Regulation of constitutive platelet-derived growth factor receptor degradation by the 105 kilodalton isoform of ankyrin3

A Thesis Submitted to the College of Graduate Studies and Research
in Partial Fulfillment of the Requirements for the Degree of
Doctor of Philosophy
in the Department of Biochemistry
University of Saskatchewan
Saskatoon

by

Levi A. Furber

PERMISSION TO USE

In presenting this thesis in partial fulfillment of the requirements for a postgraduate degree from the University of Saskatchewan, I agree that the Libraries of this University may make it freely available for inspection. I further agree that permission for copying of this thesis in any manner, in whole or in part, for scholarly purposes may be granted by the professor or professors who supervised my thesis work or, in their absence, by the Head of the Department or the Dean of the College under which this thesis work was done. It is understood that any copying or publication or use of this thesis or parts thereof for financial gain shall not be allowed without my written permission. It is also understood that due recognition shall be given to me and the University of Saskatchewan in any scholarly use which may be made of any materials in my thesis.

Requests for permission to copy or to make other use of materials in this thesis in whole or part should be addressed to:

Dr. Deborah H. Anderson
Cancer Research Cluster
Health Sciences Building, 107 Wiggins Road
University of Saskatchewan
Saskatoon, SK
S7N 5E5

ABSTRACT

Deregulation of platelet-derived growth factor receptor (PDGFR) signaling is a driving event in glioblastoma, promotes tumor progression epithelial to mesenchymal transition (EMT) in multiple cancers, modulates the tumor stroma to facilitate tumorigenesis and reduces tumor uptake of chemotherapeutics. Previous studies identified the 105 kDa isoform of ankyrin3 (Ank105) as a binding partner of the PDGFR signaling machinery and demonstrated that expression of Ank105 promoted PDGFR degradation (Ignatiuk et al., 2006)(Ignatiuk et al., 2006)(Ignatiuk et al., 2006). Receptor tyrosine kinases are targeted for degradation via endocytosis and ubiquitin-dependent trafficking to the lysosome. It was hypothesized that Ank105 promoted the constitutive degradation of the PDGFR and attenuation of PDGFR signaling by facilitating endocytosis of the PDGFR and targeting the PDGFR for lysosomal degradation via an ubiquitin-dependent mechanism. The studies in this thesis characterized the effects of Ank105 expression on PDGFR signaling and protein expression levels, determined the endocytic pathways involved in Ank105-mediated PDGFR degradation and studied the role of ubiquitin binding in Ank105 function. The most robust effect of Ank105 expression on the PDGFR was constitutive degradation as PDGFR protein expression levels in Ank105-expressing cells were significantly reduced compared to NIH 3T3 cells in the absence of PDGF ligand. Low constitutive PDGFR levels resulted in attenuated pro-proliferative AKT and mitogen-activated protein kinase (MAPK) signaling in response to ligand stimulation. To determine the endocytic requirements for Ank105-mediated constitutive PDGFR degradation, a constitutive PDGFR degradation assay was developed and the effects of several small molecule endocytosis inhibitors were evaluated. Additionally, the small molecule endocytosis inhibitors were validated by determining the effects of these inhibitors on low density lipoprotein (LDL) uptake and ligand-induced PDGFR degradation in Ank105-expressing cells. Both LDL uptake and ligand induced PDGFR degradation are known to proceed by a clathrin and dynamin dependent mechanism of endocytosis. In Ank105-expressing cells, both LDL uptake and ligand incuded PDGFR degradation were dependent upon clathrin and dynamin function. Interestingly, constitutive PDGFR degradation in Ank105-expressing cells was not dependent upon CME, but required dynamin activity. Expression of Ank105 may promote clathrin-independent, dynamin-dependent, constitutive endocytosis of the PDGFR. Additionally, acute inhibition of either lysosomal or proteasomal degradation strongly impaired constitutive PDGFR degradation, whereas ligand-

induced PDGFR degradation was less sensitive to protein degradation inhibitors, while LDL uptake was unaffected. It was unclear if PDGFR was degraded in the proteasome or if the proteasome was involved in sorting of PDGFR to the lysosome for degradation. Ubiquitination of receptors is required to target them for degradation. Ank105 was assayed for the ability to interact with ubiquitin and ubiquitinated proteins. Interestingly, Ank105 bound ubiquitin *in vitro* via the spectrin binding domain and co-immunoprecipitated with several ubiquitinated proteins, suggesting a role for Ank105 in the sorting of ubiquitinated proteins for degradation. Furthermore, Ank105 co-immunoprecipitated with a number of high and low molecular weight proteins in the absence of PDGF stimulation. Identification of Ank105 binding partners would provide further insight in the mechanism of Ank105-mediated constitutive PDGFR degradation. In summary, Ank105 promoted the attenuation of PDGFR signaling via alteration of constitutive PDGFR endocytosis and targeting of constitutive PDGFR for degradation, potentially through interaction with ubiquitin and ubiquitinated proteins. Reduction of constitutive PDGFR levels in cancers with PDGFR driver mutations, acquired PDGF responsiveness and stromal expression of PDGFR, could significantly reduce tumor proliferation, tumorigenesis and increase effectiveness of chemotherapeutics.

ACKNOWLEDGEMENTS

I would like to thank my supervisor, Dr. Deborah Anderson for her guidance and support throughout my studies. Her approach to science and mentorship has cultivated my excitement for science, challenged me to improve as a student of science and fostered my development as an independent researcher. I shall remember my time in Anderson laboratory fondly. I would also like to thank the Post-Doctoral Fellows I have encountered during the course of my studies for their mentorship, training and unique perspectives. I would also like to thank the members of the Anderson laboratory, both past and present, for their kindness and providing an excellent and encouraging work environment. I would like to thank my committee members, Drs. Anderson, Bonham, Geyer, Chelico and Lee for their advice and guidance. I also thank the funding agencies who have made this work possible and supported me throughout my studies including the Canadian Institutes of Health Research, the Saskatchewan Health Research Foundation, the Saskatchewan Cancer Agency, the Department of Biochemistry, the College of Graduate Studies and Research and the College of Medicine. Last but certainly not least, I would like to thank my friends and family for their support throughout my studies.

This work is dedicated to my wife,

Kendra

TABLE OF CONTENTS

	Page
PERMISSION TO USE	i
ABSTRACT	ii
ACKNOWLEDGEMENTS	iv
LIST OF TABLES	xi
LIST OF FIGURES	xii
LIST OF ABBREVIATIONS	xv
1.0 INTRODUCTION	1
1.1 Platelet-derived growth factor receptor biology	1
1.1.1 Structural and functional properties of platelet-derived growth factor receptor signaling	1
1.1.1.1 Platelet-derived growth factor ligands	1
1.1.1.2 The PDGFR family	1
1.1.1.3 PDGFR activation and signaling	2
1.1.2 Role of PDGFR signaling *in vivo*	6
1.1.3 Role of PDGFR signaling in disease	7
1.1.3.1 Role of PDGFR signaling in non-malignant disease	7
1.1.3.2 Role of PDGFR signaling in malignant disease	8
1.1.3.2.1 Expression and autocrine signaling of PDGF and PDGFR in human cancers	8
1.1.3.2.2 Role of paracrine PDGFR signaling in the tumor micro-environment	11
1.1.4 Summary of PDGFR signaling in biology	15
1.2 Endocytosis	16
1.2.1 Mechanisms of receptor internalization	18
1.2.1.1 Clathrin-mediated receptor internalization	18
1.2.1.1.1 Formation of clathrin coated vesicles	18
1.2.1.1.2 Dynamin-mediated vesicle scission	21
1.2.1.2 Caveolar endocytosis	22

1.2.1.3 Internalization by macropinocytosis and membrane ruffling 24
1.2.2 Endocytic trafficking and receptor degradation 26
1.2.2.1 The role of rab proteins in endosomal trafficking 26
1.2.2.2 Receptor ubiquitination and sorting into multivesicular endosomes 27
1.2.2.3 Mechanisms of protein degradation 29
1.2.2.3.1 Lysosomal degradation 29
1.2.2.3.2 Proteasomal degradation 30
1.2.3 Ligand-independent receptor degradation 32
1.2.4 Summary of endocytosis 33
1.2 Ankyrin proteins 35

2.0 RATIONALE AND OBJECTIVES 40
2.1 Hypothesis 40
2.2 Objectives 40
2.3 Specific objectives 40

3.0 MATERIALS AND METHODS 42
3.1 Materials 42
3.1.1 Reagents and supplies 42
3.2 Methods 42
3.2.1 Molecular biology 42
3.2.1.1 Generation of GST-tagged ubiquitin fusion plasmid 42
3.2.1.2 Generation of HA-tagged Ank105 fusion plasmid 42
3.2.1.3 Generation of HA-Ank105 mutant plasmids 44
3.2.1.3.1 Generation of C-terminal Ank105 deletion plasmids 44
3.2.1.3.2 Generation of spectrin binding domain and regulatory domain plasmids 44
3.2.1.3.3 Generation of C-terminal spectrin binding domain deletion plasmids 46
3.2.1.3.4 Generation of N-terminal Ank105 disordered region deletion 47

plasmids
3.2.1.3.5 Site-directed mutagenesis of potential Ank105 ubiquitin interaction motif 48
3.2.1.3.6 Site-directed mutagenesis of residues of Ank105 required for spectrin binding 49
3.2.1.3 qRT-PCR screening of knockdown cell lines 50
3.2.2 Cell culture 51
3.2.2.1 General growth conditions 51
3.2.2.2 Transient transfection of mammalian cell lines 53
3.2.2.3 Stable transfection of mammalian cell lines 53
3.2.2.4 Lentiviral transduction of mammalian cell lines 53
3.2.3 SDS-PAGE and Western blot analysis 55
3.2.3.1 Sample preparation 55
3.2.3.2 SDS-PAGE 56
3.2.3.3 Coomassie blue staining 56
3.2.3.4 Western blot analysis 56
3.2.3.4.1 Western screening of stable knockdown cell lines 58
3.2.4 Ligand stimulation of HA-Ank105-expressing cells 58
3.2.4.1 PDGF stimulation of HA-Ank105-expressing cells 58
3.2.4.2 EGF stimulation of HA-Ank105-expressing cells 58
3.2.5 Immunoprecipitations studies 59
3.2.5.1 Immunoprecipitation of PDGFR from NIH 3T3 cells 59
3.2.5.2 Immunoprecipitation of Ank105 from NIH 3T3 cells 59
3.2.5.3 Immunoprecipitation of Ank105 from HEK293 cells 60
3.2.6 Pulldown of Ank105 with an ubiquitin-GST fusion protein 61
3.2.6.1 Induction and purification of ubiquitin-GST fusion protein 61
3.2.6.2 Generation of HA-Ank105 COS-1 lysates 62
3.2.6.3 Ubiquitin-GST pulldown 62
3.2.7 Evaluation of endocytosis in HA-Ank105-expressing cells using small molecule inhibitors 63
3.2.7.1 Inducible constitutive PDGFR degradation assay 63

3.2.7.2 Preparation of small molecule inhibitors 63
3.2.7.3 Disruption of constitutive endocytosis with small molecule inhibitors 65
3.2.7.4 Optimization of Dil-LDL detection in HA-Ank105-expressing cells 67
3.2.7.5 LDL uptake assay 69
3.2.7.6 In-cell Western detection of PDGFR in HA-Ank105-expressing cells 70

4.0 RESULTS 73
4.1 Characterization of the effects of HA-Ank105 expression on PDGFR signaling and protein levels 73
4.2 Characterization of the effects of HA-Ank105 expression on EGFR protein levels 75
4.3 Effects of HA-Ank105 expression on PDGFR ubiquitination and lysosomal degradation 77
4.4 HA-Ank105 interacts with ubiquitin and ubiquitination proteins 80
4.5 HA-Ank105 interacts with ubiquitin via the spectrin binding domain 82
4.6 Inducible constitutive PDGFR degradation assay 89
4.7 Inhibition of endocytosis using small molecule inhibitors 92
4.7.1 Ank105-mediated constitutive PDGFR degradation requires dynamin activity and functional lysosomal and proteasomal pathways 95
4.7.2 LDL internalization proceeds by a clathrin and dynamin-dependent mechanism 101
4.7.3 Ligand-induced PDGFR degradation proceeds by a clathrin and dynamin-dependent mechanism and requires plasma membrane cholesterol 105
4.8 shRNA-mediated knockdown of endocytosis proteins 110
4.8.1 Inability to generate clathrin knockdown clones 111
4.8.2 Knockdown of dynamin does not recover PDGFR protein levels in HA-Ank105-expressing cells 113
4.8.3 Knockdown of tsg101 does not recover PDGFR protein levels in HA-Ank105-expressing cells 115

4.8.4 Knockdown of rab7 in HA-Ank105-expressing cells reduces PDGFR protein expression levels 117
4.9 Contributions of Ank105 binding partners to constitutive PDGFR degradation 119
4.9.1 Knockdown of βII-spectrin in HA-Ank105-expressing cells reduces PDGFR protein expression levels 119
4.9.2 Knockdown of p85α in HA-Ank105-expressing cells does not affect PDGFR protein expression levels 115
4.10 HA-Ank105 interacts with several unidentified proteins under non-stimulated conditions 121

5.0 DISCUSSION 125
5.1 Effects of Ank105 expression on PDGFR and EGFR degradation 125
5.2 Ubiquitin binding function of Ank105 128
5.3 Analysis of PDGFR endocytosis and degradation in the context of Ank105 expression 130
5.4 Knockdown of known Ank105 binding partners does not rescue constitutive PDGFR protein expression levels 137
5.5 Summary of Ank105 function and relevance to PDGFR biology 139

6.0 REFERENCES 146

LIST OF TABLES

		Page
Table 3.1	Ank105 mutagenesis primers	45
Table 3.2	PCR conditions for generation of C-terminal Ank105 deletion plasmids	46
Table 3.3	PCR conditions for generation of C-terminal Ank105 spectrin domain deletion plasmids	47
Table 3.4	PCR conditions for generation of N-terminal Ank105 deletion plasmids	48
Table 3.5	PCR conditions for generation of Ank105-S827D mutant	49
Table 3.6	PCR conditions for generation of Ank105 spectrin binding mutants	50
Table 3.7	qRT-PCR primer list	51
Table 3.8	Common buffers	52
Table 3.9	Sequences of shRNAs used for knockdown of mammalian gene expression	54
Table 3.10	Antibody list and concentrations	57
Table 3.11	Small molecule inhibitors of endocytosis	64
Table 3.12	Working concentrations of small molecule inhibitors of endocytosis	66
Table 4.1	Endocytosis inhibitor panel	93

LIST OF FIGURES

		Page
Figure 1.1	PDGFR ligand binding profiles and autophosphorylation sites	3
Figure 1.2	Prominent PDGFR cellular signaling pathways: PI3K and MAPK	5
Figure 1.3	PDGF/PDGFR mutations expressed in human cancers	9
Figure 1.4	Role of PDGFR signaling in tumorigenesis	12
Figure 1.5	Mechanisms of receptor internalization	17
Figure 1.6	Internalization, endosomal sorting and degradation of receptor tyrosine kinases	20
Figure 1.7	Domain architecture and isoforms of ankyrin3	36
Figure 3.1	Map of pHA3-Ank105 mammalian expression plasmid	43
Figure 3.2	Lentiviral transduction of GFP reporter in NIH 3T3 cells	55
Figure 3.3	Determination of optimal excitation and emission wavelengths for detection of Dil-LDL	68
Figure 3.4	Optimization of Dil-LDL uptake in HA-Ank105-expressing cells	70
Figure 3.5	In-cell Western of ligand stimulated HA-Ank105-expressing cells treated with various small molecule inhibitors	72
Figure 4.1	HA-Ank105-expression reduced PDGFR signaling and receptor levels	74
Figure 4.2	HA-Ank105 expression differentially affects EGFR degradation in HEK293 and HeLa cells	76
Figure 4.3	Ligand-induced ubiquitination of PDGFR is reduced in HA-Ank105-expressing cells while not requiring a functional lysosomal pathway for degradation	78
Figure 4.4	HA-Ank105 interacts with ubiquitin *in vitro* and several ubiquitinated proteins in cells	81
Figure 4.5	Mutation of proposed UIM of Ank105 does not prevent ubiquitin binding	83
Figure 4.6	HA-Ank105 interacts with ubiquitin through the spectrin binding domain	85

Figure 4.7	Ank105 contains several regions of disorder	86
Figure 4.8	HA-Ank105 N-terminal deletion proteins retain ubiquitin binding	88
Figure 4.9	Generation of an inducible model of constitutive PDGFR degradation	91
Figure 4.10	General endocytosis pathway and targets of small molecule inhibitors	94
Figure 4.11	Pathway specificities of the small molecule endocytosis inhibitor panel	95
Figure 4.12	Proteasomal and lysosomal degradation inhibitors MG132 and Chloroquine block constitutive PDGFR degradation	97
Figure 4.13	Ank105-mediated constitutive PDGFR degradation is blocked via inhibition of dynamin activity and cellular protein degradation	99
Figure 4.14	Dynasore treatment inhibits LDL uptake in HA-Ank105-expressing cells	102
Figure 4.15	LDL uptake proceeds by a clathrin and dynamin-dependent mechanism in HA-Ank105-expressing cells	104
Figure 4.16	Ligand-induced PDGFR degradation is dynamin-dependent in HA-Ank105-expressing cells	106
Figure 4.17	Ligand-induced PDGFR degradation requires clathrin, dynamin activity and plasma membrane cholesterol	108
Figure 4.18	General endocytosis pathway and targets of small hairpin RNAs	111
Figure 4.19	Unsucessful shRNA knockdown of clathrin heavy chain in HA-Ank105-expressing cells	112
Figure 4.20	Knockdown of dynamin in HA-Ank105-expressing cells does not impact constitutive PDGFR degradation	114
Figure 4.21	shRNA knockdown of tsg101 in HA-Ank105-expressing cells does not recover constitutive PDGFR expression	116
Figure 4.22	Knockdown of rab7 in HA-Ank105-expressing cells reduces PDGFR protein expression levels	118
Figure 4.23	Knockdown of βII-spectrin in HA-Ank105-expressing cells reduces PDGFR protein expression levels	120
Figure 4.24	Knockdown of p85α in HA-Ank105-expressing cells does not	122

affect PDGFR protein expression levels
Figure 4.25 HA-Ank105 interacted with several proteins under constitutive conditions in HEK293 cells 124
Figure 5.1 Constitutive and ligand-induced PDGFR degradation in HA-Ank105-expressing cells 141

LIST OF ABBREVIATIONS

AML	acute myeloid leukemia
Ank105	105 kDa isoform of ankyrin3
AP-2	adaptor protein-2
AP180/CALM	adaptor protein 180/clathrin-assembly lymphoid myeloid leukaemia protein
ARH	autosomal recessive hypercholesterolemia protein
BAR	Bin–Amphiphysin–Rvs
BSA	bovine serum albumin
CAF	cancer-associated fibroblast
CME	CME
CCP	clathrin-coated pits
CLIC/GEEC	clathrin-independent carriers/GPI-enriched early endosomal compartments
CML	chronic myelogenous leukemia
CMML	chronic myelomonocytic leukemia
COLIA1	collagen type Iα1
Crk	CT10 regulator of kinase
Dab2	disabled-2
Dil-LDL	dialkylcarbocyanine-labeled LDL
DMEM	Dulbecco's Modified Eagle Medium
DMSO	dimethyl sulfoxide
EEA1	early endosomal antigen 1
EDTA	ethylenediaminetetraacetic acid
EGF	epidermal growth factor
EGFR	epidermal growth factor receptor
EGTA	ethylene glycol tetraacetic acid
EIPA	5-(N-Ethyl-N-isopropyl)amiloride
Em	emission
EMT	epithelial to mesenchymal transition

ENTH	epsin N-terminal homology
Eps15	epidermal growth factor receptor substrate 15
epsin	EPS-15-interacting protein 1
E. coli	*Escherichia coli*
ESCRT	endosomal sorting complex required for transport
Ex	excitation
FasL	fas ligand
FBS	fetal bovine serum
FGF	fibroblast growth factor
FGFR	fibroblast growth factor receptor
FLK2/FLT3	fetal liver kinase 2/ Fms-like tyrosine kinase 3
Fms	colony-stimulating factor-1 receptor
GAP	GTP activating protein
GEF	GTP exchange factor
GGF	glial growth factor
Grb2	growth factor receptor-bound protein 2
hGHR	human growth hormone receptor
GST	glutathione S-transferase
G418	geneticin
HA	hemagluttinin
HEPES	2-[4-(2-hydroxyethyl)piperazin-1-yl]ethanesulfonic acid
HIP1/R	Huntingtin-interacting protein 1 related protein
Hsp40	heat shock protein 40 kDa
HRP	horseraddish peroxidase
Ig	Immunoglobulin-like
IgG	Immunoglobulin gamma
IFP	interstitial fluid pressure
IGFII	Insulin-like growth factor-II
IPTG	isopropyl β-D-1-thiogalactopyranoside
Kit	kit/stem-cell factor receptor
LAMP-1	lysosomal-associated membrane protein 1

LDL	low density lipoprotein
LDLR	low density lipoprotein receptor
LB	Luria-Bertani
MAPK	mitogen activated protein kinase
MβCD	methyl-β-cyclodextrin
MG132	carbobenzoxy-Leu-Leu-leucinal
MVE	multivesicular endosome
NCE	Non-clathrin endocytosis
NP-40	Nonidet P-40
PAGE	polyacrylamide gel electrophoresis
PBS	phosphate buffered saline
PCR	polymerase chain reaction
PDGF	platelet-derived growth factor
PDGFR	platelet-derived growth factor receptor
PH	pleckstrin homology
pHA3	HA mammalian expression plasmid
$PI4,5P_2$	phosphatidylinositol 4,5-phosphate
$PI3,4,5P_3$	phosphatidylinositol 3,4,5-phosphate
PI3K	phosphatidylinositol 3-kinase
PLC-γ	phospholipase C gamma
PP2	4-Amino-5-(4-chlorophenyl)-7-(t-butyl)pyrazolo[3,4-d] pyrimidine
pTyr	phospho-tyrosine
RasGAP	Ras GTPase activating protein
RNAi	RNA interference
RTK	receptor tyrosine kinase
SDS	sodium dodecyl sulfate
SH2	Src homology-2
shRNA	small hairpin RNA
Src	sarcoma kinase
SNARE	soluble NSF attachment proteins

STAT	SHP-2 phosphatase, signal transducer and activator of transcription
TβRI/II	transforming growth factor receptor βI/II
TEMED	N,N,N´,N´-tetra-methylethylenediamine
TGF1	transforming growth factor β 1
TfR	transferrin receptor
Tris	2-Amino-2-hydroxymethyl-propane-1,3-diol
Ub-GST	ubiquitin-GST fusion protein
UIM	ubiquitin interaction motif
VEGF	vascular endothelial growth factor
VEGFR	vascular endothelial growth factor receptor

1.0 INTRODUCTION

1.1 Platelet-derived growth factor receptor biology

1.1.1 Structural and functional properties of platelet-derived growth factor receptor signaling

1.1.1.1 Platelet-derived growth factor ligands

The platelet-derived growth factors (PDGF) are a family of soluble, protein based growth factors which exert their effects through the platelet derived growth factor receptors (PDGFR) (Kaplan *et al.*, 1979). Several cell types express PDGF including fibroblasts, leydig cells, liver endothelial cells, pericytes, astrocytes, neurons, vascular smooth muscle cells, capillary endothelial cells and macrophages, as well as several others (Heldin and Westermark, 1999). PDGF has been classically described as two polypeptide chains, being A and B, each with an approximate molecular weight of 100 kDa. The A and B chains homo- and hetero-dimerize via disulfide bond formation between 8 conserved cysteine residues to form three distinct PDGF ligands; PDGF-AA, PDGF-BB and PDGF-AB (Heldin and Westermark, 1999). The A and B chains of PDGF show a high degree of similarity, sharing 60% amino acid sequence identity (Heldin and Westermark, 1999). Two additional isoforms of PDGF have been discovered which homo-dimerize to form PDGF-CC (Li *et al*., 2000) and PDGF-DD (LaRochelle *et al*., 2001).

1.1.1.2 PDGFR family

Two PDGFR have been identified, designated α and β (Heldin and Westermark, 1999). The two PDGFR are members of the type III family of receptor tyrosine kinases (RTKs) (Heldin and Westermark, 1999) and are structurally related to the Kit/stem-cell factor receptor (Kit) (Yarden *et al*., 1987), colony-stimulating factor-1 receptor (Fms) (Coussens et al., 1986) and fetal liver kinase 2/ Fms-like tyrosine kinase 3 (FLK2/FLT3) (Rosnet *et al*., 1991). The chromosomal locations of the genes encoding these receptors are clustered. The gene encoding PDGFRα (*PDGFRA*) is located on chromosome 4q12 near the gene encoding Kit (Spritz *et al*., 1994) whereas the gene encoding PDGFRβ (*PDGFRB*) is located on chromosome 5q32 (Yarden *et al*., 1986) near the gene encoding Fms (Roberts *et al*., 1988).

The *PDGFRA* and *PDGFRB* genes encode protein products that when mature, and fully

glycosylated, are 170 and 180 kDa, respectively (Heldin and Westermark, 1999). The PDGFRα and PDGFRβ proteins are highly homologous and share a 46% amino acid sequence identity. The PDGF receptors contain three distinct regions that include an extracellular region, a transmembrane region and an intracellular region. The extracellular domain contains 5 immunoglobulin-like (Ig) domains to mediate ligand binding (Alvarez *et al*., 2006). The transmembrane domain spans the plasma membrane once. The intracellular region consists of a conserved juxtamembrane domain, a split tyrosine kinase domain containing a non-catalytic inserted sequence without homology to other kinases and a C-terminal tail (Figure 1.1) which are both implicated in inhibition of PDGFR kinase activity (Heldin and Lennartsson, 2013).

1.1.1.3 PDGFR activation and signaling

Activation of PDGFRs generates potent mitogenic and anti-apoptotic responses, as well as induces chemotaxis and actin rearrangement (Heldin and Lennartsson, 2013; Heldin and Westermark, 1999). Binding of PDGFR to ligand facilitates dimerization of receptor molecules and activation of the receptor. Binding of all PDGF isoforms except PDGF-DD promotes homo-dimerization of PDGFRα; whereas PDGFRβ homo-dimerization occurs upon binding of PDGF-BB or PDGF-DD (Heldin and Lennartsson, 2013) (Figure 1.1). PDGF-CC only binds PDGFRα (Heldin and Lennartsson, 2013). In cell lines co-expressing PDGFRα and PDGFRβ, binding PDGF-BB or PDGF-AB can direct hetero-dimerization of PDGFRα and PDGFRβ (Heldin and Lennartsson, 2013) (Figure 1.1). These ligand binding patterns have been demonstrated *in vitro*, however only PDGF-CC and PDGF-AA binding to PDGFRα and PDGF-BB binding PDGFRβ have been demonstrated *in vivo* (Andrae *et al*., 2008). Ig-like domains 2 and 3 in the extracellular region of the PDGFR mediate ligand binding (Shim *et al*., 2010). Ig-like domains 4 and 5 stabilize ligand-mediated receptor dimerization, orienting the PDGFR to facilitate trans-autophosphorylation of tyrosine residues within the intracellular regions of the PDGFR (Yang *et al*., 2008). The activation loop of the kinase domain is phosphorylated at Tyr849 and Tyr857 in PDGFRα and PDGFRβ, respectively (Baxter *et al*., 1998) (Figure 1.1). This phosphorylation event permits ATP and substrate access to the active site by changing the conformation of the activation loop, thereby fully activating tyrosine kinase activity (Baxter *et al*., 1998).

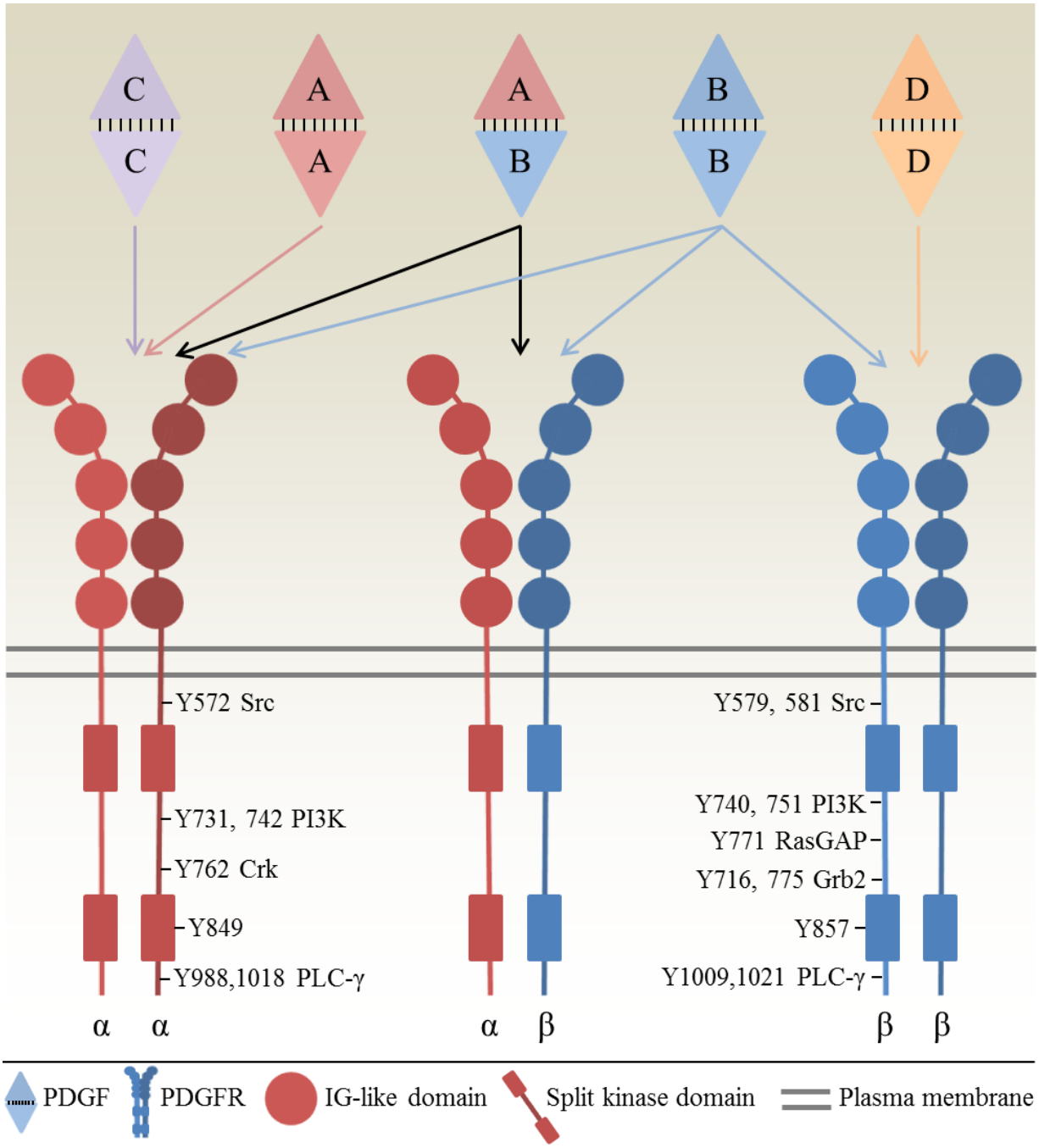

Figure 1.1: PDGFR ligand binding profiles and autophosphorylation sites
Depiction of the specificity of PDGFRα (red), PDGFRαβ (red/blue) and PDGFRβ dimers (blue) for PDGF-AA (red), PDGF-BB (blue), PDGF-AB (red/blue), PDGF-CC (purple) and PDGF-DD (orange) ligand dimers. Tyrosine (Y) residues phosphorylated on activated receptors serve as binding sites for the recruitment and activation of downstream signaling pathways including phosphatidylinositol 3-kinase (PI3K), phospholipase C gamma (PLC-γ), sarcoma kinase (Src), Ras GTPase activating protein (RasGAP), CT10 regulator of kinase (Crk) and growth factor receptor-bound protein 2 (Grb2). Phosphorylation sites in the activation loop of the split kinase domain at Y849 and Y857 of PDGFRα and PDGFRβ, respectively are depicted.

Dimerized PDGFRs trans-autophosphorylate multiple tyrosine residues within

cytoplasmic residues in the juxtamembrane domain, non-catalytic kinase insert and C-terminal tail of the PDGFR that serve as docking sites for Src homology-2 (SH2) domain containing proteins to initiate several signaling cascades (Heldin and Lennartsson, 2013) (Figure 1.1). Signaling pathways potentiated from the activation of the PDGFR include phosphatidylinositol 3-kinase (PI3K), phospholipase C gamma (PLC-γ), sarcoma kinase (Src), Ras GTPase activating protein (RasGAP), CT10 regulator of kinase (Crk), SHP-2 phosphatase, signal transducer and activator of transcription (STAT) and initiators of the mitogen activated protein kinase (MAPK) pathway (Figure 1.1; Figure 1.2) (Heldin and Lennartsson, 2013).

Class 1A PI3K is a lipid kinase composed of a regulatory subunit, p85, and a catalytic subunit, p110. The p85 subunit stabilizes and inhibits the catalytic activity of p110 (Yu *et al*., 1998). Upon activation of the PDGFR, PI3K is recruited to the receptor and binds phosphorylated Tyr731/742 and Tyr740/751 of PDGFRα and PDGFRβ, respectively, via its SH2 domains (Heldin and Westermark, 1999) (Figure 1.1; Figure 1.2). Binding of PI3K to phosphorylated receptor relieves inhibition of p85 on p110 catalytic activity (Miled *et al*., 2007). PI3K catalyzes the phosphorylation of phosphatidylinositol 4,5-phosphate ($PI4,5P_2$) at the D3 position to produce phosphatidylinositol 3,4,5-phosphate ($PI3,4,5P_3$) (Cantley, 2002) (Figure 1.2). This lipid second messenger promotes the recruitment of proteins, containing PH domains to interact with plasma membrane $PI3,4,5P_3$, and activation of several downstream signaling proteins including PDK1 Akt, p70 S6 kinase, JNK/SAPK, PKC as well as Rho family GTPases (Heldin and Westermark, 1999) (Figure 1.2). Additionally, p85 has been demonstrated to interact with proteins that regulate PDGFR endocytosis and degradation such as rab5 and the small isoforms of ankryin3 (Mellor et al., 2012).

In the context of PDGF-mediated signaling, PI3K regulates the antiapoptotic and motility responses to PDGF stimulation (Heldin and Lennartsson, 2013) (Figure 1.2). Src mediated activation of the transcription factor Myc and MAPK/ERK signaling are responsible for the growth and proliferative effects of PDGF stimulation (Heldin and Westermark, 1999) (Figure 1.2). Src binds Tyr572 of PDGFRα and Tyr579/581 of PDGFRβ (Heldin and Lennartsson, 2013) (Figure 1.1). Grb2, a component of the MAPK/ERK signaling pathway, binds PDGFRβ at Tyr716/775 (Heldin and Lennartsson, 2013) (Figure 1.1). PLC-γ binds PDGFRα at Tyr 988/1018 and PDGFRβ at Tyr1009/1021 (Heldin and Lennartsson, 2013) (Figure 1.1). The PDGFRα and

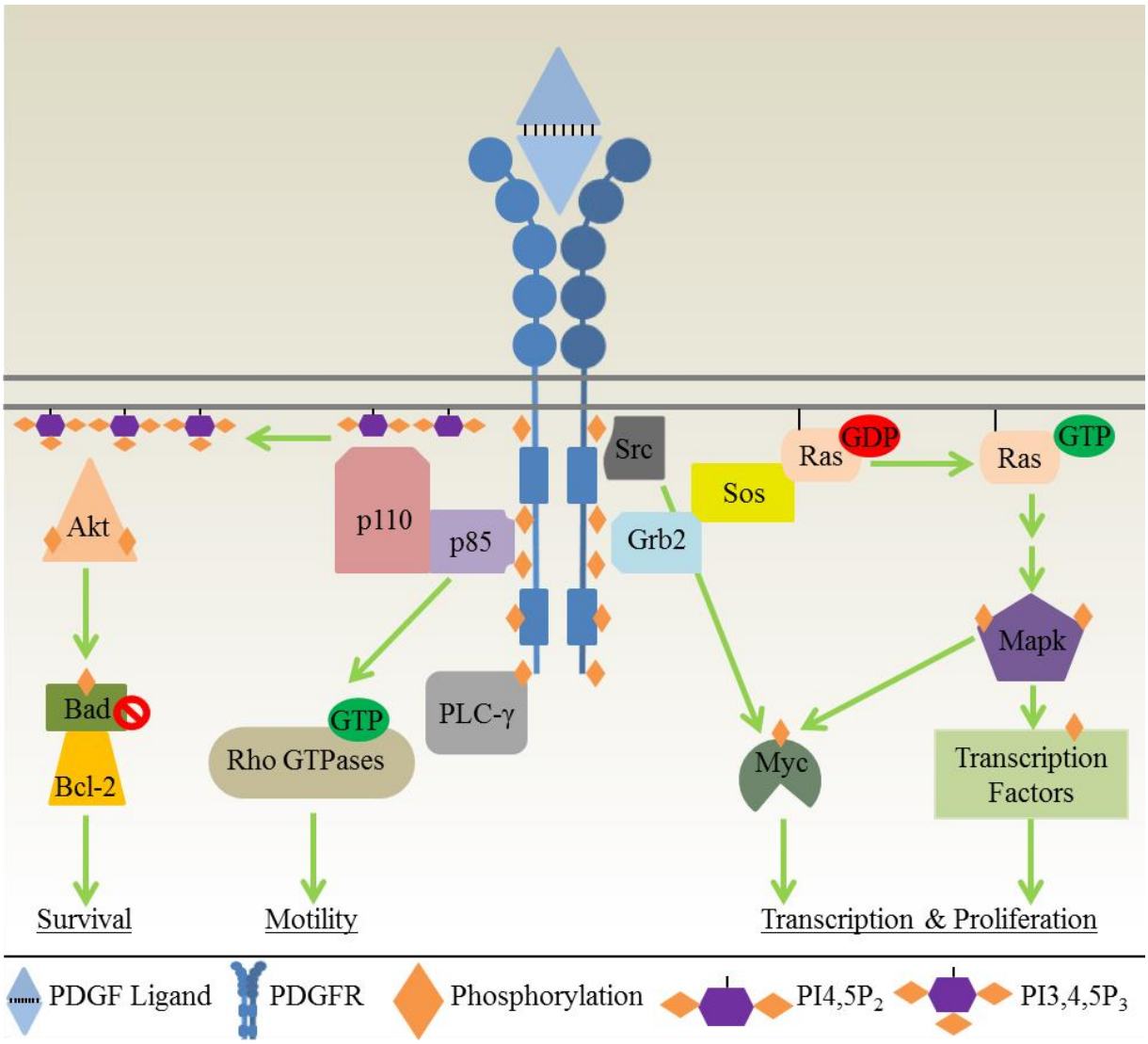

Figure 1.2: Prominent PDGFR cellular signaling pathways: PI3K and MAPK
PDGFR signaling generally inhibits apoptosis, induces cell motility and stimulates cell proliferation. Inhibition of apoptosis is initiated by PI3K mediated phosphorylation of phosphatidylinositol-4,5 bisphosphate ($PI4,5P_2$) to phosphatidylinositol-3,4,5triphosphate ($PI3,4,5P_3$) which promotes recruitment and activation Akt. The p85 subunit of PI3K regulates Rho family GTPases and cell motility. Cell proliferation is stimulated by Src and MAPK mediated activation of Myc, as well as other transcription factors. The MAPK pathway is activated via binding of a series of adaptor proteins to the PDGFR that promotes the eventual activation of MAPK.

PDGFRβ receptors share very similar signaling profiles in response to ligand, however there are differences. PDGFRα exclusively binds Crk at Tyr762 (Heldin and Lennartsson, 2013), whereas PDGFRβ binds RasGAP (Tallquist and Kazlauskas, 2004) at Tyr771 (Heldin and Lennartsson, 2013) (Figure 1.1). Indeed PDGFRα and PDGFRβ signaling can have different consequences at

the cellular level (Tallquist and Kazlauskas, 2004). While both receptor isoforms promote cell proliferation, only PDGFRβ inhibits apoptosis. Moreover activation of PDGFRβ stimulates chemotaxis whereas regulation of chemotaxis by PDGFRα is cell type dependent (Tallquist and Kazlauskas, 2004).

1.1.2 Role of PDGFR signaling *in vivo*

Both PDGFRα (Soriano, 1997) and PDGFRβ (Soriano, 1994) are required during development as deletion of genes encoding either protein in mice results in lethality. Deletion of PDGFRα results in defects in supportive connective tissue, mesenchymal type cells. Defects are observed in lung aveolar smooth muscle, kidney, and dermal mesenchymal cells as well as in oligodendrocytes (Tallquist and Kazlauskas, 2004). PDGFRα is thought to stimulate the proliferation of these cell types and removal of these signals impairs proper development (Lindahl and Betsholtz, 1998). Indeed PDGFRα knockout mice have impaired lung function, cranial deformations, impaired muscle formation and die shortly after birth (Heldin and Westermark, 1999).

Knockdown of PDGFRβ results in defects in the vascular smooth muscle cells of several organs including the kidney, eye, skin and brain (Lindahl *et al*., 1998; Lindahl *et al*., 1997b). Similar to PDGFRα, PDGFRβ signaling is thought to drive proliferation of these cell types and impairment of signaling impedes proper development (Tallquist and Kazlauskas, 2004). Knockdown of PDGFRβ impairs kidney function with reduced glomerular filtration rates and ablated development of kidney mesangial cells (Leveen *et al*., 1994; Soriano, 1994). Additionally, PDGFRβ knockout mice suffer from internal bleeding, causing death, due to impaired development of blood vessels in described cell types (Heldin and Westermark, 1999).

Knockdown of PDGF-BB produces a similar phenotype to knockdown of PDGFRβ (Lindahl *et al*., 1997a), whereas knockdown of PDGF-AA produces a more mild phenotype than knockdown of PDGFRα (Bostrom *et al*., 1996), possible due to the ability of PDGFRα to signal via other isoforms of PDGF (Heldin and Westermark, 1999). In addition to roles during development, PDGFR signaling is also implicated in wound repair, neural maintenance and regeneration, angiogenesis and recruitment of pericytes to the vascular system as well as regulation of interstitial fluid pressure (Heldin and Westermark, 1999).

1.1.3 Role of PDGFR signaling in disease

1.1.3.1 Role of PDGFR signaling in non-malignant disease

Excessive PDGFR signaling can lead to non-malignant disease characterized by over-production and deposition of connective tissue components such as collagen and glycosaminoglycans (Alvarez *et al*., 2006). Excess deposition of connective tissue components impairs proper organ function, resulting in disease. Atherosclerosis, rheumatoid arthritis, liver cirrhosis and fibrosis of the lungs and kidneys are linked to excess PDGFR signaling (Heldin and Westermark, 1999). In fibrotic disease, macrophages that have been activated by chronic inflammation secrete a number of inflammatory cytokines and growth factors, including several isoforms of PDGF. These cytokines and growth factors promote overexpression and activation of PDGFR on mesenchymal cells, driving their proliferation and production of connective tissue components (Bonner, 2004). Fibrosis of multiple organs was recapitulated in transgenic knock-in mice harboring a constitutively active PDGFRα gene (Olson and Soriano, 2009).

The principal cause of heart attack and stroke is atherosclerosis (Ross, 1993). Atherosclerosis is characterized by excessive inflammatory and fibroproliferative response to damage to the vascular and arterial smooth muscle and PDGFR signaling is thought to be one of the mediators in the pathology of atherosclerosis (Alvarez *et al*., 2006). PDGF levels expressed in the arteries are increased after arterial damage (Ross, 1993). Indeed, other atherosclerosis associated cells express PDGF including activated macrophages, smooth muscle cells, endothelial cells and platelets (Alvarez *et al*., 2006). In a cholesterol induced model of atherosclerosis, atherosclerotic lesions were significantly reduced in rabbits fed a high cholesterol diet when treated with anti-PDGF-BB antibodies (Rutherford *et al*., 1997). Individuals with diabetes are at a statistically higher risk to develop atherosclerosis (Pyorala *et al*., 1987). Indeed, 70-75% of individuals afflicted with diabetes succumb to cardiovascular disease (Uusitupa *et al*., 1990). Diabetic mice treated with the tyrosine kinase inhibitor imatinib, targeting PDGFR activity, showed reduced formation of atherosclerotic lesions in the aorta and attenuated expression of both PDGF-BB and PDGFRβ, which are both elevated in diabetic mice (Lassila *et al*., 2004).

1.1.3.2 Role of PDGFR signaling in malignant disease

1.1.3.2.1 Expression and autocrine signaling of PDGF and PDGFR in human cancers

The potential role of PDGFR signaling in malignant disease was first realized when it was discovered that simian sarcoma virus gene, sis, encoded PDGF-BB (Doolittle *et al*., 1983). The ability of the simian sarcoma virus to transform cells was abrogated by treatment with anti-PDGF antibodies (Johnsson *et al*., 1985), suggesting a role of PDGFR signaling in cellular transformation. Several human cancers show up-regulation of either mRNA or protein expression of either the PDGFR or its ligand including several brain cancers, soft tissue sarcomas, breast cancer, multiple carcinomas and several forms of leukemia (Heldin and Westermark, 1999). An interesting feature of the available tumor expression data is that both the receptor and the ligand are often co-expressed in the tumor, suggesting an autocrine signaling mechanism.

The relationship between human glioblastomas and PDGFRα signaling has been well established. PDGFRα hyper-activity has been reported in roughly 30% of glial tumors (Brennan *et al*., 2009) and PDGFRα signaling may drive glial tumor progression to a more aggressive phenotype. PDGFRα positive staining cells are observable in all grades of the tumor and the staining density increases as tumor grade increases, indicating that PDGFRα expression increases with tumor aggressiveness (Hermanson *et al*., 1996). A similar pattern is evident with the expression of PDGF-AA as ligand is expressed at low levels, if at all, in low grade tumors and expressed at high levels in high grade tumors (Heldin and Westermark, 1999). Intensification of autocrine PDGFR signaling drives glial tumor progression (Heldin and Westermark, 1999). This pattern of ligand-receptor co-expression is also observable in sarcomas (Smits *et al*., 1992; Wang *et al*., 1994).

Autocrine PDGFR signaling may be a driving event in glioblastoma tumorigenesis (Figure 1.3). Intracranial injection of simian sarcoma virus into marmosets (Heldin, 2004) or injection of a retrovirus containing the *pdgfb* gene in mice (Uhrbom *et al*., 1998) was sufficient to induce formation of glioblastoma. The prevailing mechanism of overexpression of mRNA and protein for both PDGF and PDGFR in glial tumors is unknown. Amplification of the *PDGFRA* gene has been occasionally observed in glial tumors, and this amplification promotes overexpression (Figure 1.3) (Fleming *et al*., 1992; Hermanson *et al*., 1996; Kumabe *et al*., 1992). A mutation of PDGFRα was identified where exons 8 and 9 of the extracellular domain of the

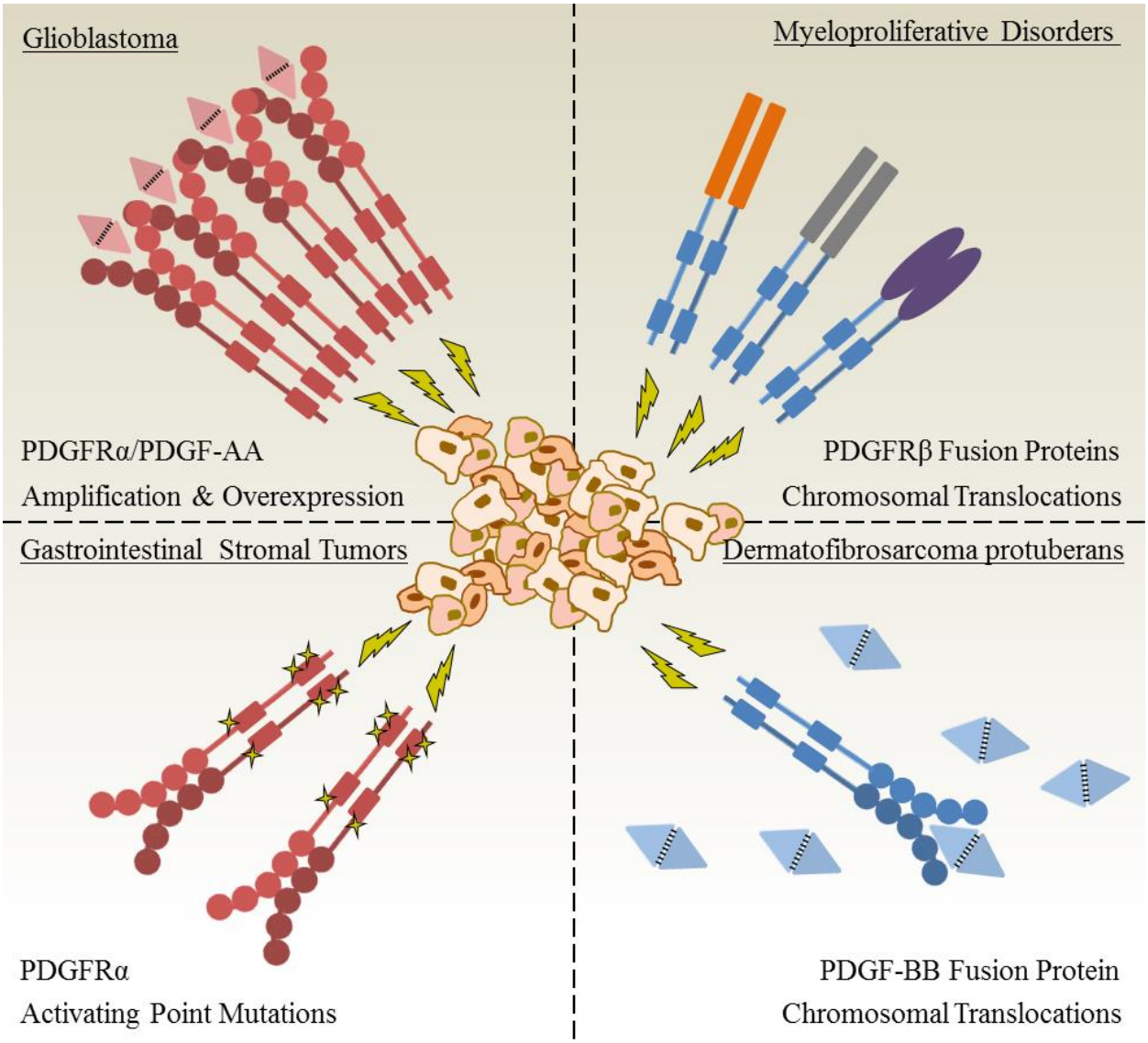

Figure 1.3: PDGF/PDGFR mutations expressed in human cancers
Depiction of PDGF and PDGFR mutations expressed in several types of human cancers that promote tumor proliferation and progression. PDGFRα and PDGF-AA are amplified and overexpressed in glioblastomas. Gastrointestinal stromal tumors harbor several point mutations resulting in ligand independent constitutive activation including V561D, D842V and D846Y. Several myeloproliferative disorders express PDGFRβ fusion proteins such as ETV6-PDGFRβ, HIP1-PDGFRβ, H4/D1OS1-PDGFRβ, CEV14-PDGFRβ and Rabaptin5-PDGFRβ that result in ligand independent constitutive activation. Dermatofibrosarcoma protuberans expresses COLIA1-PDGF-BB fusion protein resulting in excess ligand and over-active signaling. Modified with permission (Andrae *et al*., 2008).

receptor were deleted (PDGFRα-$\Delta^{8,9}$) and expression of this mutant resulted in transformation (Clarke and Dirks, 2003). Gastrointestinal stromal tumors also harbor mutations of PDGFRα that result in constitutive receptor activation and signaling. Mutations in the activation loop (D842V

and D846Y) and in the juxtamembrane domain (V561D) have been reported (Chompret *et al*., 2004; Heinrich *et al*., 2003). These mutations are thought to alter PDGFRα conformation and promote ligand independent activity (Jones and Cross, 2004) (Figure 1.3).

Myeloproliferative disorders such as acute myeloid leukemia (AML) chronic myelogenous leukemia (CML) and chronic myelomonocytic leukemia (CMML) can, albeit rarely, harbor chromosomal translocations that produce PDGFR fusion mutations which promotes constitutive PDGFR signaling (Alvarez *et al*., 2006) (Figure 1.3). Several PDGFR fusion mutants have been identified including ETV6-PDGFRβ, HIP1-PDGFRβ, H4/D1OS1-PDGFRβ, CEV14-PDGFRβ and Rabaptin5-PDGFRβ (Alvarez *et al*., 2006; Jones and Cross, 2004). These translocation mutations generally result in fusions between the intracellular domains of the PDGFR and the N-terminal regions of the fusion partner, replacing the extracellular domains of the PDGFR. The resulting fusion protein is insensitive to PDGF but is constitutively active (Jones and Cross, 2004). The N-terminal regions of the fusion partners promote dimerization that leads to constitutive activation of the PDGFR intracellular domains. Additionally, the expression of the fusion gene is under control of the regulatory elements of the fusion partner which can lead to higher expression levels of PDGFR-fusion protein than wild type PDGFR (Jones and Cross, 2004).

Several of the PDGFR fusion mutants induce cellular transformation and disease. Expression of ETV6-PDGFRβ caused cellular transformation and impaired apoptosis in cell culture models via ligand independent activation of PDGFR signaling pathways (Carroll *et al*., 1996; Jones and Cross, 2004; Jousset *et al*., 1997). Mouse bone marrow transplant models demonstrated that ETV6-PDGFRβ caused a myeloproliferative disease closely resembling CMML (Tomasson *et al*., 2000). Expression of Rabaptin5-PDGFRβ induced cellular transformation and caused myeloproliferative disease in mice that demonstrated sensitivity to imatinib treatment (Magnusson *et al*., 2001). Excitingly, treatment of patients harboring the Rabaptin5-PDGFRβ with imatinib resulted in remission (Apperley *et al*., 2002; Magnusson *et al*., 2002). In the rare soft tissue sarcoma dermatofibrosarcoma protuberans chromosomal translocation between the gene encoding PDGF-BB and collagen type Iα1 (COLIA1-PDGF-BB) have been reported (Kiuru-Kuhlefelt *et al*., 2001) (Figure 1.3). The COLIA1-PDGF-BB fusion protein is processed to PDGF-BB, resulting in autocrine stimulation of PDGFRβ receptors (Shimizu *et al*., 1999). A small group of patients with locally advanced dermatofibrosarcoma

protuberans were treated with imatinib; each of the patients responded to treatment, with 50% of the patients showing complete clinical response. One patient with metastatic dermatofibrosarcoma protuberans initially responded to imatinib treatment however, experienced disease progression after 7 months of therapy (McArthur *et al*., 2005).

Acquisition of constitutive PDGFR signaling can increase tumor invasiveness and promote metastasis. Tumors of epithelial origin are often unresponsive to PDGF stimulation (Heldin and Lennartsson, 2013). When epithelial tumors undergo epithelial to mesenchymal transition (EMT) profound alterations to gene expression occur and this transition is associated with increased invasiveness and metastasis (Thiery *et al*., 2009). Among gene expression patterns altered during EMT, PDGFRα and PDGFRβ expression was increased several fold (Jechlinger *et al*., 2003). Pharmacological inhibition of PDGFR signaling increased apoptosis and inhibited metastasis in mouse models of breast cancer (Jechlinger *et al*., 2006). PDGFRα and PDGFRβ expression positively correlated with tumor grade and invasiveness in human breast carcinoma (Jechlinger *et al*., 2006). Indeed, PDGFR was expressed in 39.2% of 181 human breast carcinoma samples tested and positively correlated with lymph node metastasis, HER-2 and Bcl-2 expression (Carvalho *et al*., 2005). Attenuation of PDGFR signaling was also shown to inhibit metastasis of hepatocellular carcinoma (Gotzmann *et al*., 2006) and prostate cancer (Dolloff *et al*., 2005; Russell *et al*., 2009). Additionally PDGF has been shown to induce EMT in PDGF responsive liver and colon cancers (Yang *et al*., 2006) and thus promote tumor invasiveness and metastasis by inducing EMT (Figure 1.4). Indeed certain carcinomas may require PDGF signaling to maintain mesenchymal phenotype (Barr *et al*., 2008).

1.1.3.2.2 Role of paracrine PDGFR signaling in the tumor micro-environment

PDGFR signaling can promote tumor invasiveness and metastasis through paracrine signaling between the cells of the carcinoma and its surrounding micro-environment. Several tumors including breast carcinoma, small-cell lung carcinoma and colorectal cancer express ligand while the stroma expresses receptor (Heldin and Westermark, 1999). The tumor stroma is composed of connective tissue components such as basement membrane and extracellular matrix, as well as several cell types including fibroblasts, vasculature and immune cells (Andrae *et al*., 2008). In normal, non-malignant, epithelial tissue the stroma plays a supportive role in regulating tissue homeostasis and is normally a barrier to tumor progression. Tumor cells

remodel the stroma to facilitate invasiveness, angiogenesis and metastasis (Bremnes *et al*., 2011; Zigrino *et al*., 2005).

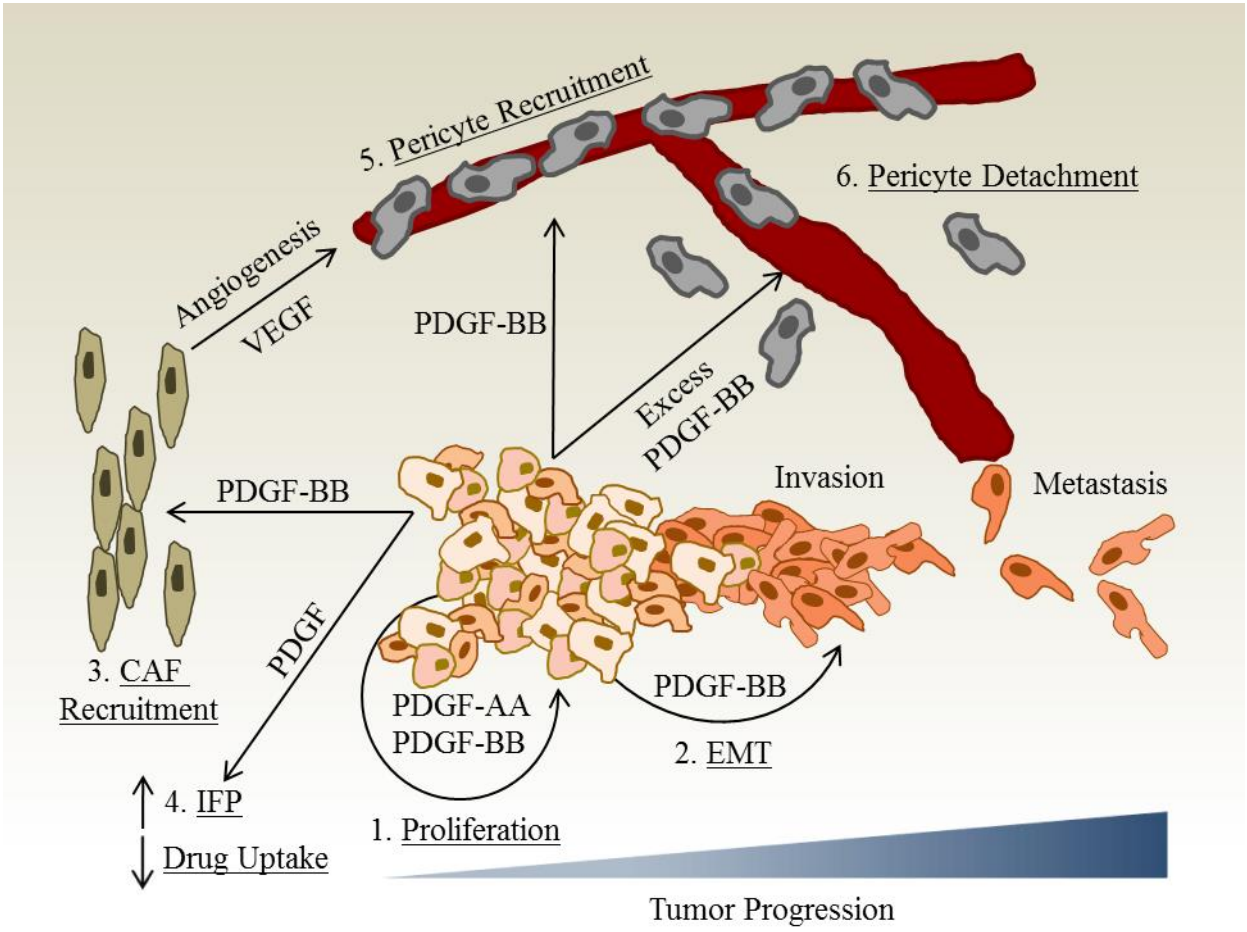

Figure 1.4: Role of PDGFR signaling in tumorigenesis
1. Autocrine PDGFR signaling, via overexpression or constitutive activation, results in cell growth and proliferation and possible inhibition of apoptosis. PDGF and PDGFR expression correlate to tumor stage in glioblastoma and sarcoma cancers. 2. Epithelial to mesenchymal transition (EMT) may be initiated or sustained by PDGF-BB facilitating tumor progression to an invasive and metastatic phenotype. 3. PDGF-AA promotes the recruitment of cancer-associated fibroblasts (CAF). CAFs secrete a number of cytokines and growth factors promoting tumorigenesis. CAF secreted vascular endothelial growth factor (VEGF) initiates angiogenesis that facilitates tumor growth and proliferation. 4. PDGF stimulates CAFs to secrete and interact with components of the stromal extracellular matrix that increases interstitial fluid pressure (IFP). Increased IFP hinders tumor uptake of chemotherapeutics. 5. PDGF-BB recruits pericytes to and stabilizes new blood vessels. Excess PDGF can induce pericyte detachment and destabilize blood vessels promoting tumor progression. Modified with permission (Andrae *et al*., 2008).

One of the key events in stroma remodeling is the recruitment and activation of carcinoma associated fibroblasts (CAFs), which are distinct from normal fibroblasts (Figure 1.4).

CAFs show distinct genetic mutations and epigenetic regulation compared to normal fibroblasts (Bremnes *et al*., 2011) and express different cell surface markers. Indeed PDGFRα and PDGFRβ expression are CAF markers (Ostman, 2004). CAFs increase tumor growth, angiogenesis, invasiveness and metastatic potential (Bremnes *et al*., 2011) and are known to secrete several types of collagens, heparin sulfate proteoglycans, matrix metalloproteinases, cytokines and growth factors including vascular endothelial growth factor (VEGF) which is critical for angiogenesis (Figure 1.4) (Bremnes *et al*., 2011). PDGF stimulates proliferation of CAFs and promotes their recruitment to sites of tumor growth (Bremnes *et al*., 2011). PDGF mediated recruitment of PDGFR expressing fibroblasts to tumor stroma has been demonstrated in several experimental models and this recruitment contributes to tumor growth. In a mouse cervical cancer model, PDGF recruited fibroblasts secreted several isoforms of fibroblast growth factor that stimulated tumor proliferation, and this proliferation was sensitive to imatinib even though the tumor itself did not express PDGFR (Pietras *et al*., 2008). Tumor cells devoid of VEGF expression show defects in initiation of angiogenesis (Andrae *et al*., 2008). VEGF knock out tumor cells that expressed PDGF-AA were transplanted into mice and promoted the recruitment of PDGFR positive fibroblasts. These PDGF recruited fibroblasts secreted VEGF and promoted angiogenesis (Dong *et al*., 2004). Indeed this mode of paracrine recruitment of fibroblasts may be relevant in human disease as recruitment of PDGFR positive fibroblasts via tumor produced PDGF has been demonstrated in human lung carcinoma (Tejada *et al*., 2006).

PDGFR signaling can also affect tumor angiogenesis via regulation of pericytes (Figure 1.4). PDGFRβ positive pericytes are recruited to newly formed blood vessels via PDGF-BB (Gerhardt and Semb, 2008). Pericytes adhere to the vascular endothelium and regulate the permeability and stability of blood vessels, preventing leakage of cells from the blood vessel (von Tell *et al*., 2006) (Figure 1.4). Indeed pericytes are required during angiogenesis for the stabilization and maturation of newly formed vasculature (Gerhardt and Semb, 2008). Given the importance of angiogenesis in promoting tumor growth, it is targeted as an anticancer therapy. VEGF is a critical component in the initiation of angiogenesis. Pharmacological inhibitors directed against the VEGF receptor show greater efficacy when combined with the PDGFR inhibitor imatinib in mouse models of pancreatic cancer, suggesting that destabilization of blood vessels by removal of pericytes, reduces tumor viability (Bergers *et al*., 2003). Other experiments in the same model system indicate that pericyte removal increases the permeability of blood

vessels and promotes tumor metastasis, as increased numbers of tumor cells were observed in the blood (Xian *et al*., 2006). Indeed many tumor types often display destabilized, leaky and inefficient vasculature generating gaps in the endothelial lining with poor pericyte coverage (Gerhardt and Semb, 2008). This type of vasculature promotes hypoxia that can drive tumor progression to an invasive and metastatic phenotype (Wilson, 2007). Thus pericyte removal from blood vessels via inhibition of PDGFR signaling may attenuate tumor growth but increase metastatic potential. Additionally, excess PDGF-BB may promote pericyte detachment (Andrae *et al*., 2008).

PDGFR stroma signaling can also modulate tumor drug uptake via regulation of interstitial fluid pressure (IFP) (Figure 1.4). The interstitial space mediates exchange of nutrients, waste, oxygen and other small molecules between tissues and the vascular system (Heldin *et al*., 2004). In normal tissue the IFP is slightly negative facilitating net movement of fluid into the interstitial space (Heldin *et al*., 2004). The IFP in many tumors including breast and colorectal carcinomas (Less *et al*., 1992) is elevated and leads to decreased interstitial transport from the vasculature in tumors (Heldin *et al*., 2004). High IFP reduces tumor uptake of chemotherapeutics, such as small molecule inhibitors and therapeutic antibodies thereby reducing therapeutic efficacy (Heldin *et al*., 2004) (Figure 1.4). Reduction of IFP was shown to increase interstitial transport of labeled small molecules and macromolecules (Brekken *et al*., 2000; Rubin *et al*., 2000). Fibroblasts are thought to contribute to IFP by increasing tension in the extracellular matrix. Fibroblasts bind to collagen in the extracellular matrix via integrins. The fibroblast bound collagen molecules in turn interact with other components of the extracellular matrix including proteoglycans and hyaluronan. The net effect is to constrict the intersitium or stroma (Heldin *et al*., 2004). PDGF stimulation was found to enhance this process and increase IFP (Clark *et al*., 1989; Gullberg *et al*., 1990) (Figure 1.4).

The tumor stroma is characterized by the presence of CAFs and increased constriction of the extracellular matrix (Heldin *et al*., 2004). As previously mentioned CAFs are highly sensitive to PDGF and actively secrete extracellular matrix components. Tumors with stromal expression of PDGFRβ including, lung, breast and colon carcinoma frequently demonstrate high IFP (Ostman and Heldin, 2001). Treatment with imatinib to inhibit PDGFRβ activity in a rat model of colon carcinoma decreased IFP and increased uptake of labeled small molecules (Pietras *et al*., 2001). Decreasing IFP and increasing interstitial transport can improve efficacy of

chemotherapeutics. In a mouse model of thyroid carcinoma expressing stromal PDGFRβ, tumor uptake and efficacy of both taxol and 5-fluorouricil was increased when treated in combination with imatinib, whereas treatment with imatinib alone did not affect tumor growth. Indeed imatinib treatment corresponded to decreased IFP (Pietras *et al*., 2002). Additionally imatinib treatment increased tumor uptake and efficacy of cyclophosphamide in mouse models of lung and pancreatic carcinoma (Falcon *et al*., 2011).

1.1.4 Summary of PDGFR signaling in biology

When activated by cognate ligand PDGFRα/β dimerize, prompting trans-autophosphorylation on multiple cytoplasmic tyrosine residues that serve as docking sites for the recruitment and activation of SH2 domain containing signaling proteins (Figure 1.1). Signaling output from PI3K and MAPK/ERK pathways are prevalent, promoting cell survival and proliferation (Figure 1.2). PDGFRs are required for correct development of the lung, kidney, nervous system and vascular system. Knockout of either isoform of PDGFR is embryonic lethal. In adults PDGFR signaling is involved in wound healing.

Hyperactivity of PDGFR signaling is implicated in both non-malignant and malignant human disease. In non-malignant disease PDGFR signaling is linked to fibrosis of multiple organs as well as to the pathogenesis of atherosclerosis. Diabetics have a statistically higher chance of developing cardiovascular disease. Diabetic mouse models show elevated expression levels of both PDGF and PDGFR. Inhibition of PDGFR signaling in non-malignant diseases, by therapeutic antibodies or small molecule inhibitors, reduced disease severity.

Multiple cancers demonstrate overexpression of PDGF or PDGFR at the level of mRNA or protein. Aberrant expression of both receptor and ligand is associated with glioblastomas and sarcoma cancers (Figure 1.3), where expression levels correlate to disease progression. Expression of both point mutations and fusion mutations of PDGFR, granting ligand independency and constitutive activation, occur in gastrointestinal tumors and myeloproliferative disorders, respectively (Figure 1.3). PDGF fusion mutations, resulting in overexpression of ligand, also occur in rare skin cancers (Figure 1.3). Autocrine signaling resulting from PDGF/PDGFR overexpression or expression of oncogenic mutants promotes tumor proliferation, inhibition of apoptosis and disease progression (Figure 1.4). PDGFR signaling can also initiate and maintain EMT, which is associated with increased invasiveness and metastasis (Figure 1.4).

Inhibition of PDGFR signaling with small molecule inhibitors can attenuate tumor growth and in some cases results in clinical clearance.

PDGFR signaling also contributes to tumorigenesis via paracrine regulation of the tumor micro-environment, or stroma (Figure 1.4). PDGF promotes the recruitment of CAFs stimulating their proliferation, secretion of extracellular matrix proteins and interaction with the extracellular matrix. Increased interaction with the extracellular matrix increases the interstitial fluid pressure of the stroma and impairs tumor uptake of chemotherapeutics (Figure 1.4). Inhibition of PDGFR signaling increased drug uptake and efficacy. CAFs promote angiogenesis via increasing secretion of VEGF. PDGF promotes recruitment of pericytes to newly formed blood vessels, increasing blood vessel stability (Figure 1.4). Inhibition of PDGFR signaling reduces pericyte coverage of blood vessels and impaired tumor growth; however, destabilization of blood vessels induces hypoxia and may increase metastatic potential.

1.2 Endocytosis

Receptor signaling is modulated by timely activation of endocytic pathways. Activated receptors at the plasma membrane are internalized via CME (CME) or non-clathrin endocytosis (NCE). Several distinct mechanisms of NCE exist including caveolar endocytosis, macropinocytosis, flotillin dependent endocytosis, lipid clustering, clathrin-independent carriers/GPI-enriched early endosomal compartments (CLIC/GEEC) endocytosis and circular dorsal membrane ruffling (Doherty and McMahon, 2009b) (Figure 1.5). While clathrin and caveolar endocytosis depend on the activity of dynamin for proper function, the majority of the NCE mechanisms of endocytosis identified function independently of dynamin activity (Doherty and McMahon, 2009b) (Figure 1.5). Many of the NCE mechanisms of endocytosis rely on actin dynamics and the presence of plasma membrane cholesterol for proper function (Doherty and McMahon, 2009b) (Figure 1.5).

Of the mechanisms of endocytosis mentioned, CME, caveolar endocytosis and macropinocytosis have been implicated in the endocytosis of RTKs whereas lipid clustering and CLIC/GEEC endocytosis are implicated in the internalization of cytokine receptors and G-protein coupled receptors, respectively (Doherty and McMahon, 2009b).These distinct mechanisms of endocytosis are thought to converge at the early endosome where cargo is either sorted for recycling back to the plasma membrane or trafficked to a degradative pathway (Le

Roy and Wrana, 2005; Mayor and Pagano, 2007) (Figure 1.5).

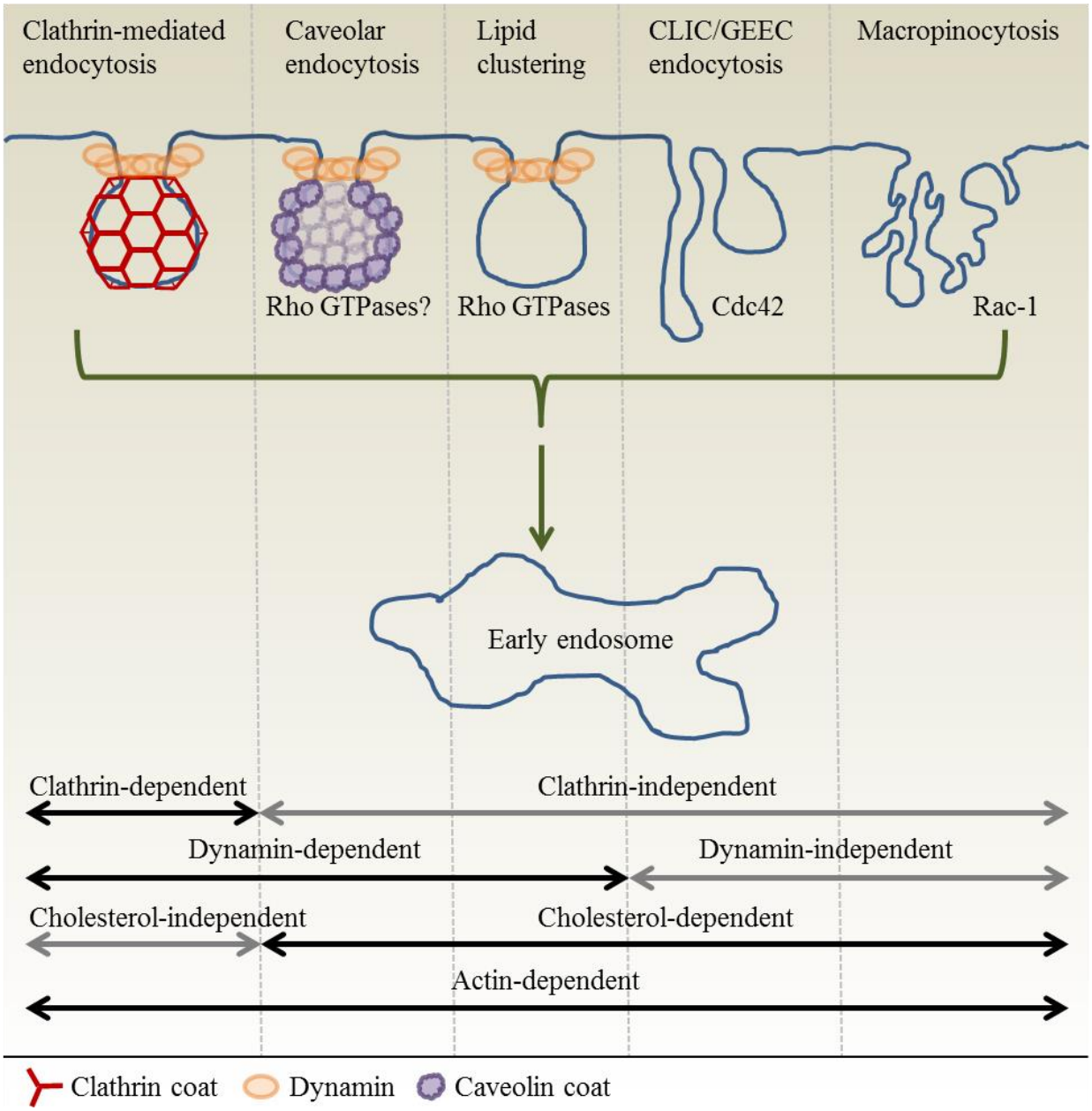

Figure 1.5: Mechanisms of receptor internalization
A diagram of different pathways of receptor internalization is shown, as well as the dependencies of these pathways on the presence of the clathrin coat protein, the GTPase dynamin, plasma membrane cholesterol and the actin cytoskeleton for proper function. Each pathway is delineated by dashed grey lines. Solid black arrows indicate dependency while solid grey arrows indicate independence. CME, caveolar endocytosis and macropinocytosis are known to internalize receptor tyrosine kinases whereas lipid clustering and CLIC/GEEC endocytosis are implicated in the internalization of cytokine receptors and G-protein coupled receptors, respectively. The different pathways of internalization are thought to converge at the early endosome.

1.2.1 Mechanisms of receptor internalization

1.2.1.1 Clathrin-mediated receptor internalization

1.2.1.1.1 Formation of clathrin coated vesicles

CME involves concentration of diverse cargo molecules into clathrin bound plasma membrane invaginations, termed clathrin-coated pits (CCPs). The clathrin lattice is composed repeating clathrin triskelions (Kirchhausen, 2000). Each triskelion is a trimer of dimers formed from clathrin heavy (190 kDa) and light chain (25 kDa) subunits (Kirchhausen, 2000). Formation of CCPs progresses in stages. First clathrin and other protein factors assemble on the cytosolic leaflet of the plasma membrane. Secondly the CCP matures, where coat proteins and membrane components generate and retain curvature to form the budding vesicle (Kirchhausen, 2000). Lastly, scission releases the clathrin coated vesicle from the plasma membrane into the cytosol (Pucadyil and Schmid, 2009) (Figure 1.6).

In the assembly stage various adaptor proteins are recruited to the plasma membrane through interactions with $PI4,5P_2$, as well as by binding specific transmembrane cargo for incorporation into CCPs (Ungewickell and Hinrichsen, 2007) (Figure 1.6). The adaptor proteins then interact with clathrin, either directly or through accessory proteins, thereby linking clathrin to the designated cargo (Figure 1.6). The large number of potential adaptor proteins is thought to provide flexibility and diversity to the clathrin machinery, allowing for internalization of many different types of cargo and facilitating the specific needs of multiple cell types (Doherty and McMahon, 2009a). Several amino acid sequences have been identified in transmembrane cargo molecules that serve as internalization signals (Ungewickell and Hinrichsen, 2007). The PDGFR contains a 14 amino acid internalization sequence between residues 952-965 which is required for endocytosis (Mori *et al*., 1991). Of the numerous clathrin adaptor proteins identified adaptor protein-2 (AP-2), autosomal recessive hypercholesterolemia protein (ARH), β-arrestin, disabled-2 (Dab2), epidermal growth factor receptor substrate 15 (Eps15), EPS-15-interacting protein 1 (epsin), numb, adaptor protein 180/clathrin-assembly lymphoid myeloid leukaemia protein (AP180/CALM) and Huntingtin-interacting protein 1 related protein (HIP1/R) are among the best characterized. Each of these adaptor proteins is able to bind clathrin directly except Eps15 (Ungewickell and Hinrichsen, 2007). AP-2 is thought to be particularly important as it forms an

interaction network with all endocytic proteins either by direct binding or binding through accessory proteins (Kirchhausen, 2000; Schmid *et al*., 2006). This AP-2 mediated interaction network reduces mobility of its components forming a gel-like micro-domain which facilitates clathrin assembly (Ungewickell and Hinrichsen, 2007). AP180/CALM simultaneously binds clathrin and $PI4,5P_2$, thereby linking clathrin to the plasma membrane (Ford *et al*., 2001).

To mature into a CCP, the clathrin lattice and underlying plasma membrane must generate and retain inward curvature. Polymerization of the clathrin lattice is energetically insufficient to generate membrane curvature (Nossal, 2001). Recruitment of proteins that penetrate the cytoplasmic leaflet of the plasma membrane is required to generate membrane curvature (Ungewickell and Hinrichsen, 2007). Proteins containing Bin–Amphiphysin–Rvs (BAR), epsin N-terminal homology (ENTH) and F-BAR domains are recruited to the plasma membrane via interaction with $PI4,5P_2$, as well as interaction with AP-2 (Kirchhausen, 2000; Ungewickell and Hinrichsen, 2007). Insertion of amphipathic helices within these domains into the plasma membrane causes deformation and generates curvature (Farsad and De Camilli, 2003) (Daumke et al., 2014). The clathrin lattice is flexible and acts as a molecular ratchet by adjusting to changes in inward membrane curvature and preserving it (Ungewickell and Hinrichsen, 2007).

Several methodologies exist to inhibit formation of the clathrin lattice and prevent clathrin-mediated internalization. Overexpression of the clathrin binding domain of AP180 is sufficient to inhibit CME by impairing the ability of the clathrin lattice to interact with the plasma membrane (Ford *et al*., 2001). Knockdown of the heavy chain of clathrin via RNA interference ablated endocytosis of EGFR and low density lipoprotein receptor (LDLR) (Motley *et al*., 2003) and inhibited transferrin uptake (Hinrichsen *et al*., 2003). Recently, small molecule inhibitors named pitstops have been developed and have been demonstrated to reversibly inhibit clathrin mediated uptake of EGF and transferrin, as well as block HIV virus entry (von Kleist *et al*., 2011). Pitstop inhibitors competitively bind the region of clathrin responsible for binding adaptor proteins and thereby prevent recruitment of clathrin to its adaptors (von Kleist *et al*., 2011).

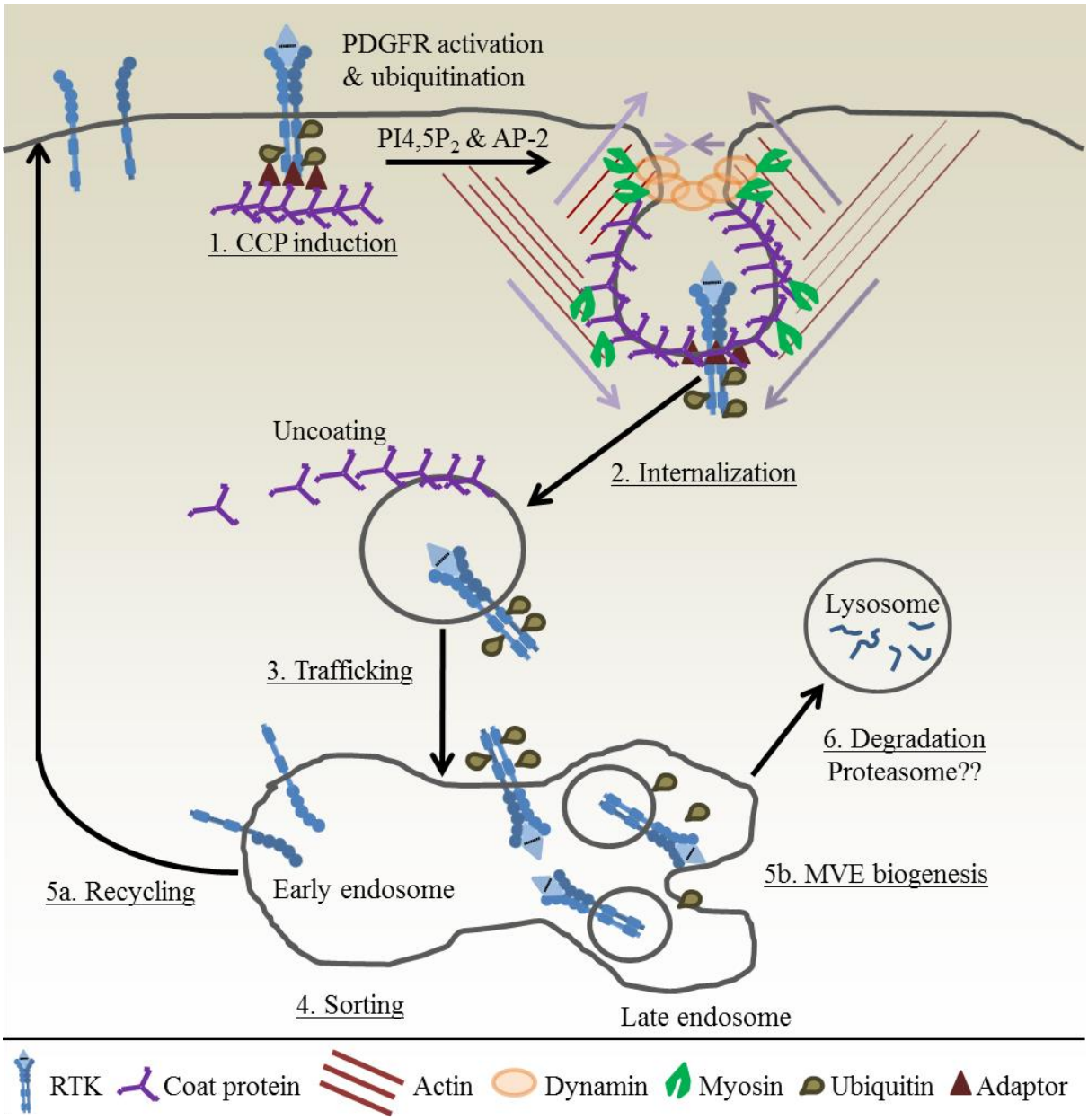

Figure 1.6: Internalization, endosomal sorting and degradation of receptor tyrosine kinases
A diagram depicting the cellular fates of ligand stimulated receptor tyrosine kinases. 1. Clathrin-coated pit (CCP) induction. Binding of ligand activates receptors prompting dimerization and trans-autophosphorylation of several cytoplasmic tyrosine residues, which creates binding sites for various endocytic adaptor proteins. Receptors are clustered and concentrated on the plasma membrane due to binding of endocytic adaptor proteins. These adaptors recruit clathrin and form a bridge between the receptor cargo and the clathrin lattice. The clathrin lattice and underlying membrane obtain curvature, generating a CCP. 2. Internalization. Scission of the clathrin-coated pit from the plasma membrane requires recruitment multiple proteins including dynamin, myosin and the actin cytoskeleton. Concerted action between dynamin and the actin cytoskeleton facilitates scission from the plasma membrane. Polymerization of dynamin constricts and tubulates the vesicle neck. Myosin motor protein associates with both dynamin and the clathrin lattice, generating force along the actin cytoskeleton and directing the vesicle toward the cell

interior. Directional lines of force are shown as light purple arrows. 3. Trafficking. The internalized vesicle is uncoated and its cargo may be ubiquitinated by E3 ubiquitin ligases. The vesicle is transported to the early endosome via the actin and microtubule cytoskeleton network. Fusion between the vesicle and the early endosome is regulated by Rab5. 4. Sorting. The majority of receptors are deactivated and recycled, whereas some receptors are targeted for degradation. 5a. Recycling. Ligand dissociates from the receptor and the receptor is dephosphorylated. The receptor is trafficked back to the plasma membrane in a Rab4-dependent manner where it can undergo additional rounds of activation and internalization. 5b. MVE biogenesis. Monoubiquitination of receptors delineate incorporation into multivesicular endosomes (MVE). Ubiquitinated receptors are recognized and concentrated on the late endosomal membrane by the ESCRT machinery. The endosomal membrane obtains inverse curvature and buds off into the lumen of the endosome via the concerted actions of Vps32 and Vps4. Cargo is de-ubiquitinated prior to inclusion in MVEs. 6. Degradation. Late endosomes containing MVEs are trafficked to the lysosome via rab7. The late endosome undergoes heterotypic fusion with the lysosome, generating a hybrid organelle where MVEs and their cargo are degraded. Inhibition of proteasomal activity impairs receptor degradation indicating a potential role of the proteasome in receptor degradation.

1.2.1.1.2 Dynamin-mediated vesicle scission

Completion of internalization requires fission of the budding vesicle from the plasma membrane (Figure 1.6). The large GTPase dynamin, 100 kDa, is recruited to budding vesicles after recruitment of AP-2 and clathrin (Ungewickell and Hinrichsen, 2007). Recruitment of dynamin to CCPs is dependent upon its activation state. Binding of GTP is required for the association of dynamin with the neck of the invaginating CCP (Chappie *et al*., 2009). Dynamin contains a C-terminal proline rich domain to interact with endocytic accessory proteins possessing SH3 domains and this interaction facilitates dynamin recruitment to invaginating CCPs (Shpetner *et al*., 1996). Dynamin contains a pleckstrin homology (PH) domain to facilitate interaction with the plasma membrane. Several amino acids of the PH domain protrude into the cytoplasmic leaflet that causes deformation of the budding vesicle neck (Ramachandran and Schmid, 2008). Assembly of dynamin on the vesicle neck stimulates its intrinsic GTPase activity and GTP hydrolysis results in disassembly from the budding vesicle neck (Chappie *et al*., 2009; Sever *et al*., 1999). Multiple rounds of GTP-mediated assembly and disassembly create a cycle of constriction and relaxation of the vesicle neck, promoting scission from the plasma membrane (Pucadyil and Schmid, 2009). Dynamin activity is inhibited by the expression of temperature sensitive mutants, the dominant negative mutant K44A and small molecule inhibitors such as dynasore (Macia *et al*., 2006a; Nankoe and Sever, 2006). Dynasore noncompetitively interferes with GTP hydrolysis without affecting the affinity of dynamin for GTP and treatment of cells

with dynasore is sufficient to prevent transferrin uptake, LDL uptake and EGFR endocytosis in response to ligand stimulation (Macia *et al*., 2006a).

F-actin dynamics are implicated in several steps in CCP formation including lateral movement of clathrin-coated patches, membrane curvature and vesicle scission (Ungewickell and Hinrichsen, 2007) (Mooren et al., 2012) (Figure 1.6). Actin and other components of the actin cytoskeleton are associated with the budding CCP at the same time as dynamin (Ungewickell and Hinrichsen, 2007) (Mooren et al., 2012). The clathrin lattice is connected to the actin cytoskeleton via the endocytic adaptor protein HIP1/R (Le Clainche *et al*., 2007). In mouse fibroblasts treatment with either the actin polymerization inhibitor latrunculin A or the actin depolymerization inhibitor jasplakinolide blocked CME and resulted in the accumulation of CCPs still attached to the plasma membrane, indicating actin dynamics primarily affect vesicle scission (Yarar *et al*., 2005). Actin motor proteins myosin VI and myosin IE may provide the force required for vesicle scission (Ungewickell and Hinrichsen, 2007) (Mooren et al., 2012). Myosin VI binds the endocytic adaptor protein Dab2 and $PI4,5P_2$, thereby linking itself to the CCP and the plasma membrane and generating force directing the vesicle inwards towards the cytoplasm (Spudich *et al*., 2007). Myosin IE binds dynamin via its SH3 domain and directs the dynamin ring towards the plasma membrane (Krendel *et al*., 2007). The pull of myosin VI on the vesicle toward the cytoplasm and the pull of myosin IE on the dynamin ring toward the plasma membrane in concert with the constriction and relaxation cycles of dynamin is thought to promote vesicle scission beneath the dynamin ring (Pucadyil and Schmid, 2009; Ungewickell and Hinrichsen, 2007) (Figure 1.6). Upon scission of the budding CCP, the clathrin coat is disassembled and the vesicle is trafficked to the endosomal system where its constituents are sorted (Figure 1.6).

1.2.1.2 Caveolar endocytosis

Caveolae are flask shaped plasma membrane invaginations that often from a network in conjunction with lipid rafts and occupy up to 40% of the plasma membrane in mammalian cells (Hommelgaard *et al*., 2005). Caveolae are enriched in caveolin-1 (22 kDa), which contribute to the spiked-like coat of caveolae (Doherty and McMahon, 2009b). Caveolin-1 forms highly ordered oligomers (Doherty and McMahon, 2009b) consisting of 14-16 caveolin-1 monomers (Sargiacomo *et al*., 1995). The ability of caveolin-1 to bind fatty acids and cholesterol is thought

to stabilize oligomerization (Monier *et al*., 1996). Oligomerization of caveolin-1 may induce membrane curvature (Parton *et al*., 2006). Extraction of plasma membrane cholesterol via methyl-β-cyclodextrin treatment flattens caveolae and attenuates caveolar endocytosis (Rothberg *et al*., 1992). Caveolin-1 binds the fatty acids portion of glycosphingolipid GM1 promoting association of caveolae with plasma membrane and detergent resistant lipid rafts (Hommelgaard *et al*., 2005). The role of caveolae in endocytosis is controversial. Study of the dynamics of caveolae reveals them to be highly immobile structures at the plasma membrane, demonstrating little turnover (Thomsen *et al*., 2002). Caveolae are rigidly linked to the actin cytoskeleton contributing to their observed immobility (Stahlhut and van Deurs, 2000). It is expected that mobility and a high turnover rate would be required for an endocytic pathway to efficiently process and internalize cargo (Hommelgaard *et al*., 2005).

Two proposed mechanisms for caveolae internalization have emerged. In one mechanism a small proportion of caveolae that are not sufficiently stabilized are infrequently internalized, resulting in removal of a vesicle from the immobilized caveolar network (Hommelgaard *et al*., 2005). In the second mechanism scission from the caveolar network occurs in coordination with Rho family GTPase-mediated remodeling of the actin cytoskeleton (Navarro *et al*., 2004). Additional studies on the dynamics of caveolae in live cells are required to further characterize caveolae-mediated internalization (Hommelgaard *et al*., 2005). Dynamin is implicated in the scission of caveolar vesicles (Mukherjee *et al*., 2006). Dynamin binds the budding neck of caveolae, colocalized with caveolin-1 and is required for the scission of caveolar vesicles (Henley *et al*., 1998; Oh *et al*., 1998). Inhibition of dynamin activity blocks caveolar-mediated uptake of cholera toxin subunit B (Henley *et al*., 1998; Oh *et al*., 1998). After scission the vesicle is transported to the early endosome and its cargo is sorted through the endosomal system.

The traditional cargos for caveolar endocytosis are cholera toxin subunit B and SV40 virus (Doherty and McMahon, 2009b). Other types of cargo including prion proteins (Peters *et al*., 2003) and several receptor tyrosine kinases have also been suggested to utilize this route of endocytosis (Mukherjee *et al*., 2006). Despite being canonically internalized by the clathrin machinery, RTKs including EGFR, PDGFR, vascular endothelia growth factor receptor 2 (VEGFR-2) and transforming growth factor receptor β (TβRI/II) have been demonstrated to be internalized via caveolar endocytosis (Mukherjee *et al*., 2006). Caveolar endocytosis of TβRI/II may occur concurrently with CME (Di Guglielmo *et al*., 2003). VEGFR-2 endocytosis proceeds

preferentially via caveolae rather than by the clathrin machinery (Labrecque *et al*., 2003). In the case of PDGFR and EGFR high concentrations of ligand are thought to promote caveolar endocytosis (De Donatis *et al*., 2008; Sigismund *et al*., 2005). One study demonstrated that low concentrations of EGF resulted in predominantly CME of EGFR whereas high ligand concentrations promoted receptor internalization by a lipid raft dependent mechanism (Sigismund *et al*., 2005). Co-localization between EGFR and caveolae was increased 10 fold in the presence of high concentrations of ligand as compared to low concentrations (Sigismund *et al*., 2005). High concentration of ligand also promoted ubiquitination and increased degradation of the EGFR (Sigismund *et al*., 2005). Ubiquitination of the EGFR and expression of ubiquitin adaptor proteins Eps15 and epsin were required for internalization (Sigismund *et al*., 2005). This observation of internalization of EGFR via caveolar endocytosis in the presence of high concentrations of ligand is controversial. Studies by another group show inhibition of caveolar endocytosis does not greatly effect EGFR internalization in the presence of low or high concentrations of ligand whereas knockdown of clathrin heavy chain does (Kazazic *et al*., 2006). Moreover high concentrations of EGF do not promote co-localization of EGFR with caveolae and caveolae remained static structures in the presence of high concentrations of EGF (Kazazic *et al*., 2006). Akin to observations with EGFR, high concentrations of PDGF promote internalization of PDGFR via caveolar endocytosis (De Donatis *et al*., 2008). This modulation of PDGFR endocytosis also differentiated PDGFR signaling output. Internalization of PDGFR via caveolar endocytosis resulted in attenuation of cell migration and promotion of mitogenic signaling in response to high concentrations of PDGF (De Donatis *et al*., 2008).

1.2.1.3 Internalization by macropinocytosis and membrane ruffling

Macropinocytosis is a distinct mechanism of endocytosis involving internalization of large portions of plasma membrane, macromolecules and extracellular fluid (Lim and Gleeson, 2011). Macropinocytosis is induced by stimulation with a number of growth factors. Treatment of cells with either PDGF or EGF promotes extensive actin polymerization at the cell surface and formation of protrusions termed membrane ruffles (Jones, 2007). Indeed, even short term stimulation produced extensive ruffling visible across the entire cell (Jones, 2007). Occasionally these membrane protrusions fold back upon the plasma membrane or upon other membrane ruffles generating vesicles called macropinosomes that allows for internalization of large

volumes of extracellular fluid and plasma membrane lipids (Swanson, 2008).

Rho family GTPases (Rac-1, Cdc42 and Rho) regulate actin polymerization and membrane ruffling (Kerr and Teasdale, 2009). Inhibition of the activity of these GTPases by small molecule inhibitors (West *et al*., 2000) or dominant negative mutation (Nobes and Marsh, 2000; Schafer *et al*., 2000) attenuates internalization by macropinocytosis. Interestingly, inhibition of Rho family GTPases does not prevent membrane ruffling, yet blocks internalization, suggesting macropinocytosis is regulated at several steps (West *et al*., 2000). Treatment of cells with the ion exchanger protein inhibitor amiloride, or its derivatives, disrupts membrane ruffling and is sufficient to inhibit macropinocytosis without affecting other mechanisms of endocytosis (Kerr and Teasdale, 2009; West *et al*., 1989). Membrane ruffles are enriched in lipid rafts which are known to contain receptor tyrosine kinases and several species of phosphoinositides (Le Roy and Wrana, 2005; Manes *et al*., 2003). Depletion of membrane cholesterol or inhibition of PI3K signaling both inhibit macropinocytosis (Grimmer *et al*., 2002).

Internalization by macropinocytosis results in the formation of large, irregular sized vesicles called macropinosomes (Lim and Gleeson, 2011). In contrast to clathrin-coated vesicles, macropinosomes are not encapsulated by a coat protein and their internalization is independent of dynamin activity (Kerr and Teasdale, 2009). Macropinosomes can be delineated from other endocytic structures via uptake of fluid phase markers including labeled dextran, horseradish peroxidase and Lucifer yellow (Lim and Gleeson, 2011). The fate of macropinosomes in the endocytic system may be cell type and/or context dependent. Macropinosomes reduce in size and acquire endocytic markers as they mature (Lim and Gleeson, 2011). In macrophages or in HEK293 cells stimulated with EGF, cargo in macropinosomes are targeted to the lysosomes (Kerr *et al*., 2006; Lim and Gleeson, 2011). At early time points of stimulation macropinosomes acquire staining of transferrin receptor which is indicative of the early endosomal system (Kerr *et al*., 2006). Transferrin receptor staining is subsequently lost, as the transferrin receptor is recycled, and Rab7 and lysosomal glycoprotein A staining is acquired, indicating trafficking to the late endosome and lysosome, respectively (Kerr *et al*., 2006; Racoosin and Swanson, 1993). In A431 cells, macropinosome cargo are not trafficked to the lysosome. Macropinosomes acquire transferrin and early endosomal antigen 1 (EEA1) staining and are eventually recycled back to the plasma membrane (Araki *et al*., 2006; Hamasaki *et al*., 2004).

While CME remains the predominant mechanism of internalization of RTKs, there are

several examples of situations promoting RTK internalization by macropinocytosis. Transformation of fibroblast cells via expression of oncogenic H-Ras (H-RasG12V) increases cellular PI3K signaling levels, possibly via interaction with the p110 subunit of PI3K (Schmees *et al*., 2012). Excessive PI3K signaling induces macropinocytic internalization of PDGFRβ as evident by PI3K dependent co-localization of PDGFRβ with fluorescently labeled dextran only in cells expressing H-RasG12V (Schmees *et al*., 2012). Indeed inhibition of PI3K activity abrogated PDGFRβ-dextran co-localization (Schmees *et al*., 2012). Internalization of PDGFRβ resulted in hyper-activation of the receptor and increased anchorage-independent proliferation of H-RasG12V transformed cells; anchorage-independent cell proliferation was sensitive to PDGFR inhibitors (Schmees *et al*., 2012). Expression of H-RasG12V in fibroblasts did not result in co-localization between EGFR and dextran; however, in non-transformed fibroblasts co-stimulation of both EGFR and PDGFR resulted in macropinocytic uptake of both receptors as evident by EGFR-dextran and PDGFR-dextran co-localization (Schmees *et al*., 2012). Stimulation of either receptor individually did not result in dextran co-localization (Schmees *et al*., 2012). Indeed co-stimulation of EGFR and PDGFR resulted in hyper-activation of each receptor and Akt (Schmees *et al*., 2012). Thus induction of macropinocytosis may be physiologically relevant as cells are likely to encounter co-stimulatory situations *in vivo*. Macropinocytic uptake of EGFR was also observed in cells with hyper-activated Rab5 (Balaji *et al*., 2012). Overexpression of Rin1, a Rab5 GTP exchange factor (GEF), was sufficient to induce macropinocytic uptake of EGFR and increased EGFR degradation (Balaji *et al*., 2012).

1.2.2 Endocytic trafficking and receptor degradation

1.2.2.1 Role of Rab proteins in endosomal trafficking

Internalized vesicles and their cargo are sorted through the endosomal network by the action of Rab proteins. Rab proteins are the gatekeepers of membrane trafficking and provide specificity to the tethering events required for vesicle-endosome fusion (Stenmark, 2009; Zerial and McBride, 2001). Rab proteins are regulated by their GTP binding state (Mellor *et al*., 2012). GEFs facilitate exchange of GDP for GTP, thereby activating the Rab protein (Mellor *et al*., 2012). Interaction with GTPase activating proteins (GAP) stimulates the intrinsic GTPase activity of Rab proteins, accelerating hydrolysis of GTP and deactivating the Rab protein

(Stenmark, 2009; Zerial and McBride, 2001). Internalized receptors are targeted to the early endosome by Rab5 (Mellor *et al*., 2012). Activated Rab proteins recruit tethering proteins that link the internalized vesicle to the early endosome and providing specificity to the soluble NSF attachment proteins (SNARE) proteins that mediated fusion of two endosomes (Zerial and McBride, 2001). Modulation of Rab5 and Rab4 GAP activity alters PDGFR activation and endocytosis, impairs receptor degradation and promotes cellular transformation (Chamberlain *et al*., 2004; Chamberlain *et al*., 2008; Chamberlain *et al*., 2010; Mellor *et al*., 2012). From the early endosome, internalized receptors can either be recycled back to the plasma membrane via Rab4 and are available for successive rounds of activation and signaling, or are incorporated into multivesicular endosomes and sorted for degradation in the lysosome via Rab7 (Zerial and McBride, 2001) (Figure 1.6). Rab proteins thus control receptor fate and signaling output through regulation of receptor trafficking to different compartments for recycling or degradation (Mellor *et al*., 2012).

1.2.2.2 Receptor ubiquitination and sorting into multivesicular endosomes

Incorporation of endosomal cargo including RTKs in multivesicular endosomes (MVEs) for lysosomal degradation requires ubiquitination of target cargo (Hicke, 2001) (Figure 1.6). Ubiquitin is a 76 amino protein which is post-translationally conjugated to target proteins. E3 ubiquitin ligases mediate isopeptide bond formation between the carboxyl group of the C-terminal glycine of ubiquitin and the ε-amino group of lysine residues in target proteins (Lu and Hunter, 2009). Additional ubiquitin molecules can be linked sequentially to several lysine residues (lysine 6, 11, 27, 29, 33, 48 and 63) of the ubiquitin conjugated to target of interest (Tanno and Komada, 2013). As such, ubiquitin chains with different linkages can be generated (Tanno and Komada, 2013).

Ligand binding of both EGFR and PDGFR induces autophosphorylation on cytoplasmic tyrosine residues creating docking sites for the E3 ubiquitin ligase Cbl promoting receptor ubiquitination (Mosesson *et al*., 2003) (Figure 1.6). Ubiquitination of receptors is not necessary for their internalization (Huang *et al*., 2007) but is required for sorting and incorporation into multivesicular endosomes (Hicke, 2001). Ubiquitinated cargo is recognized by several members of the endocytic machinery via a plethora of ubiquitin binding domains (Dikic *et al*., 2009). Ubiquitination serves as a molecular signal for several cellular responses including protein

degradation. Polyubiquitination delineates target proteins for degradation by the 26S proteasome (Ravid and Hochstrasser, 2008). In polyubiquitination, ubiquitin chains are formed where each successive ubiquitin molecule is linked via isopeptide bond to lysine residue 48 of the previous ubiquitin molecule (Lu and Hunter, 2009). Monoubiquitination and multiubiquitination, which is monoubiquitination at several lysine residues, targets activated receptor complexes for incorporation into MVEs and finally lysosomal degradation (Hicke, 2001). Polyubiquitination with lysine 63-linked chains are thought to be involved in a number of cell processes including endocytosis. Lysine 63 linked chains promote endosomal sorting and lysosomal degradation of target proteins and is thought to provide a more efficient signal than monoubiquitination (Tanno and Komada, 2013). Indeed, quantitative mass spectrometry analysis of ligand-activated EGFR demonstrated that over 50% of ubiquitin molecules conjugated to EGFR were in lysine 63 linkages (Huang et al., 2006). Monoubiquitinated and lysine 63 polyubiquitinated cargo is thought to be sorted similarly by the endocytic machinery; however lysine 63 polyubiquitin chains are recognized with a higher affinity by ubiquitin binding proteins, thereby increasing the efficiency of the ubiquitin signal (Tanno and Komada, 2013).

The endosomal sorting complex required for transport (ESCRT) machinery concentrates and packages ubiquitinated cargo into endosomal membrane invaginations (Raiborg and Stenmark, 2009). MVEs result from abscission of the budding vesicles into the lumen of the late endosome (Raiborg and Stenmark, 2009). The ESCRT machinery consists of four distinct multi-protein complexes, functioning sequentially to facilitate MVE biogenesis. ESCRT-0, composed of HRS and STAM, concentrate endosomal ubiquitinated cargo via interaction with multiple ubiquitin interaction motifs (UIM) of HRS (Raiborg and Stenmark, 2009). ESCRT-0 localizes to endosomal membranes through binding phosphatidylinositol-3 phosphate via the FYVE domain of HRS (Hanson *et al*., 2009; Raiborg and Stenmark, 2009). ESCRT-I is recruited by interaction with the PSAP motif of HRS (Raiborg and Stenmark, 2009). ESCRT-I is composed of four proteins, Tsg101 being the best characterized (Saksena *et al*., 2007). Tsg101 interacts with ubiquitinated cargo via an UEV domain and knockdown of tsg101 is sufficient to impair EGFR degradation (Saksena *et al*., 2007). ESCRT-I recruits ESCRT-II via its C-terminus (Raiborg and Stenmark, 2009). ESCRT-II is capable of binding ubiquitinated cargo, through interactions with a GLUE domain. A sequential ubiquitin hand-off model has been proposed for the different ESCRT complexes, but remains untested (Raiborg and Stenmark, 2009). ESCRTs 0-II function to

concentrate ubiquitinated cargo and recruit ESCRT-III to the site of membrane invagination (Raiborg and Stenmark, 2009). ESCRT-III, which does not bind ubiquitin, generates membrane curvature forming intraluminal invaginations, and catalyzes membrane abscission forming MVEs (Hanson *et al*., 2009; Raiborg and Stenmark, 2009). Cargo is deubiquitinated prior to inclusion in MVEs. ESCRT-III consists of numerous proteins (Raiborg and Stenmark, 2009; Saksena *et al*., 2009). Multiple molecules of highly charged Vps32 protein assemble into circular arrays on endosomal membranes and recruit the ATPase Vps4 (Raiborg and Stenmark, 2009; Saksena *et al*., 2009). Polymerization of Vps32 molecules are thought to drive constriction of the intra-luminal vesicle followed by abscission into the lumen of the endosome (Raiborg and Stenmark, 2009; Saksena *et al*., 2009). Vps4 catalyzes the de-polymerization of Vps32 and its subsequent recycling back to the cytosol (Raiborg and Stenmark, 2009; Saksena *et al*., 2009). Vesicles containing MVE, known as late endosomes, are delivered to the lysosome for degradation by a Rab7-dependent trafficking step (Raiborg and Stenmark, 2009; Zerial and McBride, 2001) (Figure 1.6).

1.2.2.3 Mechanisms of protein degradation

1.2.2.3.1 Lysosomal degradation

Lysosomes are dense membrane bound organelles and are the classical site of degradation of membrane proteins, extracellular proteins and macromolecules (Luzio *et al*., 2007). Indeed binding of ligand to PDGFR, EGFR and LDLR induces the internalization, endosomal trafficking, ubiquitin dependent sorting into MVEs and subsequent lysosomal degradation of a portion of activated receptors (Heldin and Westermark, 1999; Luzio *et al*., 2007). In the case of LDL-LDLR, the receptor and ligand dissociate and the receptor is recycled back to the plasma membrane while the ligand is degraded (Luzio *et al*., 2007).

Lysosomes contain several proteases and lipases whose activity is dependent upon low pH to facilitate protein and macromolecule degradation (Luzio *et al*., 2007). Indeed lysosomes contain ATP-dependent proton pumps to maintain a pH of 4.6-5.0 (Luzio *et al*., 2007). Treatment of cells with weak bases such as chloroquine raises the pH of the lysosome, thereby inhibiting degradation (Luzio *et al*., 2007). Lysosomes can be distinguished from other organelles of the endosomal system by the lack of mannose-6-phosphate receptor staining (Luzio *et al*., 2007) and

can be detected by the presence of lysosomal-associated membrane protein 1 (LAMP-1) (Eskelinen *et al*., 2003).

Late endosome are trafficked to the lysosome along the microtubule cytoskeleton (Piper and Luzio, 2007). An intact microtubule cytoskeleton is required for efficient trafficking of cargo to the lysosome (Piper and Luzio, 2007). Activated Rab7 on late endosomal and lysosomal membranes initiates tethering and fusion events (Zerial and McBride, 2001). Transfer of cargo to the lysosome can occur either by complete heterotypic fusion of the late endosome and the lysosome or by kiss and run exchange of cargo and lipids (Bright *et al*., 2005). The two mechanisms are not mutually exclusive and kiss and run exchange often precedes heterotypic fusion (Bright *et al*., 2005). The resulting organelle is a hybrid between the lysosome and the late endosome and is the site of degradation of endosomal cargo (Luzio *et al*., 2007; Mullock *et al*., 1998) (Figure 1.6). The lysosome is subsequently regenerated via a maturation process where the hybrid organelle losses endosomal markers and re-establishes the correct pH via the action of proton pumps (Bright *et al*., 2005; Luzio *et al*., 2007; Pryor *et al*., 2000).

1.2.2.3.2 Proteasomal degradation

Degradation of the vast majority of intracellular proteins is regulated by the ubiquitin-proteasome system. Target proteins must be recognized by the 26S proteasome, unfolded, translocated through the proteasome and degraded (Ravid and Hochstrasser, 2008). Polyubiquitination by E3 ubiquitin ligases marks target proteins for degradation by the 26S proteasome where they are proteolytically processed into oligopeptides. Ubiquitin is covalently conjugated to the ε-amino group of lysine residues on the target protein (Ravid and Hochstrasser, 2008). Successive ubiquitin molecules are added to lysine 48 of the previous ubiquitin molecule, thus extending the chain. A minimum chain length of 4 ubiquitin molecules is required to target a protein for proteasomal degradation (Sorokin *et al*., 2009).

The 26S proteasome is composed of two main subunits, the 20S proteasomal core particle and the 19S regulatory particle (Ravid and Hochstrasser, 2008). The 20S proteasomal core particle is composed of 4 heptameric rings consisting of α and β subunits that form a cylindrical barrel like structure (Coux *et al*., 1996). Eukaryotes have seven different isoforms of each α and β subunit (Sorokin *et al*., 2009). The β subunits each contain a catalytic threonine residue, conferring proteolytic activities similar to caspase, trypsin and chymotrypsin (Ravid and

Hochstrasser, 2008). Treatment of cells with the small molecule inhibitor MG132 disrupts the activity of the chymotrypsin-like catalytic site, and at higher concentrations, the activity of the caspase-like catalytic site (Goldberg, 2012). The 19S regulatory particle mediates recognition of polyubiquitinated substrates, unfolding of polypeptides and translocation into the 20S proteasomal core particle (Ravid and Hochstrasser, 2008). Prior to degradation, substrates are deubiquitinated to replenish the ubiquitin pool and facilitate the targeting and degradation of additional proteins (Ravid and Hochstrasser, 2008).

Although trafficking to the lysosome is the primary and accepted mechanism of RTK degradation in response to ligand stimulation, several lines of evidence point to a potential role of the 26S proteasome. Treatment of cells with small molecule inhibitors of either lysosomal degradation or proteasomal degradation blocks EGFR degradation in response to ligand (Ettenberg *et al*., 2001; Levkowitz *et al*., 1998; Lipkowitz, 2003). Several reports indicate that ligand induced degradation of the PDGFR is also proteasome dependent (Mori *et al*., 1992, 1993; Mori *et al*., 1995b; Mori *et al*., 1995c) and that the PDGFR is polyubiquitinated in response to stimulation (Mori *et al*., 1995a; Mori *et al*., 1992). Additionally, the degradation of other RTKs including the growth hormone receptor may proceed via the proteasome (Strous *et al*., 1996; van Kerkhof *et al*., 2000).

Several hypotheses have been proposed to account for the sensitivity of RTK degradation to proteasomal inhibitors. Inhibition of proteasomal degradation would result in accumulation of polyubiquitinated intracellular proteins and deplete the cellular pool of free ubiquitin required for lysosomal trafficking of RTKs (Swaminathan *et al*., 1999). Indeed depletion of free ubiquitin in yeast is sufficient to inhibit both proteasomal and lysosomal degradation (Swaminathan *et al*., 1999). The EGFR however, is still ubiquitinated in response to growth factor stimulation in cells treated with proteasomal inhibitors (Longva *et al*., 2002). Several lines of evidence suggest that RTKs are not direct targets of proteasomal degradation and that proteasomal mechanisms are required for lysosomal degradation. Inhibition of proteasomal activity blocks EGFR internalization (Kesarwala *et al*., 2009) and trafficking through the endosomal system (Melikova *et al*., 2006), by preventing sorting of EGFR into multivesicular endosomes (Longva *et al*., 2002). Others suggest a direct role of the proteasome where the RTK itself is degraded (Heldin and Westermark, 1999; Mori *et al*., 1992, 1993; Mori *et al*., 1995b; Mori *et al*., 1995c).

1.2.3 Ligand-independent receptor degradation

Although ligand-dependent endocytosis and lysosomal degradation is the canonical mechanism of receptor degradation, several examples of ligand-independent receptor endocytosis and degradation have been discovered. The mechanisms governing constitutive degradation are largely unknown, however; several themes are emerging, involving the modulation of endocytosis and sorting, ubiquitination and proteasomal and lysosomal degradation. Classic examples of receptors that undergo constitutive endocytosis are the transferrin receptor (TfR) and the LDLR, which are internalized in the absence of ligand and recycled back to the plasma membrane in a rab4 and rab 11-dependent manner via constitutive interaction with the clathrin adaptor AP-2 (Marmor and Yarden, 2004; Ullrich et al., 1996). The endocytosis machinery, in the case of TfR can be modulated to facilitate timely degradation of the TfR. Recent studies have demonstrated that rab12 mediated trafficking of TfR positive recycling endosomes to the lysosome for degradation in the absence of ligand (Matsui et al., 2011). Indeed, this mechanism of TfR degradation was independent of conventional receptor degradation as knockdown of rab12 or its effector proteins did not affect EGFR degradation (Matsui et al., 2011).

PDGFRβ has been demonstrated to undergo constitutive degradation, independent of PDGFR phosphorylation and kinase activity, following cell detachment (Baron and Schwartz, 2000). Detachment from the extracellular matrix reduced PDGFRβ expression levels (Baron and Schwartz, 2000). PDGFRβ expression levels recovered when cells were plated on fibronectin (Baron and Schwartz, 2000). Increased PDGFR ubiquitination was observed following cell detachment and PDGFRβ degradation was blocked by treatment with proteasomal degradation inhibitors (Baron and Schwartz, 2000).

The human growth hormone receptor (hGHR) is also targeted for ligand-independent, constitutive degradation and this degradation was blocked by the proteasomal degradation inhibitor MG132 (Mitchell et al., 2004). Indeed, the ratio of ubiquitinated hGHR to non-ubiquitinated hGHR in MG132 treated cells was low, so it is unlikely that direct ubiquitination of hGHR drives constitutive hGHR degradation (Mitchell et al., 2004).

TβRI/II undergo CME and rab4 and rab11-dependent endosomal recycling back to the plasma membrane both in the presence and absence of ligand (Mitchell et al., 2004). Indeed, the rate of internalization of TβRI/II was similar with or without ligand stimulation. TβRI/II

internalized in the absence of ligand is constitutively recycled, while TβRI/II internalized in the presence of ligand can be further sorted for degradation (Mitchell et al., 2004).

Constitutive degradation of EGFR was demonstrated to rely on interaction with HRS protein of ESCRT-0 (Katz et al., 2002). Indeed, EGFR was polyubiquitinated and colocalized with HRS positive endosomes and the UIM of HRS was shown to be capable of interacting with polyubiquitinated proteins (Katz et al., 2002). The UIM of HRS was shown to recruit the E3 ubiquitin ligase NEDD4, that resulted in the ubiquitination of HRS and this ubiquitination inhibited constitutive EGFR degradation (Katz et al., 2002). Indeed, blocking HRS ubiquitination promoted constitutive EGFR degradation (Katz et al., 2002). The related receptor ErbB3 is constitutively internalized in the absence of ligand in a clathrin dependent manner, independent of ErbB3 phosphorylation state (Sak et al., 2012).

Interestingly, benzoquinone ansamycins class drugs such as geldanamycin, herbimycin A and their derivatives induce ligand-independent proteasomal degradation of a number of trans-membrane proteins including EGFR and ErbB2 (Blagosklonny, 2002; Lipkowitz, 2003; Mimnaugh *et al*., 1996; Neckers, 2002; Sepp-Lorenzino *et al*., 1995; Tikhomirov and Carpenter, 2000). Proteasomal degradation induced by benzoquinone ansamycins is independent of the kinase activity of the receptor (Citri *et al*., 2002; Xu *et al*., 2001), whereas lysosomal degradation requires kinase activity to generate phospho-tyrosine residues on the receptor to facilitate Cbl E3 ubiquitin ligase binding, ubiquitination and subsequent trafficking through the endosomal system (Levkowitz *et al*., 1999). Benzoquinone ansamycins target chaperone proteins including Hsp90 and Grp94 which stabilize RTKs (Blagosklonny, 2002; Neckers, 2002), causing the chaperone to adopt an alternate conformation which is indicative of protein instability (Blagosklonny, 2002; Neckers, 2002). The proteins interacting with the chaperone are ubiquitinated and degraded by the proteasome (Blagosklonny, 2002; Lipkowitz, 2003; Mimnaugh *et al*., 1996; Neckers, 2002; Tikhomirov and Carpenter, 2000; Xu *et al*., 2001).

1.2.4 Summary of endocytosis

The signaling of activated RTKs is modulated by endocytosis and RTKs are internalized via several mechanisms. The classical and best-studied mechanism is internalization via clathrin coated pits. Numerous endocytic adaptor proteins, such as AP-2, interact with the plasma membrane and transmembrane cargo forming a scaffold for the assembly of the clathrin coat.

During maturation into a CCP, the clathrin lattice and underlying plasma membrane obtain inward curvature. Once mature, the vesicle absconds from the plasma membrane by the actions of dynamin and the actin cytoskeleton and the vesicle is trafficked to the early endosome in a Rab5 dependent manner (Figure 1.6). While CME is the predominant mechanism of internalization of RTKs, several examples of internalization by NCE mechanisms such as caveolar endocytosis and macropinocytosis have been discovered (Figure 1.5). Caveolar endocytosis involves internalization of cargo in vesicles coated with caveolin-1. Studies of mechanisms regulating vesicle formation and scission are limited; however, the activity of Rho family GTPases, dynamin-II and the actin cytoskeleton have been implicated in caveolar endocytosis (Figure 1.5). Macropinocytosis involves internalization of large portions of plasma membrane and extracellular fluid. Modulation of the actin cytoskeleton creates protrusions, or ruffles, of plasma membrane that fold back onto themselves, other ruffles or fold onto un-ruffled sections of the plasma membrane to generate internalized vesicles called macropinosomes. The formation of macropinosomes is independent of the activity of dynamin-II but requires the activity of Rho family GTPases, particularly Rac-1 (Figure 1.5). Both caveolar endocytosis and macropinocytosis are dependent upon the presence of cholesterol in the plasma membrane for activity (Figure 1.5).

Trafficking of internalized vesicles throughout the endosomal system is regulated by the GTP bound state of Rab proteins. Internalized vesicles are trafficked to the early endosome via Rab5. The presence of activated Rab5 on the membranes of the incoming vesicle and the endosome serve as binding sites for a number of effector proteins, including the tether EEA1 which docks the vesicle with the endosome and initiates SNARE mediated vesicle fusion. From the early endosome internalized activated receptors can either be deactivated and recycled back to the plasma membrane via Rab4, or ubiquitinated and incorporated into MVEs and then trafficked to the lysosome via Rab7 for degradation (Figure 1.6).

Ubiquitination of receptors is mediated by E3 ubiquitin ligases that form an isopeptide bond between ubiquitin and surface exposed lysine residues on the target protein. Monoubiquitination of receptors targets them for incorporation into MVEs (Figure 1.6). Components of the ESCRT machinery, like Tsg101, recognize ubiquitinated cargo via several ubiquitin binding domains. The ESCRT machinery concentrates ubiquitinated cargo to the site of MVE formation on the late endosome. The endosomal membrane obtains inverse curvature and

buds off into the lumen of the endosome via the concerted actions of Vps32 and Vps4. Cargo is de-ubiquitinated prior to inclusion in MVEs. MVEs are trafficked to the lysosome in a Rab7 dependent manner. The late endosome undergoes heterotypic fusion with the lysosome generating a hybrid organelle where MVEs and their cargo are degraded (Figure 1.6). Conjugation of polyubiquitin chains to substrates targets that substrate to the 26S proteasome for degradation. Although lysosomal degradation is the classical and accepted mechanism of RTK degradation, several lines of evidence point to a role for the proteasome.

1.3 Ankyrin proteins

Ankyrin proteins tether cytosolic domains of integral plasma membrane proteins to the cytoskeleton providing shape, structural support, and polarity to the cell (Bennett and Baines, 2001). Three different ankyrin genes have been discovered *ANK1*, *ANK2* and *ANK3* that encode ankyrin1, ankyrin2 and ankyrin3, respectively (Bennett and Healy, 2008). Each *ANK* gene is expressed as several isoforms due to alternative splicing (Bennett and Healy, 2008) (Figure 1.7). Ankyrin proteins share common domain architecture including an N-terminal integral membrane protein binding domain consisting of 24 ankyrin repeat sequences, a central spectrin/fodrin binding domain, a death domain and a C-terminal regulatory domain (Bennett and Healy, 2008) (Figure 1.7).

The N-terminal integral membrane protein binding domain and the death domain are highly conserved throughout the different ankyrin isoforms sharing 83% and 89% homology, respectively (Bennett and Healy, 2008). The spectrin binding domain and the regulatory domain are more variable sharing 78% and 53% homology, respectively (Bennett and Healy, 2008). Repeat sequences in the N-terminal domain mediate binding with numerous integral membrane proteins including cell adhesion molecules (such as L1CAMS, CD44 and E-Cadherin), ion channels (such as the anion exchanger, Na+/K+ ATPase, voltage-gated Na+ channels, Na+/Ca2+ exchanger, KCNQ2/3, Rh antigen, IP3 receptor and the ryanodine receptor) and other membrane-associated molecules (clathrin and tubulin) (Bennett and Healy, 2008).

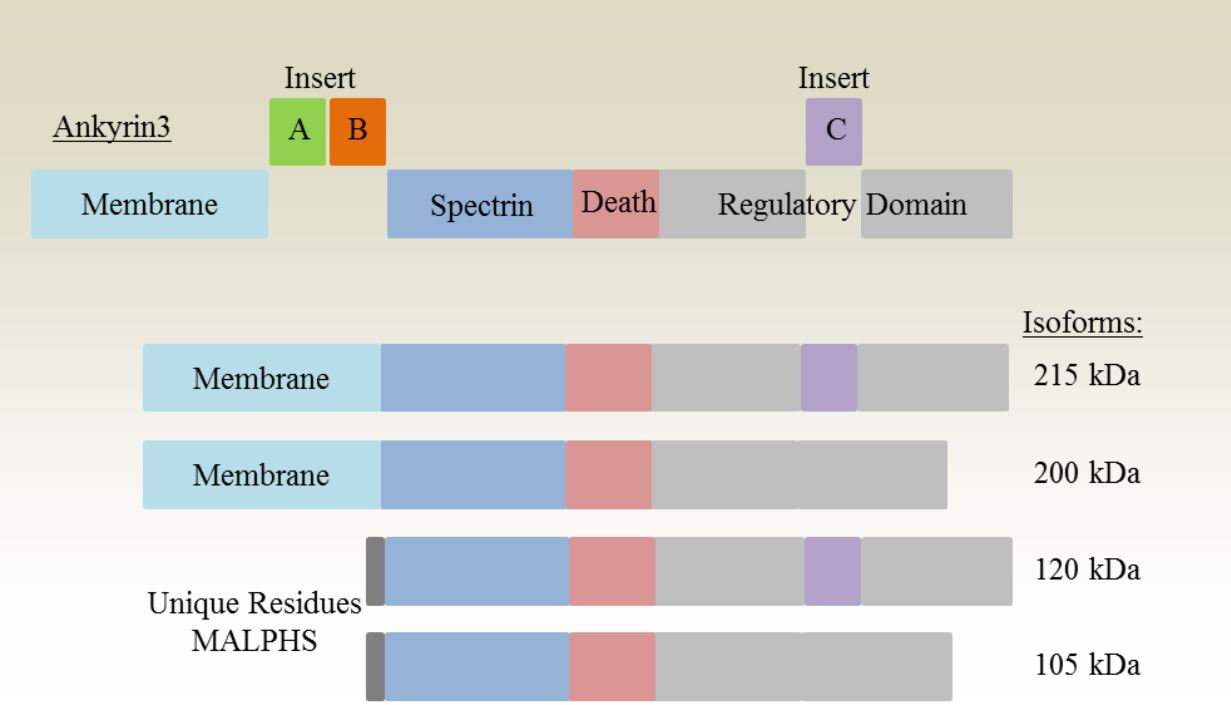

Figure 1.7: Domain architecture and isoforms of ankyrin3
A graphical representation of the general domain structure of ankyrin proteins and the different isoforms generated by alternative splicing of the ankyrin3 gene. All ankyrin proteins have the same common domain architecture consisting of an integral membrane protein binding domain (membrane) for interaction with numerous transmembrane proteins, a spectrin binding domain (spectrin) to facilitate interaction with the cytoskeleton, a death domain and a regulatory domain. Alternative splicing of the *ANK3* gene results in expression of several isoforms of varying molecular weight, including two gene products lacking the integral membrane protein binding domain and possessing 6 unique N-terminal residues.

The spectrin binding domain interacts with several isoforms of spectrin to link transmembrane proteins to the cytoskeleton (Bennett and Baines, 2001). The spectrin binding domain contains a 160 amino acid ZU5 motif which mediates interaction with spectrin (Mohler *et al*., 2004b). Mutation of conserved residues DAR999/1001 to alanine or A1024 to proline in ankyrin3 is sufficient to prevent spectrin binding (Kizhatil *et al*., 2007b). The role of the Death domain in ankyrin function is unknown; however it has been shown to bind Fas Ligand (FasL) (Bennett and Healy, 2008). The Regulatory domain has been show to bind Heat shock protein 40 kDa (Hsp40) and obscurin (Bennett and Healy, 2008).

Ankyrin proteins organize and cluster integral plasma membrane protein constituents into functional domains and disruption of ankyrin function is detrimental to cell physiology (Bennett and Healy, 2008). Ankyrin1 is expressed in human erythrocytes and provides structural support

allowing for the characteristic donut-like morphology of red blood cells (Bennett and Healy, 2008). Defects in ankyrin1 are linked to hereditary spherocytosis where red blood cells assume a spherical morphology and are more prone to osmotic lysis and physical degradation as they pass through the vasculature, resulting in hemolytic anemia (Birkenmeier and Barker, 2004; Birkenmeier *et al*., 2003; Gallagher, 2005).

Ankyrin2 is expressed in neural and cardiac tissues and links various transporters and adhesion molecules to the spectrin cytoskeleton (Bennett and Baines, 2001). While ankyrin2 knockout mice die at birth, heterozygous mice suffer from defects in cardiac conduction, heart rate variability, sinus bradycardia and sudden death (Mohler and Bennett, 2005). In humans, loss of function mutation of ankyrin2 mapped to inherited type-4 long-QT cardiac arrhythmia, termed ankyrin-B syndrome (Mohler *et al*., 2007; Mohler *et al*., 2003).

Ankyrin3 is widely expressed with highest expression levels in gut and kidney epithelium (Peters *et al*., 1995). Ankyrin3 is required for localization of voltage-gated sodium channels and L1CAM cell adhesion molecules at initial segments in Purkinje neurons (Jenkins and Bennett, 2001), for both biogenesis (Kizhatil *et al*., 2007b) and maintenance (Kizhatil *et al*., 2007a) of lateral membranes in epithelial cells and is required for localization of photoreceptors in metazoans (Kizhatil *et al*., 2009).

Interestingly, the cancer cell line encyclopedia (CCLE) showed that mRNA expression of the *ANK3* gene is frequently deregulated in numerous cancer cell lines including those derived from tumors of the central nervous system, breast, kidney and stomach tissues (http://www.broadinstitute.org/ccle/home) (Barretina et al., 2012). Indeed, downregulation of *ANK3* expression is frequently accompanied by overexpression of pro-oncogenic RTKs, while upregulation of *ANK3* expression is accompanied by attenuated RTK expression. In cancer cell lines derived from tumors of the central nervous system, including several glioblastomas attenuation of *ANK3* expression frequently demonstrate upregulation of *PDGFRa*, *PDGFRb* and fibroblast growth factor receptor (*FGFR*) expression (U118MG, LN215, LNZ308, GB1, IOMMLEE, U138MG, U178, CCFSTTG1 and LN235 cells). Indeed, cancer cell lines derived from tumor of the central nervous system that demonstrated upregulation of *ANK3* expression display downregulated expression of *PDGFRa*, *PDGFRb* and *FGFR* (SF767 and D283MED cells). In breast cancer cell lines, like central nervous system cancer cell lines, that display attenuated *ANK3* expression also frequently demonstrate upregulated *PDGFRa, PDGFRb* and

FGFR expression (HS606T, MDAMB157, BT549, HS343T, HS742T, HS739T and HS579T). Breast cancer cell lines with upregulated expression of *ANK3* frequently display attenuated expression of *PDGFRa*, *PDGFRb* and *FGFR* (HCC1428, YMB1, BT474, MDAMB415, HCC1419, BT483, EFM192A, MCF7, ZR7530, MDAMB175VII, AU565, SKBR3, MDAMB468 and HCC2157 cells). In the majority of kidney cancer cell lines, *ANK3* expression is downregulated and these cell lines also demonstrate high expression of *PDGFRb, FGFR and EGFR* (UOK101, SLR24, VMRCRZ, SLR26, SLR23, UMRC6, HK2 and KMRC2 cells). In stomach cancer cell lines with downregulated ANK3 expression, the expression of *PDGFRa* and *FGFR* is frequently up regulated (ECC12, FU97, SNU1, SH10TC, LMSU, ECC10 and AZ521 cells). Conversely, in stomach cancer cell lines with upregulated *ANK3* expression *PDGFRa* and *FGFR* expression is frequently attenuated (RERFGC1B, HS764T, SNU16, MKN45, SNU520, TGCB11TKB, NUGC2, 2313287 and SNU216 cells). Additionally, downregulation of the *ANK3* gene was recently identified as part of an 11 gene signature, a prognostic indicator of metastasis and poor clinical outcome in multiple human cancers (Glinsky *et al*., 2005). Taken together, the expression data of *ANK3* along with the reciprocal expression of pro-oncogenic RTKs in multiple cancer cell lines of different lineage suggests that ankyrin3 has a tumor suppressive role within the cell.

Previous studies from our laboratory implemented a phage display library to discover novel binding partners of the regulatory subunit of PI3K, p85 (King *et al*., 2000). Our laboratory has discovered a direct, phospho-tyrosine independent interaction between the SH2 domain of p85 and the 105 kDa isoform of ankyrin3 (Ignatiuk *et al*., 2006). Ankyrin3 is expressed as multiple isoforms (215, 200, 170 120, 105 kDa) due to two alternative transcriptional initiation sites within the *ANK3* gene and alternative splicing (Peters *et al*., 1995) (Figure 1.7). The large isoforms of ankyrin3 differ from one another by the presence or absence of amino acid inserts A, B and C (Figure 1.7). The small isoforms (120, 105 kDa) of ankyrin3 are distinguished by the presence of 15 kDa insert C within the regulatory domain and also possess six unique N-terminal amino acids not present in large isoforms (Peters *et al*., 1995) (Figure 1.7). The large isoforms of ankyrin3 are localized to the plasma membrane whereas small isoforms lacking the N-terminal repeat sequences responsible for integral membrane protein binding are localized to late endosomes/lysosomes (Hoock *et al*., 1997). Reciprocal interaction between Ank105 and p85 was confirmed via co-immunoprecipitation studies (Ignatiuk *et al*., 2006). Pulldown analysis using

purified proteins indicated that Ank105 bound the SH2 domains of p85 using both the spectrin binding domain and the regulatory domain (Ignatiuk *et al*., 2006).

Overexpression of Ank105 prompted PDGFR inactivation and degradation in response to PDGF stimulation and attenuated the ability of fibroblasts to proliferate in the presence of PDGF (Ignatiuk *et al*., 2006). Ank105 overexpression attenuated the activation of PDGFR in response to PDGF stimulation, as evident by reduced phosphorylation of the receptor (Ignatiuk *et al*., 2006). Indeed activation of downstream MAPK and PLC signaling pathways were also reduced (Ignatiuk *et al*., 2006). Co-immunofluorescence experiments showed colocalization between Ank105, p85, and PDGFR during endocytosis (Ignatiuk *et al*., 2006). Furthermore, Ank105 colocalized with LAMP-1 but not with EEA1 (Ignatiuk *et al*., 2006). Treatment of cells with the lysosomal degradation inhibitor chloroquine prevented PDGFR degradation in response to ligand (Ignatiuk *et al*., 2006). These observations indicate that Ank105 enhances the degradation of the PDGFR and attenuates signaling pathways downstream of the receptor.

2.0 RATIONALE AND OBJECTIVES

2.1 Hypothesis

Ank105 promotes the constitutive degradation of the PDGFR and attenuation of PDGFR signaling by facilitating endocytosis of the PDGFR and targeting the PDGFR for lysosomal degradation via an ubiquitin-dependent mechanism.

2.2 Objectives

The objective of the thesis work was to determine the mechanistic requirements for Ank105-mediated constitutive PDGFR degradation. The effects of Ank105 expression on PDGFR expression and signaling were determined. PDGFR endocytosis in Ank105-expressing cells was characterized with small molecule inhibitors and RNA interference targeting proteins involved in endocytosis to evaluate the mechanism of Ank105-mediated constitutive PDGFR degradation. Additionally, to determine the requirements of known Ank105 binding partners for constitutive PDGFR degradation, Ank105 binding partners were targeted for knockdown via RNA interference.

2.3 Specific objectives

1. To characterize the effects of Ank105 expression on PDGFR expression levels, activation and downstream signaling, as well as to determine whether Ank105 expression alters the phosphorylation or ubiquitination of the PDGFR. The effects of Ank105 expression on the EGFR were also examined.

2. To determine if Ank105 interacts with ubiquitin and ubiquitinated proteins and determine the region of Ank105 responsible for ubiquitin binding. Point mutations and deletion mutations were made to generate a mutant of Ank105 unable to interact with ubiquitin

3. To determine the pathway of endocytosis required for Ank105-mediated constitutive degradation using a panel of small molecule inhibitors. The effects of the small molecule inhibitors on constitutive PDGFR degradation was compared to ligand induced PDGFR degradation and LDL uptake. The effects of knockdown of key proteins involved in endocytosis on constitutive PDGFR expression were determined via RNA interference.

4. To determine the effects of knockdown of known Ank105 binding partners on

constitutive PDGFR expression via RNA interference and to identify novel binding partners of Ank105.

3.0 MATERIALS AND METHODS

3.1 Materials

3.1.1 Reagents and Supplies

All chemicals were of analytical grade or higher and purchased from VWR, Sigma Aldrich, Invitrogen, Qiagen or Fisher Scientific unless otherwise stated. Antibodies were purchased from Santa Cruz Biotechnology, Cell Signaling Technology or LI-COR biosciences unless stated otherwise.

3.2 Methods

3.2.1 Molecular biology

All standard molecular biology protocols, such as restriction digestion, ligation and transformation of competent cells were performed as per Current Protocols in Molecular Biology (Ausubel *et al*., 2007) and Current Protocols in Protein Science (Coligan *et al*., 2007). All primers were obtained from Invitrogen.

3.2.1.1 Generation of GST-tagged ubiquitin fusion plasmid

Ubiquitin-GST plasmid was provided generously by Stefan Jentsch (Max Planck Institute of Biochemistry, Munich, Germany). The isopropyl β-D-1-thiogalactopyranoside (IPTG) inducible bacterial expression vector pGEX6P1 (Amersham Pharmacia) is the backbone of the Ubiquitin-GST plasmid.

3.2.1.2 Generation of HA-tagged Ank105 fusion plasmid

Ankyrin3 cDNA was provided generously by Samuel Lux (Dana Farber Cancer Institute, Boston, MA). The 105 kDA isoform of Ankyrin3 was assembled by PCR from full length Ankyrin3 cDNA (Ignatiuk *et al*., 2006). The mammalian expression vector pRc/CMV2 (Invitrogen) was modified by the addition of three copies of the hemagluttinin (HA) epitope (YPYDVPDYA) upstream of the multiple cloning site (pHA_3), encoding HA_3-tagged fusion proteins (King *et al*., 2000). Ank105 DNA was inserted in the pHA_3 vector multiple cloning site

generating an N-terminal pHA$_3$-Ank105 fusion plasmid (Ignatiuk *et al*., 2006) (Figure 3.1).

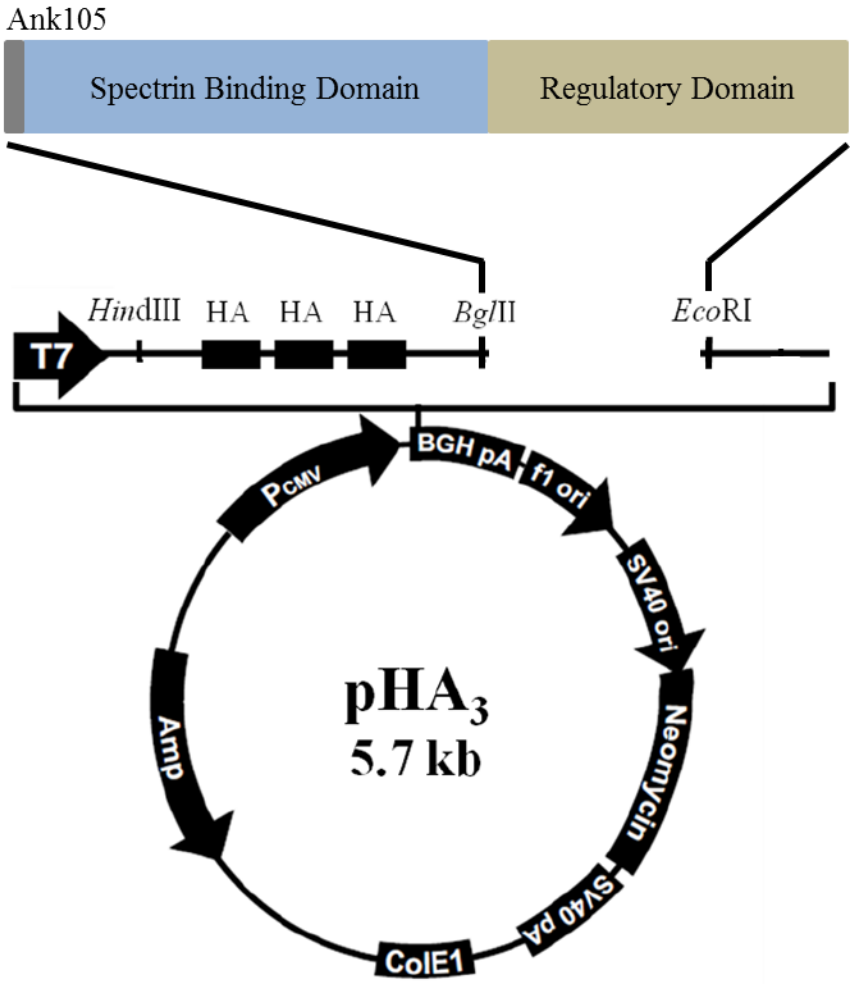

Figure 3.1: Map of pHA$_3$-Ank105 mammalian expression plasmid
Ank105 DNA containing 5′ *BglII* and 3′*EcoRI* restriction sites was inserted in the multiple cloning site of the pHA$_3$ vector, generating a pHA$_3$-Ank105 fusion plasmid. Mammalian expression is controlled by a CMV promoter and contains a bovine growth hormone (BGH) polyadenylation signal for optimal mRNA production. The vector also contains a neomycin resistance gene and an ampicillin resistance gene for mammalian and bacterial selection, respectively. Figure modified from the Invitrogen online resource website. (http://tools.invitrogen.com/content/sfs/manuals/prccmv 2_man.pdf)

3.2.1.3 Generation of HA-Ank105 mutant plasmids

3.2.1.3.1 Generation of C-terminal Ank105 deletion plasmids

C-terminal residues of Ank105 were deleted in 50 amino acid increments via polymerase chain reaction (PCR) to remove a potential ubiquitin interaction motif between residues 816 to 832 (Figure 4.5). Various amounts of pHA_3-Ank105 DNA were incubated with 5′Ank105-MALPS primer and the 3′ Ank105-ΔC primers (Table 3.1) along with other components required for the PCR (Table 3.2A). PCR was performed using PFU DNA polymerase (New England Biolabs) according to described PCR program (Table 3.2B). Successful reactions amplifying products of correct size were pooled and subjected to PCR clean up kit (Qiagen) using manufactures instructions. PCR products and empty pHA_3 were each restricted with *BglII* (New England Biolabs) and *EcoRI* (New England Biolabs) to create appropriate DNA sticky ends. Restricted PCR products were cleaned up as described above and ligated into restricted pHA_3 vector using Quick Ligation Kit (New England Biolabs) according to manufacturer's protocols and transformed into competent *Escherichia coli* (*E. coli*) TOP10 cells (Invitrogen). Single colonies of *E. coli* transformed with each Ank105 deletion plasmid were obtained via culture on Luria-Bertani (LB) broth (Sigma Aldrich) agar (Sigma Aldrich) (25mL) plates containing ampicillin (100 µg/mL) (Sigma Aldrich) at 37 °C overnight. *E. coli* cells were then inoculated into LB broth (250 mL) containing ampicillin (100 µg/mL) and cultured overnight at 37 °C. Plasmid DNA for each was purified by Maxiprep Kit (Qiagen) according to manufacturer's instruction. Plasmid inserts were verified via DNA sequencing.

3.2.1.3.2 Generation of spectrin binding domain and regulatory domain plasmids

The spectrin binding and regulatory domains of Ank105 were generated via PCR prior to commencement of thesis studies (Ignatiuk *et al*., 2006).

Table 3.1: Ank105 mutagenesis primers

List of primers used to generate deletion mutations and point mutations of Ank105. Primers are grouped and color coded based on type of mutation desired. *BglII* (AGA TCT) and *EcoRI* (GAA TTC) restriction sites are underlined. Primer nucleotides generating point mutations in Ank105 are bolded. All primers were obtained from Invitrogen.

Primer name	Sequence (5´to 3´)
5´Ank105-MALPHS	GCA AGA TCT ATG GCT TTG CCA CAC AGT GAA G
3´Ank105	CCA GAA TTC GTG GGT TTT CTT CTC CAC G
3´Ank105-ΔC50	CCA GAA TTC CTA GTC GAC CAT GCC GAC AGG CAC ACA GGG
3´Ank105-ΔC100	CCA GAA TTC CTA GTC GAC CTG TTT CCC TAT ATC GTT TTG
3´Ank105-ΔC150	CCA GAA TTC CTA GTC GAC GTC ATC CAG ACG GTC CAG TAA C
3´Ank105-ΔC200	CCA GAA TTC CTA GTC GAC CCC ATA ATC AAA TAT TGG TCC
3´Ank105-ΔC250	CCA GAA TTC CTA GTC GAC ATT GGG ATT TTC CAC ACG TAT TTG
3´Ank105-ΔC300	CCA GAA TTC CTA GTC GAC TTC AGT CAA GTA GCT GTA GCG
3´Ank105-SpecΔC50	CCA GAA TTC GGT GTC TCT GAT CTT GAT GGA AAA TTG
3´Ank105-SpecΔC100	CCA GAA TTC TTT GCT TCT GGC AAC CTC CTC GAA GTT CTC
3´Ank105-SpecΔC150	CCA GAA TTC TAT CAG CTC TCT GTA CAG CTG GGA GGC TAG CCC
3´Ank105-SpecΔC200	CCA GAA TTC TTG AGC TGG TGA GGT GCC TCC TGT GAT GCT
3´Ank105-SpecΔC250	CCA GAA TTC CGG CTC TAC CGT GAC AAT TGG GCT AAA TGT TGC
3´Ank105-SpecΔC300	CCA GGA TTC ATC CAT GCC ATT GAG AAG CTC CGC GAG GTC
3´Ank105-SpecΔC350	CCA GAA TTC ATC CAT GCC ATT GAG AAG CTC CGC GAG GTC
3´Ank105-SpecΔC400	CCA GAA TTC GGG GCC TAA AAA TTG TGC CCC CGC AGG ACC
3´Ank105-SpecΔC450	CCA GAA TTC AGG GAT GAT GAT CCG CAT CCC GTG GTG GCG
3´Ank105-SpecΔC500	CCA GAA TTC GAG GGA GTC AGA ATC AAA CTC CCT CGT
5´Ank105-ΔN127	GCA AGA TCT GGG GGC TCC ATG CGA GGA AGC
5´Ank105-ΔN169	GCA AGA TCT ATG GTG GAA GGA GAG GGA TTA G
5´Ank105-ΔN359	GCA AGA TCT TCG GGA GAA GGC GTG TCC
5´Ank105-ΔN385	GCA AGA TCT ACC TCA CCA GCT CAA TGG
5´Ank105-DAR124-26/AAA	GC TTT ATG GTG GCC GCG GCA GGG **GGC** TCC **ATG** CG
3´Ank105-DAR124-26/AAA	CG **CAT** GGA **GCC** CCC TGC CGC GGC CAC CAT AAA GC
5´Ank105-A149P	CGA AAG TGT ACG **CCC** CCC ACC CGC
3´Ank105-A149P	GCG GGT GGG **GGG** CGT ACA CTT TCG
5´Ank105-S827D	GCC TAC CAG AAA **GAT** CTG GAA GAA ACC
3´Ank105-S827D	GGT TTC TTC CAG **ATC** TTT CTG GTA GGC

Ank105 N and C-terminal primers

Ank105 N-terminal deletion primers

Ank105 C-terminal deletion primers

Site-directed mutagenesis primers

Spectrin domain C-terminal deletion primers

Table 3.2: PCR conditions for generation of C-terminal Ank105 deletion plasmids A. Concentration and volumes of each component of the PCR used to generate C-terminal Ank105 deletion fragments. B. PCR program used to generate C-terminal Ank105 deletion fragments.

A

PCR Amplification Component	Volume (µL)
PFU Reaction Buffer (10x)	5
dNTP Nucleotides (2 mM)	5
5′Ank105-MALPS Primer (5 µM)	2.5
3′Ank105-ΔC Primer (5 µM)	2.5
Template DNA (10 ng/µL)	0-5
H_20	29-34
PFU Polymerase	1
Total Volume	50

B

PCR Program Temperature (°C)	Time (Min)	
95	1	
95	1	40 Cycles
55	1	
72	15	
72	7	
4	∞	

3.2.1.3.3 Generation of C-terminal spectrin domain deletion plasmids

C-terminal residues of Ank105 spectrin binding domain were incrementally deleted via PCR to identify the region of Ank105 mediating ubiquitin binding (Figure 4.7). Purified pHA_3-Ank105 DNA was incubated with 5′Ank105-MALPS primer and each of the 3′Ank105-SpecΔC primers (Table 3.1), along with other components required for the PCR (Table 3.3A). PCR was performed using PFU DNA polymerase according to described PCR program (Table 3.3B). A gradient PCR machine was used to perform the primer-DNA binding step of the PCR at several temperatures, allowing a large number of reactions with different primers to be carried out at the same time. Successful reactions amplifying products of correct size were pooled and subjected to PCR clean up kit) using manufactures instructions. PCR products and empty pHA_3 were each restricted with *BglII* and *EcoRI* to create appropriate DNA sticky ends. Restricted PCR products were cleaned up as described above and ligated into restricted pHA_3 vector using Quick Ligation Kit according to manufacturer's protocols and transformed into competent *E. coli* TOP10 cells. Single colonies of *E. coli* transformed with each Ank105C-terminal spectrin domain deletion plasmid were obtained via culture on LB-agar (25mL) plates containing ampicillin (100 µg/mL) at 37 °C overnight. *E. coli* cells were then inoculated into LB broth (250 mL) containing ampicillin (100 µg/mL) and cultured overnight at 37 °C. Plasmid DNA for each deletion was purified by Maxiprep Kit according to manufacturer's instruction. Plasmid inserts were verified via DNA sequencing.

Table 3.3: PCR conditions for generation of C-terminal Ank105 spectrin binding domain deletion plasmids

A. Concentration and volumes of each component of the PCR used to generate C-terminal Ank105 deletion fragments. B. PCR program used to generate C-terminal Ank105 deletion fragments. Gradient PCR machine used to perform primer-DNA binding step at a series of different temperatures.

A

PCR Amplification Component	Volume (µL)
PFU Reaction Buffer (10x)	5
dNTP Nucleotides (2 mM)	5
5′Ank105-MALPS Primer (5 µM)	2.5
3′Ank105-SpecΔC Primer (5 µM)	2.5
Template DNA (10 ng/µL)	5
H_20	29
PFU Polymerase	1
Total Volume	50

B

PCR Program Temperature (°C)	Time (Min)	
95	1	
95	1	40 Cycles
58-63	1	
72	6	
72	7	
4	∞	

3.2.1.3.4 Generation of N-terminal Ank105 disordered region deletion plasmids

Disordered regions of Ank105 were identified using the Russel-Linding Globprot2.3 Software (Figure 4.7). N-terminal Ank105 deletion mutants were generated from disordered regions identified in the spectrin binding domain (Figure 4.8). Purified pHA_3-Ank105 DNA was incubated with each of the 5′Ank105-ΔN primers (Table 3.1) and the 3′Ank105 primer, along with other components required for the PCR (Table 3.4A). The PCR was performed using KOD DNA polymerase (EMD Millipore) according to described PCR program (Table 3.4B). Successful reactions amplifying products of correct size were pooled and subjected to PCR clean up kit) using manufactures instructions. PCR products and empty pHA_3 were each restricted with *BglII* and *EcoRI* to create appropriate DNA sticky ends. Restricted PCR products were cleaned up as described above and ligated into restricted pHA_3 vector using Quick Ligation Kit according to manufacturer's protocols and transformed into competent *E. coli* TOP10 cells. Single colonies of *E. coli* transformed with each pHA_3-Ank105 N-terminal disordered region deletion plasmid were obtained via culture on LB-agar (25mL) plates containing ampicillin (100 µg/mL) at 37 °C overnight. *E. coli* cells were then inoculated into LB broth (250 mL) containing ampicillin (100 µg/mL) and cultured overnight at 37 °C. Plasmid DNA for each deletion was purified by Maxiprep Kit according to manufacturer's instruction. Plasmid inserts were verified via DNA

sequencing.

Table 3.4: PCR conditions for generation of N-terminal Ank105 deletion plasmids
A. Concentration and volumes of each component of the PCR used to generate N-terminal Ank105 deletion fragments. B. PCR program used to generate N-terminal Ank105 deletion fragments. Gradient PCR machine used to perform primer-DNA binding step at a series of different temperatures.

A

PCR Amplification Component	Volume (µL)
KOD Reaction Buffer #2 (10x)	5
$MgSO_4$ (25 mM)	3
dNTP Nucleotides (2 mM)	5
5′Ank105-ΔN Primer (5 µM)	4
3′Ank105 Primer (5 µM)	4
Template DNA (12 ng/µL)	1
H_20	27.5
KOD Polymerase	0.5
Total Volume	50

B

PCR Program Temperature (°C)	Time (Seconds)	
95	30	
95	15	30 Cycles
58-63	5	
72	40	
72	300	
4	∞	

3.2.1.3.5 Site-directed mutagenesis of potential Ank105 ubiquitin interaction motif

To disrupt the ubiquitin binding function of a potential UIM within the C-terminal regulatory domain of Ank105 a conserved serine residue, essential for UIM function, was mutated to aspartic acid (Figure 4.5). This mutation was shown previously to disrupt UIM-ubiquitin interaction (Fujiwara *et al*., 2004). Purified pHA_3-Ank105 DNA was incubated with 5′Ank105-S827D and 3′Ank105-S827D primers (Table 3.1), along with other components required for the PCR (Table 3.5A). PCR products were restricted with *Dpn1* (New England Biolabs) according to manufacturer's instruction to degrade remaining wild type template and then transformed into competent TOP10 *E. coli* cells. Single colonies of *E. coli* transformed with each pHA_3-Ank105 UIM mutant plasmid were obtained via culture on LB-agar (25mL) plates containing ampicillin (100 µg/mL) at 37 °C overnight. *E. coli* cells were then inoculated into LB broth (250 mL) containing ampicillin (100 µg/mL) and cultured overnight at 37 °C. Plasmid DNA for each Ank105 UIM mutant plasmid was purified by Maxiprep Kit according to manufacturer's instruction. Plasmid inserts were verified via DNA sequencing.

Table 3.5: PCR conditions for generation of Ank105 S827D mutant

A. Concentration and volumes of each component of the PCR used to generate Ank105S827D mutant. B. PCR program used to generate Ank105S827D mutant.

A

PCR Amplification Component	Volume (µL)
PFU Reaction Buffer (10x)	5
dNTP Nucleotides (2 mM)	5
5′Ank105-S827D Primer (5 µM)	2.5
3′Ank105-S827D Primer (5 µM)	2.5
Template DNA (10 ng/µL)	10
H_20	24
PFU Polymerase	1
Total Volume	50

B

PCR Program Temperature (°C)	Time (Min)	
95	1	
95	1	18 Cycles
55	1	
68	16	
72	1	
4	∞	

3.2.1.3.6 Site-directed mutagenesis of residues of Ank105 required for spectrin binding

To disrupt the ability of Ank105 to interact with spectrin, two separate mutations, DAR124-26/AAA and A149P, were generated via PCR within the spectrin binding domain of Ank105. These two mutations were shown previously to disrupt Ankyrin3-spectrin interaction (Kizhatil *et al*., 2007a; Kizhatil *et al*., 2007b). Purified pHA_3-Ank105 DNA was incubated with 5′Ank105-DAR124-26/AAA primer and 3′Ank105-DAR124-26/AAA primer (Table 3.1), along with other components required for the PCR (Table 3.6A) to generate the Ank105-DAR124-26/AAA mutation. To generate the Ank105-A149P mutation purified pHA_3-Ank105 DNA was incubated with 5′Ank105-A149P primer and 3′Ank105-A149P primer (Table 3.1), along with other components required for the PCR (Table 3.6B). Both PCRs were performed according to the described PCR program (Table 3.6C). A gradient PCR machine was used to perform the primer-DNA annealing step of the PCR at several temperatures, allowing a large number of reactions with different primers to be carried out at the same time. PCR products were restricted with Dpn1 according to manufacturer's instruction to degrade remaining wild type template and then transformed into competent TOP10 *E. coli*. *E. coli* cells Single colonies of *E. coli* transformed with each Ank105 UIM mutant plasmid were obtained via culture on LB-agar (25mL) plates containing ampicillin (100 µg/mL) at 37 °C overnight. *E. coli* cells were then inoculated into LB broth (250 mL) containing ampicillin (100 µg/mL) and cultured overnight at 37 °C. Plasmid DNA for each Ank105 spectrin binding mutant plasmid was purified by

Maxiprep Kit according to manufacturer's instruction. Each point mutation within the spectrin binding domain was verified by DNA sequencing. Additionally, the remaining sequence of Ank105 in the spectrin binding mutant plasmids was verified by DNA sequencing to confirm that no addition mutation were erroneously introduced.

Table 3.6: PCR conditions for generation of Ank105 spectrin binding mutants
A. Concentration and volumes of each component of the PCR used to generate Ank105DAR124-26/AAA mutant. B. Concentration and volumes of each component of the PCR used to generate Ank105A149P mutant. C. PCR program used to generate Ank105DAR124-26/AAA and Ank105A149P mutants. Gradient PCR machine used to perform primer-DNA annealing step at a series of different temperatures.

A

PCR Amplification

Component	Volume (µL)
PFU Reaction Buffer (10x)	5
dNTP Nucleotides (2 mM)	5
5′Ank105-DAR124-26/AAA Primer (5 µM)	4
3′Ank105-DAR124-26/AAA Primer (5 µM)	4
Template DNA (50 ng/µL)	1
H_20	30
PFU Polymerase	1
Total Volume	50

B

PCR Amplification

Component	Volume (µL)
PFU Reaction Buffer (10x)	5
dNTP Nucleotides (2 mM)	5
5′Ank105-A149P Primer (5 µM)	4
3′Ank105-A149P Primer (5 µM)	4
Template DNA (50 ng/µL)	1
H_20	30
PFU Polymerase	1
Total Volume	50

C

PCR Program

Temperature (°C)	Time (Min)	
95	1	
95	1	18 Cycles
55-65	1	
68	16	
72	1	
4	∞	

3.2.1.4 qRT-PCR screening of knockdown cell lines

HA-Ank105-expressing cells and stable knockdown cell lines (3.2.2.4) were screened via qRT-PCR to quantify extent of target knockdown. mRNA was extracted from a confluent 6 cm^2 plate of each knockdown cell line using the RNeasy mini kit (Qiagen) according to manufacturer's instruction. cDNA was generated from isolated mRNA using the RT^2 First Strand

Kit (Qiagen) according to manufacturer's protocol. Relative expression levels of genes silenced by shRNA in each stable knockdown cell line were quantified and normalized to β-Actin expression. Taqman Gene Expression Master Mix (Invitrogen) was incubated with cDNA generated from each of the stable knockdown cell lines and the corresponding primer/probe sets (Table 3.7) and qRT-PCR was performed using the Step One Plus Real-Time PCR System (Applied Biosystems), using a carboxyfluorescein (FAM) reporter (Applied Biosystems) according to manufacturer's protocol.

Table 3.7: qRT-PCR primer list
Tabulation of primer/probe sets used to determine expression levels in knockdown cell lines.

Gene Target	Protein	Primer/Probe Set	Reporter	Species	Supplier
Actb	β-actin	Mm01205648_g1	FAM	Mouse	Invitrogen
Cltc	Clathrin Heavy Chain	Mm01303974_m1	FAM	Mouse	Invitrogen
Dnm2	Dynamin-II	Mm00514582_m1	FAM	Mouse	Invitrogen
Pik3r1	p85α	Mm00803160_m1	FAM	Mouse	Invitrogen
Rab7	Rab7	Mm01183732_g1	FAM	Mouse	Invitrogen
Spnb2	Spectrin βII	Mm00486365_m1	FAM	Mouse	Invitrogen
Tsg101	Tsg101	Mm00649956_m1	FAM	Mouse	Invitrogen

3.2.2 – Cell culture

3.2.2.1 General growth conditions

All cell lines utilized during studies were cultured in standard cell culture media (Table 3.8) and incubated at 37 °C with 5% CO_2 (v/v). Cell lines stably expressing HA-Ank105 were cultured in this standard cell culture media with the addition of geneticin (G418) (400 µg/mL) to maintain stable expression. HA-Ank105 expressing cells stably transduced with shRNA plasmids were cultured in standard cell culture media with the addition of G418 (400 µg/mL) and puromycin (2 µg/mL) to maintain stable expression. All cell lines were passaged using trypsin buffer (Table 3.8). Stocks of each cell line were generated by suspending cells in freezing media (Table 3.8) and placing them for long-term storage in liquid nitrogen.

Table 3.8: Common buffers

Buffers used to perform experiments in thesis are listed as well as the concentration/amount of their respective components. The solvent for all buffers when not directly listed is distilled H_2O.

Acrylamide	
Acrylamide	29.2% (w/v)
Bisacrylamide	0.8% (w/v)
Blocking Buffer pH 7.5	
PBS	95% (v/v)
Skim milk powder (Carnation)	5% (w/v)
Coomassie Blue Stain	
Coomassie blue R-250 (Biorad)	0.14% (w/v)
Methanol	41.4% (v/v)
Acetic acid	5.4% (v/v)
Destain	
Methanol	41.4% (v/v)
Acetic acid	5.4% (v/v)
Fixing Buffer pH 7.5	
PBS	96% (v/v)
Paraformaldehyde	4% (w/v)
Freezing Media	
Std. cell culture media	95% (v/v)
DMSO (Invitrogen)	5% (v/v)
HNTG pH 7.5	
Hepes	20 mM
Sodium Chloride	150 mM
Triton X-100	0.1% (v/v)
Glycerol	10 % (v/v)
IP Wash Buffer pH 7.5	
Tris	50 mM
Sodium Chloride	150 mM
NP-40	1% (v/v)
Lower Gel Buffer pH 8.8	
Tris	375 mM
Sodium dodecyl sulfate	0.1% (w/v)
PBS pH 7.3	
Sodium Chloride	137 mM
Potassium Chloride	2.7 mM
Potassium dihydrogen phosphate	1.4 mM
Sodium hydrogen phosphate	4.3 mM
PLC Lysis Buffer pH 7.5	
Hepes	50 mM
Sodium Chloride	150 mM
Glycerol	10 % (v/v)
Triton X-100	1% (v/v)
Magnesium Chloride	1.5 mM
EGTA	1 mM
Sodium Pyrophosphate	10 mM
Sodium Floride	100 mM
Running Buffer	
Tris	25 mM
Glycine	192 mM
Sodium dodecyl sulfate	0.1% (w/v)
SDS Sample Buffer pH 6.8	
Tris	62.5 mM
Glycerol	10% (v/v)
2-mercaptoethanol	5% (v/v)
Sodium dodecyl sulfate	2.3% (w/v)
Std. Cell Culture Media pH 7.2	
Hi glucose DMEM (Gibco)	90% (v/v)
Fetal bovine serum	10% (v/v)
Sodium bicarbonate	44 mM
Running Buffer	
Tris	25 mM
Glycine	192 mM
Sodium dodecyl sulfate	0.1% (w/v)
Transfer Buffer	
Tris	48 mM
Glycine	39 mM
Sodium dodecyl sulfate	0.0375% (w/v)
Methanol	20% (v/v)
Trypsin Buffer	
PBS	99.75% (v/v)
EDTA	6.36 mM
Trypsin (Gibco)	0.25% (v/v)
Upper Gel buffer pH 6.8	
Tris	125 mM
Sodium dodecyl sulfate	0.1% (w/v)

3.2.2.2 Transient transfection of mammalian cell lines

For transient transfection of DNA plasmids in mammalian cell lines, cells were seeded at 1/3 confluency and cultured overnight in standard cell culture media at 37°C and 5% CO_2 (v/v). The next day transfection media was prepared. For each 10 cm^2 plate of cells transfected, 3 µg of the DNA plasmid of interest and 36 µL of lipofectamine (Invitrogen) were aliquoted into 1.5 mL optimem (Gibco) and incubated at room temperature for 15 minutes. To the transfection media, 4.5 ml of DMEM per plate was added. Cells were washed once with 5 mL serum-free DMEM and then aspirated. Cells were cultured with 6 mL transfection media for 5 hours at 37 °C and 5% CO_2. Transfection media was aspirated and replaced with standard cell culture media. Cells were cultured to confluency at 37 °C and 5% CO_2.

3.2.2.3 Stable transfection of mammalian cell lines

For stable transfection of DNA plasmids in mammalian cell lines the same transfection protocol was followed as for transient transfection (3.2.2.2). When cells reach confluency they were passaged sparsely, seeding density of 1:50, in standard cell culture media with the addition of selection reagent to selectively eliminate untransfected cells from the population. G418 (400 µg/mL) was added to select for stable expression of plasmids conferring neomycin resistance whereas puromycin (2 µg/mL) was added to select for stable expression of plasmids conferring puromycin resistance. Cells were cultured until single colonies are visually identified with light microscopy. Individual colonies were isolated and seeded into 24 well plates. Cells were expanded in standard cell culture media with the appropriate selection reagent at 37 °C and 5% CO_2. Once the clones were sufficiently expanded, liquid nitrogen stocks were generated. Lysates were harvested and evaluated for expression of gene of interest by Western blot.

3.2.2.4 Lentiviral transduction of mammalian cell lines

Expression of several endocytosis related proteins was selectively knocked down via transduction of HA-Ank105-expressing cells with lentivirus packaged with a pool of three shRNA plasmids directed against each specific target (Santa Cruz Biotechnology) (Table 3.9). Lentivirus was used as a delivery system for shRNA plasmids to overcome the inherently low transient transfection efficiency of NIH 3T3 cell lines. High expression levels of shRNA plasmids were hypothesized to increase the chances of obtaining clones with a high degree of

Table 3.9: Sequences of shRNAs used for knockdown of mammalian gene expression
Tabulation of hairpin sequences of shRNA plasmids used for knockdown of mammalian gene expression. The shRNA plasmids are tranduced via lentivirus. Each commercially available lentivirus targeting each gene of interest are pooled. All lentivirus-shRNAs are species specific to mus musculus and were purchased from Santa Cruz Biotechnology. Catalogue numbers of each pooled lentivirus is provided. Sequences of each hairpin in the pool are provided and color coded to the target gene of interest.

Target	Hairpin Sequence (5′ to 3′)	Catalogue
Clathrin HC	CCACACGTGTTGAACTTGAACTTGATTCAAGAGATCAAGTTCAACACGTGTGGTTTTT	sc-35066V
	CAGTGCAGGTGTTGATTGATTCAAGAGATCAATCAACACCTGCACTGTTTTT	sc-35066V
	GAAGAATTGCTGCTTATCTTTCAAGAGAAGATAAGCAGCAATTCTTCTTTTT	sc-35066V
Dynamin-II	CCACACGTGTTGAACTTGAACTTGATTCAAGAGATCAAGTTCAACACGTGTGGTTTTT	sc-35237V
	GCATCAATCGTATCTTTCATTCAAGAGATGAAAGATACGATTGATGCTTTTT	sc-35237V
	CTAGTGGACATGACAATGATTCAAGAGATCATTGTCATGTCCACTAGTTTTT	sc-35237V
βII-spectrin	GATCCCTGCGCAGATCTTGACAAATTCAAGAGATTTGTCAAGATCTGCGCAGTTTTT	sc-36552V
	GATCCCCAGTCTCAATATTCTTCTTTCAAGAGAAGAAGAATATTGAGACTGGTTTTT	sc-36552V
	GATCCGTACATGATGTCTGAGAAATTCAAGAGATTTCTCAGACATCATGTACTTTTT	sc-36552V
p85α	GGATCAAGTTGTCAAAGAATTCAAGAGATTCTTTGACAACTTGATCCTTTTT	sc-36218V
	GCAACGAGAAAGAAATTCATTCAAGAGATGAATTTCTTTCTCGTTGCTTTTT	sc-36218V
	CCAGACGTTTCTAACCTTATTCAAGAGATAAGGTTAGAAACGTCTGGTTTTT	sc-36218V
Rab7	GTTCAGTAACCAGTACAAATTCAAGAGATTTGTACTGGTTACTGAACTTTTT	sc-270071V
	CCAGACAATTGCTCGGAATTTCAAGAGAATTCCGAGCAATTGTCTGGTTTTT	sc-270071V
Tsg101	CTGGAGCTTATTCAAATCATTCAAGAGATGATTTGAATAAGCTCCAGTTTTT	sc-36753V
	CCACAACAAGCTCACAGTATTCAAGAGATACTGTGAGCTTGTTGGTGGTTTTT	sc-36753V
	GAAGTAGCTGAAGTTGATATTCAAGAGATATCAACTTCAGCTACTTCTTTTT	sc-36753V

Clathrin HC shRNA Dynamin-II shRNA βII-spectrin shRNA p85α shRNA
Rab7 shRNA Tsg101 shRNA

knockdown of the target of interest. Indeed, transduction of NIH 3T3 cells with lentivirus packaged with a GFP-expressing plasmid (Santa Cruz Biotechnology) demonstrated the transduction efficiency to be greater than 95% (Figure 3.2). HA-Ank105-expressing cells were seeded at a density of $4.2x10^4$ cells per well in 12 well dishes. HA-Ank105-expressing cells were transduced with lentivirus packaged with a pool of three shRNA plasmids directed against endocytosis-related proteins (one of: clathrin, caveolin, p85, tsg101, rab7, spectrin β-II and dynamin II) (Santa Cruz Biotechnology) as well as control scrambled shRNA plasmids (Santa Cruz Biotechnology) with no specific target. Lentiviral transduction of NIH 3T3 cells stably expressing HA-Ank105 was performed according to the manufacturer's instruction (http://datasheets.scbt.com/shrna_lv_protocol.pdf). Sequences of small hairpin RNAs used to target mammalian gene expression are provided (Table 3.9). Single, stable knockdown clones

were isolated with culture in standard cell culture media with the addition of G418 (400 µg/mL; for stable expression of pHA$_3$-Ank105 plasmid) and puromycin (2 µg/mL; for stable expression of shRNA plasmid) as previously described.

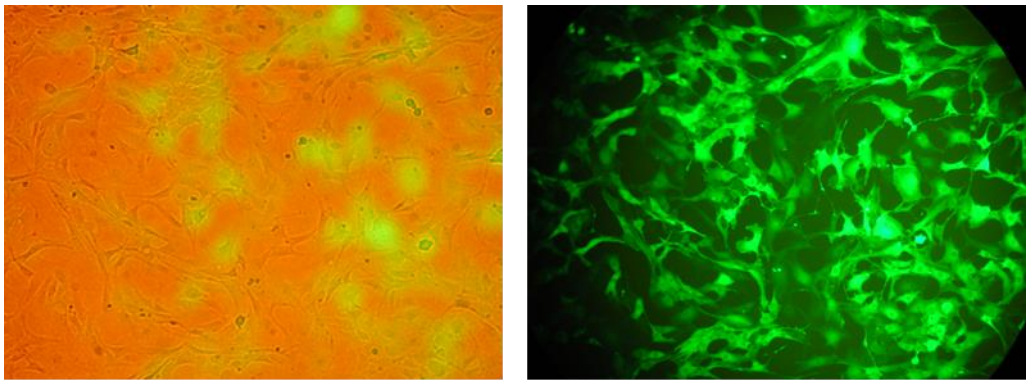

Figure 3.2: Lentiviral transduction of GFP reporter in NIH 3T3 cells
NIH 3T3 cells were transduced with lentivirus encoding a GFP reporter. Cells were visualized 24 hours post transduction with both light and fluorescent microscopy.

3.2.3 SDS-PAGE and Western blot analysis

3.2.3.1 Sample preparation

When denaturing lysis conditions were desirable, as for Western blot of cellular lysate to determine protein expression levels, cells were lysed in SDS sample buffer (Table 3.8). Cells were scraped in 150 µL SDS sample buffer per 10 cm^2 plate. Lysates were collected and heated at 95 °C for 5 minutes. Samples were sonicated to reduce viscosity. Prior to SDS-PAGE and Western blot analysis, samples were normalized to total cellular protein content using Total Protein Micro Lowry Kit, Peterson's modification (Sigma Aldrich) according to the manufacturer's instructions.

When non-denaturing lysis conditions were desirable, as for pulldown experiments, cells were lysed in PLC lysis buffer (Table 3.8). Cells were scraped in150 µL PLC lysis buffer (Table 3.8) per 10 cm^2 plate. Samples were centrifuged at 7000 g to pellet the triton insoluble fraction of the cell lysate. Supernatant was aliquoted and stored and the pellet was discarded. After experimentation with these samples, samples were mixed 1:1 with SDS sample buffer and heated

at 95 °C for 5 minutes prior to resolution by SDS-PAGE.

3.2.3.2 SDS-PAGE

Protein content of cellular lysates was resolved via SDS-PAGE. Resolving gels were composed of 7.5-15% acrylamide (Table 3.8) in SDS-PAGE lower gel buffer (Table 3.8). Resolving gels were polymerized with the addition of 0.06% (w/v) ammonium persulfate and 0.1% (v/v) N,N,N′,N′-tetra-methylethylenediamine (TEMED). Stacking gels were composed of 4.5% acrylamide in upper gel buffer (Table 3.8) and poured on top of the resolving gel. A loading comb was inserted to created loading wells. Stacking gels were polymerized as described for resolving gels. Gels were placed in Mini-Protean-3 System (Biorad). Mini-Protean-3 buffer tank was filled with SDS-PAGE running buffer (Table 3.8) Samples, prepared as described previously, were loaded into wells. Prestained or unstained protein ladder (Fermentas) was also loaded as a reference for molecular weight. Samples were resolved at 225 V until the bromophenol blue dye from SDS sample buffer ran off the bottom of the gel.

3.2.3.3 Coomassie blue staining

To visualize the protein content of SDS-PAGE resolved samples gels were covered with Coomassie blue stain (Table 3.8) and incubated at room temperature for 30 minutes on a nutator to allow incorporation of stain. Stain was discarded and gels were incubated with destain (Table 3.8) until protein bands were visible. Gels were imaged using the Gel Doc XR+ System (Biorad) and analyzed using Quantity One Software (Biorad).

3.2.3.4 Western blot analysis

Following SDS-PAGE gels were placed in transfer buffer (Table 3.8) for 15 minutes. Proteins were then transferred from gels to a nitrocellulose membrane using a semi-dry OWL separation system (VWR) at 500 mA for 15 minutes per gel. Nitrocellulose membranes were then placed into blocking buffer (Table 3.8) for 1 hour at room temperature. Nitrocellulose membranes were then incubated with 5 mL primary antibody (Table 3.10) in blocking buffer for 1 hour at room temperature. Nitrocellulose membranes were washed 3 times for 5 minutes with copious amounts of PBS (Table 3.8). Following washing, nitrocellulose membranes were

Table 3.10: Antibody list and concentrations

Antibodies and their respective working concentrations are listed. Antibodies are grouped and color coded according to functionality.

Antibody	Manufacturer	Isotype	Cat. Number	Conc.
anti-Akt	Cell Signaling	Rabbit IgG	9272	1:1000
anti-Caveolin	BD Biosciences	Rabbit IgG	610060	1:1000
anti-Clathrin heavy chain	Pierce Thermo	Rabbit IgG	PA5-17347	1:1000
anti-Dynamin (H300)	Santa Cruz	Rabbit IgG	sc-11362	2 µg/mL
anti-EGFR (1005)	Santa Cruz	Rabbit IgG	sc-03	1:500
anti-Erk1 (MK12)	BD Biosciences	Rabbit IgG	610030	1:1000
anti-GAPDH (6C5)	Invitrogen	Mouse IgG_1	AM4300	1 µg/mL
anti-HA (F7)	Santa Cruz	Mouse $IgG2_a$	sc-7392	5 µg/mL
anti-PDGFRβ (958)	Santa Cruz	Rabbit IgG	sc-432	2 µg/mL
anti-PDGFRβ (2B3)	Cell Signaling	Mouse IgG	3175	1:500
anti-PDGFRβ (C82A3)	Cell Signaling	Rabbit IgG	4564	1:500
anti-PI3 kinase, p85 N-SH3 (AB6)	EMD Millipore	Mouse IgG	05-212	1:500
anti-Ubiquitin (P4D1)	Santa Cruz	Mouse IgG_1	sc-8017	2 µg/mL
anti-phospho-Akt (Ser 473)	Cell Signaling	Rabbit IgG	9271	1:1000
anti-phospho-Tyrosine (pY20)	Santa Cruz	Mouse IgG_{2b}	sc-508	2 µg/mL
anti-phospho-p44/42 (Erk1/2)	Cell Signaling	Rabbit IgG	9101	1:1000
anti-HA (F7) Agarose Conjugated	Santa Cruz	Mouse $IgG2_a$	sc-7392 AC	10 µg/IP
anti-mouse IgG Agarose Conjugated	Santa Cruz	Goat IgG	sc-2058	10 µg/IP
anti-rabbit IgG Agarose Conjugated	Santa Cruz	Goat IgG	sc-2007	10 µg/IP
anti-mouse IgG HRP Conjugated	Santa Cruz	Goat IgG	sc-2005	1:5000
anti-mouse IgG IRDye 680RD	LI-COR	Goat IgG	926-68070	1:5000
anti-mouse IgG IRDye 800CW	LI-COR	Goat IgG	926-33221	1:5000
anti-rabbit IgG HRP Conjugated	Santa Cruz	Goat IgG	sc-2004	1:5000
anti-rabbit IgG IRDye 680RD	LI-COR	Goat IgG	926-68071	1:5000
anti-rabbit IgG IRDye 800CW	LI-COR	Goat IgG	926-32210	1:5000

Primary antibodies Phospho-specific antibodies Immunoprecipitation antibodies

Secondary antibodies

incubated with 5 mL of secondary antibody (Table 3.10) in blocking buffer for 1 hour at room temperature. Next they were washed 3 times for 5 minutes with 50-75 mL PBS. For secondary antibodies conjugated to horseradish peroxidase, membranes were incubated with HRP substrate kit (Biorad) according to manufacturer's instruction and imaged with the Molecular Imager® Gel Doc™ XR+ (Biorad) and Quantity One Software. For secondary antibodies conjugated to an infrared tag, membranes were imaged using the Odyssey Infrared Imaging System (LI-COR Biosciences) and analyzed using Odyssey Infrared Imaging System Application Software V3.0 (LI-COR Biosciences).

3.2.3.4.1 Western screening of stable knockdown cell lines

HA-Ank105-expressing stable knockdown cells that demonstrated extensive knockdown of target mRNA levels as indicated by qRT-PCR screening (3.1.2.4) were further screened by Western blot to confirm knockdown of target at the protein level. Lysates were generated from one 10 cm^2 plate of each knock down cell lines, as well as Ank105 parental and scrambled shRNA controls, under denaturing conditions (3.2.3.1), normalized to total protein content (3.2.3.1) and resolved by SDS-PAGE (3.2.3.2). Gels were transferred to nitrocellulose and protein expression was analyzed via Western blot (3.2.3.4) with anti-PDGFRβ (958), anti-GAPDH and target specific antibodies (Table 3.10).

3.2.4 Ligand stimulation of HA-Ank105-expressing cells

3.2.4.1 PDGF stimulation of HA-Ank105-expressing cells

The effects of Ank105 expression on PDGFR levels and signaling in NIH 3T3 cells stably expressing HA-Ank105 (Figure 4.1) were determined. Cells were cultured overnight in hi glucose DMEM with the addition of 0.5% FBS at 37 °C and 5% CO_2. Cells were either lest unstimulated, or stimulated for 30 minutes with PDGF (50 ng/mL) in serum free hi glucose DMEM (2 mL). Cells were placed on ice and stimulation media was aspirated. Cells were washed with cold PBS (5 mL). Cells were lysed under denaturing conditions in SDS sample buffer (3.2.3.1), normalized to total protein content (3.2.3.1), resolved by SDS-PAGE (3.2.3.2) and analyzed by Western blot (3.2.3.4) with indicated antibodies (Table 3.10) (Figure 4.1).

3.2.4.2 EGF stimulation of HA-Ank105-expressing cells

The effects of HA-Ank105 expression on EGFR levels and signaling in HEK293 and HeLa cells transiently transfected with HA-Ank105 were determined (Figure 4.2). HEK293 and HeLa cells were each transiently transfected with HA-Ank105 (3.2.2.2). When cell confluency reached approximately 80%, cells were cultured overnight in hi glucose DMEM with the addition of 0.5% FBS at 37 °C and 5% CO_2. Cells were either left unstimulated, or stimulated for indicated times (Figure 4.2) with EGF (80 nM) in serum free hi glucose DMEM (2 mL). Cells were placed on ice and stimulation media was aspirated. Cells were washed with cold PBS (5 mL). Cells were lysed under denaturing conditions in SDS sample buffer (3.2.3.1), normalized to

total protein content (3.2.3.1), resolved by SDS-PAGE (3.2.3.2) and analyzed by Western blot (3.2.3.4) with indicated antibodies (Table 3.10) (Figure 4.2).

3.2.5 Immunoprecipitation Studies

3.2.5.1 Immunoprecipitation of PDGFR from NIH 3T3 cells

The PDGFR was immunoprecipitated to determine the effects of HA-Ank105 expression on receptor activation and ubiquitination (Figure 4.3). HA-Ank105-expressing cells were cultured in standard cell culture media at 37 °C and 5% CO_2. When cell confluency reached approximately 80%, cells were cultured overnight in hi glucose DMEM with the addition of 0.5% FBS at 37 °C and 5% CO_2. Cells were stimulated for 0, 10 or 30 minutes with PDGF (50 ng/mL) in serum free hi glucose DMEM (2 mL). Cells were placed on ice and stimulation media was aspirated. Cells were washed with cold PBS (5 mL). Lysates of HA-Ank105-expressing cells were generated under non-denaturing conditions in PLC lysis buffer (3.2.3.1) with protease inhibitor cocktail (1 tablet per 50 mL) (Roche) and normalized to total protein content (3.2.3.1). Lysate (1 mg) was pre-cleared with rabbit IgG conjugated to agarose (Table 3.10) (10 µg) with the addition of protein A Sepharose beads (30 µL) (Sigma Aldrich) to immunoprecipitate proteins that non-specifically interact with IgG and beads. Lysates were nutated for 1 hour at 4 °C. Beads were pelleted by centrifugation and supernatant was saved for subsequent immunoprecipitations. To immunoprecipitate PDGFR, anti-PDGFR (958) antibody (10 µg) (Table 3.9) and protein A agarose beads (30 µL) were added to the supernatant. Samples were nutated at 4 °C for 90 minutes. Beads were pelleted by centrifugation and supernatant was aspirated. Beads were washed three times with HNTG wash buffer (1 mL) (Table 3.9). Immunoprecipitants were denatured (3.2.3.1), resolved by SDS-PAGE (3.2.3.2) and analyzed by Western blot (3.2.3.4) with indicated antibodies (Table 3.9) (Figure 4.3).

3.2.5.2 Immunoprecipitation of HA-Ank105 from NIH 3T3 cells

To determine if Ank105 interacts with ubiquitinated proteins, Ank105 was immunoprecipitated from HA-Ank105 stable cell lines and immunoprecipitants were analyzed for ubiquitinated proteins which co-immunoprecipitate with HA-Ank105 (Figure 4.4). HA-Ank105-expressing cells were cultured in standard cell culture media at 37 °C and 5% CO_2.

When cell confluency reach approximately 80%, cells were cultured overnight in hi glucose DMEM with the addition of 0.5% FBS at 37 °C and 5% CO_2. Cells were stimulated for 0, 3, 5 or 10 minutes with PDGF (50 ng/mL) in serum free hi glucose DMEM (2 mL). Cells were placed on ice and stimulation media was aspirated. Cells were washed with cold PBS (5 mL). Lysates of HA-Ank105-expressing cells were generated under non-denaturing conditions in PLC lysis buffer (3.2.3.1) with protease inhibitor cocktail (1 tablet per 50 mL). The three plates of lysate (1 mL total volume) were subjected to immunoprecipitation. Lysate was pre-cleared with mouse IgG conjugated to agarose (Table 3.9) (10 µg) with the addition of protein A Sepharose beads (30 µL) to immunoprecipitate proteins that non-specifically interact with IgG and beads. Lysates were nutated for 1 hour at 4 °C. Beads were pelleted by centrifugation and supernatant collected. To immunoprecipitate HA-Ank105, anti-HA (F7) antibody conjugated to agarose (10 µg) (Table 3.9) and protein A Sepharose beads (30 µL) were added to the supernatant. Samples were nutated at 4 °C overnight. Beads were pelleted by centrifugation and supernatant was aspirated. Beads were washed three times with HNTG was buffer (1 mL) (Table 3.9). Immunoprecipitants were denatured (3.2.3.1), resolved by SDS-PAGE (3.2.3.2) and analyzed by Western blot (3.2.3.4) with indicated antibodies (Table 3.9) (Figure 4.4). As a control, the immunoprecipitation procedure was also performed on untransfected NIH 3T3 cells; no ubiquitinated protein co-immunoprecipitated (data not shown).

3.2.5.3 Immunoprecipitation of HA-Ank105 from HEK293 cells

As a preliminary step to mass spectrometry, HA-Ank105 was immunoprecipitated from transiently transfected HEK293 cells to determine if a viable amount of Ank105 binding partners could be isolated for further analysis (Figure 4.25). HEK293 cells were transiently transfected with HA-Ank105 (3.2.2.2). When cells reached confluency, lysates were generated under non-denaturing conditions in PLC lysis buffer (3.2.3.1) with protease inhibitor cocktail (1 tablet per 50 mL). Amendment to lysis protocol: cellular debris was not immediately pelleted to increase solubilization of lysate. Five plates of lysate (1 mL total volume) were subjected to immunoprecipitation. Lysate was pre-cleared with mouse IgG conjugated to agarose (Table 3.9) (10 µg) with the addition of protein A Sepharose beads (30 µL) to immunoprecipitate proteins that non-specifically interacted with IgG and beads. Lysates were nutated for 1 hour at 4 °C. Beads and cellular debris were pelleted by two rounds of centrifugation at 14 x g. To

immunoprecipitate HA-Ank105, anti-HA antibody conjugated to agarose (10 µg) (Table 3.9) and protein A Sepharose beads (30 µL) were added to the supernatant. Samples were nutated at 4 °C for 2 hours. Beads were pelleted by centrifugation and supernatant was aspirated. Beads were washed five times with IP wash buffer (1 mL) (Table 3.9). Immunoprecipitants were denatured (3.2.3.1), resolved by SDS-PAGE (3.2.3.2) and analyzed by sypro ruby stain (Invitrogen) according to manufacturer's protocol. Sypro ruby stain is an effective alternative to Coomassie staining as it rapid, sensitive, low background, UV detectable stain and allows for the detection of low abundance proteins (Berggren *et al*., 2000). As a control an IP was performed with non-specific mouse IgG conjugated to agarose (Table 3.9) (10 µg) with the addition of protein A Sepharose beads (30 µL). In this manner, only proteins which specifically immunoprecipitate with anti-HA (F7) antibody are considered as HA-Ank105 binding partners.

3.2.6 Pulldown of HA-Ank105 with an ubiquitin-GST fusion protein

3.2.6.1 Induction and purification of ubiquitin-GST fusion protein

Ubiquitin-GST fusion plasmid (3.2.1.1), under the control of an IPTG inducible promoter, was transformed into competent BL21 *E. coli* (Novagen) and inoculated into 50 mL LB Broth containing ampicillin (100 µg/mL). Proteins containing GST without ubiquitin were also prepared similarly. Cultures were incubated overnight at 37 °C in a shaking incubator. Cultures were inoculated into LB broth (1 L) containing ampicillin (100 µg/mL) and incubated at 37 °C until the culture reached an optical density (600 nm) of 0.6 then induced with IPTG (0.1 mM) and incubated overnight at room temperature in a shaking incubator. Cells were divided into aliquots (100 mL) and pelleted by centrifugation at 4200 x g for 20 minutes at 4 °C. Supernatant was discarded. Cells were resuspended in PBS (10 mL) containing protease inhibitor cocktail (1 tablet per 50 mL) and lysozyme (1 mg/mL) (Sigma Aldrich) and incubated 1 hour at 4 °C to facilitate cell lysis. Lysate was sonicated three times for 30 seconds at setting 3 using a Model 250/450 Sonifier (Branson Ultrasonics). Triton X-100 (1% v/v) was added to lysate to facilitate solubilization. The triton x-100 insoluble fraction was pelleted by centrifugation at 12,000 x g for 30 minutes at 4 °C. Supernatant was passed through a 0.8 micron cellulose acetate membrane filter (Nalgene). Glutathione Sepharose beads (Amersham Biosciences) were prepared in PBS (50% v/v) according to manufacturer's instructions. Glutathione Sepharose

slurry (1 mL) was added to filtered lysate and incubated for 1 hour at 4°C. Beads were pelleted by centrifugation at 800 x g for 5 minutes at 4 °C. Beads were washed 3 times with cold PBS (50 mL). Beads were suspended in PBS (50% v/v) and stored at 4°C. A sample of the beads was prepared under denaturing conditions (3.2.3.1) and resolved by SDS-PAGE (3.2.3.2). Protein expression was examined and concentrations were approximated against bovine serum albumin (BSA) standards using Coomassie blue staining (3.2.3.3).

3.2.6.2 Generation of HA-Ank105 COS-1 lysates

pHA$_3$-Ank105 (3.2.1.2), pHA$_3$-Ank105 C-terminal deletion plasmids (3.2.1.3.1), pHA$_3$-Ank105 UIM mutant (3.2.1.3.5), pHA$_3$-Ank105 spectrin domain, pHA$_3$-Ank105 regulatory domain (3.2.1.3.2), pHA$_3$-Ank105 spectrin domain C-terminal deletion plasmids (3.2.1.3.3) and pHA$_3$-Ank105 N-terminal deletion plasmids (3.2.1.3.4) were individually transiently transfected (3.2.2.2) in COS-1 cells. Lysates were prepared under non-denaturing conditions (3.2.3.1) and stored at -20 °C. A sample of each lysate was denatured in SDS sample buffer (3.2.3.1), resolved by SDS-PAGE (3.2.3.2) and analyzed by Western blot (3.2.3.4) with anti-HA (F7) antibody (Table 3.9) for expression of each protein. Lysates were normalized according to the lowest expressing protein by diluting lysates with lysate from untransfected COS-1 cells.

3.2.6.3 Ubiquitin-GST pulldown

Pulldown experiments with ubiquitin-GST fusion protein (3.2.6.1) were performed with lysates expressing HA-Ank105 and various HA-Ank105 mutants (3.2.6.2) to assay ubiquitin binding and determine the region of Ank105 required for interaction with ubiquitin. Each of the normalized lysates (200 µL) were precleared with GST bound to glutathione Sepharose beads (100 µg) and glutathione Sepharose beads (30 µL) for 1 hour at 4 °C on a nutator to remove proteins from the lysate which non-specifically interact with GST or glutathione sepharose beads. Beads were pelleted by centrifugation at 14,000 x g for 10 min at 4 °C. Supernatant was collected and beads discarded. GST glutathione Sepharose beads (10 µg) or ubiquitin-GST glutathione Sepharose beads (10 µg) along with unbound glutathione Sepharose beads (30 µL) was added to each the normalized, precleared lysate (200 µL). Pulldowns were nutated at 4 °C for 90 minutes. Beads were pelleted by centrifugation at 5000 x g for 2 minutes at 4°C. Supernatant was aspirated and beads were washed 3 times with IP wash buffer (1 mL) (Table

3.8). SDS sample buffer was added to each pulldown (3.2.3.1) resolved by SDS-PAGE (3.2.3.2) and analyzed by Western blot (3.2.3.4) with anti-HA (F7) antibody (Table 3.9) to detect HA-Ank105 proteins that interact with ubiquitin.

3.2.7 Evaluation of endocytosis in HA-Ank105-expressing cells using small molecule inhibitors

3.2.7.1 Inducible constitutive PDGFR degradation assay

An inducible assay was developed to study constitutive PDGFR degradation in HA-Ank105-expressing cells (Figure 4.9). Constitutive degradation is the change in baseline PDGFR protein expression levels in the absence of ligand stimulation. HA-Ank105-expressing cells were cultured hi glucose DMEM (at pH 7.2) containing 1% FBS over night at 37 °C and 5% CO_2 to increase constitutive PDGFR levels. Media was replaced with standard cell culture media and cells were incubated for 0, 30 60 120 and 240 minutes at 37 °C and 5% CO_2 to induce constitutive PDGFR degradation. Lysate was generated under denaturing conditions (3.2.3.1) and normalized to total protein content (3.2.3.1). Lysates were resolved by SDS-PAGE (3.2.3.2) and analyzed by Western blot (3.2.3.4) with anti-PDGFR (958) and anti-GAPDH antibodies (Table 3.9).

3.2.7.2 Preparation of small molecule inhibitors

Each inhibitor was resuspended in either DMSO or water depending on solubility requirements (Table 3.11). Inhibitors were aliquoted and stored at -20 °C. A literature search revealed appropriate working concentrations of each of the inhibitors in the small molecule endocytosis inhibitor panel. For inhibitors preventing proper vesicle coat formation, pitstop concentrations from 10-30 μM have been demonstrated to inhibit CME (Dutta *et al*., 2012). A chlorpromazine concentration of 20 μM has also been demonstrated to significantly inhibit CME (Marina-Garcia *et al*., 2009). Acute treatment of cells with 10 mM MβCD has been demonstrated to deplete plasma membrane cholesterol (Rodal *et al*., 1999). To inhibit vesicle internalization, a concentration of 80 μM of dynasore impaired dynamin activity (Macia *et al*., 2006b). To inhibit cdc42 activity, a concentration of 10 μM is typically used, with no off target cellular effects observed with concentrations up to 100 μM (Martin-Granados *et al*., 2012; Surviladze Z, 2010).

Rac-1 activity was previously shown to be significantly inhibited with a 50 µM concentration of

Table 3.11: Small molecule inhibitors of endocytosis
Table lists small molecule inhibitors used in endocytosis studies along with their respective targets, molecular weights (M.W.) (g/mol), solvents in which they are soluble, catalogue numbers and suppliers. Inhibitors with similar function, such as blocking internalization, are grouped together and color coded.

Inhibitor	Catalogue	M.W.	Solubility	Target	Supplier
Pitstop2	ab120687	409.3	DMSO	Clathrin	Abcam
Chlorpromazine	C8138	355.33	H_2O	Clathrin	Sigma Aldrich
Methyl-β-cyclodextrin	C4555	1310	H_2O	Caveolin	Sigma Aldrich
Dynasore	ab120192	322.31	DMSO	Dynamin	Abcam
ML141	SML0407	407.49	DMSO	Cdc42	Sigma Aldrich
NSC 23766	553502	530.96	H_2O	Rac-1	EMD Millipore
Latrunculin A	L5288	421.55	DMSO	Actin	Sigma Aldrich
Jasplakinolide	J4580	709.68	DMSO	Actin	Sigma Aldrich
Nocodazole	M1404	301.3	DMSO	Microtubules	Sigma Aldrich
Monensin	M5273	692.85	DMSO	Na^+H^+ exchanger	Sigma Aldrich
EIPA	A3085	299.76	DMSO	Na^+ Channel	Sigma Aldrich
PP2	P0042	301.77	DMSO	SRC kinases	Sigma Aldrich
Wortmannin	W1628	428.43	DMSO	PI3K	Sigma Aldrich
MG132	474790	475.62	DMSO	Proteasome	Calbiochem
Chloroquine	C6628	515.86	H_2O	Lysosome	Sigma Aldrich

Inhibitors blocking coat formation
Inhibitors blocking internalization
Cytoskeleton inhibitors
Inhibitors of implicated proteins
Inhibitors of degradation pathways

NCS 23766 (Gao *et al*., 2004). For cytoskeletal inhibitors, latrunculin A concentrations from 0.01-1 µM have been demonstrated to inhibit actin dynamics (Krucker *et al*., 2000). Jasplakinolide concentrations from 0.05 to 5 µM have been demonstrated to inhibit actin polymerization (Bubb *et al*., 2000; Wang *et al*., 2002). Microtubule polymerization was inhibited at a concentration of 30 µM of nocodazole (Ausubel *et al*., 2007). Working concentrations of monensin range from 10-50 µM and disrupted proton gradients and endocytosis (Chen *et al*., 2009; Ippoliti *et al*., 1998). Macropinocytosis was inhibited by 100 µM 5-(N-Ethyl-N-isopropyl) amiloride (EIPA) (Gold *et al*., 2010; Meier *et al*., 2002), however a lower concentration of 40 µM have been demonstrated to inhibit sodium channels, the target of EIPA (Praetorius *et al*., 2000). Inhibition of Src family kinases with 4-Amino-5-(4-chlorophenyl)-7-(t-

butyl)pyrazolo[3,4-d]pyrimidine (PP2) has been demonstrated in the literature at a variety of concentrations. Inhibition of Src family kinase signaling generated from PDGFR signaling was accomplished at concentrations ranging from 10-50 μM (Yang *et al*., 2010), whereas inhibition of Src family kinases in endocytosis is often accomplished at lower concentrations of 0.01-10 μM (Balzac *et al*., 2005; Singh *et al*., 2006; Sorkina *et al*., 2002). For the inhibition studies performed in the thesis, concentration range of PP2 between 12.5-50 μM was employed (Table 3.12) Inhibition of PI3K signaling with wortmannin was accomplished with concentrations ranging from 0.1-5 μM (Clarke *et al*., 2001; Kjeken *et al*., 2001). To inhibit proteasomal degradation, concentrations of carbobenzoxy-Leu-Leu-leucinal (MG132) ranging between 1-10 μM are employed (Amanso *et al*., 2011; Ortiz-Lazareno *et al*., 2008). Lysosomal degradation is inhibited via chloroquine with concentrations ranging between 2-100 μM (Ignatiuk *et al*., 2006; Karch *et al*., 2012; Verschooten *et al*., 2012). While, the high range of chloroquine is listed as 50μM (Table 3.12) it was found that a concentration of 100 μM was most effective at inhibiting PDGFR degradation (Ignatiuk *et al*., 2006) and was used in LDL uptake (Figure 4.15), as well as constitutive (Figure 4.13) and ligand induced (Figure 4.17) PDGFR degradation studies. For each inhibitor used to study constitutive PDGFR endocytosis a range of concentrations were tested (Table 3.12). In the majority of cases the medium concentration of inhibitor was sufficient to observe the effect of the inhibitor and the medium concentration was used in subsequent experiments.

3.2.7.3 Disruption of constitutive endocytosis with small molecule inhibitors

To determine the effects of inhibition of endocytosis on constitutive PDGFR degradation in HA-Ank105-expressing cells, a range of concentrations of each inhibitor used (Table 3.12) (Figure 4.12; Figure 4.13). One 10 cm^2 plate of HA-Ank105-expressing cells per inhibitor treatment was cultured in standard cell culture media at 37 °C and 5% CO_2 to 80% confluency. Cells were then cultured in hi glucose DMEM containing 1% FBS over night at 37 °C and 5% CO_2 to increase constitutive PDGFR levels. Cells were then incubated with DMEM containing low, medium or high concentrations of each inhibitor (Table 3.12) for 30 minutes at 37 °C and 5% CO_2. This media was replaced with DMEM containing 10% FBS in the presence of each

Table 3.12: Working concentrations of small molecule inhibitors of endocytosis
Table lists small molecule inhibitors used in endocytosis studies along with their respective stock and working concentrations. Inhibitors with similar function, such as blocking internalization,

are grouped together and color coded.

Inhibitor	Stock (mM)	Low (µM)	Medium (µM)	High (µM)
Pitstop2	12.5	12.5	25	50
Chlorpromazine	14	25	50	100
Methyl-β-cyclodextrin	38.17	2000	5000	10000
Dynasore	100	40	80	160
ML141	25	12.5	25	50
NSC 23766	25	25	50	100
Latrunculin A	1	0.5	1	2
Jasplakinolide	1	0.5	1	2
Nocodazole	16.6	12.5	25	50
Monensin	28.26	12.5	25	50
EIPA	83.4	20	40	80
PP2	15	12.5	25	50
Wortmannin	5	2.5	5	10
MG132	10	5	10	20
Chloroquine	9.7	12.5	25	50

Inhibitors blocking coat formation
Inhibitors blocking internalization
Cytoskeleton inhibitors
Inhibitors of implicated proteins
Inhibitors of degradation pathways

respective inhibitor at low medium or high concentrations. Cells were incubated for 240 minutes at 37 °C and 5% CO_2 to induce constitutive PDGFR degradation, as determined previously (3.2.7.1). Control conditions where HA-Ank105-expressing cells were not cultured in 1% FBS (but cultured in 10% FBS), and HA-Ank105-expressing cells that were cultured overnight in media containing 1% FBS but were not stimulated in media containing 10% FBS were generated to provide a baseline of PDGFR expression levels in constitutive and serum-restricted conditions, respectively. Lysate was generated under denaturing conditions (3.2.3.1) and normalized to total protein content (3.2.3.1). Lysates were resolved by SDS-PAGE, transferred to a nitrocellulose membrane (3.2.3.2), and analyzed by Western blot (3.2.3.4) with anti-PDGFR (958) and anti-GAPDH antibodies (Table 3.10). Relative expression was quantified using Odyssey Infrared Imaging System Application Software V3.0 (LI-COR Biosciences) and replicate experiments were averaged. Statistical significance was determined for each inhibitor after 240 minutes of FBS incubation compared to untreated HA-Ank105-expressing cells after 240 minutes of FBS incubation by t-test (Microsoft Excel).

3.2.7.4 Optimization of Dil-LDL detection in HA-Ank105-expressing cells

In order to validate observations made on the effects of endocytosis inhibitors on constitutive PDGFR degradation in HA-Ank105-expressing cells the effects of these inhibitors were determined for the endocytosis of LDL. Uptake of LDL has been extensively characterized and proceeds by a clathrin and dynamin dependent mechanism and is trafficked to the lysosome (Luzio *et al*., 2007). LDL endocytosis was studied by quantifying uptake of LDL labeled with the lipophilic fluorescent dye dialkylcarbocyanine (Dil-LDL) (Invitrogen) in HA-Ank105-expressing cells. The reported excitation/emission maxima for Dil-LDL are 554 nm and 571 nm, respectively (Invitrogen).

The excitation and emission wavelengths used to detect Dil-LDL were optimized to facilitate Dil-LDL detection under experimental conditions and with available equipment. A range of concentrations of Dil-LDL (0, 10, 25, 50 and 100 μg/mL) were prepared in DMEM media and aliquoted into a standard 96 well cell culture plate (BD Falcon) (50 μL per well). Each concentration of Dil-LDL was tested with 4 replicate wells. Spectral excitation analysis was performed at a range of excitation wavelengths (530, 535, 540, 545, 550 and 555 nm) and a fixed emission (580 nm) wavelength with an emission cut off filter (570 nm) using a Spectramax M5 Multi-mode Microplate Reader (Molecular Devices) (Figure 3.3A). The excitation wavelength of 550 nm was chosen because it demonstrated the next highest level of fluorescence as compared to the reported excitation maxima, but with significantly less background (Figure 3.3A). Next a spectral emission analysis was performed. The excitation wavelength was fixed (550 nm) and fluorescence was measured at a range of emission wavelengths (570, 575, 580, 585, 590, 595 and 600 nm) with an emission cut of filter at 570 nm (Figure 3.3B). An emission wavelength of 580 nm was chosen because it demonstrated the highest fluorescence signal with low background signal (Figure 3.3B).

The experimental excitation (550 nm) and emission (580 nm) wavelengths for Dil-LDL in DMEM media were used to determine the optimal concentration of Dil-LDL in HA-Ank105-expressing cells. HA-Ank105-expressing cells were seeded into standard 96 well cell culture plates at a density of $5x10^4$ cells per well in standard cell culture media and cultured overnight at

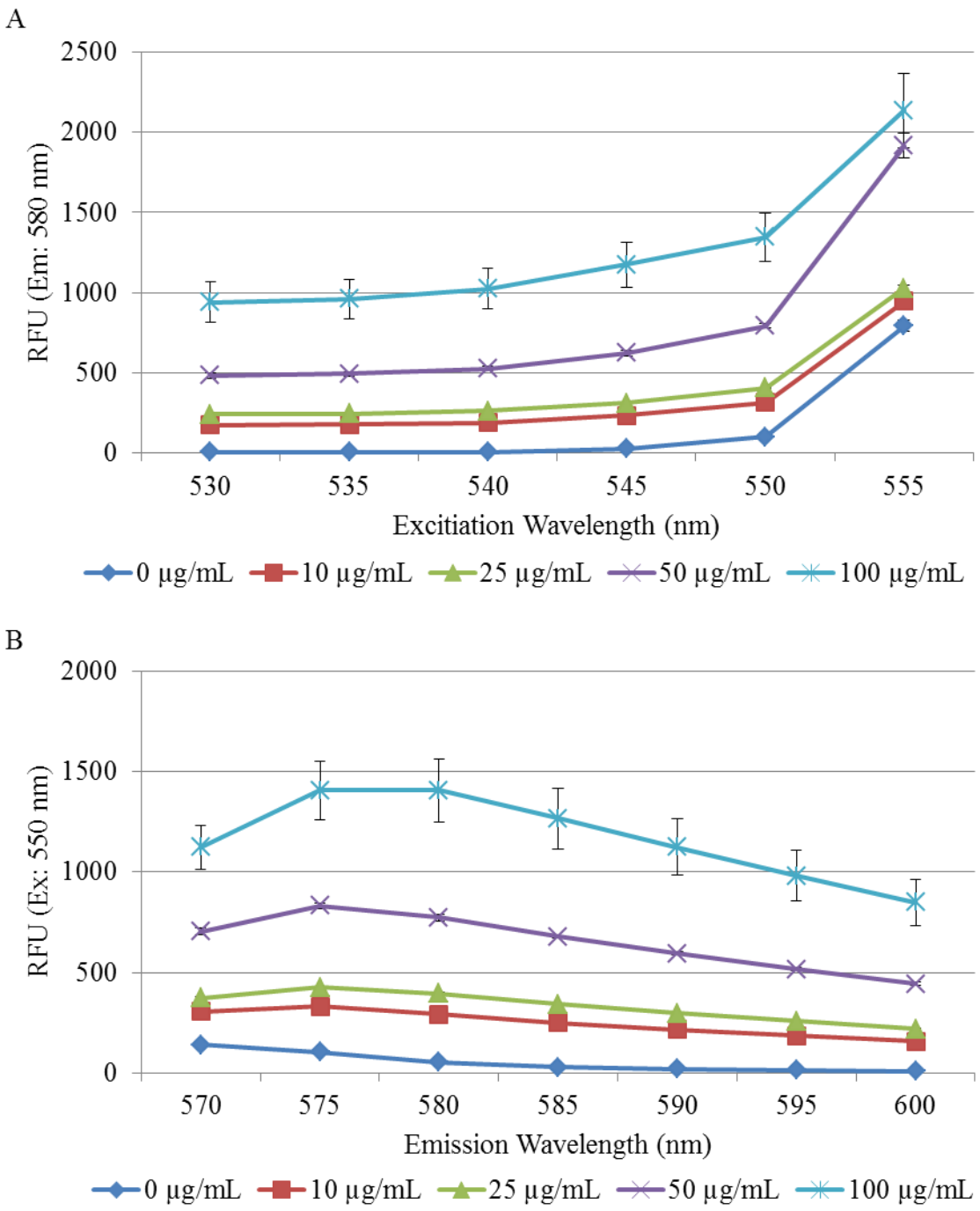

Figure 3.3: Determination of optimal excitation and emission wavelengths for detection of Dil-LDL.

Several concentrations of dialkylcarbocyanine-labeled LDL (Dil-LDL) were suspended in DMEM and aliquoted in 96 well cell culture plates. A. Spectral excitation and B. spectral emission analysis were performed using a Spectramax M5 Multi-mode Microplate Reader (Molecular Devices) to determine optimal experimental excitation and emission wavelengths for Dil-LDL.

37 °C and 5% CO_2. Media was aspirated and replaced with DMEM containing 0.5% FBS to maximize uptake of LDL. Cells were cultured overnight at 37 °C and 5% CO_2. Media was aspirated and HA-Ank105-expressing cells were incubated with increasing concentrations of Dil-LDL (10, 25, 50 and 100 μg/mL) (50 μL per well) for indicated times (0, 30, 60, 120, 240, 300 minutes). Each concentration of Dil-LDL and time point was tested with 4 replicate wells. Upon completion of incubation cells were placed on ice and washed gently 3 times with cold serum free DMEM (200 μL) to remove excess Dil-LDL. After the last wash step cells were placed in cold serum free DMEM (50 μL). LDL uptake was quantified as relative fluorescence signal intensity at excitation and emission wavelengths of 550 and 580 nm, respectively (Figure 3.4). The optimal concentration of Dil-LDL was determined to be 50 μg/mL, as the extent of uptake of Dil-LDL at a concentration of 50 μg/mL was similar to Dil-LDL at a concentration of 100 μg/mL (Figure 3.4).

3.2.7.5 LDL uptake assay

The effects of endocytosis inhibitors on LDL uptake in HA-Ank105-expressing cells were next determined (Figure 4.14; Figure 4.15). HA-Ank105-expressing cells were seeded into standard 96 well cell culture plates at a density of $5x10^4$ cells per well in standard cell culture media and cultured overnight at 37 °C and 5% CO_2. Media was aspirated and replaced with DMEM containing 0.5% FBS to maximize uptake of LDL. Cells were cultured overnight at 37 °C and 5% CO_2. Media was aspirated. Each of the small molecule endocytosis inhibitors were diluted to medium working concentration (Table 3.12) in DMEM and incubated with cells (50 μL per well) for 30 minutes at 37 °C and 5% CO_2 to allow equilibration of cells with each inhibitor prior to incubation with Dil-LDL. Media was aspirated. Both Dil-LDL (50 μg/mL) (3.2.7.4) and medium working concentrations of each small molecule endocytosis (Table 3.12) were suspended in DMEM and added to HA-Ank105-expressing cells (50 μL per well). Untreated HA-Ank105-expressing cells were incubated in DMEM (50 μL per well) containing only Dil-LDL (50 μg/mL). Cells were incubated at 37 °C and 5% CO_2 for a range of times (0, 30, 60, 120, 240, 300 minutes). Each condition was replicated in 4 wells to facilitate statistical analysis. Upon completion of incubation cells were placed on ice and washed gently 3 times with cold serum free DMEM (200 μL) to remove excess Dil-LDL. After the last wash step cells were placed in cold serum free DMEM (50 μL). LDL uptake was quantified as relative fluorescence

signal intensity at excitation and emission wavelengths of 550 and 580 nm, respectively. LDL uptake for each time point with each inhibitor was averaged and expressed as percent LDL uptake in untreated (no inhibitor) HA-Ank105-expressing cells after 300 minutes of incubation with Dil-LDL. Statistical significance was determined for each inhibitor after 300 minutes of Dil-LDL incubation compared to untreated HA-Ank105-expressing cells after 300 minutes of Dil-LDL incubation by t-test (Microsoft Excel).

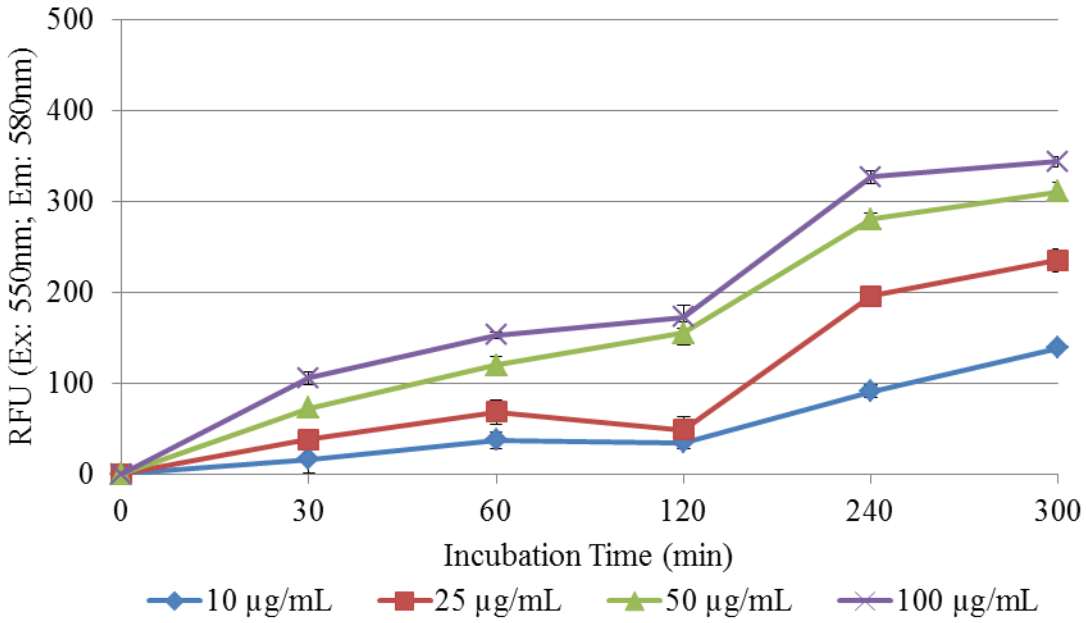

Figure 3.4: Optimization of Dil-LDL uptake in HA-Ank105-expressing cells.
HA-Ank105-expressing cells were seeded onto 96 well plates ($5x10^4$ cells per well) and cultured overnight. Cells were then starved overnight in DMEM containing 0.5% FBS. Cells were incubated with increasing concentrations (0, 25, 50, 100 µg/mL) of dialkylcarbocyanine-labeled LDL (Dil-LDL) for indicated times (0, 30, 60, 120, 240, 300). Cells were washed and LDL uptake was quantified relative fluorescence intensity at excitation/emission spectra of 550/580 nm.

3.2.7.6 In-cell Western detection of PDGFR in HA-Ank105-expressing cells

To study the effects of small molecule endocytosis inhibitors on ligand-mediated PDGFR degradation in HA-Ank105-expressing cells an in-cell Western methodology was developed to facilitate rapid screening of each inhibitor. HA-Ank105-expressing cells were seeded onto a 96 well plate at a density of $5x10^4$ cells per well and cultured overnight in standard cell culture media (150 µL per well) at 37 °C and 5% CO_2. Media was aspirated and cells were cultured in

DMEM containing 0.5% FBS overnight at 37 °C and 5% CO_2 to maximize effects of ligand stimulation. Each of the small molecule endocytosis inhibitors were diluted to medium working concentration (Table 3.12) in DMEM and incubated with cells (100 µL per well) for 30 minutes at 37 °C and 5% CO_2 to allow equilibration of cells with each inhibitor prior to stimulation with PDGF. Media was aspirated. Both PDGF (50 ng/mL) and medium working concentrations of each small molecule endocytosis (Table 3.12) were suspended in DMEM and added to HA-Ank105-expressing cells (100 µL per well). Untreated HA-Ank105-expressing cells were incubated in DMEM (100 µL per well) containing only PDGF (50 ng/mL). Cells were incubated at 37 °C and 5% CO_2 for a range of times (0, 30, 60, 120 and 240 minutes). Each condition was replicated in 4 wells to facilitate statistical analysis. Media was aspirated and cells were incubated in fixing buffer (Table 3.8) (200 µL per well) for 30 minutes at room temperature. Buffer was aspirated and replaced with PBS (Table 3.8) containing 0.5% (v/v) triton X-100 (sigma) (200 µL per well) to permeabilize the cell membrane. Cells were incubated at room temperature for 30 minutes on a nutator. Buffer was aspirated. Cells were incubated with blocking buffer (Table 3.8) (200 µL per well) for 30 minutes at room temperature on a nutator. Buffer was aspirated. Blocking buffer containing anti-PDGFRβ (C82A3) primary antibody (Table 3.10) was added to cells (50 µL per well) and incubated at room temperature for 1 hour on a nutator. Primary antibody solution was aspirated and cells were washed gently 3 times with PBS (150 µL per well). Cells were incubated with blocking buffer (50 µL per well) containing anti-rabbit IgG 680RD secondary antibody (Table 3.10) at room temperature for 1 hour on a nutator. Secondary antibody solution was aspirated and cells were washed gently 3 times with PBS (150 µL per well). PBS (100 µL per well) was placed on cells and the plate was imaged using the Odyssey Infrared Imaging System (LI-COR Biosciences) using a focal offset of 4 mm to focus on the surface containing the cells (Figure 3.5) and quantified using Odyssey Infrared Imaging System Application software V3.0.

Serum starved HA-Ank105-expressing cells not stimulated with PDGF demonstrate the highest signal intensity (Figure 3.5). Upon ligand stimulation PDGFR is degraded with the most extensive degradation, and lowest signal intensity, occurring after 240 minutes of stimulation. Indeed the in-cell Western methodology can detect effects of endocytosis inhibitors on PDGFR degradation. In dynasore treated HA-Ank105-expressing cells, the signal intensity after 240 minutes of ligand stimulation is similar to unstimulated cells (Figure 3.5). Relative PDGFR

expression was quantified using Odyssey Infrared Imaging System Application software V3.0 (LiCOR Biosciences) and replicate experiments were averaged. Statistical significance was determined for each inhibitor after 240 minutes of PDGF stimulation compared to untreated HA-Ank105-expressing cells after 240 minutes of PDGF stimulation by t-test (Microsoft Excel).

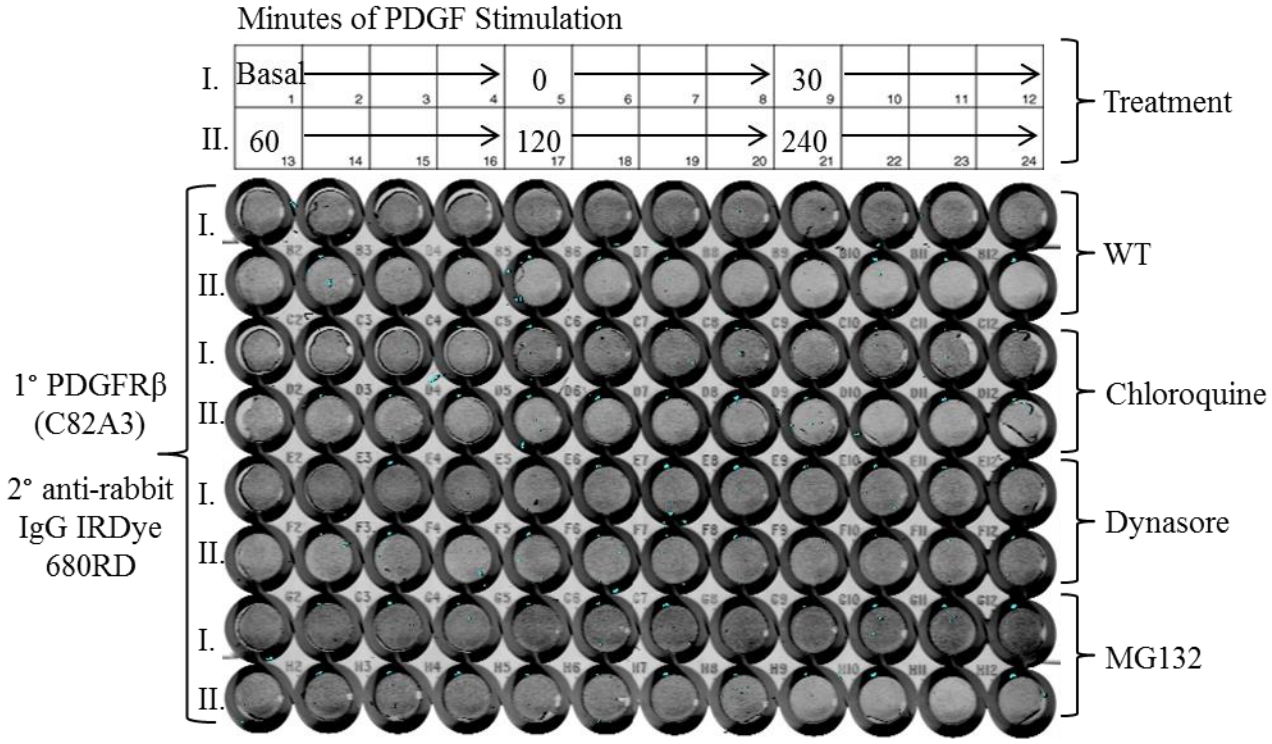

Figure 3.5: In-cell detection of PDGFR in ligand stimulated HA-Ank105-expressing cells treated with various small molecule endocytosis inhibitors

Serum starved HA-Ank105-expressing cells were treated with indicated inhibitors (Table 3.12) and then stimulated media containing PDGF (50 ng/mL) and inhibitor for a range of times (0, 30, 60, 120 and 240 minutes) according to provided scheme. Cells were fixed, permeabilized and incubated with primary antibody (Table 3.10), followed by secondary antibody (Table 3.10) to detect PDGFR levels.

4.0 RESULTS

4.1 Characterization of the effects of HA-Ank105 expression on PDGFR signaling and protein levels

Our laboratory had identified Ank105 as a binding partner of the regulatory subunit of PI3K (Ignatiuk *et al*., 2006). Since PI3K is a downstream component of the PDGFR signaling cascade, the effects of Ank105 expression were examined in the context of PDGFR and PI3K signaling. It was shown that overexpression of Ank105 enhanced degradation of the PDGFR (Ignatiuk *et al*., 2006). Since this observation was made in a single stable clonal NIH 3T3 cell line, initial studies were carried out to determine if the level of Ank105 expression was proportional to PDGFR degradation. Cell lines showing a range in Ank105 expression were selected for analysis. Parental NIH 3T3 cells and cells stably expressing low, medium and high levels, respectively, of hemagluttinin tagged Ank105 (HA-Ank105) were stimulated for 30 minutes with PDGF. Lysates were harvested, normalized to total protein content and analyzed via SDS-PAGE and Western blot analysis to evaluate HA-Ank105 expression, PDGFR expression, PDGFR activation, as well as activation of downstream signaling pathways, namely AKT and MAPK (Figure 4.1).

Parental NIH 3T3 cells qualitatively show activation of the PDGFR, as indicated by phospho-tyrosine (pTyr) specific antibody detecting pTyr on the PDGFR after 30 minutes of ligand stimulation, as well as robust activation of downstream AKT and MAPK pathways. PDGFR protein levels are predictably reduced upon ligand stimulation, indicating a functional degradation pathway. The total levels of AKT and MAPK on the other hand did not change in response to stimulation. Qualitatively, expression of increasing levels of HA-Ank105 led to decreased constitutive (no stimulation) expression levels of PDGFR compared to parental cells. Stimulation of HA-Ank105-expressing cells with PDGF predictably reduced PDGFR levels further. Levels of activated PDGFR, AKT and MAPK after 30 minutes of PDGF stimulation were dramatically reduced in HA-Ank105-expressing cells as compared to parental cells, with the greatest impact being on the activation of PDGFR and MAPK. The total levels of AKT and MAPK proteins themselves remained consistent across the low, medium and high Ank105-expressing cell lines. Ank105-mediated constitutive PDGFR degradation is dependent on the level of HA-Ank105 expression. The extent of reduction in constitutive PDGFR levels and

signaling activation in response to ligand tended to increase as HA-Ank105 expression increased. This trend was most evident when the activation of the PDGFR was examined as the high Ank105-expressing cell line appeared most attenuated when stimulated with ligand.

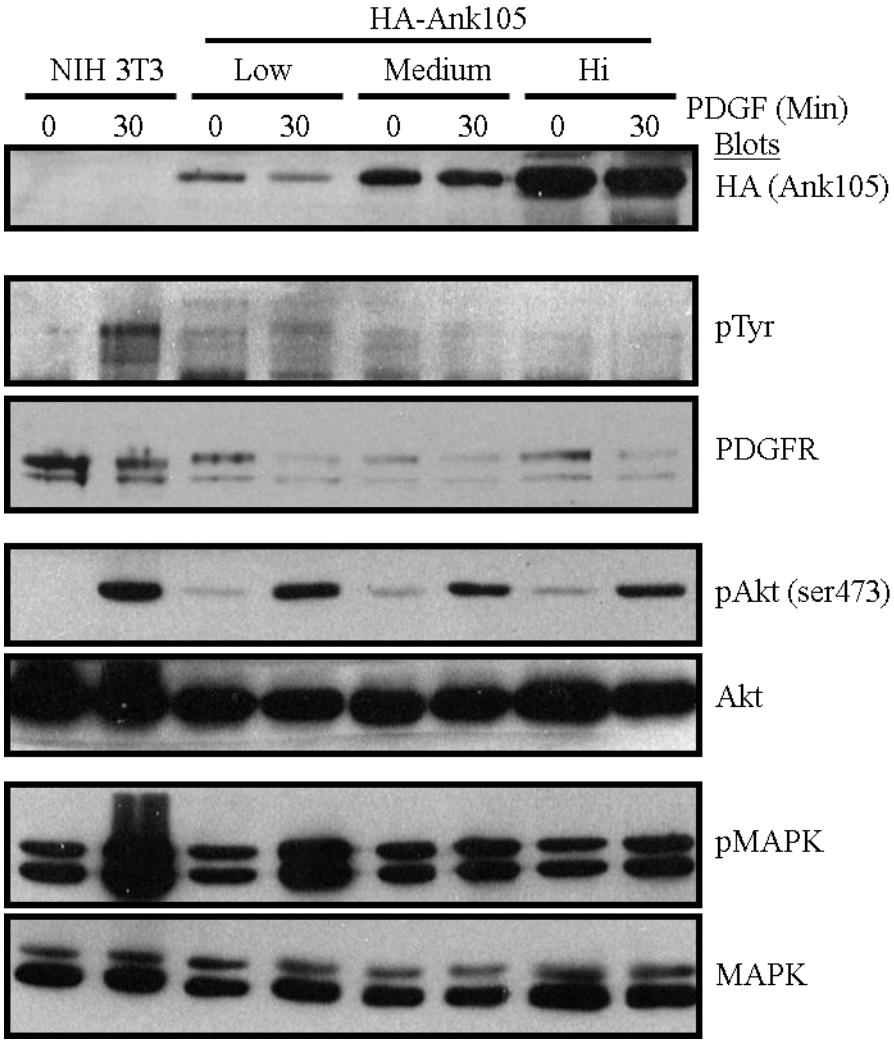

Figure 4.1: HA-Ank105 expression reduced PDGFR signaling and receptor levels
Untransfected control NIH 3T3 cells and cells stably expressing low, medium and high levels of HA-Ank105 were either left untreated (0 ng/mL) or treated for 30 minutes with PDGF (50 ng/mL) for 30 minutes. Cell lysates (20 μg) were resolved by SDS-PAGE and transferred to a nitrocellulose membrane. The nitrocellulose membranes were analyzed via Western blot to detect Ank105 expression (HA), PDGFR expression and activation (pTyr), Akt expression and activation (pAkt), as well as MAPK expression and activation (pMAPK). Western blots were developed using chemiluminescence and evaluated qualitatively. Results are representative of those from 3 independent experiments (N=3).

One caveat is the cell line expressing the highest level of HA-Ank105 has higher levels of constitutive PDGFR than the cell line expressing medium levels of HA-Ank105. It may be

possible that at very high expression levels of Ank105, the endocytic cellular machinery became over saturated with Ank105 and excess Ank105 could sequester its binding partners, thereby impairing Ank105 function. Quantitatively determining the relative expression of each band proved challenging as Western blots were developed using chemiluminescence. Oversaturation of several bands made analysis by densitometry difficult. However, caveats aside, this experiment demonstrated the trend that expression of Ank105 in NIH 3T3 cells promoted PDGFR degradation and attenuated PDGFR signaling in response to ligand. Indeed, phosphorylation of Akt was detected in all Ank105 stable cell lines in the absence of PDGF stimulation, possibly due to overexposure of the Western blot. Since the cell line that expressed medium levels of Ank105 demonstrated the most significant effect on constitutive PDGFR protein levels, this cell line was used in all subsequent experiments unless indicated otherwise.

4.2 Characterization of the effects of HA-Ank105 expression on EGFR protein expression levels

Since Ank105 promoted the degradation of PDGFR, we next determined whether HA-Ank105 expression could promote the degradation of other related RTKs. The effect of HA-Ank105 expression was determined for EGFR degradation. Increasing amounts of HA-Ank105 were transiently transfected into HEK293 and HeLa cells. Both cell lines endogenously express EGFR. Cells were stimulated with EGF for indicated times. Lysates were harvested, normalized to total protein content and analyzed via SDS-PAGE and Western blot analysis to evaluate HA-Ank105 expression, EGFR expression and EGFR activation, as approximated by Western blot detection of tyrosine phosphorylation at the expected molecular weight of EGFR (Figure 4.2). In HEK293 cells constitutive EGFR levels decreased as HA-Ank105 expression increased. The extent of EGFR activation was reduced in HA-Ank105-expressing HEK293 cells upon EGF stimulation as compared to untransfected control cells. Transfection of the spectrin binding domain of Ank105, lacking the regulatory domain, was sufficient to induce EGFR degradation; whereas, transfection of the regulatory domain, lacking the spectrin binding domain, did not affect EGFR degradation (data not shown). In HeLa cells, constitutive EGFR levels did not change in response to HA-Ank105 transfection. EGFR was activated to a similar extent upon EGF stimulation in HA-Ank105-expressing HeLa cells as untransfected control cells. HeLa cells also endogenously express PDGFR, albeit at much lower levels than NIH 3T3 cells. Expression

of HA-Ank105 in HeLa cells ablated PDGFR expression as compared to untransfected control cells. Thus HA-Ank105 expression differentially affects constitutive EGFR levels in HEK293 cells versus HeLa cells. It may be that HEK293 cells express some additional factor, such as an adaptor protein, that sensitizes EGFR to Ank105-mediated degradation that is not expressed in HeLa cells; however this possibility was not explored further.

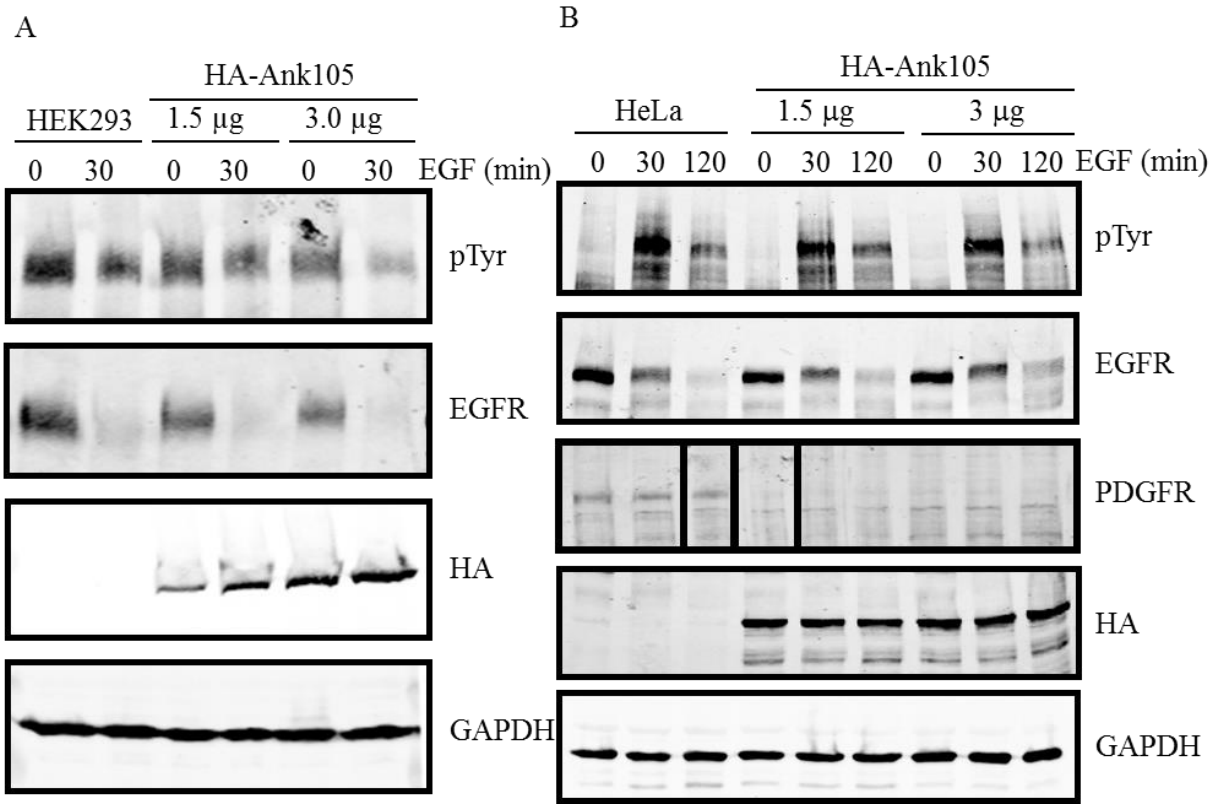

Figure 4.2: HA-Ank105 expression differentially affects EGFR degradation in HEK293 and HeLa cells.

A. HEK293T cells transiently transfected with increasing concentrations of HA-Ank105 (0, 1.5, 3.0 µg DNA) were either left unstimulated (0 ng/mL) or stimulated with EGF (20 ng/mL) for indicated times. Cell lysates (50 µg) were resolved by SDS-PAGE and transferred to a nitrocellulose membrane. The nitrocellulose membranes were analyzed via Western blot to detect Ank105 expression (HA), EGFR expression and EGFR activation (pTyr). Results are representative of those from 3 independent experiments (N=3). B**.** HeLa cells transiently transfected with increasing concentrations of HA-Ank105 (0, 1.5, 3.0 µg DNA) were stimulated with EGF (20 ng/mL) for indicated times. Lysates (50 µg) were analyzed with indicated antibodies Cell lysates (50 µg) were resolved by SDS-PAGE and transferred to a nitrocellulose membrane. The nitrocellulose membranes were analyzed via Western blot to detect Ank105 expression (HA), EGFR expression, EGFR activation (pTyr) and PDGFR expression. N=1.

4.3 Effects of HA-Ank105 expression on PDGFR ubiquitination and lysosomal degradation

Trafficking of activated receptor complexes to the lysosome for degradation requires monoubiquitination of receptor. Since Ank105 promoted degradation of the PDGFR, we examined PDGFR ubiquitination in HA-Ank105-expressing cells. NIH 3T3 cells and cells stably expressing HA-Ank105 were stimulated for a time course up to 30 minutes with PDGF. Lysates were generated and PDGFR was immunoprecipitated from each sample. Immunoprecipitants were resolved via SDS PAGE and examined via Western blot for PDGFR levels, PDGFR activation and PDGFR ubiquitination (Figure 4.3A). In NIH 3T3 cells, immunoprecipitated PDGFR is highly phosphorylated and ubiquitinated after 10 minutes of PDGF stimulation, which persists to 30 minutes of stimulation. PDGFR levels are only slightly reduced after 10 minutes of stimulation (Figure 4.3A). HA-Ank105-expressing cells again show a dramatic reduction in constitutive PDGFR levels as compared to parental cells and are hardly detectable after 30 minutes of stimulation (Figure 4.3A). The PDGFR was ubiquitinated after 10 minutes of stimulation in HA-Ank105-expressing cells, but to a lesser extent than the parental cells. The level of PDGFR ubiquitination was dramatically reduced after 30 minutes of stimulation; whereas PDGFR ubiquitination in parental cells was robust after 30 minutes of stimulation (Figure 4.3A). The PDGFR was phosphorylated after 10 minutes of stimulation; however the level phosphorylation is markedly reduced after 30 minutes of stimulation. In contrast the parental cells demonstrate robust PDGFR phosphorylation after 30 minutes of stimulation (Figure 4.3A). Interestingly the PDGFR displays a different phosphorylation pattern in HA-Ank105-expressing cells than in parental cells. The anti-phospho-tyrosine antibody detects higher molecular weight species in HA-Ank105-expressing cells, suggesting the PDGFR may be more highly phosphorylated upon stimulation in HA-Ank105-expressing cells than in parental cells (Figure 4.3A). Cells were not stimulated past 30 minutes in this experiment as phosphorylation and ubiquitination of the PDGFR in HA-Ank105-expressing cells occurred predominantly after 10 minutes of stimulation and the signal attenuated after 30 minutes. The lack of extensive smearing and laddering in the ubiquitination blots of immunoprecipitated PDGFR in both NIH 3T3 and HA-Ank105-expressing cell indicated that the PDGFR was likely monoubiquitinated (Figure 4.3A). Taken together these results indicate that HA-Ank105 expression reduced PDGFR phosphorylation and ubiquitination in response to ligand stimulation, possibly by inducing constitutive degradation of PDGFR.

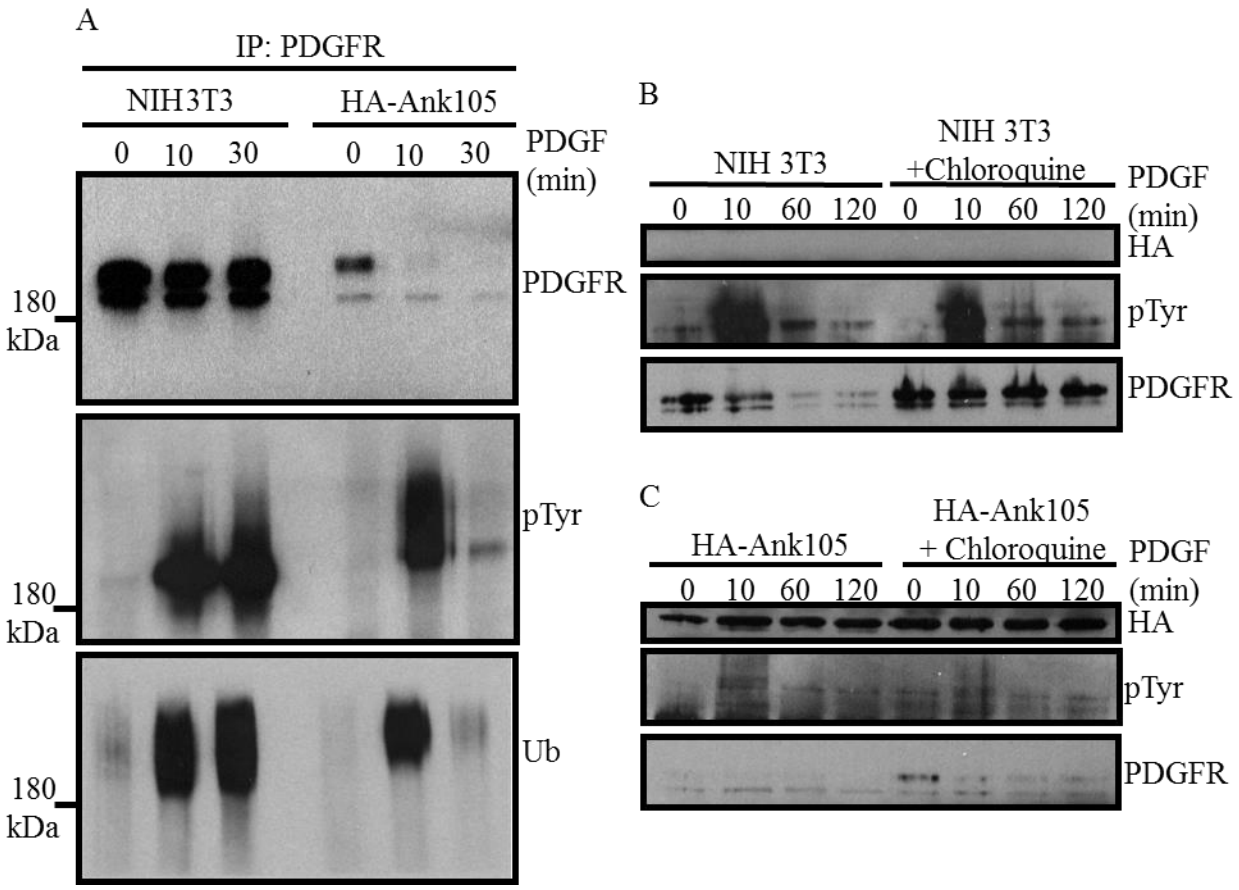

Figure 4.3: Ligand-induced ubiquitination of PDGFR is reduced in HA-Ank105-expressing cells while not requiring a functional lysosomal pathway for degradation.
A. NIH 3T3 or HA-Ank105-expressing cells were either left unstimulated (0 ng/mL) or stimulated for indicated times with PDGF (50 ng/mL). PDGFR was immunoprecipitated from cell lysates, resolved via SDS PAGE, transferred to a nitrocellulose membrane and analyzed via Western blot for PDGFR levels, activation (pTyr) and ubiquitination (Ub). Results are representative of those from 3 independent experiments (N=3). B. NIH 3T3 cells and C. HA-Ank105-expressing cells were either left untreated or treated for 4 hours with chloroquine (100 μM) and stimulated for indicated times with PDGF (50 ng/mL). Lysates were normalized to total protein content (50 μg), resolved via SDS-PAGE, transferred to a nitrocellulose membrane and analyzed by Western blot for HA-Ank105 expression, PDGFR expression and PDGFR activation (pTyr). Results are representative of those from 3 independent experiments (N=3).

Since activated, ubiquitinated receptors are sorted to the lysosome for degradation it was next determined whether HA-Ank105-expressing cells required a functional lysosomal pathway to target ligand stimulated PDGFR for degradation. NIH 3T3 cells and cells stably expressing HA-Ank105 were either untreated or treated for 4 hours with the lysosomal degradation inhibitor chloroquine (Figure 4.3B,C). Chloroquine is a tertiary amine that raises the pH of the lysosome, thereby inactivating low pH-dependent proteases required for protein degradation (Heldin *et al*.,

1982). After treatment with chloroquine, cells were stimulated for a 120 minute time course with PDGF. Lysates were harvested, normalized to total protein content, resolved by SDS-PAGE and analyzed by Western blot for HA-Ank105 expression, PDGFR expression and PDGFR activation.

In NIH 3T3 cells not treated with chloroquine the PDGFR is progressively degraded following PDGF stimulation, with the greatest extent of degradation after 120 minutes of stimulation (Figure 4.3B). The PDGFR is phosphorylated to the highest extent after 10 minutes of stimulation and tapers off as the time course progresses (Figure 4.3B). Treatment of NIH 3T3 cells with chloroquine inhibits ligand induced PDGFR degradation. In chloroquine treated cells, the level of PDGFR present after 120 minutes of PDGF stimulation is similar to the constitutive level observed prior to stimulation (Figure 4.3B). With regards to receptor phosphorylation, the activation profile of PDGFR in chloroquine treated cells mirrors untreated cells, with the highest extent of phosphorylation occurring after 10 minutes of stimulation and tapering off at later time points (Figure 4.3B).

In Ank105-expressing cells not treated with chloroquine, constitutive PDGFR expression levels are markedly reduced as compared to parental cells, as expected. Stimulation of HA-Ank105-expressing cells with PDGF lead to further reduction in receptor levels (Figure 4.3C). When examined for receptor activation, HA-Ank105-expressing cells showed peak phosphorylation levels after 10 minutes of stimulation, which decreased at later time points. The level of phosphorylation in HA-Ank105-cells was significantly lower than parental cells (Figure 4.3C). In chloroquine treated HA-Ank105-expressing cells there was a slight increase in constitutive PDGFR levels, however the level was still much lower than constitutive PDGFR in control cells (Figure 4.3C). Chloroquine treatment partially blocked PDGFR degradation in response to ligand in HA-Ank105-expressing cells whereas chloroquine treatment completely blocked ligand induced degradation in control NIH 3T3 cells. The PDGFR phosphorylation profile upon ligand stimulation in chloroquine treated HA-Ank105-expressing cells mirrored that of non-chloroquine treated HA-Ank105-expressing cells (Figure 4.3C). Thus inhibition of lysosomal degradation via chloroquine treatment completely inhibited ligand induced degradation in NIH 3T3 cells and partially inhibited degradation in HA-Ank105-expressing cells. Treatment of HA-Ank105-expressing cells with chloroquine partially recovered constitutive PDGFR levels. This data suggests that Ank105 may promote constitutive PDGFR degradation by

a lysosomal-mediated mechanism. Possible explanations for only a slight increase in constitutive PDGFR levels is that PDGFR in this cell model is under control of an endogenous promoter and 4 hours of chloroquine treatment may be insufficient to increase PDGFR levels to those observed constitutively in NIH 3T3 cells. Treatment times longer than 4 hours have proved toxic. An alternative explanation is that Ank105 mediates the majority of its effect on PDGFR levels via proteasomal degradation.

4.4 HA-Ank105 interacts with ubiquitin and ubiquitinated proteins

An overlying trend in the sorting of ubiquitinated cargo for lysosomal degradation is the ability of the sorting machinery is to recognize monoubiquitinated cargo by interacting with the ubiquitin tag itself. Additionally, these proteins are often ubiquitinated themselves. Since HA-Ank105 promotes degradation of the PDGFR, the ability of HA-Ank105 to interact with monoubiquitin using a pulldown methodology was determined. pHA_3-Ank105 was transiently transfected into COS-1 cells. COS-1 cells were chosen due to high transfection efficiency and high protein expression levels of transfected proteins. Lysates from COS-1 cells transiently overexpressing HA-Ank105 were incubated with either purified monoubiquitin-glutathione-S transferase (Ub-GST) fusion protein or glutathione-S transferase (GST) protein, both of which were bound to glutathione sepharose beads. Following incubation, beads were separated from lysate by several centrifugation and washing steps. Samples were then resolved by SDS-PAGE and analyzed via Western blot to detect the presence of HA-Ank105 (Figure 4.4A). If HA-Ank105 specifically interacts with ubiquitin it will be bound to Ub-GST beads, but not to GST beads. Indeed, HA-Ank105 was readily detectable in an Ub-GST pulldown but not in a control GST pulldown (Figure 4.4B), indicating that HA-Ank105 interacted with monoubiquitin *in vitro*.

Given that HA-Ank105 interacted with purified recombinant ubiquitin in an *in vitro* assay it was next determined whether HA-Ank105 was able to interact with ubiquitinated proteins in cells. NIH 3T3 cells stably expressing HA-Ank105 were stimulated for indicated times with PDGF and HA-Ank105 was immunoprecipitated from resulting lysates at each time point. Immunoprecipitants were resolved by SDS-PAGE and analyzed by Western blot for ubiquitinated proteins that co-immunoprecipitate with HA-Ank105. Western blot reveals that

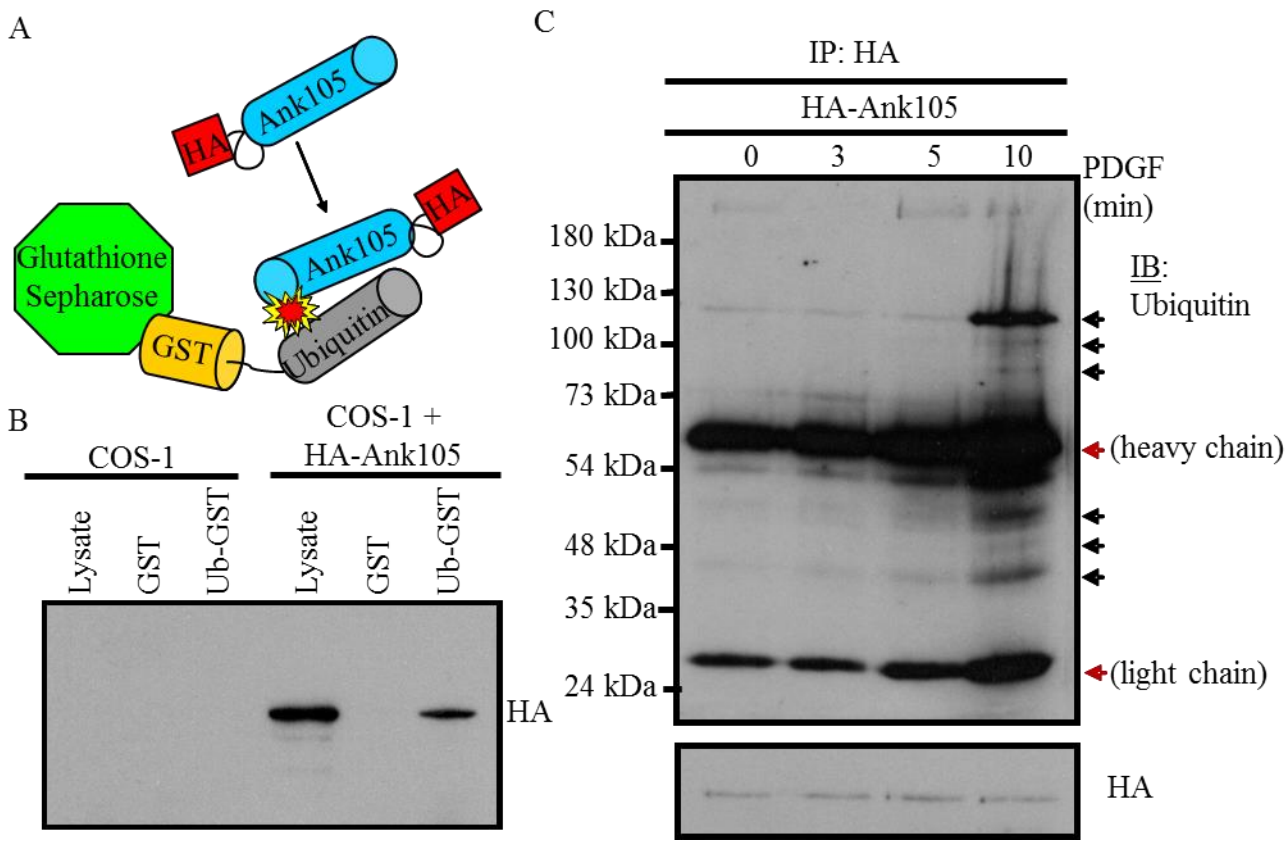

Figure 4.4: HA-Ank105 interacts with ubiquitin *in vitro* and several ubiquitinated proteins in cells.
A. Diagram of pulldown experiment. B. Lysates from untransfected COS-1 cells and cells transiently transfected with HA-Ank105 were incubated with either GST (100 µg) or ubiquitin-GST (Ub-GST) (100 µg) immobilized on glutathione sepharose beads. Proteins bound to beads were resolved via SDS-PAGE and analyzed by Western blot for the presence of HA-Ank105. Results are representative of those from 3 independent experiments (N=3). C. NIH 3T3 cells stably expressing HA-Ank105 were starved overnight in DMEM containing 0.5% FBS and then stimulated for indicated times with PDGF (50 ng/mL). HA-Ank105 was immunoprecipitated with anti-HA antibody immobilized on protein G-sepharose beads. Immunoprecipitants were resolved by SDS-PAGE. Ubiquitinated proteins which co-immunoprecipitate with HA-Ank105 were detected with an anti-ubiquitin antibody via Western blot. Ubiquitinated proteins are indicated with black arrows and the light and heavy antibody chains are indicated with red arrows. N=1.

several ubiquitinated proteins co-immunoprecipitated with HA-Ank105 after 10 minutes of PDGF stimulation (Figure 4.4C). An intense band is visible between the 100 and 130 kDa molecular weight markers, a weight range that may correspond to HA-Ank105 (Figure 4.4C). Since the antibodies used for immunoprecipitation of HA-Ank105 and detection of ubiquitin had the same species origin, the heavy and light antibody chains are present in all time points tested

(Figure 4.4C). The Western blots in this this experiment were developed by chemiluminescence and as a result, the bands representing the heavy and light chains were overexposed. This overexposure was necessary to observe low abundance ubiquitinated proteins that co-immunoprecipitated with HA-Ank105 (Figure 4.4). This data suggests that HA-Ank105 interacts with several ubiquitinated proteins under conditions that induce ligand-mediated PDGFR degradation and that HA-Ank015 may be ubiquitinated.

4.5 HA-Ank105 interacts with ubiquitin via the spectrin binding domain

Since HA-Ank105 interacted with purified ubiquitin *in vitro* and several ubiquitinated proteins in cells it was next determined how HA-Ank105 interacted with ubiquitin. The primary sequence of Ank105 revealed a potential ubiquitin interaction motif (UIM) from amino acids 1880 to 1894 within the regulatory domain. This potential UIM of Ank105 conformed well to the published consensus sequence (Fujiwara *et al*., 2004) and contained conserved alanine and serine residues (Figure 4.5A). UIMs fold into a single α-helix that interact with surface residues of ubiquitin (Fujiwara *et al*., 2004). In order to determine if this putative UIM facilitated Ank105-ubiquitin interaction, a rational mutagenesis strategy was employed. The conserved serine residue 1891 (Figure 4.5B) was mutated to aspartic acid as this mutation was previously shown to abrogate UIM-ubiquitin binding (Fujiwara *et al*., 2004). As a complimentary methodology, deletion mutagenesis was also performed. Truncation mutants of HA-Ank105 were generated to progressively remove 50 amino acids at a time from the C-terminus of Ank105 until the putative, predicted, UIM was deleted (Figure 4.5B). Removal of 100 C-terminal amino acids was sufficient to delete the putative UIM. These proteins were evaluated for the ability to interact with ubiquitin via an Ub-GST pulldown experiment. Point mutation of the conserved serine residue to aspartic acid has been shown previously to prevent UIM-ubiquitin interaction (Fujiwara *et al*., 2004). The HA-Ank105-S1891D mutant retained the ability to interact with the Ub-GST fusion protein (Figure 4.5B,C). Indeed, HA-Ank105-C-terminal deletion mutants where the putative UIM was entirely removed also retained the ability to interact with ubiquitin. Thus, all mutants retained the ability to interact with ubiquitin (Figure 4.5B,C). Of note, the proteins showed some background binding to the GST control; however the band intensity of Ub-GST were consistently greater (Figure 4.5B,C). This data suggests that this putative UIM, which conformed well to the consensus sequence, does not mediate the Ank105-ubiquitin interaction

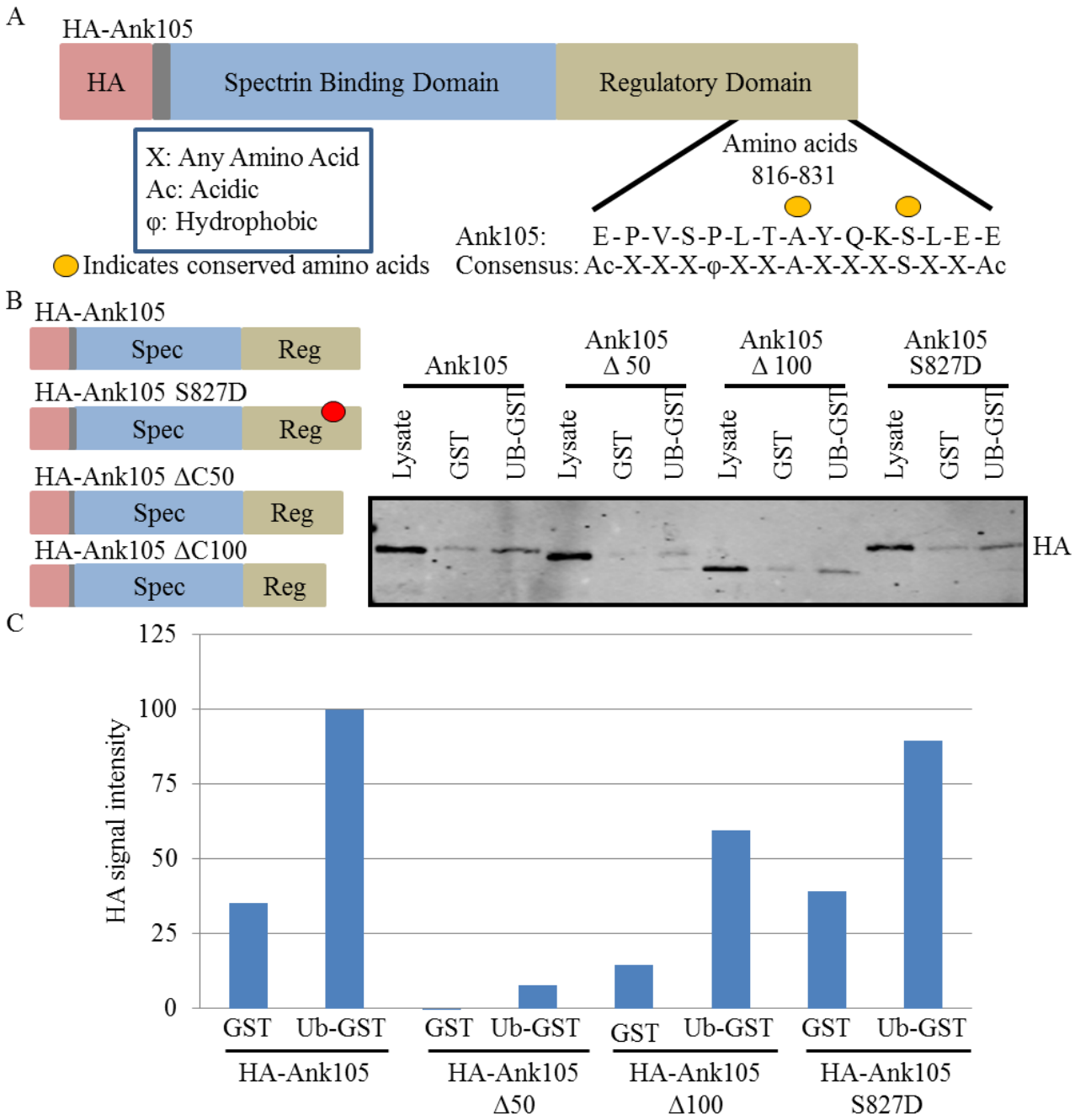

Figure 4.5: Mutation of proposed UIM of Ank105 does not prevent ubiquitin binding

A. Potential UIM within the C-terminal regulatory domain of Ank105 and its consensus sequence. The essential amino acids are highlighted. B**.** COS-1 cells were transiently transfected with indicated HA-Ank105 mutant proteins. Lysates were incubated with either GST (100 µg) or ubiquitin-GST (Ub-GST) (100 µg) immobilized on glutathione sepharose beads. Proteins bound to beads were resolved via SDS-PAGE, transferred to a nitrocellulose membrane and analyzed by Western blot for the presence of HA-Ank105 mutant proteins. Results are representative of those from 3 independent experiments (N=3). C. Quantification of Figure 4.5B. Only one blot was quantified as other replicates were developed using chemilumenescence. Yellow dots indicate conserved amino acids. Red dots indicate point mutations.

and raised the question as to which region of Ank105 confers the ability to bind ubiquitin.

To determine the region of Ank105 responsible for mediating ubiquitin interaction the domains of Ank105, being the spectrin binding domain and the regulatory domain, were individually evaluated for the ability to bind ubiquitin using Ub-GST pulldown experiments (Figure 4.6). Both full length HA-Ank105 and the HA-spectrin-binding-domain, lacking the regulatory domain, interacted with the Ub-GST fusion protein (Figure 4.6A,B). The HA-regulatory-domain, lacking the spectrin binding domain, was unable to interact with the Ub-GST fusion protein (Figure 4.6A,B). Even though the overall signal intensity is relatively weak and each of the GST control lanes contains background binding (Figure 4.6A), the signal intensity of the Ub-GST lanes are consistently higher than the GST lanes. This data suggests that the Ank105-ubiquitin interaction is mediated via spectrin binding domain and not the regulatory domain.

Several C-terminal deletion spectrin binding domain mutants were generated to determine the region of the spectrin-binding domain responsible for the interaction with ubiquitin. Amino acids were progressively removed from the C-terminus of the spectrin-binding domain, deleting 250, 350, 400 and 450 C-terminal amino acids, respectively (Figure 4.7A). Once the deletion mutants were successfully generated, the resulting plasmids were transfected into COS-1 cells to evaluate and normalize expression levels for subsequent Ub-GST pulldown experiments. Unfortunately, all of the HA-spectrin-binding-domain-C-terminal-deletion mutants were not expressed when transfected into COS-1 cells, whereas full-length HA-Ank105 and full length HA-spectrin-binding-domain were expressed at the expected molecular weights (Figure 4.7A). It was hypothesized that C-terminal deletion of amino acids at these particular positions (Figure 4.7A) in the spectrin binding domain compromised secondary and/or tertiary protein folding and this instability negatively impacted expression.

The primary amino acid sequence of Ank105 was analyzed by Russell/Linding Globprot software to determine positions in the Ank105 sequence where amino acid deletions would be tolerated, allowing for transient protein expression of deletion proteins. The Russell Linding Globprot software distinguishes regions of a protein that have high polypeptide flexibility and a consistent lack of secondary structure from regions that have a high degree of order and packaged into globular units (Linding *et al*., 2003). In other words, the software identifies and distinguishes the globular/ordered regions of a protein from the disordered regions. The software

achieves this by analyzing the propensity of each amino acid residue in a primary sequence to be in an ordered or disordered state. The disorder propensities of each amino acid are summed and graphed versus residue number. Decreasing sums on the graph indicate regions of order whereas

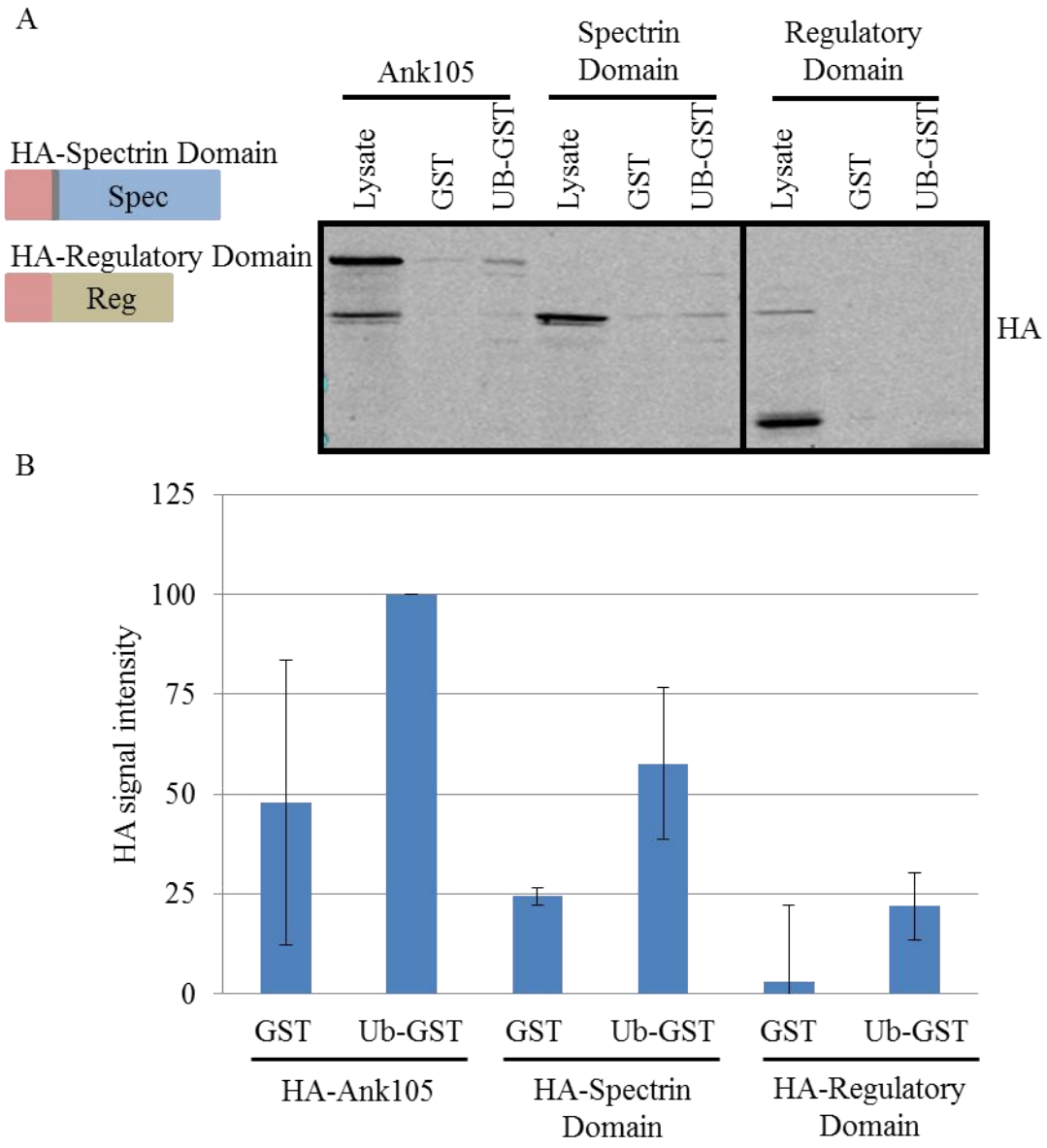

Figure 4.6: HA-Ank105 interacts with ubiquitin through the spectrin binding domain
A. COS-1 cells were transiently transfected HA-Ank105 spectrin binding domain or regulatory domain proteins. Lysates were incubated with either GST (100 µg) or Ub-GST (100 µg) immobilized on glutathione sepharose beads. Proteins bound to beads were resolved via SDS-PAGE, transferred to a nitrocellulose membrane and analyzed by Western blot for the presence of HA-Ank105 domain proteins. Results are representative of those from 3 independent experiments (N=3). Quantification and graphical representation of Figure 4.6A (mean +/- S.D). Data compared to Ub-GST HA-Ank105 pulldown.

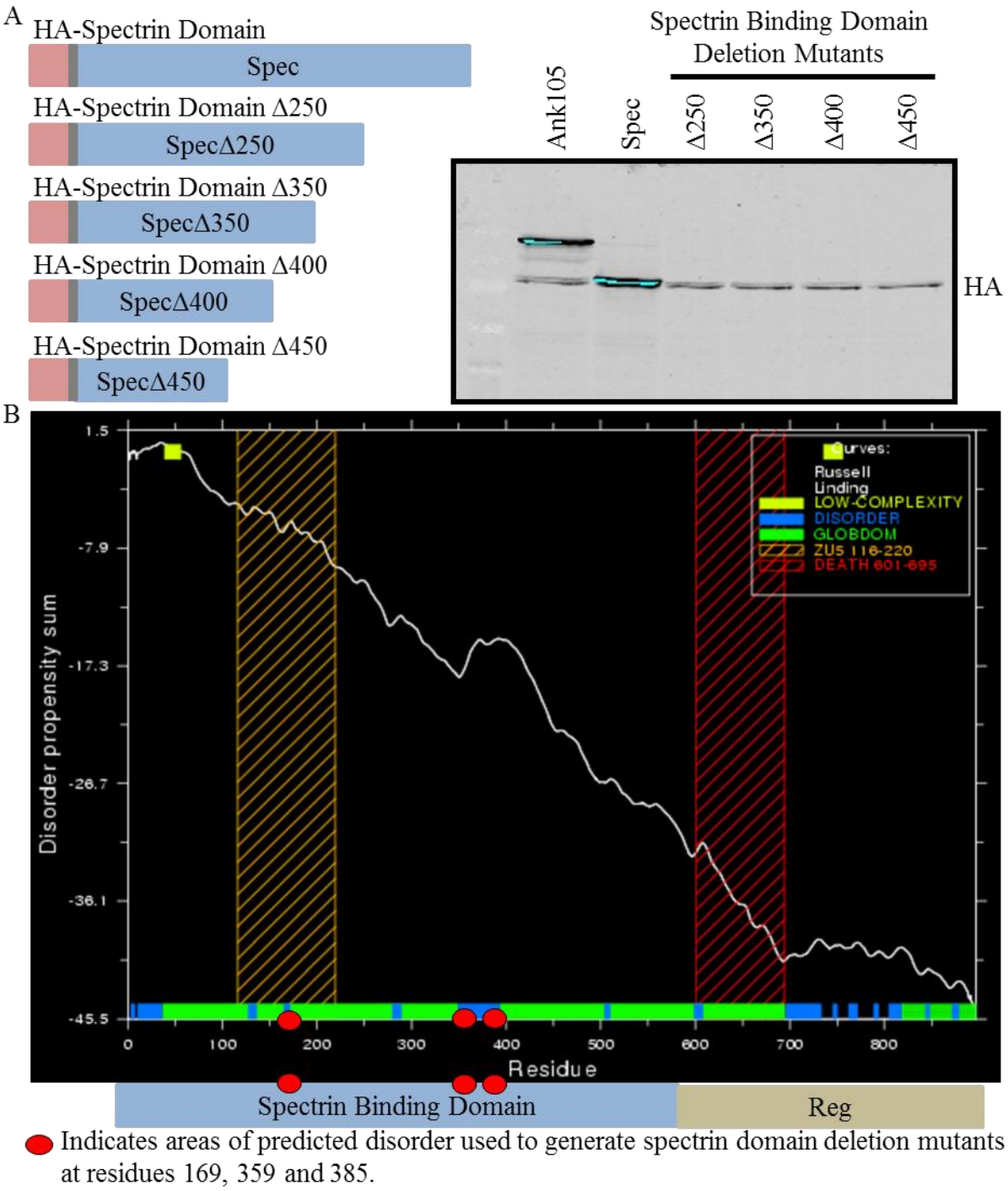

Figure 4.7: Ank105 contains several regions of disorder

A**.** Spectrin binding domain C-terminal deletion proteins were transiently transfected into COS-1 cells. Lysates (50 µg) were resolved via SDS-PAGE and transferred to a nitrocellulose membrane. Expression of deletion proteins was analyzed by Western blot using an anti-hemagluttinin antibody. N=1. B. The primary amino acid of An105 was analyzed by the Russell/Linding Globprot2.3 software http://globplot.embl.de/ to identify regions of order and disorder. Downwards trends in the disorder propensity sum versus residue graph indicate regions

with a high propensity for order whereas upwards trends identify regions with a high propensity for disorder (Linding *et al*., 2003). A domain map showing the spectrin binding domain and the regulatory domain compared to Ank105 residue is located directly below the graph. Disordered regions identified for generation of spectrin domain deletion mutants are indicated (amino acid residues 169, 359 and 385).

increasing sums indicate regions of disorder (Linding *et al*., 2003) (Figure 4.7B).

The Russell/Linding software identified several regions of disorder in the primary sequence of Ank105 (Figure 4.7B). Amino acids within several of these disordered regions were selected as candidates for deletion mutagenesis. It was hypothesized that generating deletion mutants within disordered regions would have less impact on the overall protein folding since these regions show a high degree of disorder. Several N-terminal deletion mutants of Ank105 were generated in regions predicted to be disordered, truncating Ank105 at residues 169, 359 and 385, respectively (Figure 4.8A). N-terminal deletion mutants are generated from full length HA-Ank105 rather than the spectrin domain. By keeping the regulatory domain intact protein stability would be increased. Full length HA-Ank105 interacted with ubiquitin and the regulatory domain itself did not, thus the presence of the regulatory domain should not hinder screening of these mutants for ubiquitin binding. The N-terminal deletion mutants were transfected into COS-1 cells and analyzed for protein expression. The HA-Ank105-NΔ169, HA-Ank105-NΔ359 and HA-Ank105-NΔ385 deletion mutants each were expressed at the expected molecular weights (Figure 4.8A).

The N-terminal deletion mutants were evaluated for the ability to interact with ubiquitin via Ub-GST pulldown experiments. The HA-Ank105-NΔ385 deletion mutants interact with Ub-GST fusion protein however the signal intensity was very low. The HA-spectrin-binding-domain was used as a positive control and bound Ub-GST, but with low signal intensity (Figure 4.8B). The HA-Ank105-NΔ169 and HA-Ank105-NΔ359 proteins did not appear to interact with Ub-GST. The lack of interaction is odd considering the proteins with more significant amino acid deletions retained the ability to bind ubiquitin (Figure 4.8B). The absence of observable ubiquitin binding with the HA-Ank105-NΔ169 and HA-Ank105-NΔ359 mutant could be due to the low overall signal intensity or complications in protein expression, as the HA-Ank105-NΔ169 protein is expressed as a doublet. Addition replicate experiments are required to improve signal intensity and determine the efficacy of HA-Ank105-NΔ169 ubiquitin binding, potentially using more input lysate to increase signal intensity. Assuming the HA-Ank105-NΔ385 proteins

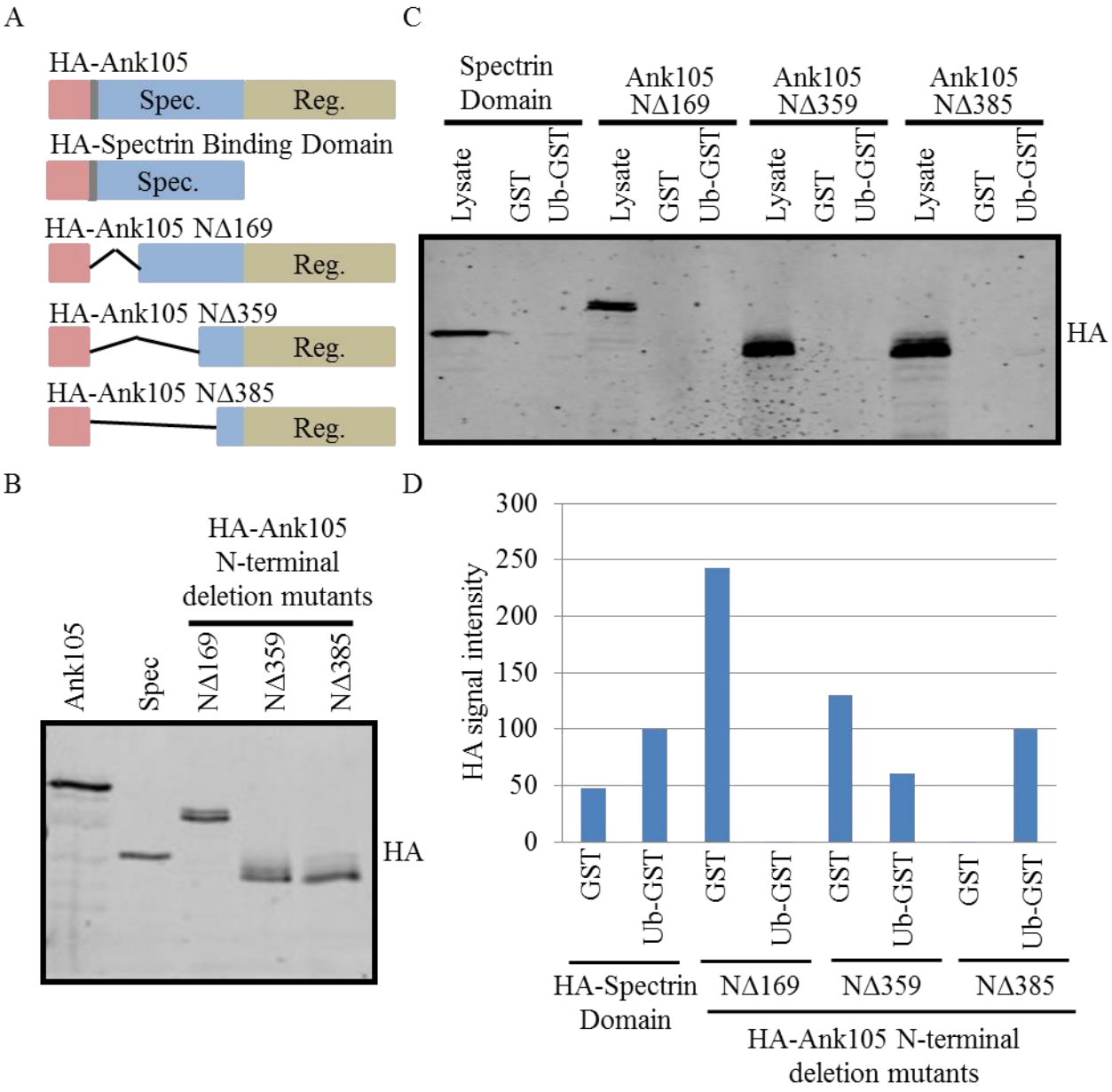

Figure 4.8: HA-Ank105 N-terminal deletion proteins retain ubiquitin binding
A. Domain map of HA-Ank105 N-terminal deletion proteins. B. HA-Ank105 N-terminal deletion proteins were transiently transfected into COS-1 cells. Lysates (50 µg) were resolved via SDS-PAGE and transferred to a nitrocellulose membrane. Expression of deletion proteins was analyzed by Western blot using an anti-hemagluttinin (HA) antibody. N=1. C. COS-1 cells were transiently transfected with indicated HA-Ank105-N-terminal deletion mutant proteins. Lysates were incubated with either GST (100 µg) or Ub-GST (100 µg) immobilized on glutathione sepharose beads. Proteins bound to beads were resolved via SDS-PAGE, transferred to a nitrocellulose membrane and analyzed by Western blot for the presence of HA-Ank105 mutants via Western blot with an anti-hemagluttinin (HA) antibody. N=1. D. Quantification and graphical representation of Figure 4.8C. Data compared to signal in Ub-GST HA-Spectrin domain pulldown.

interact with ubiquitin, the region of Ank105 mediating ubiquitin binding may be located between amino acids 360 and 588, which is the remainder of the spectrin binding domain. The Russell/Linding software predicts a small disordered region shortly after the 500th residue position of Ank105 (Figure 4.7B). Deletion mutagenesis in this region could generate proteins to more closely pinpoint the region of Ank105 mediating ubiquitin interaction.

4.6 Inducible constitutive PDGFR degradation assay

Ank105 promoted the constitutive degradation of PDGFR and EGFR, possibly by an endocytic mechanism involving Ank105 interaction with ubiquitinated proteins and targeting of receptors for degradation. Distinct mechanisms of endocytosis are distinguished by small molecule inhibitors (von Kleist and Haucke, 2012). Treatment of HA-Ank105-expressing cells with a panel of endocytosis inhibitors was used to determine the pathway by which Ank105 functioned. As such, inhibition of an endocytosis pathway required for Ank105 function was expected to elevate PDGFR levels above levels in untreated HA-Ank105-expressing cells. One challenge of studying Ank105-mediated constitutive receptor degradation was that Ank105 function is constitutive and occurred in the absence of ligand stimulation of the PDGFR. HA-Ank105 expression under standard cell culture conditions (DMEM + 10% FBS + 5% CO_2) was sufficient for Ank105 function; the receptor does not need to be stimulated to be degraded. Using small molecule inhibitors in a constitutively active system as in Ank105-expressing cells raised potential concerns. The PDGFR in HA-Ank105-expressing cells was under the control of an endogenous promoter and long inhibitor treatment times, potentially overnight, would be required to observe significant changes in PDGFR expression. Such long treatment times raised the possibility that changes observed in PDGFR expression may be due to off-target effects of the inhibitor. Thus a system permitting acute inhibitor treatment was desirable.

It was observed that PDGFR expression levels were sensitive to the level of available nutrients in the culture media. When HA-Ank105-expressing cells were cultured in media contained low serum (1% FBS), the expression level of PDGFR was elevated approximately 2 fold as compared to cells cultured with standard levels of serum (10% FBS) (Figure 4.9A). Given that serum restriction increased PDGFR levels HA-Ank105-expressing cells, it was next determined whether constitutive PDGFR degradation could be induced by incubation of low

serum treated cells in media containing normal levels of serum. HA-Ank105-expressing cells were cultured in low serum media (1% FBS) overnight to increase PDGFR levels. Overnight treatment with low serum increased PDGFR expression two fold as compared to cells cultured in normal serum levels (Figure 4.9B,C). The low serum treated cells were then re-incubated with media containing 10% FBS over time and induced PDGFR degradation (Figure 4.9B,C). After 4 hours of incubation with 10% FBS containing media, the level of PDGFR expression was comparable to control HA-Ank105-expressing cells not incubated with low serum media (Figure 4.9B,C). PDGFR levels did not decrease below control cells, as low serum treated cells incubated overnight with 10% FBS containing media expressed PDGFR at comparable levels (Figure 4.9B,C). An alternative explanation for the increase in PDGFR levels upon serum restriction is that serum contains a protein factor that promotes PDGFR degradation; however HA-Ank105-expressing cells cultured with the low protein content serum, Nuserum (Gibco), expressed PDGFR to similar levels as cells cultured in FBS (data not shown). Indeed, proteomic analysis of the growth factor content of several lots of FBS for different suppliers by mass spectrometry did not detect the presence of PDGF. Fibroblast growth factor (FGF), glial growth factor (GGF), transforming growth factor β-1 (TGF1) and insulin-like growth factor-II (IGFII) were readily and consistently detected in FBS (Zheng et al., 2006). Taken together this data suggests that restriction of nutrients and growth factors diverts PDGFR from Ank105-mediated degradation, presumably to prime the cell for maximum responsiveness to future nutrients and growth factors. When cells were re-exposed to sufficient levels of serum, PDGFR is shunted back to an Ank105-sensitive mechanism of degradation.

Given that serum restriction elevated PDGFR levels in HA-Ank105-expressing cells and re-introduction of serum promoted constitutive PDGFR degradation, this model of inducible, constitutive PDGFR degradation was utilized to study the effects of small molecule inhibitors on constitutive PDGFR degradation. By using this inducible model of PDGFR degradation, the sensitivity issue of the PDGFR being under the control of an endogenous promoter was avoided. Furthermore, using this model allowed for acute inhibitor treatment and alleviated some of the potential concerns of off-target inhibitor effects with prolonged treatment times. To further address concerns of off-target effects of inhibitor treatment, the inhibitors used were validated by studying their effects on ligand induced PDGFR degradation and the endocytosis of LDL. The endocytosis of LDL follows a distinct and well characterized pathway, and will be discussed in

subsequent sections of the thesis.

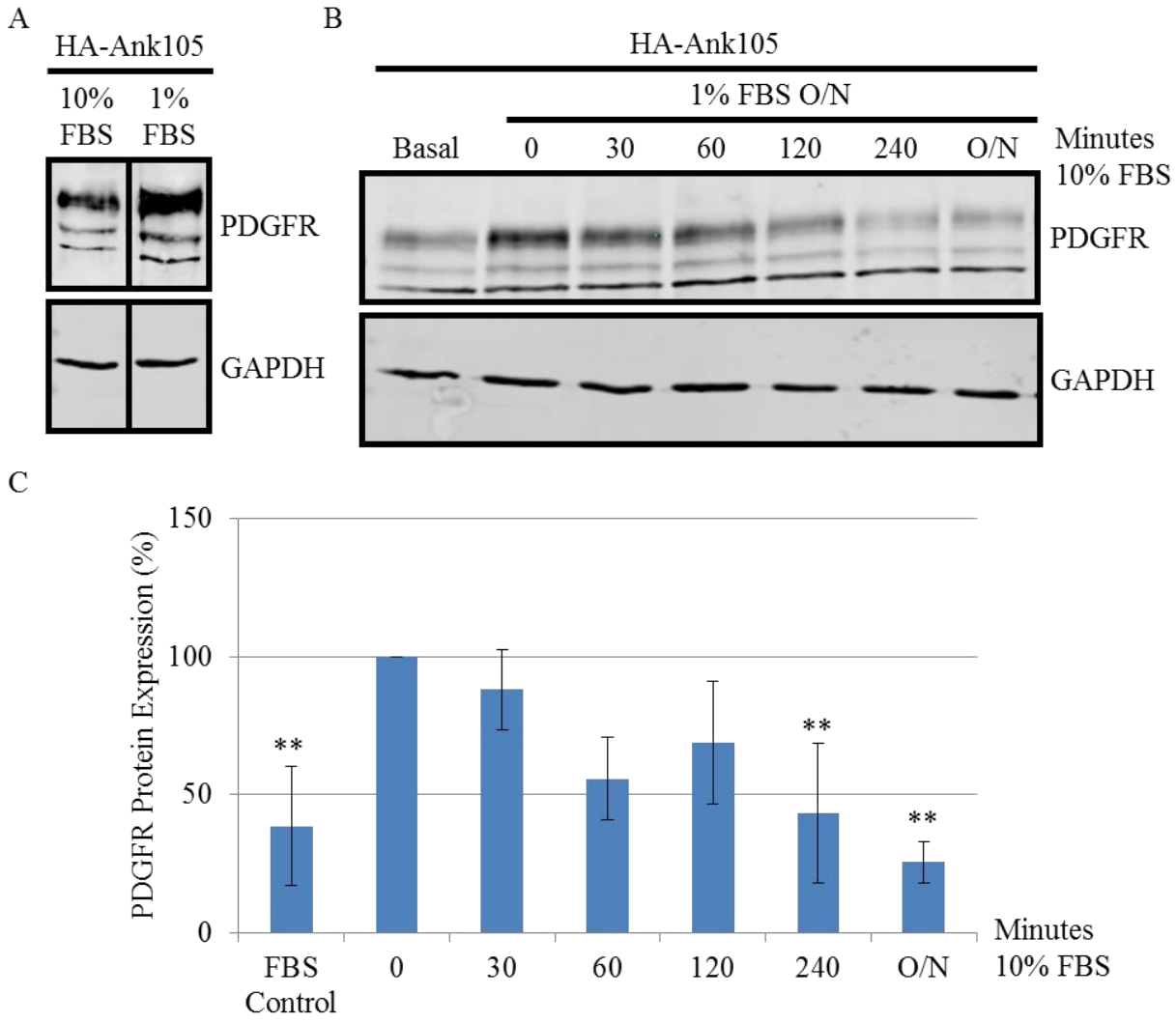

Figure 4.9: Generation of an inducible model of constitutive PDGFR degradation
A. HA-Ank105-expressing cells were grown in DMEM containing 10% FBS or 1% FBS. Lysates were generated, normalized for total protein content, resolved by SDS-PAGE (100 µg), transferred to a nitrocellulose membrane and analyzed via Western blot for PDGFR and GAPDH expression. N=1. B. HA-Ank105-expressing cells were grown overnight in DMEM containing 1% FBS to increase PDGFR levels and stimulated with DMEM containing 10% FBS for indicated times. Lysates for each time point were collected, normalized for total protein content, resolved by SDS-PAGE (100 µg), transferred to a nitrocellulose membrane and analyzed via Western blot for PDGFR and GAPDH expression. Expression was quantified as per 3.2.3.4. C. Quantification and graphical representation of Figure 4.9b (Mean +/- S.D.). Data compared to expression in Ank105 0min sample. Results are representative of those from 3 independent experiments (N=3) (** indicates P value <0.01).

4.7 Inhibition of endocytosis using small molecule inhibitors

Several distinct mechanisms of endocytosis exist and may serve as routes promoting Ank105-mediated constitutive PDGFR degradation. CME, caveolar endocytosis and macropinocytosis are the most likely candidate pathways for constitutive PDGFR endocytosis since these pathways have been previously shown to internalize RTKs. The lipid clustering and CLIC/GEEC pathways are also candidates for constitutive PDGFR endocytosis; however cargo identified for these pathways is limited to IgE and GPI-anchored proteins, respectively. CME is by far the best-studied endocytic mechanism and has been extensively characterized in the endocytosis of RTKs. The clathrin-independent pathways of internalization are emerging in the literature and the range of cargo is largely unknown. Thus, it is prudent to inhibit each of these potential pathways.

A 'top-down' strategy was employed to specifically inhibit each of these endocytosis mechanisms. The small molecule inhibitors chosen for these studies target several events in endocytosis such as coat formation, GTPases regulating internalization, endosomal pH, cytoskeleton dynamics, mechanisms of degradation, as well as kinases implicated in endocytic events (Table 4.1) (Figure 4.10). Pitstop-2 and chlorpromazine inhibit CME by preventing adaptor protein binding and inducing coat mis-assembly, respectively (Figure 4.10). Methyl-β-cyclodextrin (MβCD) extracts membrane cholesterol and flattens caveolae, thereby preventing caveolar endocytosis (Figure 4.10). Next, small molecule inhibitors were selected to inhibit the internalization step of endocytosis. The small molecule dynasore inhibits dynamin GTPase activity, thereby blocking dynamin-mediated internalization (Figure 4.10). ML141 inhibits CLIC/GEEC endocytosis by attenuating the GTPase activity of Cdc42, while NCS 23766 inhibits macropinocytosis by attenuating Rac-1 GTPase activity (Figure 4.10). Macropinocytosis can also be targeted by inhibiting the activity of proteins thought to be required for function. Inhibition of SRC family kinases by PP2, and sodium-proton exchange by EIPA block macropinocytosis (Figure 4.10).

The actin cytoskeleton is implicated during the internalization step in all of the major pathways of endocytosis. Actin polymerization and depolymerization are inhibited by latrunculin A and jasplakinolide, respectively (Figure 4.10). Lysosomal degradation and proteasomal degradation are the two pathways of protein degradation in the cell. Although lysosomal degradation is the canonical endpoint of endocytosis, several lines of evidence suggest the

Table 4.1: Endocytosis inhibitor panel
Small molecule inhibitors used to study Ank105-mediated constitutive PDGFR degradation, ligand induced PDGFR degradation and LDL uptake are tabulated and listed according to their respective targets. Inhibitors with similar function, such as blocking internalization, are grouped together and color coded.

Inhibitor	Abbr.	Target	Mechanism
Pitstop2	-	Clathrin	Prevent adaptor protein binding
Chlorpromazine	-	Clathrin	Induce coat mis-assembly
Methyl-β-cyclodextrin	MβCD	Caveolin	Cholesterol extraction
Dynasore	-	Dynamin	Inhibit GTPase activity
ML141	-	Cdc42	Inhibit GTPase activity
NSC 23766	iRac-1	Rac-1	Inhibit GTPase activity
Monensin	-	Na^+H^+ exchanger	Inhibit proton exchange
5-(N-Ethyl-N-isopropyl) amiloride	EIPA	Na^+ Channel	Inhibit Na+ channel activity
Latrunculin A	LatA	Actin	Inhibit actin polymerization
Jasplakinolide	-	Actin	Inhibit actin de-polymerization
Nocodazole	-	Microtubules	Inhibit microtubule polymerization
PP2	-	SRC kinases	SRC family kinase inhibitor
Wortmannin	-	PI3K	Inhibit PI3K lipid kinase activity
carbobenzoxy-Leu-Leu-leucinal	MG132	Proteasome	Inhibit proteasomal degradation
Chloroquine	-	Lysosome	Increase lysosomal pH

Inhibitors blocking coat formation
Inhibitors blocking internalization
Broad/non-specific inhibitors
Cytoskeleton inhibitors
Inhibitors of implicated proteins
Inhibitors of degradation pathways

proteasome is involved in endocytosis-mediated protein degradation. Lysosomal degradation and proteasomal degradation are inhibited by chloroquine and MG132, respectively. Lastly, the cellular proton gradient and PI3K activity have been implicated broadly in many pathways of endocytosis. The proton gradient can be disrupted with monensin and PI3K activity can be inhibited by wortmannin (Figure 4.10). Several of the small molecule endocytosis inhibitors used to study Ank105-mediated constitutive PDGFR degradation are not specific to one endocytosis pathway, but rather affect several pathways at a common junction. Although the endocytosis pathways discussed are distinct, certain pathways use common mechanisms, such as internalization, to function. Several endocytosis pathways, including CME, caveolar endocytosis and lipid clustering require dynamin to drive internalization whereas others, including CLIC/GEEC and macropinocytosis, are independent of dynamin activity (Figure 4.11). MβCB can inhibit both CME and caveolar endocytosis; however caveolar endocytosis is thought to be

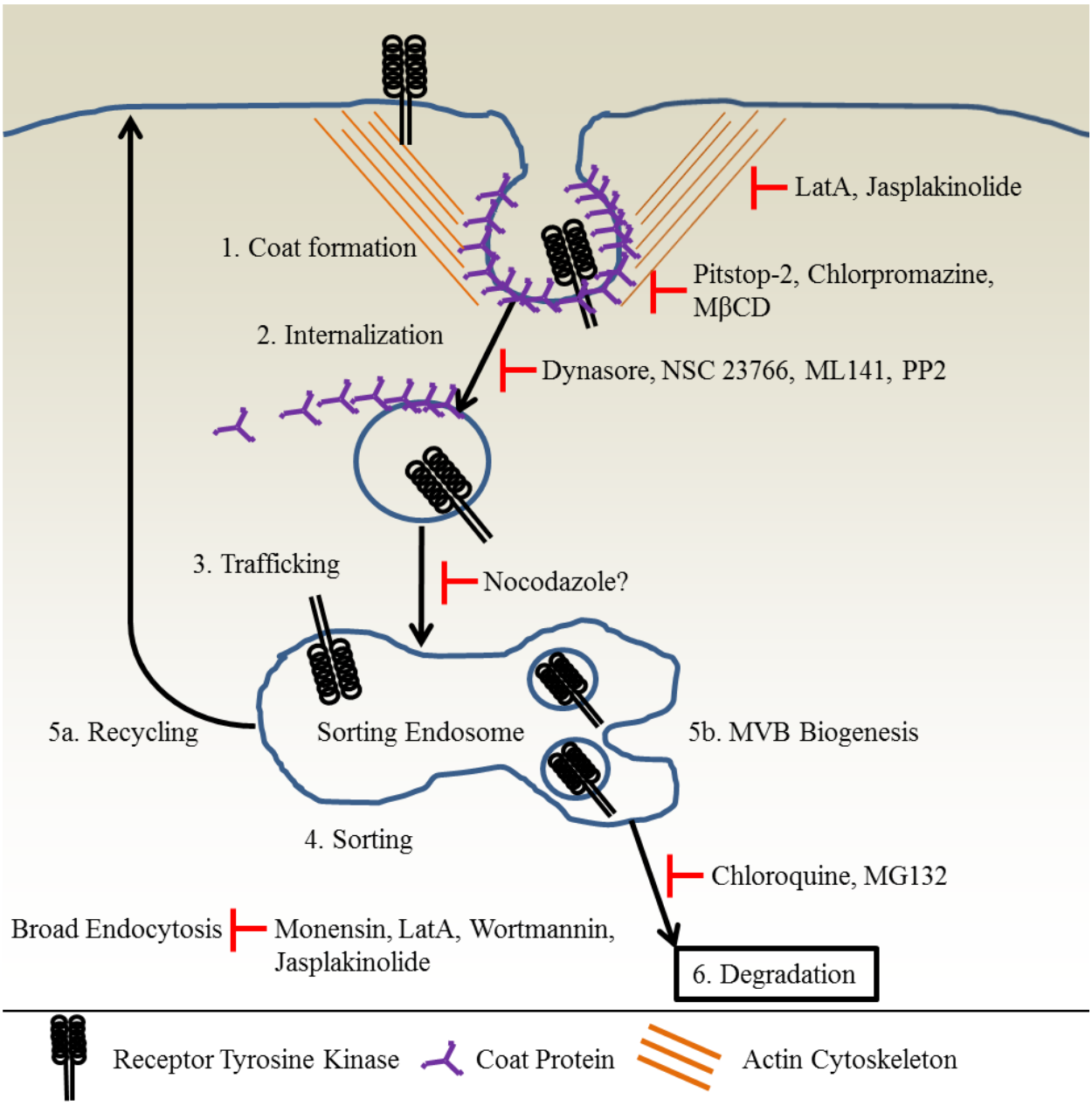

Figure 4.10: General endocytosis pathway and targets of small molecule inhibitors
Depicts a general scheme of endocytosis common to major pathways, as well as delineates stages of endocytosis affected by various small molecule inhibitors. Cell surface receptors are incorporated into budding, protein coated vesicles (1.). Budding vesicles are internalized (2.), often requiring dynamin activity. Internalized vesicles are trafficked to the sorting endosome (3.) where they are sorted (4.) and either recycled back to the plasma membrane (5a.) or incorporated into multivesicular bodies (5b.) and subsequently trafficked for degradation (6.).

more sensitive to plasma membrane cholesterol levels (Figure 4.11). Several inhibitors can be considered broad endocytosis inhibitors and affect multiple endocytosis pathways (Figure 4.11).

Thus by studying the effects of the endocytosis inhibitor panel on Ank105-mediated constitutive degradation, the pathway by which Ank105 functions was characterized.

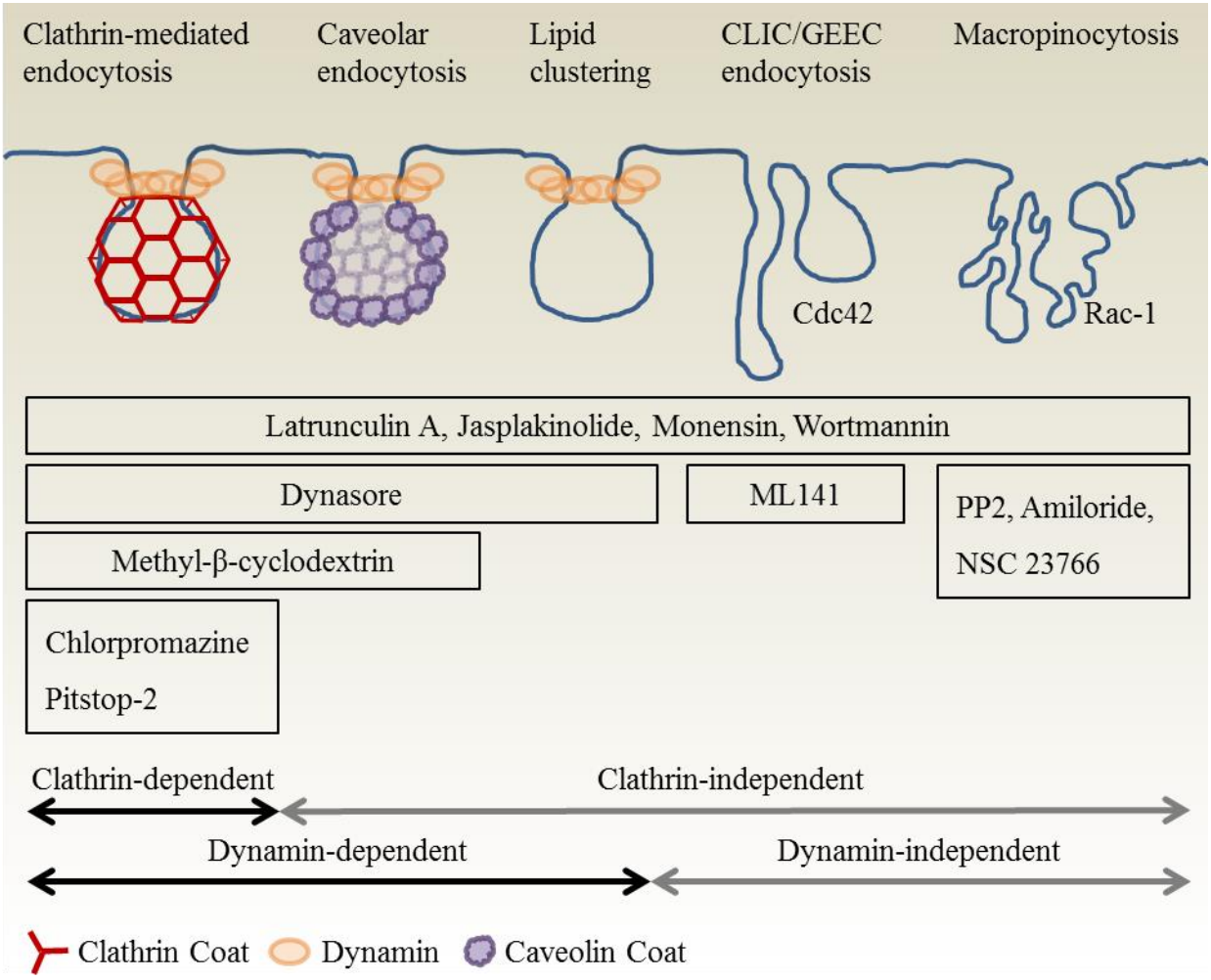

Figure 4.11: Pathway specificities of the small molecule endocytosis inhibitor panel
Small molecule endocytosis inhibitors used to study Ank105-mediated constitutive PDGFR degradation, ligand induced PDGFR degradation and LDL uptake are organized according to which endocytosis pathways they affect. Text box size delineates endocytosis pathways affected. Endocytosis pathways are organized based upon the requirement of clathrin and/or dynamin for proper function. Modified from with permission from (von Kleist and Haucke, 2012).

4.7.1 Ank105-mediated constitutive PDGFR degradation requires dynamin activity and functional lysosomal and proteasomal pathways

PDGFR expression levels in HA-Ank105-expressing cells were increased by overnight culture in low serum media. Serum restricted cells were incubated with ranging concentrations of each small molecule endocytosis inhibitor (Table 4.1) for 30 minutes then incubated in media containing 10% FBS in the presence of inhibitor. Control conditions where HA-Ank105-

expressing cells were cultured in either 10% FBS or 1% FBS overnight, not treated with inhibitor and not stimulated with 10% FBS were generated to provide a baseline of constitutive and serum restricted PDGFR protein expression levels. These control conditions were compared to serum restricted HA-Ank105-expressing cells treated with inhibitor and stimulated with 10% FBS. Lysates were collected, normalized to total protein content and analyzed for PDGFR protein expression. Western blot analysis of PDGFR expression again demonstrated that serum restriction in HA-Ank105-expressing cells increased PDGFR protein levels by approximately 2 fold, and those levels return to base line after 4 hours of incubation with media containing 10% FBS (Figure 4.12A,B). Treatment of serum restricted cells with increasing concentrations chloroquine partially inhibited constitutive PDGFR degradation in response to incubation with media containing 10% FBS (Figure 4.12A,B). The PDGFR protein expression levels are similar between the medium (10 μM) and high (20 μM) concentrations of chloroquine indicating that the medium concentration elicits the maximum effect. It is possible that more robust response to chloroquine may be observed if the concentration is increased further as the difference between the medium and high concentrations is only 2 fold. Treatment of serum restricted cells with increasing concentrations of MG132 to inhibit proteasomal degradation completely blocked constitutive PDGFR degradation in response to incubation with media containing 10% FBS (Figure 4.12A,B). PDGFR expression levels were similar across all concentrations of MG132 used (Figure 4.12B). The data indicates that both a functional lysosome and proteasome are required for constitutive PDGFR degradation. Lysosomal degradation and proteasomal degradation are associated with monoubiquitination and polyubiquitination, respectively. It would prove interesting to evaluate the ubiquitination state of the receptor in degradation-impaired HA-Ank105-expressing cells to gain insight to the mechanism of PDGFR degradation promoted by Ank105.

Due to the large amount of data collected the remainder of the data from each of the other endocytosis inhibitors in the panel is summarized (Figure 4.12A,B). To simplify the comparison of the effects of these different inhibitors on Ank105-mediated constitutive PDGFR degradation the mid-range concentration for each inhibitor was used rather than comparing the effect of a range of inhibitor concentrations on constitutive PDGFR degradation. Indeed PDGFR expression levels were very similar amongst inhibitor concentrations in the same set, for instance, low, medium and high concentrations of MG132 display similar PDGFR expression levels (Figure

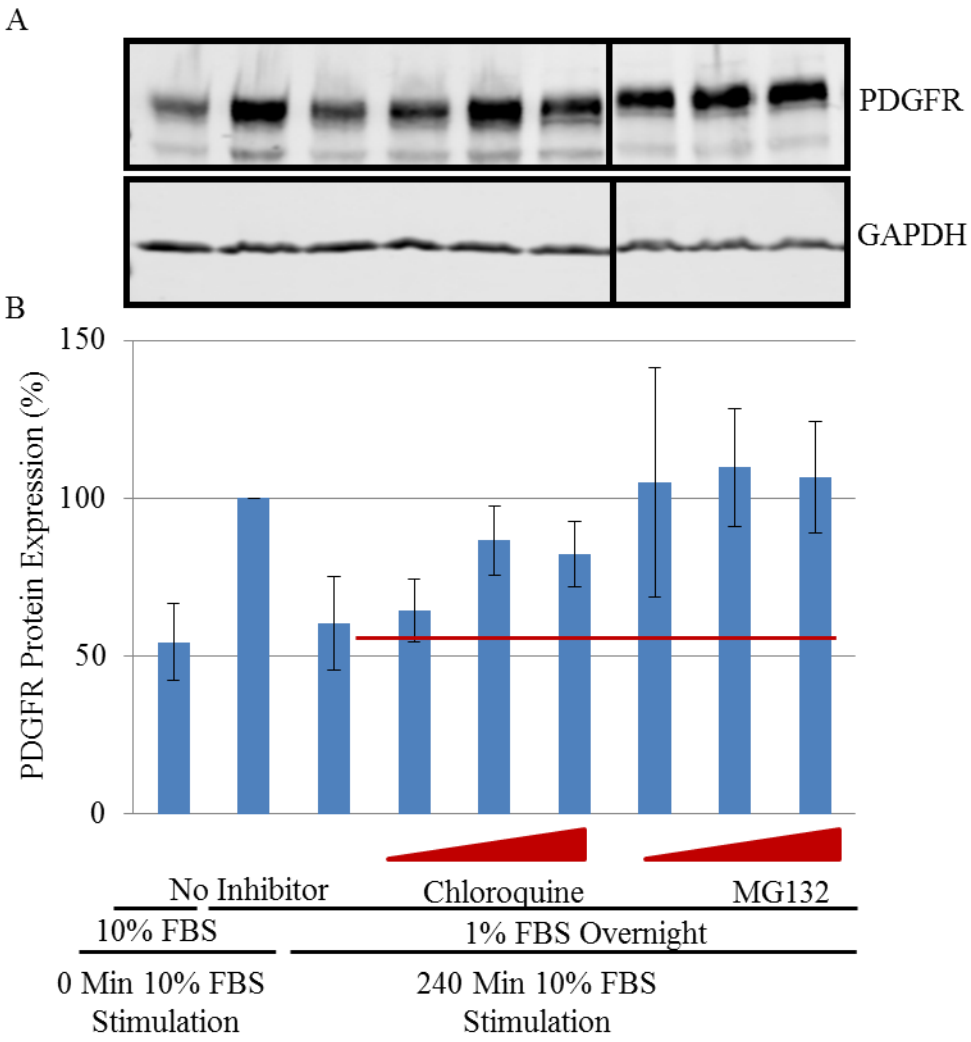

Figure 4.12: Proteasomal and lysosomal degradation inhibitors MG132 and chloroquine block constitutive PDGFR degradation

A. HA-Ank105-expressing cells were cultured overnight in media containing 1% FBS to increase PDGFR levels. Control cells were cultured overnight in media containing 10% FBS. Cells were either left untreated treated with increasing concentrations of chloroquine (5 µM, 10 µM and 20 µM) or MG132 (5 µM, 10 µM and 20 µM) for 30 minutes. Cells were stimulated with media containing 10% FBS for 240 minutes. Control cells, one set which were cultured in media containing 10% FBS overnight and another set in media containing 1% FBS overnight, were not stimulated with media containing 10% FBS as to provide base line levels of constitutive and recovered PDGFR, respectively. Lysates for each time point were collected, normalized for total protein content, resolved via SDS-PAGE (100 µg), transferred to a nitrocellulose membrane and analyzed by Western blot for PDGFR and GAPDH expression. PDGFR protein expression was quantified as per 3.2.3.4. Results are representative of those from 3 independent experiments (N=3). B. Quantification and graphical representation of PDGFR expression data in Figure 4.12A and additional replicate experiments (Mean +/- S.D.). Data was compared to expression in Ank105 240min sample.

4.12A,B). This pattern held true for the majority of inhibitors tested (data not shown). Chloroquine concentrations were increased to those used in previous acute treatment experiments (100 μM) (Figure 4.3B,C).

PDGFR protein expression data from serum restricted cells treated with the medium concentration of each inhibitor was compiled (Figure 4.13) and organized according to mechanism of action of each inhibitor (Table 4.1). PDGFR protein expression levels for each inhibitor were compared to untreated control cells and analyzed for statistical significance. In examining PDGFR protein expression levels in samples treated with inhibitors preventing proper clathrin vesicle coat formation, it is evident that treatment with either pitstop (Pvalue 0.44) or chlorpromazine (Pvalue 0.45) did not affect constitutive PDGFR degradation (Figure 4.13). Inhibition of caveolar endocytosis via extraction of plasma membrane cholesterol with MβCD also did not affect constitutive PDGFR degradation (Pvalue 0.26) (Figure 4.13). This data suggests that inhibition of CME with chlorpromazine or pitstop did not affect Ank105-mediated constitutive degradation. Additionally, Ank105-mediated constitutive PDGFR degradation is independent of caveolar endocytosis.

The effect of internalization inhibitors on constitutive PDGFR degradation was next determined. Inhibition of dynamin activity with dynasore did not affect Ank105-mediated constitutive PDGFR degradation. PDGFR protein expression levels in dynasore treated cells were elevated as compared to untreated control cells (Pvalue 0.015) (Figure 4.13). This data indicates that constitutive PDGFR degradation is partially dependent upon dynamin function. Inhibition of Cdc42 regulated CLIC/GEEC pathway with ML141 did not affect Ank105-mediated constitutive PDGFR degradation. PDGFR protein expression levels in ML141 treated cells were similar to untreated control cells (Pvalue 0.29) (Figure 4.13). This data indicates that constitutive PDGFR degradation is independent the CLIC/GEEC pathway. Targeting of macropinocytosis via inhibition of Rac-1 activity with NCS 27366 produced interesting results. Serum restricted cells treated with NCS 27366 showed a decrease in PDGFR protein expression as compared to untreated control cells (Pvalue 0.031) (Figure 4.13). This data suggests that disruption of macropinocytosis promoted constitutive PDGFR degradation, possibly by directing a greater proportion of PDGFR towards Ank105-mediated constitutive degradation. A potential caveat is that treatment of the macropinocytosis inhibitor EIPA did not affect PDGFR protein expression levels as compared to control cells (Pvalue 0.17) (Figure 4.13). It may be possible

that HA-Ank105-expressing cells are insensitive to EIPA treatment or greater concentrations may be required to produce an effect. Additionally, Src kinase activity is thought to be implicated in macropinocytosis (Doherty and McMahon, 2009b) and treatment of serum restricted cells with

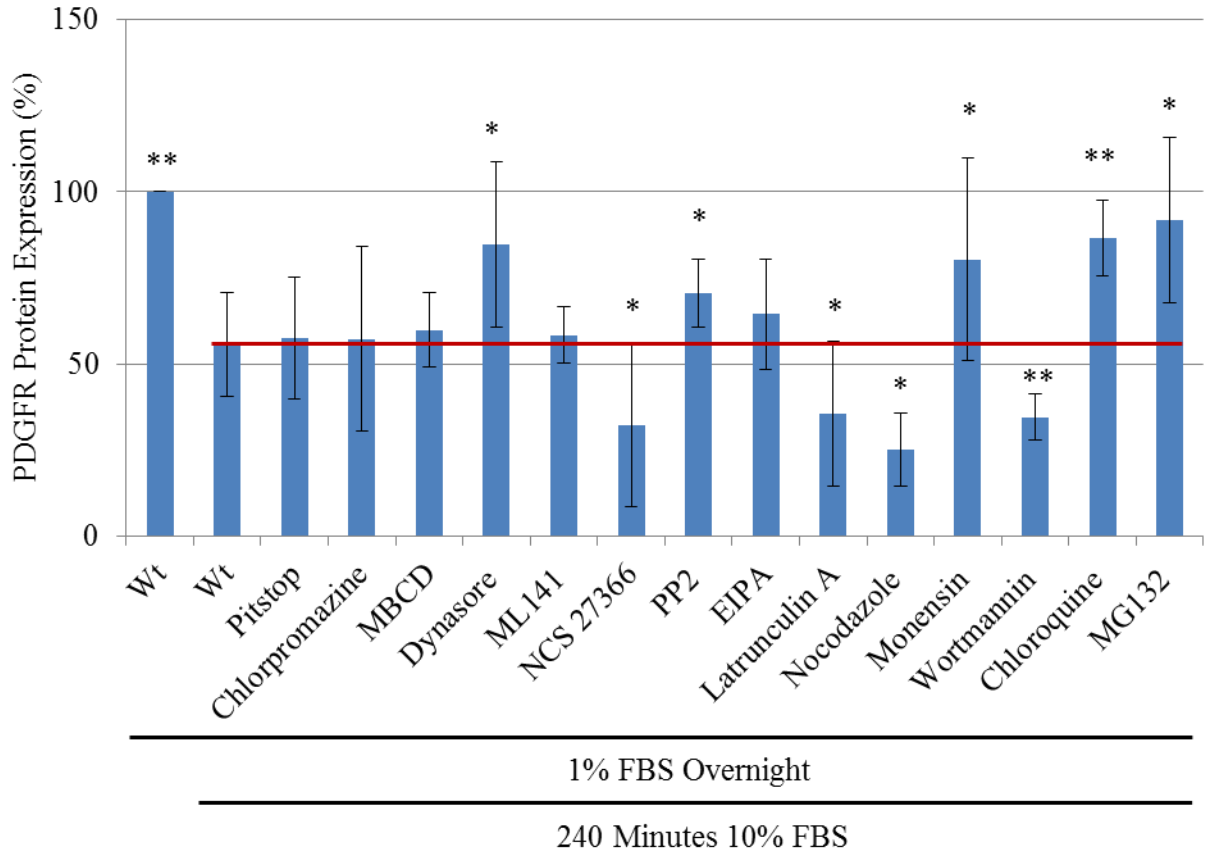

Figure 4.13: Ank105-mediated constitutive PDGFR degradation is blocked via inhibition of dynamin activity and cellular protein degradation
HA-Ank105-expressing cells were grown overnight in media containing 1% FBS to increase PDGFR levels. Cells were treated with the small molecule endocytosis inhibitor panel for 30 minutes then stimulated with media containing 10% FBS for 240 minutes. Lysates for each time point were collected, normalized for total protein content, resolved via SDS-PAGE (100 µg), transferred to a nitrocellulose membrane and analyzed by Western blot for PDGFR protein expression. PDGFR expression levels were quantified and summarized for each inhibitor (Mean +/- S.D.). Data compared to expression in Ank105 240min sample and analyzed for statistical significance by t-test (* indicates Pvalue <0.05, ** indicates Pvalue <0.001). Results were compiled from 3 independent experiments (N=3).

PP2 slightly inhibited PDGFR degradation (Pvalue 0.012) (Figure 4.13) which is the opposite effect as observed with NCS 27366. SRC family kinases are also implicated in other endocytosis pathways including caveolar endocytosis (Doherty and McMahon, 2009b) and flotillin-mediated endocytosis (Doherty and McMahon, 2009b). The role of implicated proteins such as Src is

likely to be cell type specific (Doherty and McMahon, 2009b).

The effects of cytoskeletal inhibitors on constitutive PDGFR degradation were determined. Treatment of serum restricted cells with actin polymerization inhibitor latrunculin A resulted in a statistically significant decrease in PDGFR protein expression as compared to untreated control cells (Pvalue 0.048) (Figure 4.13). Similarly, treatment of serum restricted cells with microtubule de-polymerization agent nocodazole also decreased PDGFR protein expression levels as compared to untreated control cells (Pvalue 0.011) (Figure 4.13) This data suggests that inhibition of polymerization of either actin or microtubules promotes Ank105-mediated constitutive PDGFR degradation. The effect of latrunculin A on constitutive PDGFR degradation is particularly surprising considering actin dynamics are thought to contribute extensively to many pathways of endocytosis.

The effects of other broad endocytosis inhibitors, monensin and wortmannin, were also studied. Treatment of serum restricted cells with the proton gradient disruptor monensin inhibited constitutive PDGFR degradation. Indeed, monensin treated cells had elevated PDGFR protein levels as compared to control cells stimulated with 10% FBS containing media (Pvalue 0.034) (Figure 4.13), indicating an intact proton gradient may be required for Ank105 function. The data obtained with the inhibitor monensin did however demonstrate high degree of variance, as evident by the large values of standard deviation (Figure 4.13). Treatment with wortmannin to inhibit PI3K activity promoted Ank105 function. Serum restricted cells treated with wortmannin had significantly lower PDGFR protein levels than untreated control cells (Pvalue 0.00011) (Figure 4.13), indicating that inhibition of PI3K activity promotes Ank105 function.

The requirement of functional lysosomal and proteasomal pathways for Ank105-mediated constitutive PDGFR degradation was also determined. Inhibition of lysosomal degradation with chloroquine blocked constitutive PDGFR degradation. Chloroquine treated cells had similar PDGFR protein levels as untreated control cells which were not stimulated with 10% FBS containing media (Pvalue 0.00012) (Figure 4.13). Inhibition of proteasomal degradation with MG132 robustly inhibited constitutive PDGFR degradation. MG132 treated cells had similar PDGFR protein levels as untreated control cells which were not stimulated with 10% FBS containing media (Pvalue 0.0063) (Figure 4.13). Taken together this data indicates that functional lysosomal and proteasomal degradation pathways are required for Ank105-mediated constitutive PDGFR degradation.

Several of the treatment conditions, such as monensin, dynasore and MG132 has a large degree of error in measurement of PDGFR protein levels following incubation in media containing 10% FBS. One potential shortcoming of the constitutive PDGFR degradation assay is the low dynamic range of the assay as receptor levels are only 2 fold less in cells incubated with serum as serum restricted cells (Figure 4.13), whereas ligand-induced PDGFR degradation studies had a much higher dynamic range as the difference in PDGFR expression levels between stimulated and unstimulated cells was more substantial (Figure 4.17). The lower dynamic range of the constitutive PDGFR degradation assay combined with error in measurement between replicate sets could potentially reduce the statistical significance of the observed effects of the small molecule inhibitors on constitutive PDGFR degradation. Perhaps additional replicate experiments for these particular inhibitors would reduce error and improve statistical analysis. Additional experiments with alternative methodologies such as fluorescence activated cell sorting could be employed to also address these issues.

4.7.2 LDL internalization proceeds by a clathrin and dynamin-dependent mechanism

In order to validate observations made with the effects of inhibitor treatment on constitutive PDGFR degradation, the effects of endocytosis inhibitor panel were determined for uptake of LDL. Endocytosis of LDL has been extensively studied and is known to proceed by a clathrin and dynamin dependent mechanism. HA-Ank105-expressing cells were incubated with chloroquine, dynasore and MG132 for 30 minutes. Cells were then incubated with dialkylcarbocyanine-labeled LDL (Dil-LDL) for indicated times; after several washing steps uptake of Dil-LDL was measured by fluorescence signal intensity (Figure 4.14). Untreated HA-Ank105-expressing cells internalized LDL in a linear fashion over time, with the highest levels of internalized LDL after 300 minutes (Figure 4.14A,B). Treatments with chloroquine and MG132 did not appear to affect LDL uptake in HA-Ank105-expressing cells (Figure 4.14A,B). Indeed, cells treated with chloroquine and MG132 internalized LDL in a linear fashion with respect to time, similar to control cells. In addition, cells treated with chloroquine or MG132 internalized LDL to the same extent as control cells (Figure 4.14A,B). Treatment with dynasore strongly inhibited LDL uptake in HA-Ank105-expressing cells. After 300 minutes of incubation with Dil-LDL, 90% of LDL uptake was inhibited (Figure 4.14A,B).

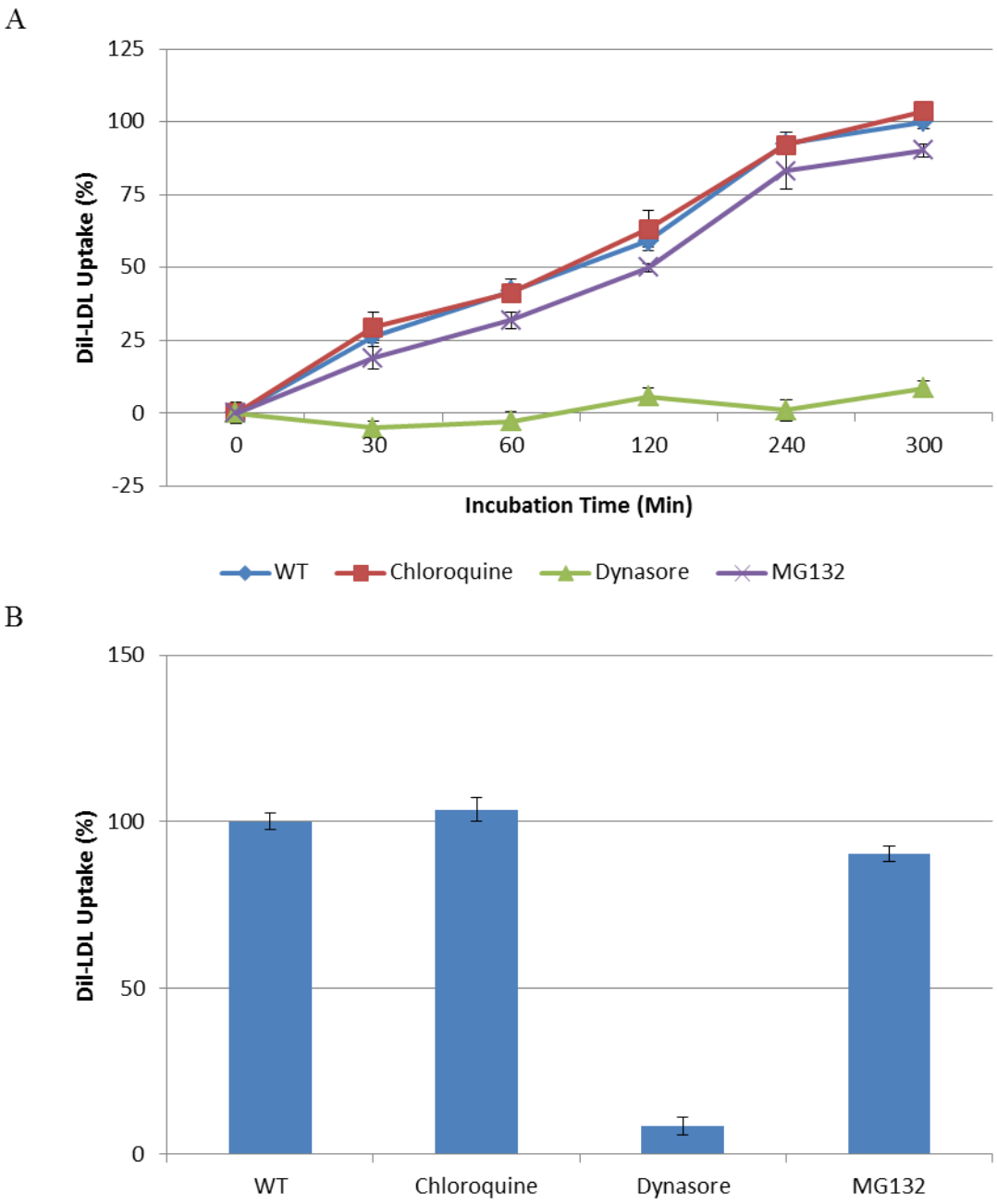

Figure 4.14: Dynasore treatment inhibits LDL uptake in HA-Ank105 expressing cells
A. HA-Ank105-expressing cells were cultured overnight in media containing 0.5% FBS, treated with chloroquine (25 µM), dynasore (80 µM) or MG132 (10 µM) for 30 minutes then incubated with serum-free media containing Dil-LDL (50 µg/mL) in the presence of inhibitor for indicated times. Dil-LDL uptake was measured as fluorescence signal intensity (Ex: 540 nm; Em: 580 nm). B. Quantification and graphical representation of LDL uptake of 300 minute time point (Mean +/- S.D.). Results were compiled from 3 independent experiments (N=3).

Due to the large amount of data collected the remainder of the data from each of the other endocytosis inhibitors in the panel is summarized (Figure 4.15). To simplify the comparison of the effects of these different inhibitors on Dil-LDL uptake, the 300 minute time point for each inhibitor was used rather than comparing the effects of each inhibitor over a range of times. In examining LDL uptake in samples treated with inhibitors preventing proper vesicle coat formation, it is evident that treatment with the clathrin endocytosis inhibitor pitstop-2 strongly inhibits LDL uptake (Figure 4.15). Treatment with pitstop-2 inhibited 75% of LDL uptake in HA-Ank105-expressing cells (Pvalue 0.00038) (Figure 4.15). Similarly, treatment with the clathrin endocytosis inhibitor chlorpromazine partially blocked LDL uptake by 40% (Pvalue 0.0044) (Figure 4.15). Taken together, this data indicates that LDL internalization proceeds by a clathrin-dependent mechanism. Extraction of plasma membrane cholesterol with MβCD partially inhibited LDL uptake in HA-Ank105-expressing cells, reducing uptake by 15% (Pvalue 0.038) (Figure 4.15). This slight inhibition could be due to the effects of MβCD on caveolar endocytosis or CME. The data indicates that CME is the predominant mechanism of internalization of LDL in HA-Ank105-expressing cells.

The effect of internalization inhibitors on constitutive PDGFR degradation was next determined. Inhibition of dynamin activity with dynasore ablated LDL uptake in HA-Ank105-expressing cells. Indeed, dynasore treatment inhibits 90% of LDL uptake (Pvalue 7.65×10^{-18}) (Figure 4.15), indicating that dynamin activity is essential for LDL internalization. Inhibition of the CLIC/GEEC pathway with Cdc42 inhibitor ML141 did not affect LDL uptake. Cells treated with ML141 internalized LDL to a similar extent as untreated cells (Pvalue 0.20) (Figure 4.15). Inhibition of macropinocytosis with Rac-1 inhibitor NCS 27366 also did not affect LDL uptake. Cells treated with NCS 27366 internalized LDL to an extent comparable to untreated HA-Ank105-expressing cells (Pvalue 0.17) (Figure 4.15). Similarly, treatment with additional macropinocytosis inhibitors PP2 (Pvalue 0.17) and EIPA (Pvalue 0.27) also did not affect LDL uptake (Figure 4.15). The data indicates that LDL internalization in HA-Ank105-expressing cells proceeds by a dynamin-dependent mechanism and does not involve dynamin-independent pathways.

The effects of cytoskeletal inhibitors on LDL uptake were next determined. Treatment either with the actin polymerization inhibitor latrunculin A did not affect LDL uptake in HA-Ank105-expressing cells (Pvalue 0.37) (Figure 4.15). Treatment with the actin de-polymerization

inhibitor jasplakinolide slightly impaired LDL uptake compared to untreated cells (Pvalue 0.037) (Figure 4.15). Treatment of HA-Ank105-expressing cells with the microtubule polymerization inhibitor nocodazole also did not affect LDL internalization (Pvalue 0.30) (Figure 4.15). Taken together, the data suggests that the aspects of cytoskeletal dynamics tested are not extensively involved in LDL internalization in HA-Ank105-expressing cells.

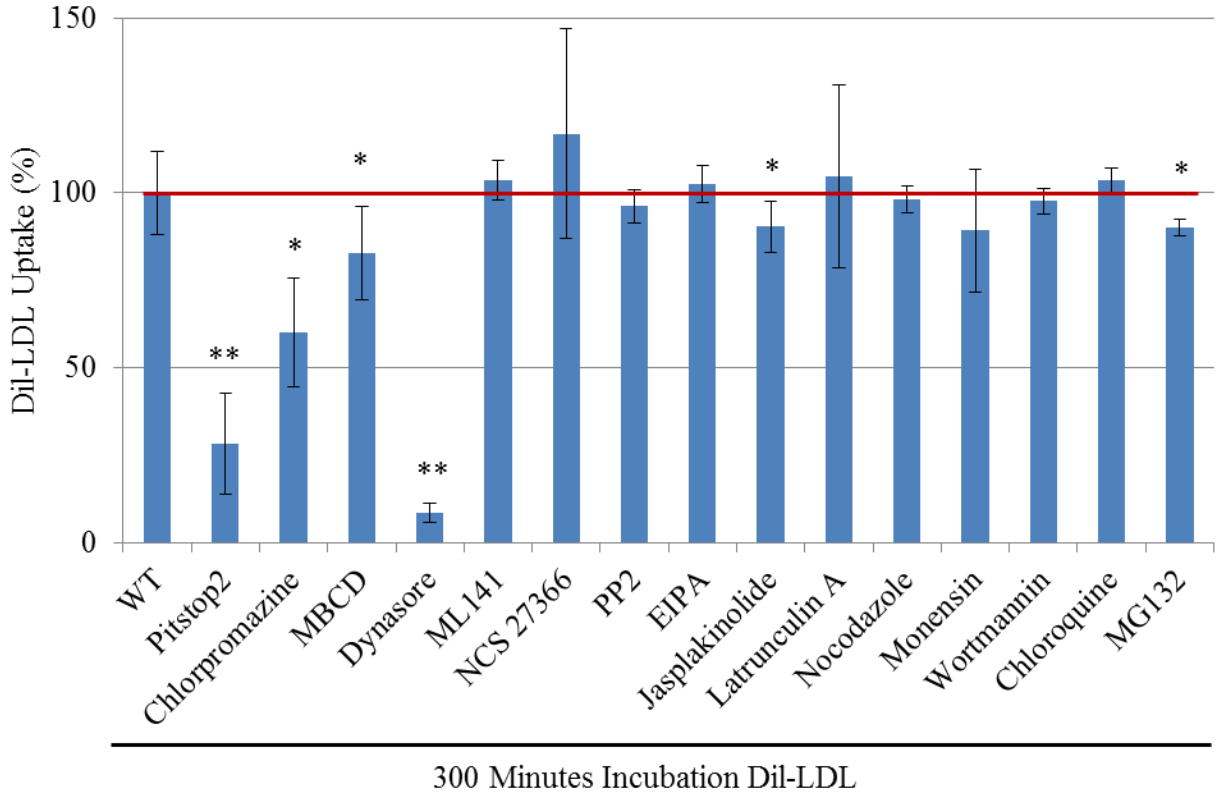

Figure 4.15: LDL uptake proceeds by a clathrin and dynamin-dependent mechanism in HA-Ank105-expressing cells
HA-Ank105-expressing cells were treated with each inhibitor of the small molecule endocytosis inhibitor panel for 30 minutes then incubated with Dil-LDL (50 µg/mL) for 300 minutes in the presence of inhibitor. Excess inhibitor was washed away. Internalized LDL was quantified as fluorescent signal intensity (Ex: 540 nm; Em: 580 nm) (Mean +/- S.D.). Data for each inhibitor is compared to untreated cells and analyzed for statistical significance by t-test (* indicates Pvalue <0.05, ** indicates Pvalue <0.001). Results were compiled from 3 independent experiments (N=3).

The effects of other broad endocytosis inhibitors, monensin and wortmannin, were also studied. Treatment of HA-Ank105-expressing cells with the proton gradient disruptor monensin did not inhibit LDL uptake (Figure 4.15). Monensin treated cells internalized LDL to a similar

extent as untreated control cells (Pvalue 0.15) (Figure 4.15), indicating cellular proton gradient is not required for LDL uptake. Likewise, inhibition of PI3K activity with wortmannin did not affect LDL uptake in HA-Ank105-expressing cells (Pvalue 0.26) (Figure 4.15).

The requirement of functional lysosomal and proteasomal pathways for LDL uptake in HA-Ank105-expressing cells was also determined. Inhibition of lysosomal degradation with chloroquine did not affect LDL uptake as cells treated with chloroquine internalized LDL to the same extent as untreated cells (Pvalue 0.16) (Figure 4.15). Treatment with the proteasomal degradation inhibitor MG132 blocked LDL uptake by 10% as compared to untreated HA-Ank105-expressing cells (Pvalue 0.003) (Figure 4.15). This data indicates that lysosomal degradation is not required for internalization of LDL in HA-Ank105-expressing cells.

4.7.3 Ligand-induced PDGFR degradation proceeds by a clathrin and dynamin-dependent mechanism and requires plasma membrane cholesterol

Next the effects of the endocytosis inhibitor panel were determined for ligand-induced PDGFR degradation to elucidate differences between constitutive degradation promoted by Ank105 and the canonical mechanism of receptor degradation. HA-Ank105-expressing cells were starved overnight in media containing 0.5% FBS to maximize responsiveness to stimulation. Cells were then treated with each of the small molecule endocytosis inhibitor panel. Cells were then stimulated for indicated times with PDGF (50 ng/mL) in the presence of inhibitor. Cells were analyzed by in-cell Western to quantify PDGFR protein expression levels (Figure 4.16A). As an example, full time course data set is shown for chloroquine, dynasore and MG132. In untreated cells overnight starvation in media containing 0.5% FBS increases PDGFR protein levels (Figure 4.16A). PDGFR is degraded over time in response to PDGF stimulation with the highest extent of degradation occurring after 240 minutes of ligand stimulation. PDGFR is degraded slower in chloroquine treated cells as compared to untreated control cells, with higher PDGFR protein expression levels at each time point (Figure 4.16A). Treatment with chloroquine increases PDGFR protein expressions levels by approximately 20% after 240 minutes of PDGF stimulation (Figure 4.16A,B). Treatment of HA-Ank105-expressing cells with dynasore inhibits ligand-induced PDGFR degradation. PDGFR expression levels are approximately 80% the level of unstimulated cells at each time point (Figure 4.16A,B). Treatment of HA-Ank105-expressing cells with MG132 impairs ligand-induced PDGFR

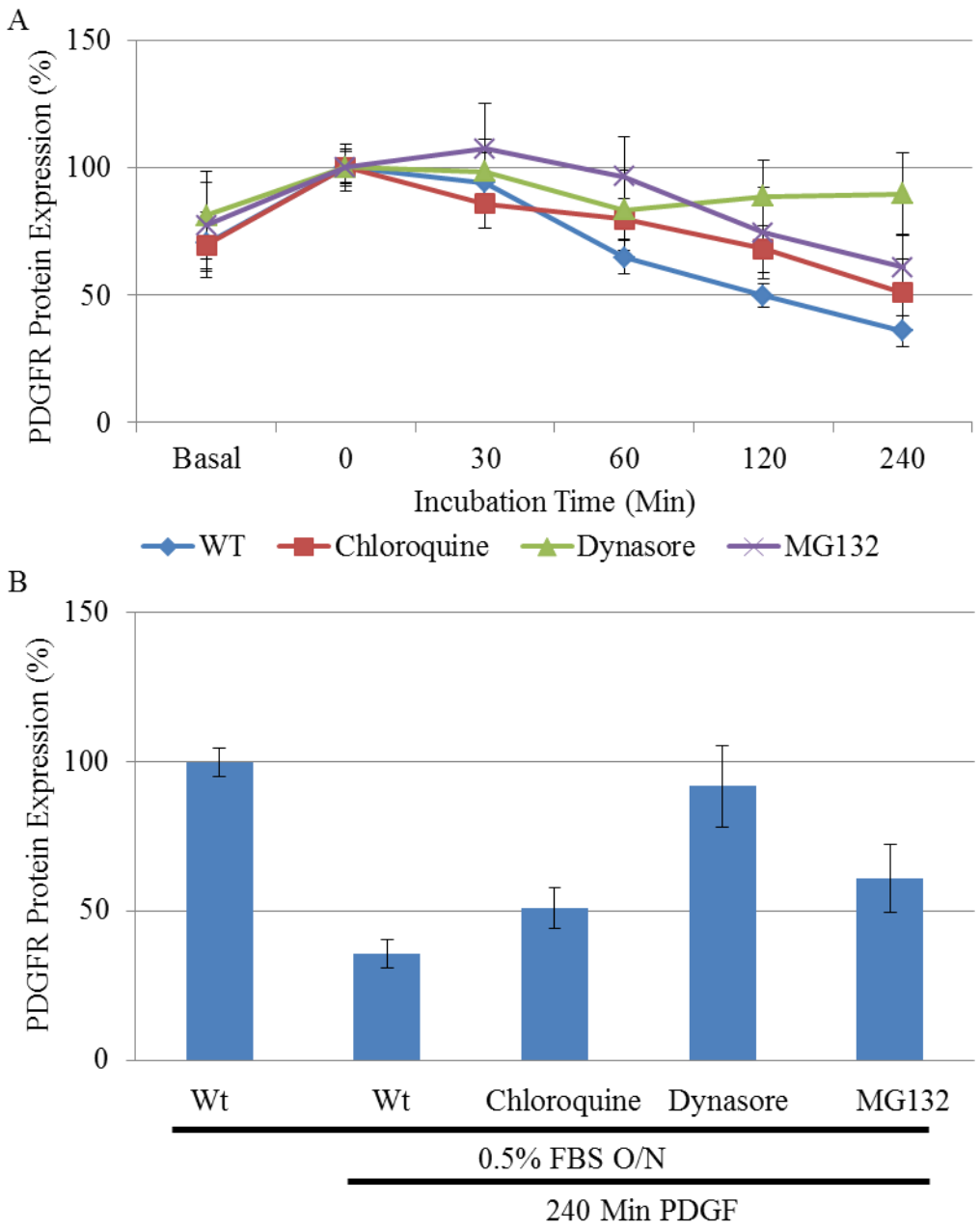

Figure 4.16: Ligand-induced PDGFR degradation is dynamin-dependent in HA-Ank105-expressing cells

A. HA-Ank105-expressing cells were cultured overnight in media containing 0.5% FBS to increase PDGFR levels and maximize responsiveness to stimulation. Cells were treated with chloroquine (25 µM), dynasore (80 µM) or MG132 (10 µM) for 30 minutes then stimulated with media containing PDGF (50 ng/mL) in the presence of inhibitor for indicated times. PDGFR protein expression was quantified by in-cell Western. B. Quantification and graphical representation (Mean +/- S.D.) of the 240 min time point of each treatment condition. Results were compiled from 3 independent experiments (N=3).

degradation. PDGFR is degraded slower in MG132 treated cells as compared to untreated control cells, with higher PDGFR protein expression levels at each time point (Figure 4.16A). Treatment with MG132 increases PDGFR protein expressions levels by approximately 30% after 240 minutes of PDGF stimulation (Figure 4.16A,B).

Due to the large amount of data collected the remainder of the data from each of the other endocytosis inhibitors in the panel is summarized (Figure 4.17). To simplify the comparison of the effects of these different inhibitors on ligand-induced PDGFR degradation, the 240 minute time point for each inhibitor is evaluated rather than the entire stimulation time course. In examining inhibitors affecting vesicle coat formation, chlorpromazine did not have an effect on ligand-induced degradation (Pvalue 0.97), however treatment of HA-Ank105-expressing cells with the CME inhibitor pitstop impaired ligand induced PDGFR degradation and increased PDGFR protein levels by approximately 2 fold as compared HA-Ank105-expressing cells not treated with inhibitor (Pvalue $8.5x10^{-4}$) (Figure 4.17). The data with the pitstop inhibitor strongly indicated that ligand induced PDGFR degradation in HA-Ank105-expressing cells occurs by a clathrin-dependent mechanism, possibly independent from the mechanism of action of chlorpromazine. Recall the different mechanisms of these two inhibitors; chloropromazine induces misassembly of the clathrin lattice on endosomes whereas pitstop prevents adaptor assembly.

Extraction of plasma membrane cholesterol with MβCD partially inhibited ligand induced degradation (Figure 4.17). PDGFR protein expression levels in HA-Ank105-expressing cells treated with MβCD were approximately 2 fold higher after 240 minutes of ligand stimulation as compared to control cells (Pvalue $1.5x10^{-7}$) (Figure 4.17). This data suggests that ligand induced PDGFR degradation is sensitive to levels of plasma membrane cholesterol. Some proportion of ligand-induced internalization may proceed by caveolar endocytosis. MβCD treatment did not have an extensive effect on LDL uptake (Figure 4.15), a molecule known to be internalized by a clathrin-dependent mechanism, whereas MβCD treatment partially inhibited ligand-induced degradation. Additionally chlorpromazine treatment inhibited 40% of LDL uptake (Figure 4.15) but did not affect ligand induced degradation (Figure 4.17).

The effect of internalization inhibitors on ligand-induced PDGFR degradation was next determined. Inhibition of dynamin activity with dynasore strongly inhibited PDGFR degradation in HA-Ank105-expressing cells. Indeed, dynasore treatment inhibits 90% of PDGFR degradation

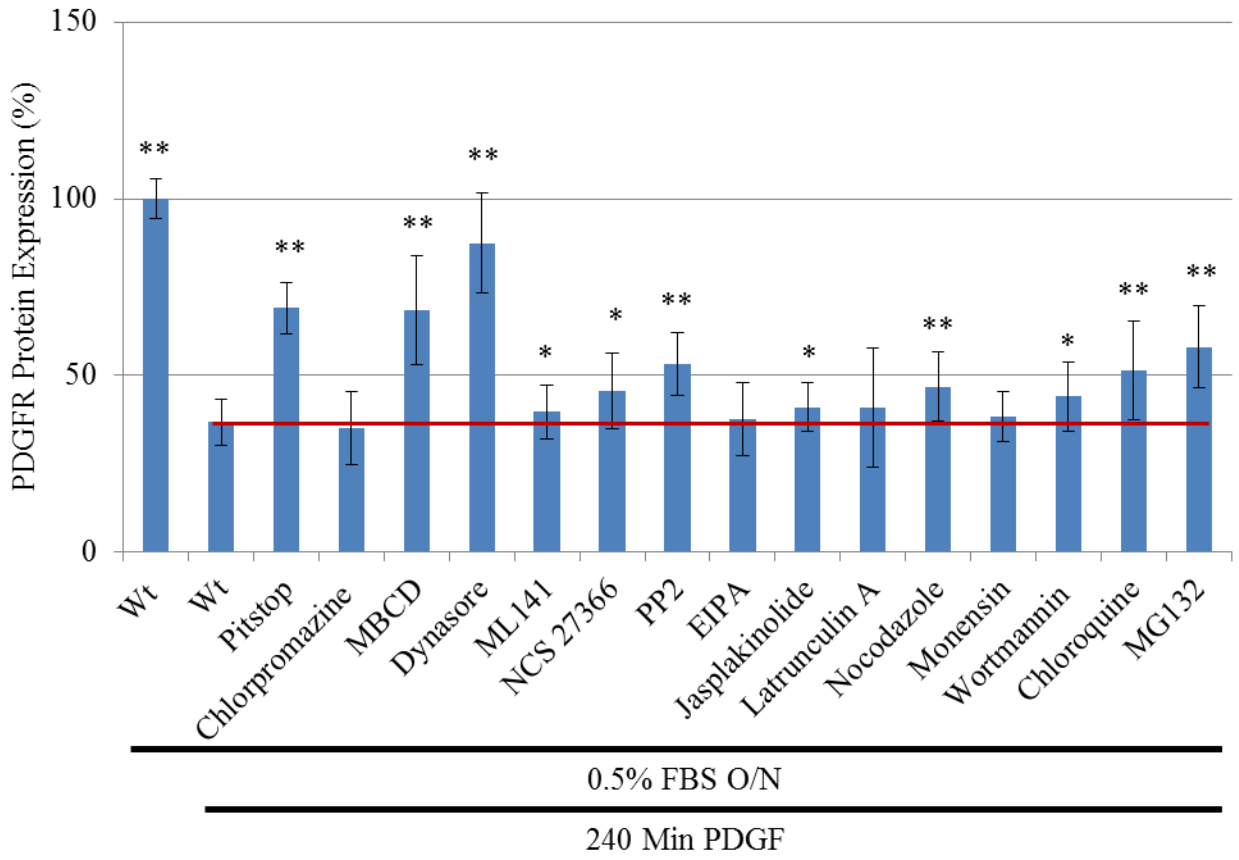

Figure 4.17: Ligand-induced PDGFR degradation requires clathrin, dynamin activity and plasma membrane cholesterol
HA-Ank105-expressing cells were cultured overnight in media containing 0.5% FBS to increase PDGFR levels and maximize responsiveness to stimulation. Cells were treated with each inhibitor of the small molecule endocytosis inhibitor panel for 30 minutes then stimulated with media containing PDGF (50 ng/mL) in the presence of inhibitor for indicated times. PDGFR protein expression was quantified by in-cell Western (Mean +/- S.D.). Data for each inhibitor is compared to untreated cells stimulated for 240 minutes with PDGF and analyzed for statistical significance by t-test (* indicates Pvalue <0.05, ** indicates Pvalue <0.001). Results were compiled from 3 independent experiments (N=3).

(Pvalue 4.1×10^{-11}) (Figure 4.17), indicating that dynamin activity is essential for ligand-induced PDGFR degradation. Inhibition of the CLIC/GEEC pathway with Cdc42 inhibitor ML141 did not affect ligand-induced PDGFR degradation. The PDGFR protein expression levels in ML141 treated cells are only 5% higher than untreated control cells after 240 minutes of PDGF stimulation (Pvalue 0.043) (Figure 4.17). Inhibition of macropinocytosis with Rac-1 inhibitor NCS 27366 also slightly inhibited ligand-induced PDGFR degradation (Figure 4.17). The PDGFR protein expression levels in NCS 27366 treated cells are only 10% higher than untreated

control cells after 240 minutes of PDGF stimulation (Pvalue 0.00158) (Figure 4.17). Treatment of HA-Ank105-expressing cells with Src family kinase inhibitor PP2 partially inhibited ligand-induced PDGFR degradation. PDGFR protein expression levels in PP2 treated cells are 20% higher than untreated control cells after 240 minutes of PDGF stimulation (Pvalue $2.1x10^{-7}$) (Figure 4.17). Treatment with EIPA however did not affect ligand-induced PDGFR degradation (Figure 4.17). Cell treated with EIPA had similar PDGFR expression levels as control cells after 240 minutes of PDGF stimulation (Pvalue 0.37) (Figure 4.17). Taken together the data with internalization inhibitors suggest that ligand-induced PDGFR degradation proceeds predominantly by a dynamin-dependent mechanism. The CLIC/GEEC and macropinocytotic endocytosis mechanisms may play a sight role in ligand-induced PDGFR degradation. Treatment with PP2 inhibits ligand- induced degradation to a greater extent than NCS 27366, possibly due to the fact that SRC family kinases are implicated in endocytosis pathways other than macropinocytosis, such as caveolar endocytosis (Doherty and McMahon, 2009b).

The effects of cytoskeletal inhibitors on LDL uptake were next determined. Treatment with the actin de-polymerization inhibitor jasplakinolide slightly inhibited ligand-induced PDGFR degradation (Figure 4.17). The PDGFR protein expression levels in jasplakinolide treated cells are 7% higher than in untreated control cells stimulated for 240 minutes with PDGF (Pvalue 0.008) (Figure 4.17). Treatment with the actin polymerization inhibitor latrunculin A did not affect ligand-induced degradation as latrunculin A treated cells had similar PDGFR protein expression levels as untreated cells (Pvalue 0.29) (Figure 4.17). Treatment with the microtubule polymerization inhibitor nocodazole slightly inhibited ligand-induced PDGFR degradation (Figure 4.17). Nocodazole treated cells expressed approximately 12% more PDGFR protein than untreated control cells stimulated with PDGF for 240 minutes (Pvalue 0.00024) (Figure 4.17). Taken together the data suggests that the actin cytoskeleton may have a minimal role in ligand-induced PDGFR degradation, whereas the microtubule cytoskeleton may be more involved.

The effects of other broad endocytosis inhibitors, monensin and wortmannin, were also studied. Treatment of HA-Ank105-expressing cells with the proton gradient disruptor monensin did not affect ligand-induced PDGFR degradation as the expression level of PDGFR protein in monensin treated cells are similar to untreated control cells (Pvalue 0.13) (Figure 4.17). Treatment with wortmannin slightly inhibited ligand-induced PDGFR degradation (Figure 4.17). Wortmannin treated cells expressed approximately 10% more PDGFR protein than untreated

control cells stimulated with PDGF for 240 minutes (Pvalue 0.003) (Figure 4.17).

The requirement of functional lysosomal and proteasomal pathways for ligand-induced PDGFR degradation in HA-Ank105-expressing cells was also determined. Inhibition of lysosomal degradation with chloroquine and proteasomal degradation with MG132 both partially inhibited PDGFR degradation (Figure 4.17). Cells treated with chloroquine expressed 16% more PDGFR protein after 240 minutes of PDGF stimulation than untreated control cells (Pvalue 0.00034) and cells treated with MG132 expressed 23% more PDGFR protein than untreated control cells (Pvalue $3.9x10^{-7}$) (Figure 4.17).

4.8 shRNA-mediated knockdown of endocytosis proteins

To further define the endocytosis pathway by which Ank105-mediated constitutive PDGFR degradation occurs, proteins involved in several stages of endocytosis were targeted for knockdown via small hairpin RNA (shRNA) (Figure 4.18). Coat formation in clathrin-mediated and caveolar endocytosis was targeted for inhibition by transfection of HA-Ank105-expressing cells with shRNA plasmids directed against the heavy chain of clathrin and caveolin-1, respectively (Figure 4.18). The internalization step of endocytosis was targeted for inhibition with shRNA specific for dynamin-II (Figure 4.18). Multivesicular body biogenesis was targeted with shRNA directed against tsg101 (Figure 4.18). Trafficking to the lysosome was targeted via knockdown of rab7 (Figure 4.18). Known binding partners of Ank105 were also targeted for shRNA mediated knockdown including p85 and spectrin β-II (Figure 4.18). HA-Ank105-expressing cells were also transfected with control shRNA plasmids, which are not specific for any known protein. If the proteins targeted for knockdown are required for Ank105-mediated constitutive PDGFR degradation, then reduction of expression would lead to an increase in PDGFR protein expression levels. Knockdown of proteins required for Ank105 function should revert the phenotype cause by HA-Ank105 overexpression. For each shRNA transduced into HA-Ank105-expressing cells, 24 clones were isolated under puromycin selection. Those clones surviving expansion were analyzed for mRNA expression of target knockdown genes.

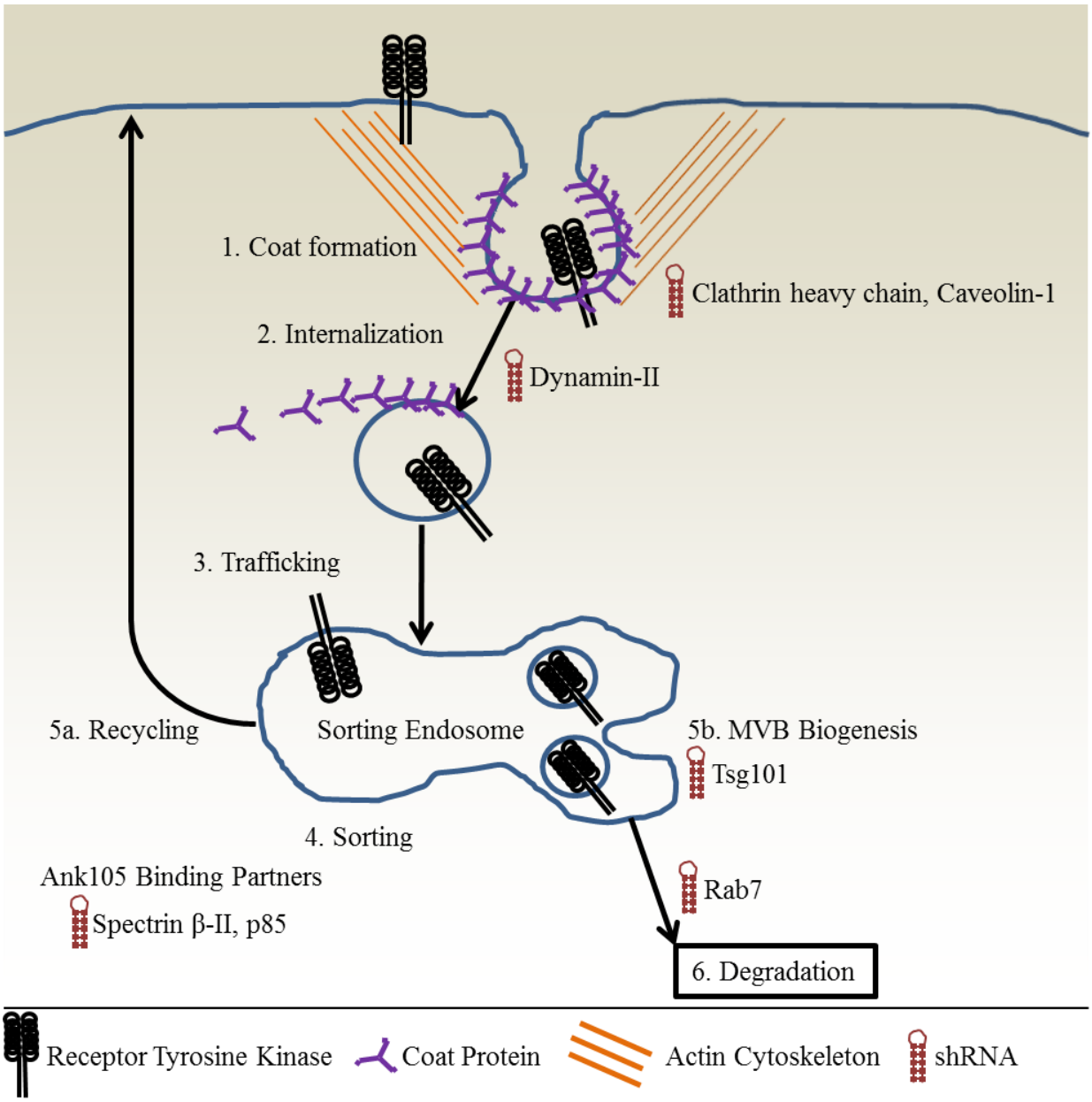

Figure 4.18: General endocytosis pathway and targets of small hairpin RNAs
Depicts a general scheme of endocytosis common to major pathways, as well as delineates stages of endocytosis targeted by various small hairpin RNAs (shRNA). Cell surface receptors are incorporated into budding, protein coated vesicles (1.). Budding vesicles are internalized (2.), often requiring dynamin activity. Internalized vesicles are trafficked to the sorting endosome (3.) where they are sorted (4.) and either recycled back to the plasma membrane (5a.) or incorporated into multivesicular bodies (5b.) and subsequently trafficked for degradation (6.).

4.8.1 Inability to generate clathrin knockdown clones

HA-Ank105-expressing cells were lentivirally transduced with shRNA directed against the heavy chain of clathrin. Stable clathrin knockdown clones were generated under puromycin

selection (Figure 4.19). Clathrin heavy chain mRNA expression was evaluated by RT-PCR in

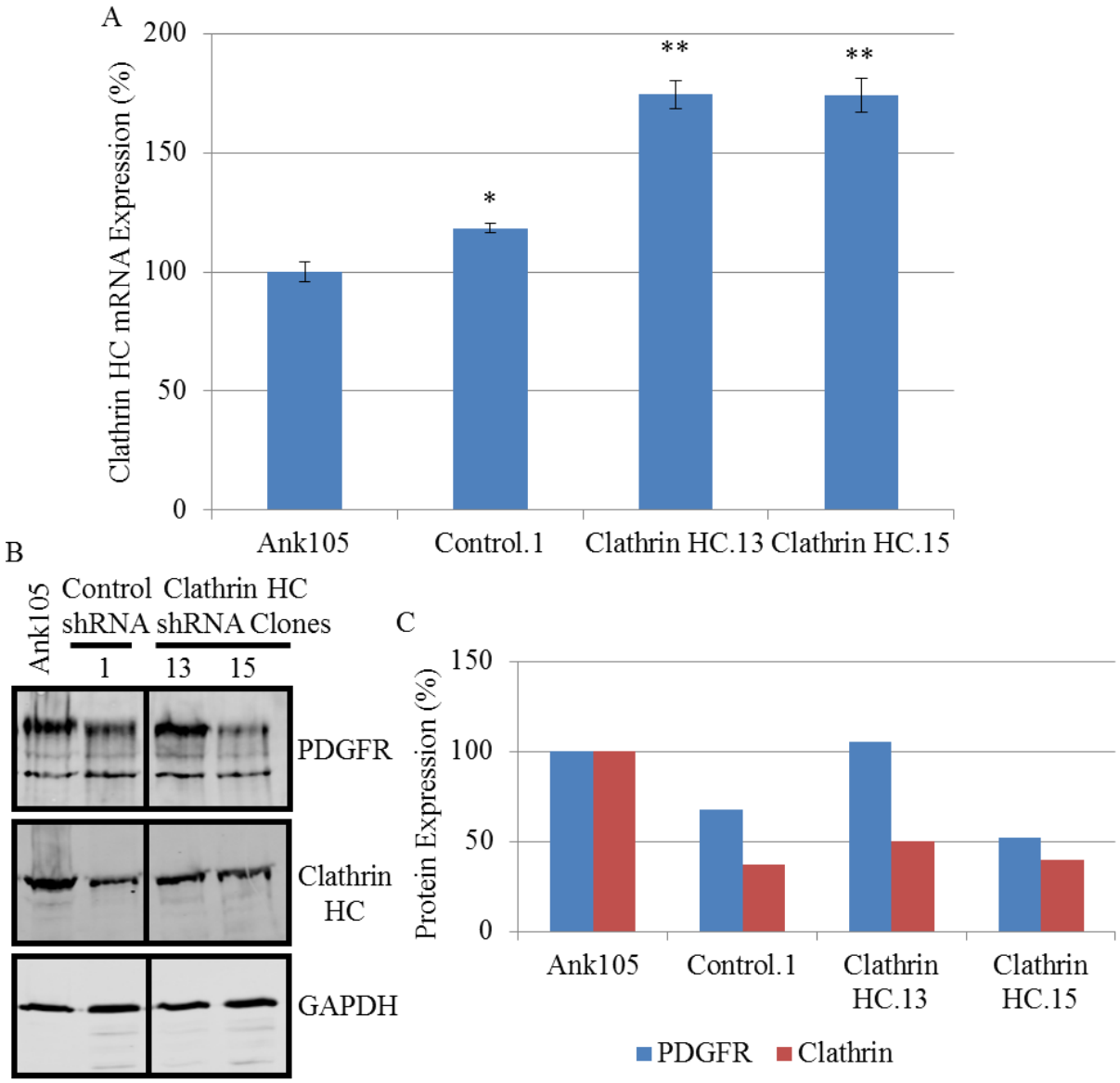

Figure 4.19: Unsuccessful shRNA knockdown of clathrin heavy chain in Ank105-expressing cells

HA-Ank105-expressing cells stably transduced with scrambled shRNA or shRNA specifically targeting clathrin heavy chain (clathrin HC) were generated. A. mRNA was purified, converted to cDNA and analyzed for clathrin HC expression via qRT-PCR and normalized to β-actin expression. (* indicates Pvalue <0.05; ** indicates Pvalue <0.001) Results were compiled from 3 independent experiments (N=3). B. Lysates were resolved by SDS-PAGE (100 µg) and analyzed via Western blot for PDGFR, clathrin heavy chain and GAPDH expression. C. Quantification and graphical representation of Figure 4.19b. Data compared to expression in Ank105 Samples. N=1.

stable knockdown cell lines and compared to HA-Ank105-expressing cells and HA-Ank105-

expressing cells stably transduced with control scrambled shRNA (Figure 4.19A). The two clones obtained, Clathrin HC.13 and Clathrin HC.15, did not demonstrate knockdown in clathrin heavy chain expression (Figure 4.19A). Indeed, clathrin heavy chain mRNA expression was higher in clathrin HC.13 and clathrin HC.15 than HA-Ank105-expressing cells (Figure 4.19A). Clathrin heavy chain mRNA expression levels were slightly higher in cells transduced with control scrambled shRNA HA-Ank105-expressing cells (Figure 4.19A). Additionally, clathrin heavy chain protein expression levels were robust when examined by Western blot (Figure 4.19B,C). Only two stable clathrin heavy chain knockdown cell lines were obtained, suggesting that clathrin heavy chain expression may be essential for viability in HA-Ank105-expressing cells.

4.8.2 Knockdown of dynamin-II does not recover PDGFR protein levels in HA-Ank105-expressing cells.

Two isoforms of dynamin are expressed. Dynamin-I is expressed in neuronal cells while dynamin-II is expressed ubiquitously (Altschuler *et al*., 1998). HA-Ank105-expressing cells were lentivirally transduced with shRNA directed against dynamin-II. Stable dynamin knockdown clones were generated under puromycin selection. Dynamin-II mRNA expression was evaluated by qRT-PCR in stable knockdown cell lines and compared to HA-Ank105-expressing cells and HA-Ank105-expressing cells stably transduced with control scrambled shRNA (Figure 4.20A). Two cells lines were identified reduction in dynamin-II mRNA expression. The dynamin-II.15 cell line showed the greatest level of knockdown, with expression levels reduced 50% as compared to HA-Ank105-expressing cells (Pvalue 0.014) (Figure 4.20A). The dynamin-II.17 cell displayed expression levels reduced 40% as compared to control cells (Pvalue 0.022) (Figure 4.20A). Dynamin-II mRNA expression levels were similar between HA-Ank105-expressing cells and cells transduced with control scrambled shRNA (Pvalue 0.08) (Figure 4.20A). Cell lines showing reduction in dynamin-II mRNA were examined by Western blot for PDGFR and dynamin protein expression (Figure 4.20B,C). Dynamin-II.15 (Pvalue 0.04) and dynamin-II.17 (Pvalue 0.04) cell lines also demonstrated reduction in dynamin protein expression levels (Figure 4.20B,C). Knockdown of dynamin-II in these cell lines did not increase PDGFR levels. PDGFR protein expression levels in dynamin-II.15 (Pvalue 0..07) and dynamin-

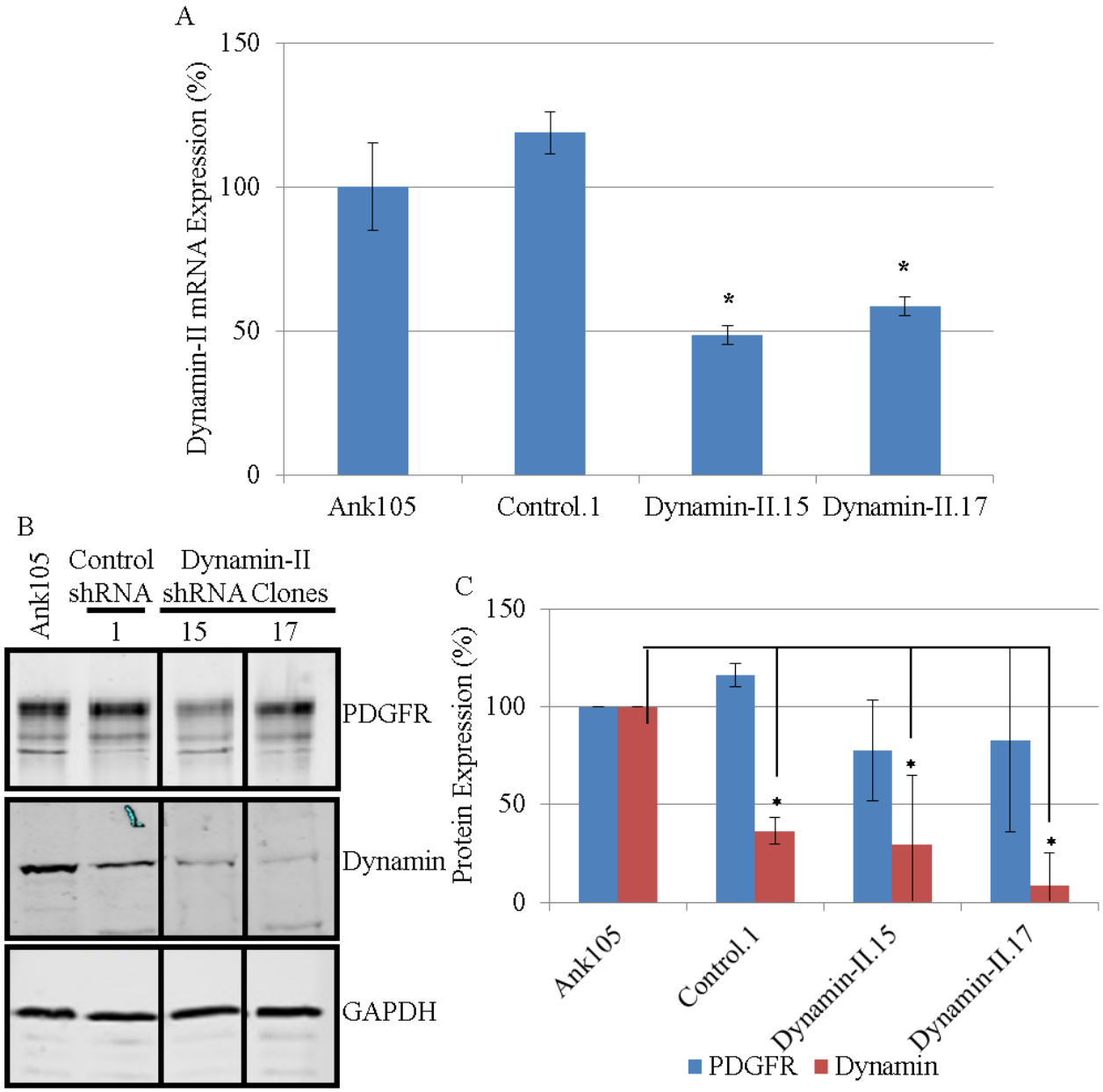

Figure 4.20: Knockdown of dynamin in Ank105-expressing cells does not impact constitutive PDGFR degradation

HA-Ank105-expressing cells stably transduced with scrambled shRNA or shRNA specifically targeting dynamin-II were generated. A. mRNA was purified, converted to cDNA and analyzed for dynamin-II expression via qRT-PCR and normalized to β-actin expression. Results were compiled from 3 independent experiments (N=3). B. Lysates were resolved by SDS-PAGE (100 µg), transferred to a nitrocellulose membrane and analyzed via Western blot for PDGFR, dynamin-II and GAPDH expression. C. Quantification of Figure 4.20b (Mean +/- S.D.). Data compared to expression in Ank105 samples via t-test. (* indicates Pvalue <0.05; ** indicates Pvalue <0.001). Results were compiled from 3 independent experiments (N=3).

II.17 (Pvalue 0.10) knockdown cell lines was similar to HA-Ank105-expressing cells (Figure 4.20B,C). A caveat with this data there is a large degree of variance in quantification of PDGFR protein levels across these cells lines (Figure 4.20C). Additionally, dynamin protein expression levels in cells transduced with control scrambled shRNA are reduced as compared to HA-Ank105-expressing cells (Figure 4.20B,C). This result is unexpected considering the two cell lines have similar dynamin-II mRNA expression levels (Figure 4.20A). It may be prudent to examine additional scrambled shRNA controls for dynamin-II mRNA and protein expression levels as well as perform additional replicates to decrease variance in the data.

4.8.3 Knockdown of tsg101 does not recover PDGFR protein levels in HA-Ank105-expressing cells.

HA-Ank105-expressing cells were lentivirally transduced with shRNA directed against tsg101 to impair MVE formation. Stable tsg101 knockdown clones were generated under puromycin selection. Tsg101 mRNA expression was evaluated by RT-PCR in stable knockdown cell lines and compared to HA-Ank105-expressing cells and HA-Ank105-expressing cells stably transduced with control scrambled shRNA (Figure 4.21A). Several cell lines were identified showing a statistically significant reduction in tsg101 mRNA expression. The tsg101.3 cell line demonstrated the greatest extent of knockdown, with levels reduced 75% as compared to HA-Ank105-expressing cells (Pvalue 1.79×10^{-5}) (Figure 4.21A). Tsg101 mRNA expression levels in the other stable knockdown cell lines, tsg101.7 (Pvalue 7.10×10^{-5}), tsg101.13 (Pvalue 2.31×10^{-5}) and tsg101.14 (Pvalue 0.00067), were reduced approximately 50% as compared to HA-Ank105-expressing cells (Figure 4.21A). Cells transduced with control scrambled shRNA had slightly elevated tsg101 mRNA expression levels as compared to HA-Ank105-expressing cells(Pvalue 0.039) (Figure 4.21A).

The cell lines showing knockdown of tsg101 mRNA expression were evaluated for PDGFR and GAPDH protein expression (Figure 4.21B,C). Tsg101.3 (Pvalue 0.16), tsg101.7 (Pvalue 0.44) tsg101.13 (Pvalue 0.18) and tsg101.14 (Pvalue 0.40) knockdown cell lines all displayed PDGFR protein expression levels similar to HA-Ank105-expressing cells (Figure 4.21B,C). PDGFR protein expression levels in cells transduced with control scrambled shRNA were similar to HA-Ank105-expressing cells (Pvalue 0.054) (Figure 4.21B,C). The tsg101 knockdown cell lines were also evaluated for tsg101 protein expression levels. However, despite

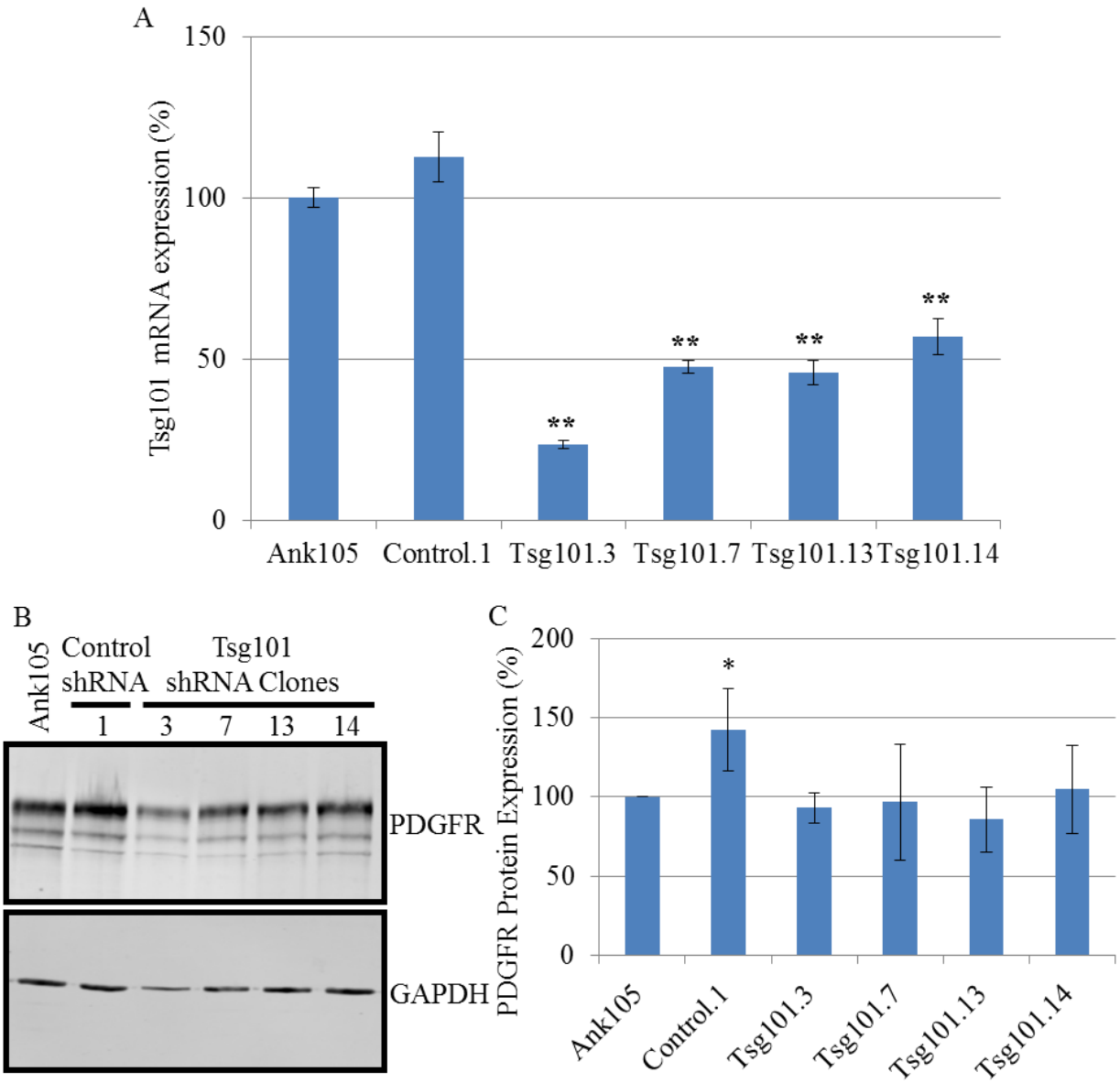

Figure 4.21: shRNA knockdown of tsg101 in HA-Ank105-expressing cells does not recover constitutive PDGFR expression

HA-Ank105-expressing cells stably transduced with scrambled shRNA or shRNA specifically targeting tsg101 were generated. A. mRNA was purified, converted to cDNA and analyzed for tsg101 expression via qRT-PCR and normalized to β-actin expression. Results were compiled from 3 independent experiments (N=3). B. Lysates were resolved by SDS-PAGE (100 µg) and analyzed via Western blot for PDGFR and GAPDH expression. C. Quantification and graphical representation of Figure 4.21b (Mean +/- S.D.). Data compared to expression in Ank105 samples by t-test. (* indicates Pvalue <0.05; ** indicates Pvalue <0.001). Results were compiled from 3 independent experiments (N=3).

testing several commercially available antibodies, suitable antibodies for Western blot detection

of tsg101 protein expression in HA-Ank105-expressing cells were not obtained. Assuming the reduction in tsg101 mRNA expression levels correspond to reduction in tsg101 protein levels, the data indicates that Ank105-mediated constitutive PDGFR degradation may be independent of tsg101 function since 75% knockdown of tsg101 mRNA levels does not increase constitutive PDGFR protein levels. Tsg101 has been shown to be required for sorting ligand activated EGFR into multivesicular bodies and subsequent degradation. An alternative explanation is that the level of knockdown achieved is insufficient to disrupt tsg101 function.

4.8.4 Knockdown of rab7 in HA-Ank105-expressing cells reduces PDGFR protein expression levels

Ha-Ank105-expressing cells were lentivirally transduced with shRNA directed against rab7. Stable rab7 knockdown clones were generated under puromycin selection. Rab7 mRNA expression was evaluated by RT-PCR in stable knockdown cell lines and compared to HA-Ank105-expressing cells and Ank105-expressing cells stably transduced with control scrambled shRNA (Figure 4.22A). Several cells lines were identified showing a statistically significant reduction in rab7 mRNA expression. Rab7 mRNA expression in the rab7.4 knockdown cell line was reduced 85% as compared to HA-Ank105-expressing cells (Pvalue 0.003) (Figure 4.22A). The rab7.11 cell line showed an 80% reduction in rab7 mRNA levels (Pvalue 0.0033) (Figure 4.22A). The rab7.15 cells line displayed a 60% reduction in rab7 mRNA as compared to HA-Ank105-expressing cells (Pvalue 0.006) (Figure 4.22A). The rab7.17 cell line had the greatest level of knockdown, expressing 87% less rab7 mRNA as HA-Ank105-expressing cells (Pvalue 0.005) (Figure 4.22A). The rab7 mRNA expression levels in cells transduced with control scrambled shRNA were similar to HA-Ank105-expressing cells (Pvalue 0.19) (Figure 4.22A).

The cell lines showing knockdown of rab7 mRNA expression were evaluated for PDGFR and GAPDH protein expression (Figure 4.22B,C). The majority of the rab7 knockdown cells lines showed reduction in PDGFR protein expression levels. The rab7.4 cell line had 25% reduced PDGFR protein expression levels as compared to HA-Ank105-expressing cells (Pvalue 0.011) (Figure 4.22B,C). The PDGFR expression levels in the rab7.11 cell line were 55% less than HA-Ank105-expressing cells (Pvalue 0.004) (Figure 4.22B,C). Rab7.15 displayed the greatest reduction in PDGFR protein expression levels, being 65% less than HA-Ank105-

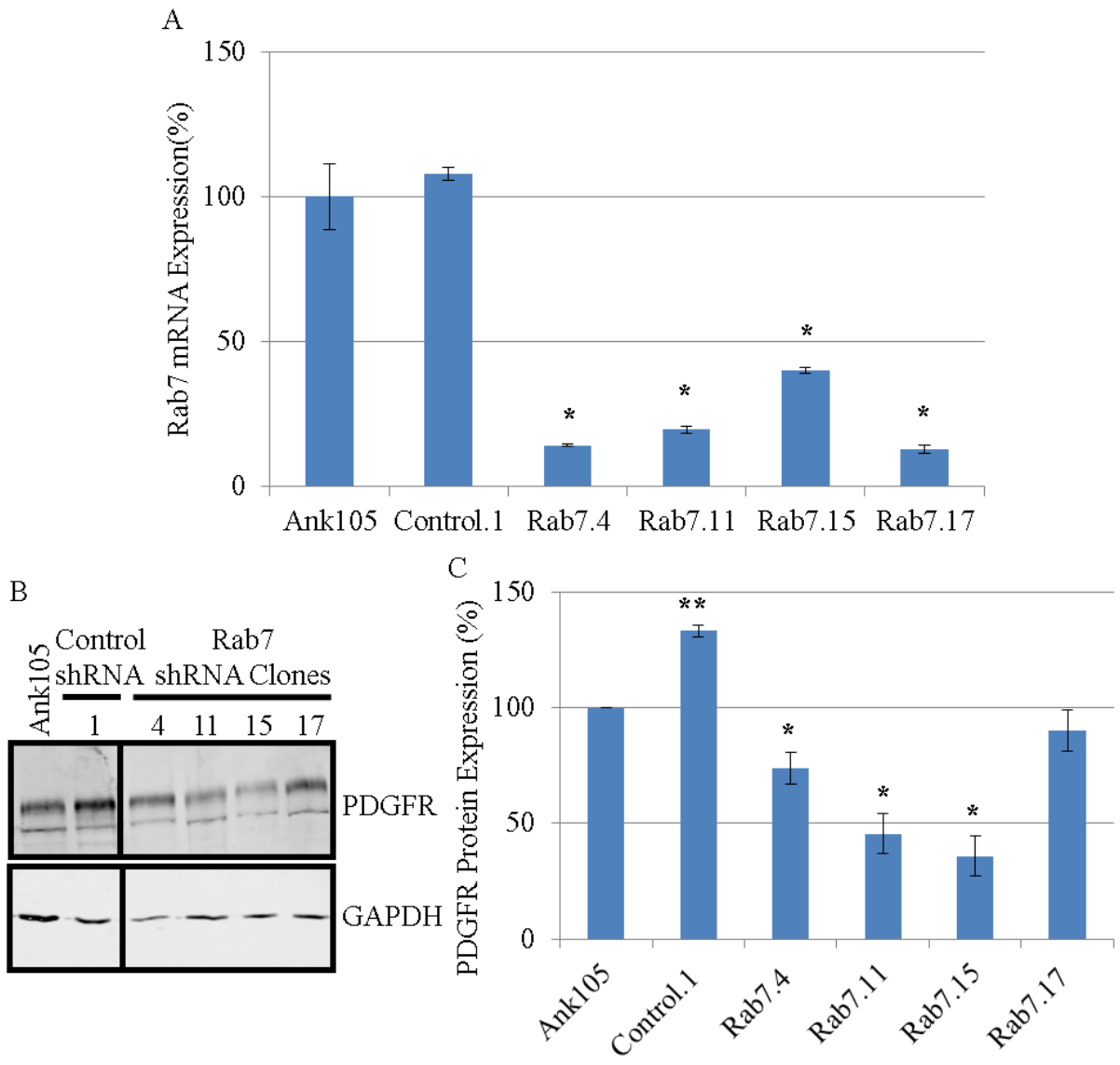

Figure 4.22: Knockdown of rab7 in HA-Ank105-expressing cells reduces PDGFR protein expression levels

HA-Ank105-expressing cells stably transduced with scrambled shRNA or shRNA specifically targeting rab7 were generated. A. mRNA was purified, converted to cDNA and analyzed for rab7 expression via qRT-PCR and normalized to β-actin expression. Results were compiled from 3 independent experiments (N=3). B. Lysates were resolved by SDS-PAGE (100 µg), transferred to a nitrocellulose membrane and analyzed via Western blot for PDGFR and GAPDH expression. C. Quantification and graphical representation of Figure 4.22b (Mean +/- S.D.). Data compared to expression in Ank105 samples by t-test. (* indicates Pvalue <0.05; ** indicates Pvalue <0.001). Results were compiled from 3 independent experiments (N=3).

expressing cells (Pvalue 0.0031) (Figure 4.22B,C). The trend with reduction of PDGFR levels does not follow the level of rab7 mRNA expression in knockdown cell lines. The cell lines with

the highest extent of rab7 mRNA knockdown do not necessarily show the greatest reduction in PDGFR protein expression. The cell line with the lowest PDGFR expression level, being rab7.15, has the highest rab7 mRNA expression levels of the knockdown cell lines characterized (Figure 4.22B,C). The cell line showing most extensive knockdown of rab7 mRNA, rab7.17, had PDGFR protein expression levels similar to HA-Ank105-expressing cells (Pvalue 0.10). PDGFR protein expression levels in cells transduced with control scrambled shRNA were 30% higher than Ank-105-expressing cells (Pvalue 0.001) (Figure 4.22B,C), highlighting the need to characterize these cell lines with additional scrambled shRNA controls. The rab7 knockdown cell lines were also evaluated for rab7 protein expression levels. However, despite testing several commercially available antibodies, I was unable to identify an antibody suitable for Western blot detection of rab7 protein expression in HA-Ank105-expressing cells. Assuming the reduction in rab7 mRNA expression levels correspond to reduction in rab7 protein levels, the data indicates that knockdown of rab7, in the majority of cell lines tested, promotes reduction in PDGFR protein expression. One potential explanation is that inhibition of lysosomal trafficking promotes alternative mechanisms of degradation, such as proteasomal degradation. Indeed Ank105-mediated constitutive PDGFR degradation was completely inhibited by MG132 treatment (Figure 4.13).

4.9 Contributions of Ank105 binding partners to constitutive PDGFR degradation

4.9.1 Knockdown of βII-spectrin in HA-Ank105-expressing cells reduces PDGFR protein expression levels

HA-Ank105-expressing cells were lentivirally transduced with shRNA directed against the Ank105 binding partner βII-spectrin. Stable βII-spectrin knockdown clones were generated under puromycin selection. βII-spectrin mRNA expression was evaluated by RT-PCR in stable knockdown cell lines and compared to HA-Ank105-expressing cells and HA-Ank105-expressing cells stably transduced with control scrambled shRNA (Figure 4.23A). Two cells lines were identified showing a statistically significant reduction in βII-spectrin mRNA expression. The βII-spectrin.1 cell line had the greatest level of knockdown, expressing 85% less βII-spectrin mRNA as HA-Ank105-expressing cells (Pvalue 0.0008) (Figure 4.23A). The βII-spectrin.7 cell line expressed 65% less βII-spectrin mRNA than HA-Ank105-expressing cells (Pvalue 0.001)

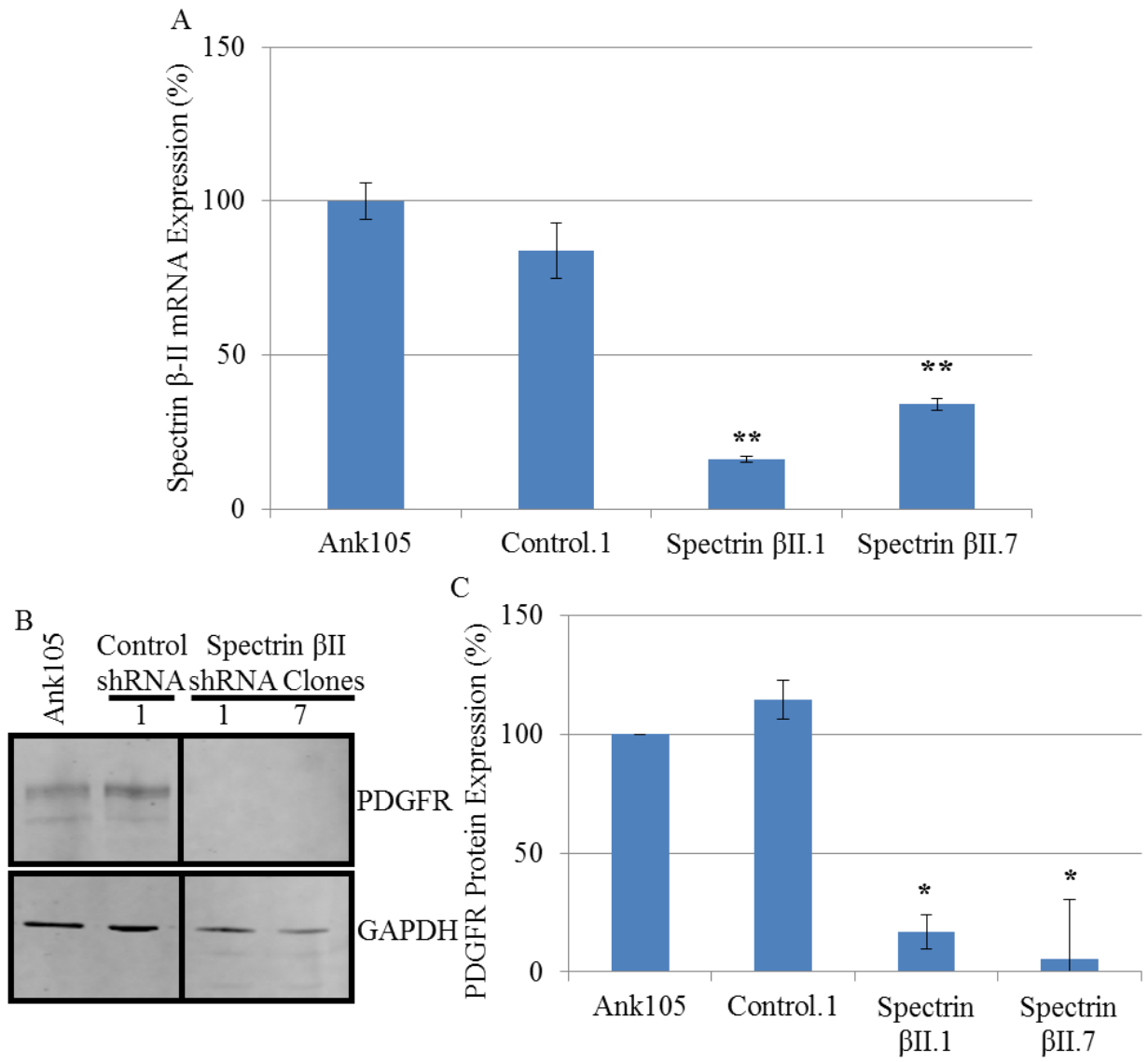

Figure 4.23: Knockdown of βII-spectrin in HA-Ank105-expressing cells reduces PDGFR protein expression levels

HA-Ank105-expressing cells stably transduced with scrambled shRNA or shRNA specifically targeting βII-spectrin were generated. A. mRNA was purified, converted to cDNA and analyzed for βII-spectrin expression via qRT-PCR and normalized to β-actin expression. Results were compiled from 3 independent experiments (N=3). B. Lysates were resolved by SDS-PAGE (100 µg), transferred to a nitrocellulose membrane and analyzed via Western blot for PDGFR and GAPDH expression. C. Quantification and graphical representation of Figure 4.23b (Mean +/- S.D.). Data compared to expression in Ank105 samples by t-test. (* indicates Pvalue <0.05; ** indicates Pvalue <0.001). Results were compiled from 3 independent experiments (N=3).

(Figure 4.23A). Cells transduced with control scrambled shRNA had similar βII-spectrin mRNA expression levels as HA-Ank105-expressing cells (Pvalue 0.05) (Figure 4.23A). The cell lines

showing knockdown of βII-spectrin mRNA expression were evaluated for PDGFR and GAPDH protein expression (Figure 4.23B,C). PDGFR protein expression levels were significantly reduced in the βII-spectrin.1 cell line, expressing 83% less PDGFR than HA-Ank105-expressing cells (Pvalue 0.0012) (Figure 4.23B,C). The βII-spectrin.7 cell line expressed 95% less PDGFR than HA-Ank105-expressing cells (Pvalue 0.011) (Figure 4.23B,C). PDGFR expression levels were similar in cells transduced with control scrambled shRNA as compared to HA-Ank105-expressing cells (Pvalue 0.05) (Figure 4.23B,C).

4.9.2 Knockdown of p85α in HA-Ank105-expressing cells does not affect PDGFR protein expression levels

As p85α was identified by our laboratory as a binding partner of Ank105 (Ignatiuk *et al*., 2006), the requirement of p85α expression for constitutive PDGFR degradation in Ank105-expressing cells was determined by RNA interference. If p85α is indeed required to mediate Ank105 function, knockdown of p85α would be expected to elevate constitutive PDGFR expression levels. HA-Ank105-expressing cells were lentivirally transduced with shRNA directed against the Ank105 binding partner p85α. Stable p85α knockdown mixed populations were generated under puromycin selection. A control mixed population was also generated via transduction of HA-Ank105-expressing cells with scrambled shRNA, followed by selection in puromycin. Lysates from HA-Ank105-expressing cells, control scrambled shRNA mixed population and p85α knockdown mixed population cell lines were evaluated for PDGFR, p85α and GAPDH protein expression via Western blot (Figure 4.24A,B). PDGFR protein expression levels were similar in HA-Ank105-expressing, control scrambled shRNA mixed population (Pvalue 0.42) and p85α knockdown mixed population cell lines (Pvalue 0.10), while only the p85α knockdown mixed population cell line demonstrated reduction in p85α protein expression levels (Figure 4.24A,B). Indeed, p85α protein expression was attenuated by 80% in the p85α knockdown mixed population cell line (Pvalue 0.007) as compared to HA-Ank105-expressing and the control scrambled shRNA mixed population cell line (Pvalue 0.31) (Figure 4.24A,B). These results indicate that p85α is not required for Ank105-mediated constitutive PDGFR degradation. Even though p85α was demonstrated to be a binding partner of Ank105 via both binding studies with purified proteins and co-immunoprecipitation studies in cells (Ignatiuk *et al*., 2006), the interaction of Ank105 and p85α may be involved in other cellular pathways other

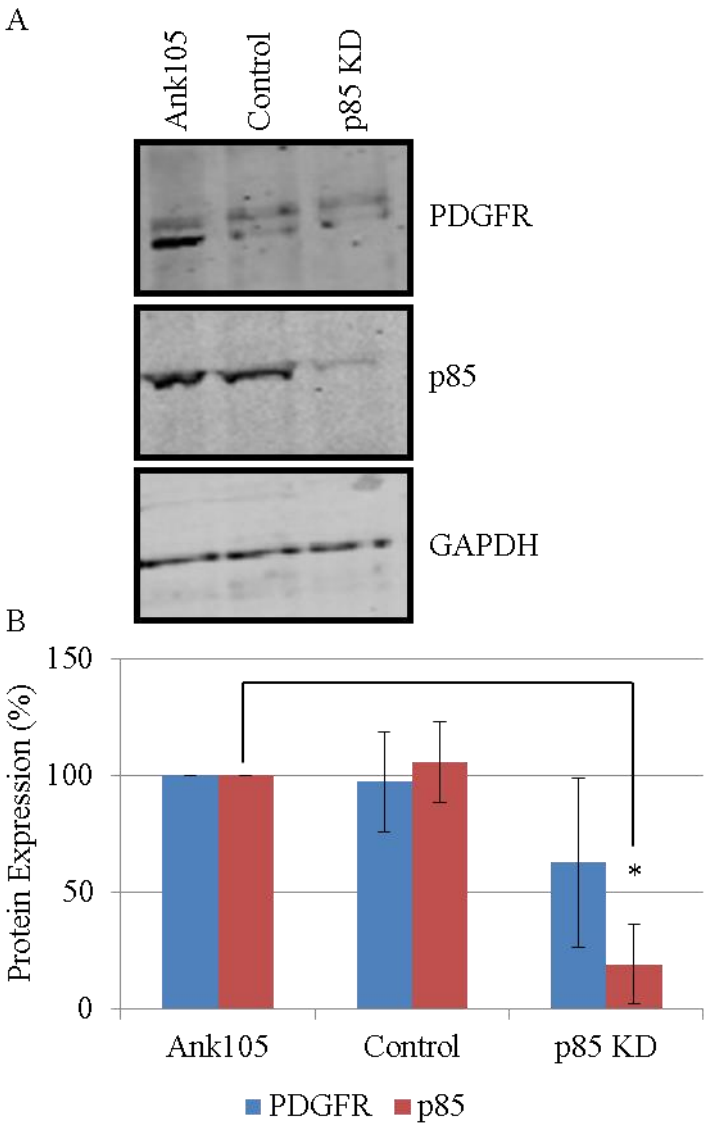

Figure 4.24: Knockdown of p85α in HA-Ank105-expressing cells does not affect PDGFR protein expression levels

Mixed populations were generated by transducing HA-Ank105-expressing cells with scrambled shRNA or shRNA specifically targeting p85α, followed by selection in puromycin. A. Lysates for HA-Ank105-expressing cells (Ank105), control scrambled mixed populations (control) and p85α knockdown mixed populations (p85 KD) were collected, normalized to total protein content, resolved by SDS-PAGE (50 µg), transferred to a nitrocellulose membrane and analyzed by Western blot for PDGFR, p85α and GAPDH protein expression. Results are representative of those from 3 independent experiments (N=3). B. Quantification of Figure 4.24A. PDGFR and p85α protein expression levels were compared to those from HA-Ank105-expressing cells. Data analyzed for statistical significance via t-test (* indicates Pvalue <0.05). Results were compiled from 3 independent experiments.

than Ank105-mediated constitutive PDGFR degradation. Since PI3K is a regulator of cell motility (Qian et al., 2003), it may be possible that Ank105-p85α interaction promotes cell motility as HA-Ank105-expressing cells migrate at a significantly faster rate than NIH 3T3 cells when seeded on glass cover slips (data not shown), however this possibility was not tested further. Indeed Ank105-p85α interaction occurred reciprocally in the absence of PDGF stimulation (Ignatiuk et al., 2006).

4.10 HA-Ank105 interacts with several unidentified proteins under non-stimulated conditions

Since knockdown of known Ank105 binding partners, being βII-spectrin and p85α, did not elevate PDGFR expression levels, identification of novel binding partners of Ank105 could provide insight into the mechanism of Ank105-mediated constitutive PDGFR degradation. HA-Ank105 plasmid DNA was transiently transfected into HEK293 cells to generate high protein expression levels of HA-Ank105. Indeed, HEK293 cells are a suitable model to pursue Ank105 binding partners as transient expression of HA-Ank105 in HEK293 cells induces constitutive degradation of the EGFR. Cells were not stimulated with growth factor in order to facilitate isolation and identification of proteins that interact with Ank105 under constitutive conditions. HA-Ank105 was immunoprecipitated from lysate prepared under non-denaturing conditions using anti-HA antibody. As controls, lysates from untransfected HEK293 cells and HEK293 cells transiently transfected with HA-Ank105 were subjected to immunoprecipitation using anti-HA and non-specific IgG antibodies, respectively, to identify those proteins which specifically interact with HA-Ank105. Samples were denatured, resolved by SDS-PAGE and proteins were visualized by sypro ruby staining and UV light. HA-Ank105 interacted with a number of high (Figure 4.25A) and low (Figure 4.25B) molecular weight proteins. Immunoprecipitated HA-Ank105, as well as the light and heavy antibody chains was also observed (Figure 4.25A,B). Our laboratory is actively collaborating with the laboratory of Dr. Mohan Babu (University of Regina) to determine the identity of proteins that interact with Ank105 via mass spectrometry, both in HEK293 cells and in NIH 3T3 cells stably expressing HA-Ank105.

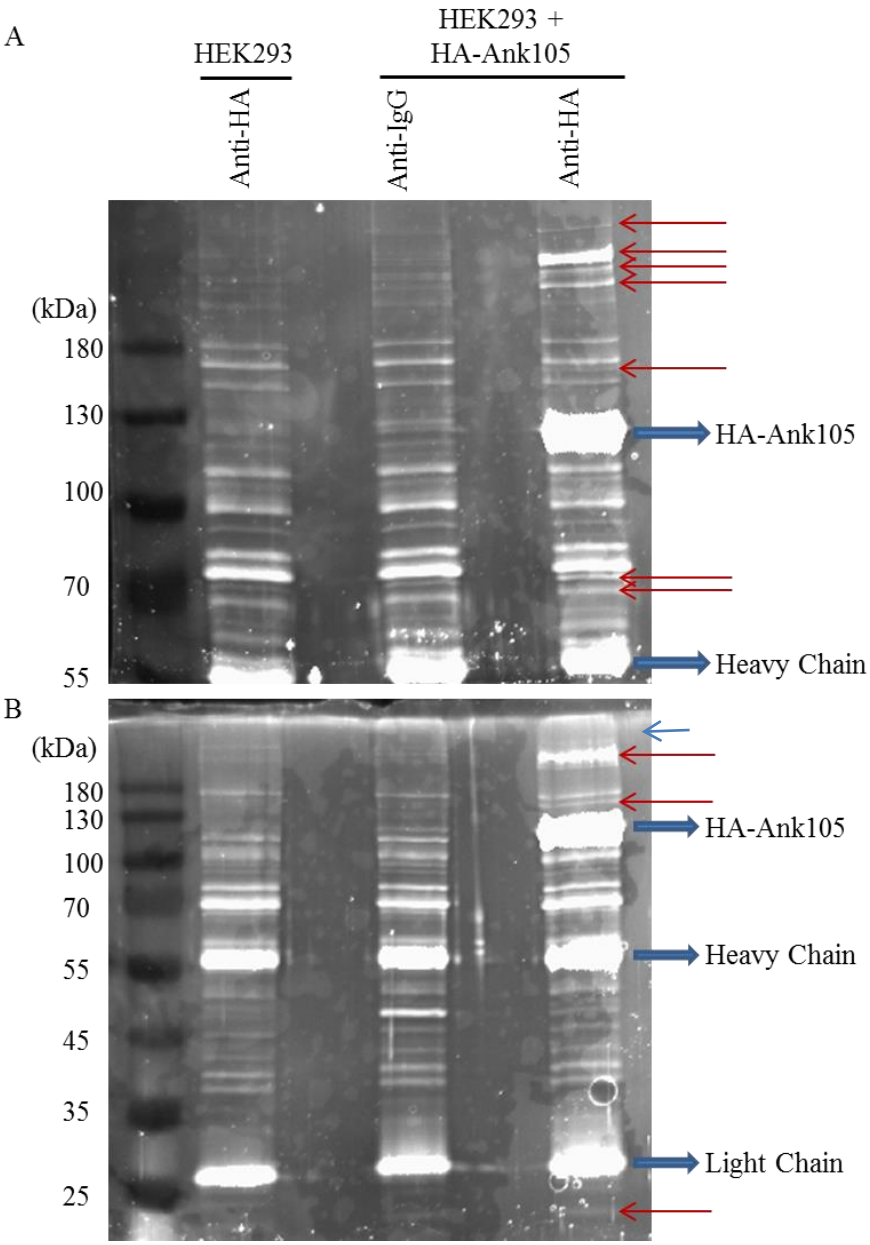

Figure 4.25: HA-Ank105 interacted with several proteins under constitutive conditions in HEK 293 cells

HA-Ank105 was transiently transfected in HEK293 cells. HA-Ank105 was immunoprecipitated from lysate prepared under non-denaturing conditions using and anti-HA antibody (10 µg). As controls, lysates from untransfected HEK293 cells and HEK293 cells transiently transfected with HA-Ank105 were subjected to immunoprecipitation using anti-HA (10 µg) and non-specific IgG antibodies (10 µg), respectively. Samples were denatured, resolved by SDS-PAGE and visualized via sypro ruby staining and UV light. A. Sypro ruby stained image of immunoprecipitants resolved by SDS-PAGE in a 7.5% poly-acrylamide gel. B. Sypro ruby stained image of immunoprecipitants resolved by SDS-PAGE in a 12% poly-acrylamide gel. Red arrows indicate unidentified proteins that co-immunoprecipitated with HA-Ank105. Blue arrows indicate antibody chains and HA-Ank105.

5.0 DISCUSSION

5.1 Effects of Ank105 expression on PDGFR and EGFR degradation

Previous work using a phage display library identified Ank105 as a binding partner of p85 (King *et al*., 2000). Ank105 interacts with the SH2 domains of p85 in a phosphotyrosine-independent manner via residues located in both the spectrin binding domain and regulatory domain (Ignatiuk *et al*., 2006). Interaction between p85 and Ank105 was confirmed in cells via reciprocal co-immunoprecipitation (Ignatiuk *et al*., 2006). Besides its well documented role in PI3K/PTEN signaling (Chagpar *et al*., 2010; Mellor *et al*., 2012), p85 stimulates the intrinsic GTPase activity of Rab5 thereby modulating the endocytosis of the PDGFR (Chamberlain et al., 2008; Chamberlain et al., 2010; Mellor et al., 2012). Binding of p85 and Ank105 suggests that Ank105 may have a role in the regulation of PI3K signaling and PDGFR endocytosis. The effects of HA-Ank105 overexpression were studied in NIH 3T3 cells which endogenously express high levels of PDGFR. Overexpression of HA-Ank105 prompted PDGFR inactivation and degradation in response to PDGF stimulation and reduced the ability of fibroblasts to proliferate in the presence of PDGF (Ignatiuk *et al*., 2006). HA-Ank105 overexpression attenuated the activation of PDGFR in response to PDGF stimulation, as evident by reduced phosphorylation of the receptor (Ignatiuk *et al*., 2006). Indeed activation downstream Shc and PLC signaling pathways were also reduced (Ignatiuk *et al*., 2006). Co-immunofluorescence experiments show co-localization between Ank105, p85, and PDGFR during endocytosis (Ignatiuk *et al*., 2006). Furthermore, HA-Ank105 co-localized with the lysosomal marker protein LAMP-1, but not with the early endosomal marker protein EEA1 (Ignatiuk *et al*., 2006) and treatment of cells with chloroquine inhibited PDGFR degradation in response to ligand (Ignatiuk *et al*., 2006). These observations indicate that Ank105 enhances the lysosomal degradation of the PDGFR and attenuates signaling pathways downstream of the receptor.

To evaluate the effect of HA-Ank105 expression on PDGFR expression and signaling, several cell lines were selected showing increasing amounts of HA-Ank105 expression (Figure 4.1). Each Ank105-expressing cell line had reduced PDGFR levels as compared to untransfected controls (Figure 4.1). Additionally, activation of the receptor itself as well as downstream AKT and MAPK signaling pathways was also attenuated in HA-Ank105-expressing cells in response to PDGF stimulation, as compared to untransfected NIH 3T3 cells (Figure 4.1). The extent of

reduction in constitutive PDGFR levels and signaling activation in response to ligand tended to increase as HA-Ank105 expression increased. The expression levels of constitutive PDGFR is slightly higher in the high HA-Ank105-expressing cell line than in the medium HA-Ank105-expressing cell line; however PDGFR phosphorylation and phosphorylation of both AKT and MAPK are increasingly attenuated as HA-Ank105 expression increases (Figure 4.1). It may be possible that at very high expression levels of Ank105, the endocytic cellular machinery became over saturated with Ank105 and excess Ank105 could sequester its binding partners, thereby impairing Ank105 function. Importantly expression of HA-Ank105 does not affect the expression levels of the MAPK and AKT proteins themselves (Figure 4.1). Both MAPK and AKT signaling are increasingly attenuated in HA-Ank105-expressing cells however reduction of MAPK activation is much more pronounced. Activation of AKT signaling primary occurs at the plasma membrane (Cantley, 2002) whereas MAPK activation and signaling is thought to occur on endosomes (von Zastrow and Sorkin, 2007). Alterations in endosomal trafficking of PDGFR in HA-Ank105-expressing cells could explain the difference observed in differential sensitivity of AKT and MAPK activation to HA-Ank105 expression. An alternative explanation is that since AKT activation depends on the production of lipid second messengers AKT signaling would be less dependent on total receptor levels for efficacy than the MAPK pathway. The production of second messengers amplifies the original signal, rendering downstream signaling less sensitive to the intensity of the original signal.

The degradation of both transmembrane cargo (Hicke, 2001) and intracellular proteins (Ravid and Hochstrasser, 2008) requires ubiquitination. The PDGFR was immunoprecipitated from untransfected NIH 3T3 cells and HA-Ank105-expressing cells in order to examine activation and ubiquitination of the PDGFR in response to ligand stimulation. PDGFR immunoprecipitated from NIH 3T3 cells showed a more intense overall ubiquitination signal than PDGFR from HA-Ank105-expressing cells (Figure 4.3A). The increased signal intensity in NIH 3T3 cells is expected due the significant decrease in constitutive PDGFR levels in HA-Ank105-expressing cells, as more receptor was expressed and available for activation, phosphorylation and ubiquitination (Figure 4.3A). Despite HA-Ank105-expressing cells demonstrating less overall PDGFR ubiquitination, the ubiquitin moieties on the PDGFR appear to be at the same molecular weight as in NIH 3T3 cells, suggesting PDGFR is ubiquitinated similarly in NIH 3T3 and HA-Ank105-expressing cells in response to stimulation (Figure 4.3A).

This hypothesis would need to be confirmed by mass spectrometry of PDGFR immunoprecipitated from stimulated cells to identify ubiquitination sites on the PDGFR.

Interestingly, the PDGFR appears to be differentially phosphorylated upon ligand stimulation in NIH 3T3 cells and HA-Ank105-expressing cells (Figure 4.3A). Phosphorylation of the PDGFR, as indicated by Western blotting with antibody specifically detecting phosphorylated tyrosine residues, significantly increases the molecular weight of immunoprecipitated PDGFR in HA-Ank105-expressing cells as compared to NIH 3T3 cells (Figure 4.3A). Additional phosphorylation of the PDGFR in HA-Ank105-expressing cells could provide docking sites not present in NIH 3T3 cells for endocytic adaptor proteins to promote degradation of the PDGFR. To confirm this speculation, PDGFR could be immunoprecipitated from ligand stimulated, untransfected NIH 3T3 cells and HA-Ank105-expressing cells and examined via mass spectrometry to determine which intracellular tyrosine residues of the PDGFR are indeed phosphorylated.

The classical pathway of degradation of receptor tyrosine kinases upon growth factor stimulation is lysosomal degradation. Treatment of untransfected NIH 3T3 cells with chloroquine for 4 hours prior to PDGF stimulation inhibits receptor degradation (Figure 4.3B). The PDGFR phosphorylation profile in response to PDGFR stimulation in chloroquine treated NIH 3T3 cells was the same as untreated cells, indicating the PDGFR is still activated and de-activated normally even though the lysosomal degradation pathway is perturbed (Figure 4.3B). In HA-Ank105-expressing cells treatment with chloroquine for 4 hours prior to PDGF stimulation only partially inhibited receptor degradation (Figure 4.3C). The constitutive PDGFR levels in chloroquine treated HA-Ank105-expressing cells were slightly higher than the constitutive PDGFR levels in untreated HA-Ank105-expressing cells and this increased receptor is degraded in response to PDGF stimulation (Figure 4.3C). Like untransfected NIH 3T3 cells, the activation profile of the PDGFR in HA-Ank105-expressing cells is similar with and without chloroquine treatment (Figure 4.3B,C). Possible explanations for only a slight increase in constitutive PDGFR levels is that PDGFR in this cell model is under control of an endogenous promoter and 4 hours of chloroquine treatment may not be sufficient to increase PDGFR levels to those observed constitutively in untransfected NIH 3T3 cells. Treatment times longer than 4 hours have proved toxic. An alternative explanation is that Ank105 mediates the majority of its effect on PDGFR levels via a mechanism other than lysosomal degradation. Indeed PDGFR present

after chloroquine treatment was degraded in response to PDGF stimulation.

Determining the receptor target range of Ank105 could provide a mechanism to attenuate pro-oncogenic RTK signaling in multiple cancers. Given that Ank105 promotes the degradation of PDGFR, the effect of HA-Ank105 expression on the degradation of EGFR was also determined. HA-Ank105 was transiently expressed in HEK293 cells and HeLa cells, both of which endogenously express EGFR. In HEK293 cells transfected with pHA_3-Ank105, the level of constitutive EGFR expression decreased as HA-Ank105 expression increased in a dose-dependent manner (Figure 4.2A). Expression of HA-Ank105 also attenuated phosphorylation of the EGFR even though phosphorylation of EGFR in this particular cell line appears to be independent of growth factor stimulation (Figure 4.2A). Transfection of the spectrin binding domain of Ank105 alone was sufficient to induce EGFR degradation; whereas, transfection of the regulatory domain of Ank105 alone did not induce EGFR degradation (data not shown). Expression of HA-Ank105 in HeLa cells did not affect EGFR expression levels. EGFR levels were similar in untransfected HeLa cells and cells transiently transfected increasing amounts of HA-Ank105 (Figure 4.2B). Indeed, EGFR activation and degradation profiles in response to EGF stimulation was consistent between untransfected HeLa cells and cells expressing HA-Ank105 (Figure 4.2B). Interestingly, HeLa cells also express PDGFR at low levels and PDGFR levels are decreased upon HA-Ank105 expression. Thus, HA-Ank105 expression differentially affects constitutive EGFR levels in HEK293 cells and HeLa cells. It may be that HEK293 cells express some additional factor specific to the EGFR such as an endocytic adaptor protein that sensitizes EGFR to Ank105-mediated degradation that is not expressed in HeLa cells; however this possibility was not explored further. It may prove interesting to immunoprecipitate EGFR from these two cell lines and compare the compliment of co-immunoprecipitating proteins. Differences in proteins interacting with the EGFR may provide insight into the mechanism of Ank105 function. Additionally it would be of value to determine the effects of HA-Ank105 expression on the degradation of other RTKs, such as VEGFR or FGFR

5.2 Ubiquitin binding function of Ank105

A common theme in the sorting of ubiquitinated cargo for lysosomal degradation is the ability of the sorting machinery to recognize monoubiquitinated cargo by interacting with the ubiquitin tag itself. Since Ank105 promotes degradation of the PDGFR, the ability of Ank105 to

interact with ubiquitin and ubiquitinated proteins was investigated. HA-Ank105 co-immunprecipitated with several ubiquitinated proteins, particularly after ten minutes of ligand stimulation (Figure 4.4C), and interacted with monoubiquitin via an *in vitro* pulldown assay (Figure 4.4B). The ability of Ank105 to interact with polyubiquitin chains was not determined. It would prove interesting to determine if Ank105 could interact with lysine63-linked chains, as lysine63-linked chains are thought to provide a more efficient lysosomal degradation signal compared to monoubiquitin. Additionally, it would prove interesting to determine if Ank105 interacts with lysine48-linked ubiquitin chains, as lysine48-linked ubiquitin chains target substrates for proteasomal degradation. Indeed, disruption of either lysosomal or proteasomal degradation with small molecule inhibitors dramatically impaired constitutive PDGFR degradation in HA-Ank105-expressing cells (Figure 4.13).

In order to determine if the ubiquitin binding function of Ank105 was required to mediate the effect of Ank105 expression on PDGFR degradation, point mutations and deletion mutations were employed to abrogate ubiquitin binding. Neither point mutation (HA-Ank105-S827D) nor deletion of the potential ubiquitin interaction motif (HA-Ank105-CΔ50, HA-Ank105-CΔ100) within the C-terminal regulatory domain disrupted ubiquitin binding (Figure 4.5A,B). The spectrin binding domain of Ank105 was shown to interact with ubiquitin while the regulatory domain itself did not bind ubiquitin (Figure 4.5C).

To determine the region of the spectrin binding domain responsible for ubiquitin binding a series of deletion mutations were generated in regions of disorder in the spectrin domain of full length HA-Ank105 (Figure 4.8A). The region of the spectrin binding domain mediating ubiquitin binding remains elusive. Ubiquitin-GST pulldown experiments indicate that the HA-Ank105-NΔ169 and HA-Ank105-NΔ359 proteins did not possess the ability to interact with ubiquitin while and HA-Ank105-NΔ385 deletion mutant retained ubiquitin binding (Figure 4.8B). The HA-Ank105-NΔ169 and HA-Ank105-NΔ359 proteins not binding ubiquitin while the HA-Ank105-NΔ385 proteins retained ubiquitin binding is unexpected as the HA-Ank105-NΔ385 protein has the same N-terminal amino acid residues deleted. The absence of observable ubiquitin binding with the HA-Ank105-NΔ169 and HA-Ank105-NΔ359 proteins could be due to the low overall signal intensity or complications in protein expression and folding, as the HA-Ank105-NΔ169 protein is expressed as a doublet. One method to determine whether the HA-Ank105-NΔ169 was properly folder or not would be to express this protein in NIH 3T3 or HEK

293 cells and determine whether if expression of this protein promotes degradation of the PDGFR or EGFR, respectively. Addition replicate experiments are required to improve signal intensity and determine the efficacy of HA-Ank105- NΔ169 ubiquitin binding, possibly by using more input lysate to increase signal intensity. Assuming the HA-Ank105-NΔ385 protein is able to interact with ubiquitin, the region of Ank105 mediating ubiquitin binding may be located between amino acids 360 and 588, which is the remainder of the spectrin binding domain. Deletion mutagenesis in this region could generate proteins to more closely pinpoint the region of Ank105 mediating ubiquitin interaction. The primary amino acid sequence of the spectrin binding domain does not correspond to the consensus sequences of any common ubiquitin binding domains, therefore Ank105 may bind ubiquitin by a novel mechanism. Identification and mutation of the amino acid residues in the spectrin binding domain which confer ubiquitin binding is required to determine if the ability of Ank105 to bind ubiquitin is linked to the observed phenotype of constitutive receptor tyrosine kinase degradation upon Ank105 overexpression. If indeed the ability of Ank105 to recognize ubiquitin and ubiquitinated cargo is required for Ank105-mediated constitutive PDGFR and EGFR degradation then abrogation of ubiquitin binding via site directed mutagenesis would increase constitutive PDGFR and EGFR expression.

5.3 Analysis of PDGFR endocytosis and degradation in the context of HA-Ank105 expression

HA-Ank105-expressing cells were treated with a panel of small molecule endocytosis and protein degradation inhibitors to gain insight into the mechanism of Ank105-mediated constitutive PDGFR degradation. One challenge of studying Ank105-mediated constitutive receptor degradation is that Ank105 function is constitutive. Using small molecule inhibitors in a constitutively active system like Ank105 raises potential concerns. The PDGFR in HA-Ank105-expressing cells is under the control of an endogenous promoter. Long inhibitor treatment times, potentially overnight, may be required to observe significant changes in PDGFR expression. Such long treatment times raise the possibility that changes observed in PDGFR expression may be due to off-target effects of the inhibitor. Thus a system permitting acute inhibitor treatment is desirable. Constitutive PDGFR levels in HA-Ank105-expressing cells are sensitive to the amount of serum used in the culture media. Culture of HA-Ank105-expressing cells in low levels of

serum increased constitutive PDGFR levels approximately 2 fold (Figure 4.9A). Incubation of low serum cultured cells in media containing normal serum levels induced degradation of the PDGFR and incubation in normal serum levels for 4 hours reduced PDGFR levels to those observed prior to serum restriction (Figure 4.9B,C). This system of inducible constitutive PDGFR degradation was used to study the effects of acute treatment of HA-Ank105-expressing cells with various small molecule inhibitors of endocytosis and protein degradation. Inhibition of endocytic and degradation pathways required for Ank105-mediated constitutive PDGFR degradation would result inhibition of PDGFR degradation (observed as increased levels of PDGFR protein) in serum restricted HA-Ank105-expressing cells when re-introduced to media containing normal serum levels. The small molecule inhibitors used were validated via comparison of the effects of these inhibitors on ligand induced PDGFR degradation and LDL uptake.

Cellular uptake of LDL is known to proceed via a clathrin and dynamin dependent mechanism of endocytosis. LDL uptake is impaired in HA-Ank105-expressing cells treated with inhibitors targeting clathrin or dynamin. Treatment with pitstop and chlorpromazine inhibited clathrin mediated uptake of LDL by 75% and 40%, respectively, whereas inhibition of dynamin activity with dynasore blocked 90% of LDL uptake (Figure 4.15). Extraction of plasma membrane cholesterol with MβCD slightly impaired LDL uptake. Inhibitors targeting clathrin independent mechanisms of internalization (Table 4.1, Figure 4.10, Figure 4.11) such as macropinocytosis (NCS 27366, EIPA), membrane ruffling (cytoskeleton inhibitors) and CLIC/GEEC (ML141) did not affect LDL uptake in HA-Ank105-expressing cells (Figure 4.15). The remainder of the inhibitors targeting broad endocytosis (monensin, wortmannin, nocodazole, latrunculin A and jasplakinolide) or protein degradation (chloroquine and MG132) also did not impact LDL uptake (Figure 4.15). Taken together, the small molecule endocytosis inhibitor panel confirmed the clathrin and dynamin dependent endocytosis of LDL. One caveat is the lack of effect of inhibitors targeting cytoskeleton dynamics. Indeed most mechanisms of endocytosis, including CME, are thought to require actin dynamics to function (Figure 4.11). Perhaps the involvement of actin in clathrin dependent uptake varies in different cell types.

The effects of the small molecule endocytosis inhibitor panel were examined for ligand induced degradation of the PDGFR in HA-Ank105-expressing cells. Stimulation of HA-Ank105-expressing cells with PDGF for 240 minutes was sufficient to induce degradation of the PDGFR,

where PDGFR expression levels were reduced greater than 2 fold compared to unstimulated cells (Figure 4.17). Treatment with pitstop or dynasore inhibited 69% and 90% of PDGFR degradation, respectively (Figure 4.17), indicating that ligand induced PDGFR degradation occurs via a clathrin and dynamin dependent mechanism similar to LDL uptake. However there were differences between LDL uptake and ligand induced PDGFR degradation. Chlorpromazine treatment did not affect ligand induced PDGFR degradation (Figure 4.17), whereas chlorpromazine treatment reduced LDL uptake by 40% (Figure 4.15). Ligand induced PDGFR degradation is more sensitive to the level of cholesterol present in the plasma membrane. PDGFR expression levels in MβCD treated cells were 2 fold higher than in non-treated cells after PDGF stimulation (Figure 4.17), whereas MβCD treatment only slightly impaired LDL uptake (Figure 4.15). Additionally, treatment with the Src kinase inhibitor PP2 partially inhibited ligand induced PDGFR degradation (Figure 4.17) while having no effect on LDL uptake (Figure 4.15). Similar to LDL uptake, inhibitors targeting clathrin independent pathways of endocytosis such as macropinocytosis (NCS 27366, EIPA), membrane ruffling (cytoskeleton inhibitors) and CLIC/GEEC (ML141), as well as broad endocytosis inhibitors (monensin, wortmannin, nocodazole, latrunculin A and jasplakinolide) did not impact ligand induced PDGFR degradation (Figure 4.15; Figure 4.17). Treatment with the lysosomal degradation inhibitor chloroquine and the proteasomal degradation inhibitor MG132 both partially inhibited ligand induced PDGFR degradation (Figure 4.17). Interestingly, ligand induced PDGFR degradation in untransfected NIH 3T3 cells was more sensitive to lysosomal degradation inhibitors than HA-Ank105-expressing cells. Treatment of untransfected NIH 3T3 cells with chloroquine prior to ligand stimulation completely inhibits PDGFR degradation (Figure 4.3B), whereas the effect is much less pronounced in HA-Ank105-expressing cells (Figure 4.3C; Figure 4.17). It may be possible that the lower sensitivity of HA-Ank105-expressing cells to protein degradation inhibitors prior to PDGF stimulation may reflect the ability of Ank105 to interact with ubiquitinated proteins upon ligand stimulation. Alterations in trafficking of ubiquitinated PDGFR could result in differences in sorting of ubiquitinated cargo through the endosomal system for degradation in HA-Ank105-expressing cells as compared to untransfected NIH 3T3 cells. Taken together, results from the small molecule endocytosis inhibitors indicate that both ligand induced PDGFR degradation and LDL uptake occur by a clathrin and dynamin dependent mechanism in HA-Ank105-expressing cells, and ligand induced PDGFR degradation is sensitive to the level of

cholesterol present in the plasma membrane and partially sensitive to both lysosomal and proteasomal degradation inhibitors.

Culturing HA-Ank105-expressing cells in low serum overnight increases PDGFR expression levels 2 fold and incubation of serum restricted cells in media containing normal serum levels for 240 minutes induces degradation of PDGFR, decreasing PDGFR expression levels to those prior to serum restriction (Figure 4.9). The effects of the small molecule endocytosis inhibitor panel were markedly different for constitutive PDGFR degradation than for ligand induced PDGFR degradation and LDL uptake. Inhibitors of CME (pitstop and chlorpromazine) did not significantly impair constitutive PDGFR degradation (Figure 4.13), whereas treatment of cells with pitstop dramatically impaired both ligand induced PDGFR degradation (Figure 4.17) and LDL uptake (Figure 4.15). Additionally, constitutive PDGFR degradation was insensitive to the level of cholesterol present in the plasma membrane (Figure 4.13) whereas treatment with MβCB impaired ligand induced PDGFR degradation (Figure 4.17).

Inhibitors targeting macropinocytosis and other endocytosis pathways relying on a dynamic cytoskeleton slightly increased constitutive PDGFR degradation (Figure 4.13). Treatment with the macropinocytosis inhibitor EIPA did not affect constitutive degradation (Figure 4.13), indicating that inhibition of alternative clathrin independent mechanisms of endocytosis, such as membrane ruffling, may increase constitutive PDGFR degradation. Inhibition of those clathrin independent pathways, sensitive to Rac-1 and PI3K activity as well as cytoskeletal dynamics, may increase the efficiency of constitutive PDGFR degradation, possibly by directing a greater proportion of the PDGFR population to an Ank105-mediated degradation pathway.

Lysosomal and proteasomal degradation inhibitors demonstrate a more pronounced effect on constitutive PDGFR endocytosis, resulting in almost complete inhibition (Figure 4.13), as compared to ligand induced PDGFR degradation where the effects of these protein degradation inhibitors was much less pronounced (Figure 4.17; Figure 4.3C) Indeed, treatment of untransfected NIH 3T3 cells with the same concentration of chloroquine is sufficient to inhibit ligand induced PDGFR degradation. It is unclear whether constitutive PDGFR degradation is mediated by the lysosome, the proteasome or some combination of the two. Indeed, inhibition of either pathway was sufficient to significantly impair constitutive PDGFR degradation. Some research has suggested that the PDGFR is polyubiquitinated and degraded by the proteasome

(Ettenberg *et al*., 2001; Levkowitz *et al*., 1998; Lipkowitz, 2003). It remains possible that treatment of HA-Ank105-expressing cells with MG132 depletes the pool of free ubiquitin in the cell, thus impeding sorting and delivery of the PDGFR to the lysosome for degradation (Swaminathan *et al*., 1999). Other lines of evidence suggest proteasomal activity is required for sorting receptors into MVEs (Longva *et al*., 2002). Perhaps co-localization studies between PDGFR and endocytic marker protein with both lysosomal and proteasomal marker proteins in MG132 and chloroquine treated HA-Ank105-expressing cells would concretely identify the mechanism of constitutive PDGFR degradation. Interestingly inhibition of dynamin activity affected constitutive PDGFR degradation (Figure 4.13), ligand induced degradation (Figure 4.17) and LDL uptake (Figure 4.15) indicating that these different examples of endocytosis share a common feature required for internalization. Similar to ligand induced PDGFR degradation (Figure 4.17), inhibition of SRC kinase activity with PP2 partially impaired constitutive PDGFR degradation (Figure 4.13).

It is certainly unusual for a mechanism of endocytosis to be independent of both clathrin and plasma membrane cholesterol, yet still be sensitive inhibition of dynamin activity. Indeed lipid clustering mechanisms of endocytosis which are independent of clathrin and plasma membrane cholesterol, yet still dependent upon dynamin activity, have been identified and are responsible for the endocytosis of the IgGE receptor (Figure 4.11) (von Kleist and Haucke, 2012). It is possible that the observed clathrin independence of constitutive PDGFR degradation is an artifact of the inhibitors used. The pitstop inhibitor functions by competitively binding the region of clathrin responsible for interacting with adaptor proteins thereby preventing recruitment of clathrin to its adaptors (von Kleist *et al*., 2011). If constitutive PDGFR degradation relies on a different subset of adaptor proteins for endocytosis than ligand induced PDGFR degradation, these adaptor proteins may interact with clathrin in a manner which is not inhibited by pitstop. Indeed the clathrin-adaptor protein network is known to be extensive, complex and adaptive (Doherty and McMahon, 2009a).

In order to confirm the observations made with small molecule inhibitors, expression of clathrin and dynamin and were targeted for knockdown via shRNA. Unfortunately, knockdown of the clathrin heavy chain proved to be detrimental to cell physiology. Only two stable cell lines were obtained after puromycin selection and neither of these clones demonstrated reduction of clathrin heavy chain expression via qRT-PCR. To evaluate the role of CME in Ank105-mediated

constitutive PDGFR degradation it would be prudent to transfect HA-Ank105-expressing cells with the clathrin binding domain of AP180. Overexpression of the clathrin binding domain of AP180 was sufficient to inhibit CME by impairing the ability of the clathrin lattice to interact with the plasma membrane (Ford *et al*., 2001).

Dynamin-II was then targeted for shRNA-mediated knockdown and two stable cell lines were obtained, each showing approximately 50% reduction in dynamin-II expression via RT-PCR (Figure 4.21A). Knockdown of dynamin-II was also confirmed via Western blot (Figure 4.21B,C). One caveat with the Western blot data is that the scrambled shRNA control cell line also showed reduced dynamin-II protein expression levels (Figure 4.21B,C), but did not differ from HA-Ank105-expressing cells in dynamin-II mRNA levels (Figure 4.21A). Interestingly, PDGFR protein expression levels were similar in dynamin-II knockdown cell lines compared to HA-Ank105-expressing cells, as well as control scrambled shRNA cells (Figure 4.21B,C). Constitutive PDGFR endocytosis studies in dynasore treated HA-Ank105-expressing cells showed strong inhibition of PDGFR degradation (Figure 4.13), indicating a requirement of dynamin activity in Ank105-mediated constitutive PDGFR degradation. Since only a 50% reduction in dynamin mRNA levels was observed, it remains possible that dynamin was still expressed at a sufficient level for proper endocytosis to occur. Another possibility is that dynamin expression is sufficiently repressed to abrogate dynamin activity, and the cells have adjusted their endocytic machinery to bypass the requirement of dynamin function for receptor internalization and undergo endocytosis by an alternative mechanism (such as macropinocytosis or caveolar endocytosis). It may prove beneficial to evaluate both LDL uptake and ligand induced PDGFR degradation in dynamin knockdown cell lines using the small molecule inhibitors to determine differences between HA-Ank105-expressing cells and dynamin knockdown cell lines. Both LDL uptake and ligand induced PDGFR degradation were exquisitely sensitive to inhibition of dynamin activity. If LDL uptake and/or ligand induced PDGFR degradation are impaired in dynamin knockdown cells and constitutive degradation is not, it would suggest that constitutive degradation is proceeding via an alternative mechanism in the context of dynamin knockdown. Additionally, transfection of the dominant negative dynamin K44A mutant in HA-Ank105-expressing cells would be prudent to evaluate the role of dynamin in Ank105-mediated constitutive degradation. Dynamin K44A impairs endocytosis at the vesicle scission step, resulting in accumulation of committed “U-shaped” pits in the plasma membrane

(Macia *et al*., 2006a; Nankoe and Sever, 2006). Knockdown of the dynamin protein itself may produce a different phenotype where receptor cargo is not committed to dynamin-dependent endocytosis and can enter the cell via alternate mechanisms.

To further evaluate the role of lysosomal degradation in Ank105-mediated constitutive PDGFR degradation, tsg101 and rab7 were targeted for knockdown via shRNA. tsg101 is a critical component of the ESCRT machinery, required for sorting ubiquitinated cargo into MVEs which are subsequently trafficked to the lysosome and degraded (Raiborg and Stenmark, 2009). Knockdown of tsg101 was sufficient to impair EGFR degradation and results in accumulation of EGFR in late endosomal structures (Saksena *et al*., 2007). Indeed tsg101 is an interesting candidate for knockdown studies in HA-Ank105-expressing cells as HA-Ank105 binds ubiquitin and several ubiquitinated proteins, suggesting a role for Ank105 in sorting of ubiquitinated cargo for degradation. Several stable tsg101 knockdown cell lines demonstrated significant attenuation of tsg101 mRNA expression (Figure 4.22), yet had similar PDGFR protein expression levels as compared to HA-Ank105-expressing cells (Figure 4.22B,C). This could suggest that constitutive PDGFR degradation in HA-Ank105-expressing cells is independent of tsg101 and ESCRT sorting. Indeed ESCRT independent sorting of EGFR to the lysosome has been reported (Stuffers *et al*., 2009). Alternatively, the level of tsg101 knockdown in these cell lines may not be sufficient to adequately disrupt tsg101 function. As mRNA expressions and protein expression levels do not always directly correlate, tsg101 protein expression levels must be examined to determine the full extent of tsg101 knockdown. Development of in-house polyclonal rabbit antibodies would allow evaluation of tsg101 protein expression.

The requirement of rab7 for constitutive PDGFR degradation in HA-Ank105-expressing cells was then determined as rab7 is the regulator of late endosome to lysosome trafficking (Zerial and McBride, 2001). The majority of rab7 knockdown cell lines showed a least an 80% reduction in rab7 mRNA expression as compared to control cells (Figure 4.23A) and a number of the rab7 knockdown cell lines showed decreased PDGFR levels as compared to HA-Ank105-expressing cells (Figure 4.23B,C). It is expected that if lysosomal trafficking is the mechanism mediating PDGFR degradation then knockdown of rab7 would increase constitutive PDGFR levels. Acute treatment with the lysosomal degradation inhibitor chloroquine impairs constitutive PDGF degradation in serum restricted HA-Ank105-expressing cells (Figure 4.13). It would be of interest to study the effects of chloroquine and MG132 on constitutive PDGFR degradation in

rab7 knockdown cells to determine whether receptor degradation is still sensitive to inhibition of lysosomal degradation or if there is a greater sensitivity to proteasomal degradation inhibitors. Alternatively, HA-Ank105-expressing cells could be transfected with dominant negative mutants of rab7 and evaluated for constitutive PDGFR levels. Transfection of Rab7N125I in HeLa cells impairs EGFR degradation and promotes accumulation of EGFR in late endosomal structures (Ceresa and Bahr, 2006).

5.4 Knockdown of known Ank105 binding partners does not rescue constitutive PDGFR protein expression levels

Previously identified Ank105 binding partners βII-spectrin and p85 were targeted for knockdown via shRNA. Interaction of the large isoforms of Ank3, which possess the N-terminal integral membrane protein binding domain, with βII-spectrin is required for Ank3 function. As abrogation of spectrin binding disrupts lateral membrane formation in epithelial cells (Kizhatil *et al*., 2007a; Kizhatil *et al*., 2007b), βII-spectrin was a candidate protein regulating Ank105-mediated constitutive PDGFR degradation. Two cell lines showing significant reduction in βII-spectrin mRNA expression via RT-PCR were obtained (Figure 4.24A). These cell lines were then screened by Western blot for βII-spectrin and PDGFR protein expression levels. Unfortunately, a suitable commercial antibody for the detection of endogenous βII-spectrin expression could not be obtained, and it is possible that βII-spectrin mRNA expression levels do not correlate to βII-spectrin protein expression levels. To evaluate the effect of βII-spectrin knockdown, it could prove interesting to measure the rate of proliferation between HA-Ank105-expressing cells and βII-spectrin knockdown cells as knockdown of βII-spectrin has been previously shown to reduce thymidine incorporation in proliferation assays (Tang et al., 2003). Interestingly, PDGFR protein expression levels in βII-spectrin knockdown cell lines were dramatically reduced, suggesting potential roles for βII-spectrin in PDGFR biosynthesis or regulation of PDGFR turnover. If βII-spectrin was required to mediate constitutive PDGFR degradation in HA-Ank105-expressing cells, then it is expected that knockdown of βII-spectrin would increase constitutive PDGFR expression levels. Since β-spectrin is expressed as several isoforms, it remains possible that other β-spectrin isoforms capable of interacting with Ank105 are still expressed. To further address the role Ank105-spectrin interaction, NIH 3T3 cells were stably transfected with GFP-tagged Ank105 containing mutations DAR999/1001 to alanine or A1024 to proline, that were previously

shown to abrogate spectrin binding (Kizhatil *et al*., 2007a; Kizhatil *et al*., 2007b). Unfortunately, these stable GFP-Ank105 mutant clones lost expression overtime, complicating analysis of the effects of these mutations on constitutive PDGFR expression (data not shown). The Ank105-spectrin binding mutations were transferred to the HA vector, which has previously facilitated long term stable Ank105 expression, and stable clones in NIH 3T3 cells were generated. However, due to time constrains these cell lines were not evaluated.

The requirement of p85α for constitutive PDGFR degradation in HA-Ank105-expressing cells was then determined as p85α is binding partner of Ank105 (Ignatiuk *et al*., 2006). The p85α protein is an excellent candidate for regulation of Ank105-mediated constitutive PDGFR degradation as p85α directly binds the PDGFR and mediates downstream signaling of the PI3K/PTEN pathway (Chagpar et al., 2010; Mellor et al., 2012), as well as modulates PDGFR endocytosis via regulation of Rab5 activity (Chamberlain et al., 2008; Chamberlain et al., 2010; Mellor et al., 2012). HA-Ank105-expressing cells were transduced with shRNA targeting p85α to generate a mixed population and evaluated for PDGFR and p85α protein expression. Additionally, a mixed population of HA-Ank105-expressing cells transduced with scrambled control shRNA was also generated and screened. In the p85α knockdown mixed population cell line, p85α protein expression levels were reduced by 81% compared to the scrambled shRNA control mixed population cell line and HA-Ank105-expressing cells (Figure 4.24). Knockdown of p85α did not increase PDGFR expression levels as compared to control cell lines (Figure 4.24), indicating p85α is not required for Ank105-mediated constitutive PDGFR degradation. The interaction between Ank105 and p85α may serve some purpose other than facilitating constitutive PDGFR degradation.

Given that knockdown of known Ank105 binding proteins βII-spectrin and p85α did not result in increased constitutive PDGFR expression, the identification of novel Ank105 binding partners could provide mechanistic insight into Ank105-mediated constitutive PDGFR degradation. To isolate potential binding partners, HA-Ank105 was immunoprecipitated from HA-Ank105-expressing cells and immunoprecipitants were analyzed via syproruby staining for proteins which co-immunoprecipitate with HA-Ank105. Indeed a number of high molecular weight (Figure 4.25A) and low molecular weight (Figure 4.25B) proteins were observed to co-immunoprecipitate with HA-Ank105 and not from control samples. The Anderson laboratory is participating in an active collaboration with the laboratory of Dr. Mohan Babu (University of

Regina) to determine the identities of proteins which co-immunoprecipitate with HA-Ank105 via mass spectrometry. An additional complimentary experiment would be to immunoprecipitate PDGFR under constitutive and stimulated conditions in HA-Ank105-expressing cells, as well as untransfected NIH 3T3 cells, to determine the compliment of endocytic adaptor proteins, scaffold proteins and signaling molecules that interact with the PDGFR. These cell lines could potentially be cultured in low serum or treated with protein degradation inhibitors, as needed, to increase the relative abundance of proteins interacting with PDGFR. In this manner, proteins that specifically interact with the PDGFR in the context of HA-Ank105 expression could be identified. Indeed this may provide mechanistic insight into the regulation of constitutive and ligand induced PDGFR degradation in HA-Ank105 expressing cells.

5.5 Summary of Ank105 function and relevance to PDGFR biology

Stable expression of HA-Ank105 in NIH 3T3 cells reduced constitutive PDGFR protein expression levels and attenuated pro-proliferative AKT and MAPK signaling pathways in response to ligand stimulation. Ank105 also promoted constitutive degradation of the EGFR; however this observation was cell type dependent. Expression of HA-Ank105 in NIH 3T3 cells alters the phosphorylation profile of intracellular tyrosine residues on the PDGFR in response to ligand stimulation and alters sensitivity of PDGFR degradation to chloroquine. NIH 3T3 cells are exquisitely sensitive to chloroquine, as chloroquine treatment drastically inhibited ligand induced PDGFR degradation, whereas chloroquine treatment of HA-Ank105-expressing cells has little effect on ligand induced PDGFR degradation. The greatest effect of HA-Ank105 expression on the PDGFR appears to be constitutive degradation as PDGFR expression levels in HA-Ank105-expressing cells are significantly reduced compared to NIH 3T3 cells in the absence of PDGF ligand.

PDGFR protein expression levels in HA-Ank105-expressing cells are sensitive to serum levels in the growth media. Overnight culture of HA-Ank105-expressing cells in media containing low levels of serum increased PDGFR protein expression levels by 2 fold and incubation of serum restricted cells in media containing standard levels of serum induced PDGFR degradation, with levels returning to those observed in non-serum restricted cells after 2 hours, providing an inducible assay to study constitutive PDGFR degradation. Both LDL uptake and ligand induced PDGFR degradation in HA-Ank105-expressing cells are dependent upon

proper function of CME and dynamin activity, and are not greatly affected by protein degradation inhibitors (Figure 5.1B). Ligand induced PDGFR degradation is also dependent on the presence of cholesterol in the plasma membrane (Figure 5.1B). In contrast, constitutive PDGFR degradation in HA-Ank105-expressing cells is not dependent upon CME or cholesterol levels in the plasma membrane for function; however acute inhibition of dynamin activity impairs constitutive PDGFR degradation (Figure 5.1A). Expression of HA-Ank105 may promote the clathrin-independent, but dynamin dependent, constitutive endocytosis of the PDGFR. Of note, stable knockdown of dynamin-II in HA-Ank105-expressing cells does not increase constitutive PDGFR protein expression levels, however the extent of knockdown of dynamin-II may not have been sufficient to fully impair dynamin function or alternative mechanisms of internalization were up-regulated to compensate for long term attenuation of dynamin activity. Additional experiments with dominant negative mutants affecting dynamin activity and CME are required to explore the mechanism of internalization utilized for constitutive PDGFR degradation in HA-Ank105-expressing cells.

Acute inhibition of either lysosomal or proteasomal degradation impairs constitutive PDGFR degradation (Figure 5.1A). It not clear if PDGFR is degraded in the proteasome or if the proteasome is involved in sorting of PDGFR to the lysosome for degradation (Figure 5.1A). The independence of ligand-induced PDGFR degradation to protein degradation inhibitors is surprising as PDGFR is effectively degraded post PDGF stimulation (Figure 5.1B), yet untransfected NIH 3T3 cells are exquisitely sensitive to inhibition of lysosomal degradation. These results could signify that, in the context of HA-Ank105 expression, degradation of the PDGFR in the absence of ligand proceeds by a novel mechanism compared to ligand induced degradation of the receptor (Figure 5.1A,B). The role of the proteasome in Ank105-mediated constitutive PDGFR degradation may share similarities to the mechanism of action of the benzoquinone ansamycins class drugs. Benzoquinone ansamycins class drugs induce ligand-independent proteasomal degradation of a number of trans-membrane proteins including EGFR and ErbB2 (Blagosklonny, 2002; Lipkowitz, 2003; Mimnaugh *et al*., 1996; Neckers, 2002; Sepp-Lorenzino *et al*., 1995; Tikhomirov and Carpenter, 2000). Proteasomal degradation induced by benzoquinone ansamycins is independent of the kinase activity of the receptor (Citri *et al*., 2002; Xu *et al*., 2001), whereas lysosomal degradation requires kinase activity to generate phospho-tyrosine residues on the receptor to facilitate Cbl E3 ubiquitin ligase binding, ubiquitination and

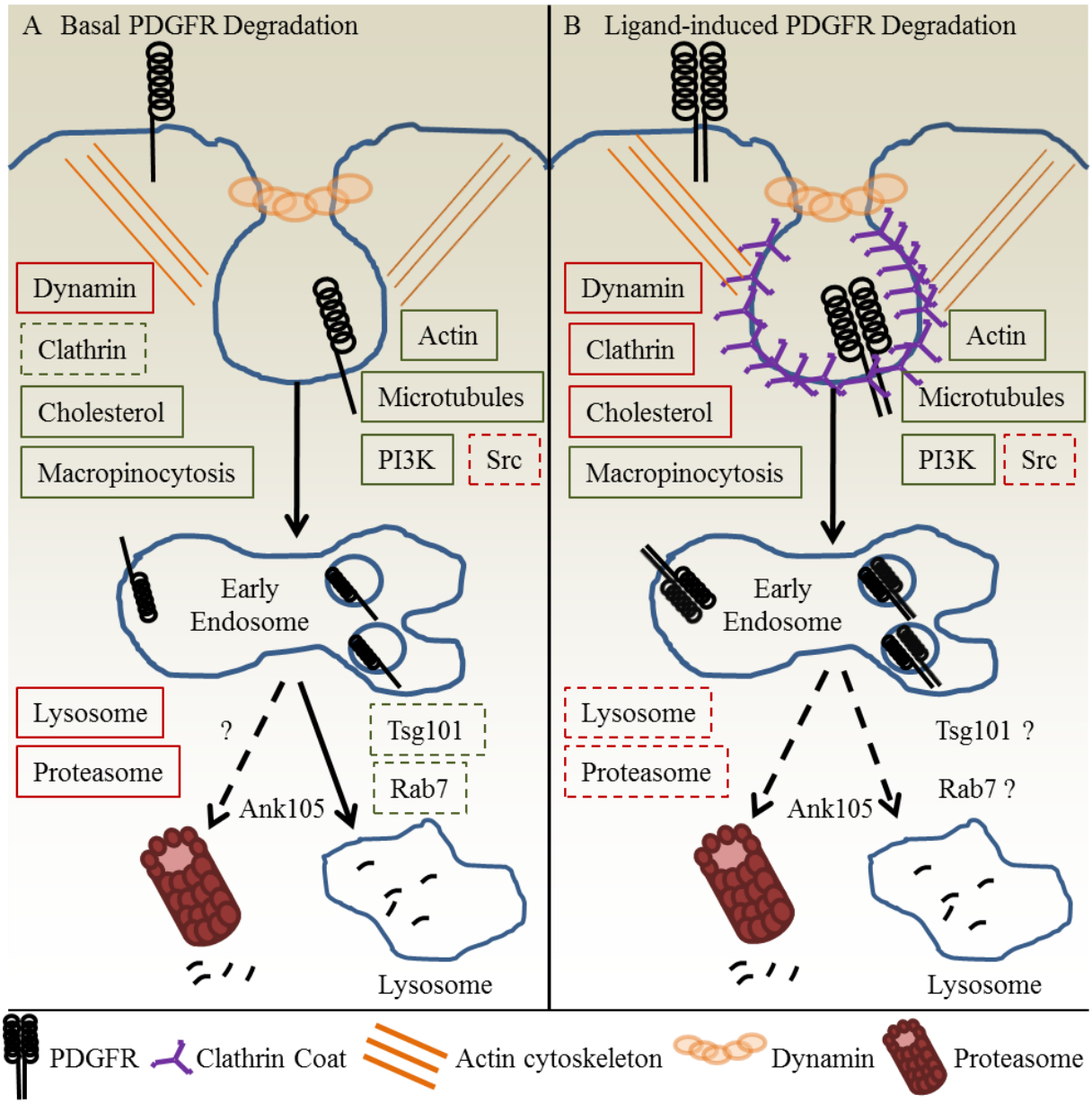

Figure 5.1: Constitutive and ligand-induced PDGFR degradation in HA-Ank105-expressing cells.
A. Diagram of the effects of small molecule inhibitors on constitutive PDGFR degradation in Ank105-expressing cells. Cellular pathways that impair constitutive PDGFR degradation when inhibited are boxed in red and pathways that only slightly impair constitutive degradation when inhibited are boxed red dashed lines. Cellular pathways that do not affect constitutive PDGFR degradation when inhibited are boxed in green. B. Diagram of the effects of small molecule inhibitors on ligand induced PDGFR degradation in Ank105-expressing cells. Cellular pathways that impair ligand induced PDGFR degradation when inhibited are boxed in red and pathways which only slightly impair ligand induced degradation when inhibited are boxed red dashed lines. Cellular pathways which do not affect ligand induced PDGFR degradation when inhibited are boxed in green.

subsequent trafficking through the endosomal system (Levkowitz *et al*., 1999). Benzoquinone ansamycins target chaperone proteins including Hsp90 and Grp94 which stabilize RTKs (Blagosklonny, 2002; Neckers, 2002), causing the chaperone to adopt an alternate conformation which is indicative of protein instability (Blagosklonny, 2002; Neckers, 2002). The proteins interacting with the chaperone are ubiquitinated and degraded by the proteasome (Blagosklonny, 2002; Lipkowitz, 2003; Mimnaugh *et al*., 1996; Neckers, 2002; Tikhomirov and Carpenter, 2000; Xu *et al*., 2001). Ankyrin2 was previously shown to interact with the molecular co-chaperone Hsp40 via the regulatory domain (Mohler *et al*., 2004a). Perhaps ankyrin3 and its isoforms are also capable of binding heat shock proteins, and the interaction between Ank105, PDGFR and a heat shock protein targets the PDGFR for ubiquitination and proteasomal degradation. Determining the identity of Ank105 binding partners via mass spectrometry could determine if Ank105 does indeed interact with heat shock proteins and provide an interesting avenue for further investigation.

Tsg101 and rab7 were targeted for knockdown to address the role of the lysosome for constitutive PDGFR degradation, as constitutive degradation but not ligand induced PDGFR degradation. Knockdown of either tsg101 or rab7 did not increase constitutive PDGFR protein expression levels, indicating that Ank105-mediated PDGFR degradation may proceed independently of ESCRT mediated sorting of ubiquitinated cargo to MVEs and rab7-mediated trafficking of MVEs to the lysosome (Figure 5.1A). Again, similar to dynamin-II knockdown cell lines, knockdown of tsg101 and rab7 may not have been sufficient to fully impair their respective functions. Further compounding this issue is that lack of robust commercial reagents for the detection of endogenous tsg101 and rab7 protein. If knockdown is sufficient in these cell lines, the data suggests that Ank105-mediated degradation promotes the sorting and degradation of PDGF independently of the canonical ESCRT/rab7 dependent lysosomal trafficking pathway (Figure 5.1A).

Interestingly, HA-Ank105 binds ubiquitin *in vitro* via the spectrin binding domain and co-immunoprecipitated with several ubiquitinated proteins in response to short term PDGF stimulation, suggesting a role for Ank105 in the sorting of ubiquitinated proteins for degradation. This hypothesis must be confirmed by studying the effects of Ank105 mutants that cannot bind ubiquitin on constitutive and ligand induced PDGFR degradation. Furthermore, HA-Ank105 co-immunoprecipitated with a number of high and low molecular weight proteins in the absence of

PDGF stimulation. Identifying and validating these potential Ank105 binding partners could provide insight into the mechanism of Ank105-mediated PDGFR degradation, and for example, identify proteins which are required for constitutive PDGFR degradation in the context of HA-Ank105 expression.

Aberrant expression and signaling of the PDGFRα is implicated as a driving event in several malignant diseases including glioblastomas, gastrointestinal stromal tumors, skin tumors and myeloproliferative disorders (Figure 1.3). In the case of glioblastomas where amplification and overexpression of the PDGFR or its ligand is common, as well as gastrointestinal tumors where activating point mutations in the juxtamembrane regions of the PDGFR (Chompret *et al*., 2004; Heinrich *et al*., 2003) promote ligand independent activity (Jones and Cross, 2004), Ank105-mediated down-regulation of constitutive PDGFR expression could alleviate excess proliferative autocrine signaling, thereby reducing tumorigenesis. Indeed PDGFR hyperactivity has been reported in 30% of glial tumors (Brennan *et al*., 2009) and PDGFR expression positively correlates to tumor grade and aggressiveness (Hermanson *et al*., 1996). In the case of myeloproliferative disorders harboring constitutively active fusion mutations, the effectiveness of Ank105 expression on constitutive degradation on each of the fusion mutants would need to be individually investigated as regions interacting with Ank105 may be disrupted or the fusion mutant may not be available to Ank105 if the fusion mutation alters the endocytosis or cellular localization of the mutant receptor.

Several types of epithelial tumors, including breast carcinoma, hepatocellular carcinoma, prostate and colon cancers, are initially unresponsive to PDGF stimulation (Heldin and Lennartsson, 2013); however these tumors acquire PDGFR expression while undergoing epithelial-to-mesenchymal transition (Jechlinger *et al*., 2003) and PDGFR signaling is thought to promote maintenance of the mesenchymal phenotype (Barr *et al*., 2008). Indeed PDGFR expression positively correlates with tumor grade, invasiveness and metastasis in breast carcinoma (Carvalho *et al*., 2005; Jechlinger *et al*., 2006). In the case of hepatocellular carcinoma and prostate cancer, attenuation of PDGFR signaling inhibited metastasis (Dolloff *et al*., 2005; Gotzmann *et al*., 2006; Russell *et al*., 2009). Thus, targeting PDGFR for Ank105-mediated constitutive PDGFR degradation could attenuate PDGFR signaling and promote transition to an epithelial-like phenotype, thereby reducing tumorigenesis and metastasis in epithelial-based cancers with acquired PDGFR expression.

PDGFR signaling can also have extensive paracrine effects in the tumor micro-environment, promoting remodeling of the stroma to facilitate invasiveness, angiogenesis and metastasis as the tumor itself often expresses PDGF and the cells of the stroma express the receptor (Bremnes *et al*., 2011; Heldin and Westermark, 1999; Zigrino *et al*., 2005). Tumor based production of PDGF promotes the recruitment and proliferation of CAFs, which in turn secrete extracellular matrix, cytokines, matric metalloproteinases and VEGF to remodel the tumor stroma and promote angiogenesis (Figure 1.4) (Bremnes *et al*., 2011). Additionally, PDGFR signaling recruits pericytes to newly formed blood vessels promoting their stabilization and maturation (Figure 1.4) (Gerhardt and Semb, 2008). Pharmacological inhibitors targeting the VEGFR in pancreatic cancer models show greater efficacy when combined with the PDGFR inhibitor imatinib, causing blood vessel destabilization via removal of pericytes and reducing tumor viability by the ensuing hypoxic phenotype (Figure 1.4) (Bergers *et al*., 2003). Additional experiments in the same model system indicate that hypoxia induced by this leaky vasculature can drive tumor progression to a more invasive and metastatic phenotype (Figure 1.4) (Xian *et al*., 2006). In the case of paracrine PDGFR signaling in the tumor microenvironment, induction of Ank105-mediated constitutive PDGFR degradation could have the most benefit in low grade tumors that do not have an established vasculature by reduction of CAF recruitment and proliferation. In this manner up-regulation of Ank105-mediated constitutive PDGFR degradation in the tumor stroma could attenuate CAF-mediated stromal remodeling, deposition of extracellular matrix, VEGF secretion and angiogenesis. Additionally, CAF recruitment and deposition of extracellular matrix increases tumor IFP, which in turns impairs tumor uptake of chemotherapeutics (Figure 1.4). Indeed tumors with stromal expression of PDGFR such as lung, breast and colon carcinoma frequently demonstrate high IFP (Ostman and Heldin, 2001). In a thyroid cancer model system, uptake and efficacy of both taxol and 5-fluorouricil was increased when treated in combination with imatinib to reduce IFP, while imatinib treatment alone did not affect tumor growth (Pietras *et al*., 2002). Imatinib treatment was also demonstrated to decrease IFP and increase tumor uptake and efficacy of cyclophosphamide in both lung and pancreatic carcinomas (Falcon *et al*., 2011). Attenuation of stromal PDGFR signaling via Ank105-mediated PDGFR degradation and reduction of CAF recruitment could lower tumor IFP, thereby allowing increased tumor uptake and efficacy of chemotherapeutics.

The *ANK3* gene, as part of an 11 gene signature, was previously demonstrated by micro-

array analysis to be down-regulated in multiple human cancers (Glinsky *et al*., 2005). Indeed down-regulation of the *ANK3* gene was a prognostic indicator of metastasis and poor clinical outcome (Glinsky *et al*., 2005), suggesting *ANK3* has a potential tumor suppressive role. Perhaps down-regulation of Ank105 expression in these cancers elevates constitutive RTK levels and increases pro-oncogenic autocrine and paracrine RTK signaling, thereby contributing to tumor progression. Analysis of mRNA expression of multiple cancer cell lines from distinct lineages demonstrated that *ANK3* expression is frequently attenuated and is often accompanied by increased expression of pro-oncogenic RTKs. Studying the mechanism of Ank105-mediated PDGFR degradation by determining the specific pathway of PDGFR endocytosis in Ank105-expressing cells and by identifying Ank105 binding partners could lead to the identification of novel therapeutic targets to promote Ank105 function and re-expression of Ank105 in cancer cell lines with elevated RTK levels could provide an avenue of future study to determine the effects of Ank105 expression on tumorigenicity. Indeed, expression studies in cell lines with reduced *ANK3* expression will allow for the determination of the effect of each ankyrin3 isoform, independently of each other. Reduction of constitutive PDGFR levels in cancers with PDGFR driver mutations, acquired PDGF responsiveness and stromal expression of PDGFR could significantly reduce tumor proliferation, tumorigenesis and increase effectiveness of chemotherapeutics.

6.0 REFERENCES

Altschuler, Y., Barbas, S.M., Terlecky, L.J., Tang, K., Hardy, S., Mostov, K.E., and Schmid, S.L. (1998). Redundant and distinct functions for dynamin-1 and dynamin-2 isoforms. Journal of Cell Biology *143*, 1871-1881.

Alvarez, R.H., Kantarjian, H.M., and Cortes, J.E. (2006). Biology of platelet-derived growth factor and its involvement in disease. Mayo Clin Proc *81*, 1241-1257.

Amanso, A.M., Debbas, V., and Laurindo, F.R.M. (2011). Proteasome Inhibition Represses Unfolded Protein Response and Nox4, Sensitizing Vascular Cells to Endoplasmic Reticulum Stress-Induced Death. PLoS ONE *6*, e14591.

Andrae, J., Gallini, R., and Betsholtz, C. (2008). Role of platelet-derived growth factors in physiology and medicine. Genes & Development *22*, 1276-1312.

Apperley, J.F., Gardembas, M., Melo, J.V., Russell-Jones, R., Bain, B.J., Baxter, E.J., Chase, A., Chessells, J.M., Colombat, M., Dearden, C.E.*, et al.* (2002). Response to imatinib mesylate in patients with chronic myeloproliferative diseases with rearrangements of the platelet-derived growth factor receptor beta. New England Journal of Medicine *347*, 481-487.

Araki, N., Hamasaki, M., Egami, Y., and Hatae, T. (2006). Effect of 3-methyladenine on the fusion process of macropinosomes in EGF-stimulated A431 cells. Cell Structure & Function *31*, 145-157.

Ausubel, F.M., Brent, R., Kingston, R.E., Moore, D.D., Seidman, J.G., Smith, J.A., and Struhl, K.e. (2007). Current Protocols in Molecular Biology (Somerset, Wiley).

Balaji, K., Mooser, C., Janson, C.M., Bliss, J.M., Hojjat, H., and Colicelli, J. (2012). RIN1 orchestrates the activation of RAB5 GTPases and ABL tyrosine kinases to determine the fate of EGFR. Journal of Cell Science *125*, 5887-5896.

Balzac, F., Avolio, M., Degani, S., Kaverina, I., Torti, M., Silengo, L., Small, J.V., and Retta, S.F. (2005). E-cadherin endocytosis regulates the activity of Rap1: a traffic light GTPase at the crossroads between cadherin and integrin function. Journal of Cell Science *118*, 4765-4783.

Baron, V., and Schwartz, M. (2000). Cell adhesion regulates ubiquitin-mediated degradation of the platelet-derived growth factor receptor beta. J Biol Chem *275*, 39318-39323.

Barr, S., Thomson, S., Buck, E., Russo, S., Petti, F., Sujka-Kwok, I., Eyzaguirre, A., Rosenfeld-Franklin, M., Gibson, N.W., Miglarese, M.*, et al.* (2008). Bypassing cellular EGF receptor dependence through epithelial-to-mesenchymal-like transitions. Clin Exp Metastasis *25*, 685-693.

Barretina, J., Caponigro, G., Stransky, N., Venkatesan, K., Margolin, A.A., Kim, S., Wilson, C.J., Lehar, J., Kryukov, G.V., Sonkin, D.*, et al.* (2012). The Cancer Cell Line Encyclopedia enables predictive modelling of anticancer drug sensitivity. Nature *483*, 603-607.

Baxter, R.M., Secrist, J.P., Vaillancourt, R.R., and Kazlauskas, A. (1998). Full activation of the platelet-derived growth factor beta-receptor kinase involves multiple events. Journal of Biological Chemistry *273*, 17050-17055.

Bennett, V., and Baines, A.J. (2001). Spectrin and ankyrin-based pathways: metazoan inventions for integrating cells into tissues. Physiol Rev *81*, 1353-1392.

Bennett, V., and Healy, J. (2008). Organizing the fluid membrane bilayer: diseases linked to spectrin and ankyrin. Trends Mol Med *14*, 28-36.

Bergers, G., Song, S., Meyer-Morse, N., Bergsland, E., and Hanahan, D. (2003). Benefits of targeting both pericytes and endothelial cells in the tumor vasculature with kinase inhibitors. Journal of Clinical Investigation *111*, 1287-1295.

Berggren, K., Chernokalskaya, E., Steinberg, T.H., Kemper, C., Lopez, M.F., Diwu, Z.,

Haugland, R.P., and Patton, W.F. (2000). Background-free, high sensitivity staining of proteins in one- and two-dimensional sodium dodecyl sulfate-polyacrylamide gels using a luminescent ruthenium complex. Electrophoresis *21*, 2509-2521.

Birkenmeier, C.S., and Barker, J.E. (2004). Hereditary haemolytic anaemias: unexpected sequelae of mutations in the genes for erythroid membrane skeletal proteins. J Pathol *204*, 450-459.

Birkenmeier, C.S., Gifford, E.J., and Barker, J.E. (2003). Normoblastosis, a murine model for ankyrin-deficient hemolytic anemia, is caused by a hypomorphic mutation in the erythroid ankyrin gene Ank1. Hematol J *4*, 445-449.

Blagosklonny, M.V. (2002). Hsp-90-associated oncoproteins: multiple targets of geldanamycin and its analogs. Leukemia *16*, 455-462.

Bonner, J.C. (2004). Regulation of PDGF and its receptors in fibrotic diseases. Cytokine Growth Factor Rev *15*, 255-273.

Bostrom, H., Willetts, K., Pekny, M., Leveen, P., Lindahl, P., Hedstrand, H., Pekna, M., Hellstrom, M., Gebre-Medhin, S., Schalling, M.*, et al.* (1996). PDGF-A signaling is a critical event in lung alveolar myofibroblast development and alveogenesis. Cell *85*, 863-873.

Brekken, C., Hjelstuen, M.H., Bruland, O.S., and de Lange Davies, C. (2000). Hyaluronidase-induced periodic modulation of the interstitial fluid pressure increases selective antibody uptake in human osteosarcoma xenografts. Anticancer Research *20*, 3513-3519.

Bremnes, R.M., Donnem, T., Al-Saad, S., Al-Shibli, K., Andersen, S., Sirera, R., Camps, C., Marinez, I., and Busund, L.T. (2011). The role of tumor stroma in cancer progression and prognosis: emphasis on carcinoma-associated fibroblasts and non-small cell lung cancer. J Thorac Oncol *6*, 209-217.

Brennan, C., Momota, H., Hambardzumyan, D., Ozawa, T., Tandon, A., Pedraza, A., and Holland, E. (2009). Glioblastoma subclasses can be defined by activity among signal transduction pathways and associated genomic alterations. PLoS ONE [Electronic Resource] *4*, e7752.

Bright, N.A., Gratian, M.J., and Luzio, J.P. (2005). Endocytic delivery to lysosomes mediated by concurrent fusion and kissing events in living cells. Current Biology *15*, 360-365.

Bubb, M.R., Spector, I., Beyer, B.B., and Fosen, K.M. (2000). Effects of Jasplakinolide on the Kinetics of Actin Polymerization: AN EXPLANATION FOR CERTAIN IN VIVO OBSERVATIONS. Journal of Biological Chemistry *275*, 5163-5170.

Cantley, L.C. (2002). The phosphoinositide 3-kinase pathway. Science (New York, N.Y.) *296*, 1655-1657.

Carroll, M., Tomasson, M.H., Barker, G.F., Golub, T.R., and Gilliland, D.G. (1996). The TEL/platelet-derived growth factor beta receptor (PDGF beta R) fusion in chronic myelomonocytic leukemia is a transforming protein that self-associates and activates PDGF beta R kinase-dependent signaling pathways. Proceedings of the National Academy of Sciences of the United States of America *93*, 14845-14850.

Carvalho, I., Milanezi, F., Martins, A., Reis, R.M., and Schmitt, F. (2005). Overexpression of platelet-derived growth factor receptor alpha in breast cancer is associated with tumour progression. Breast Cancer Res *7*, R788-795.

Ceresa, B.P., and Bahr, S.J. (2006). rab7 Activity Affects Epidermal Growth Factor:Epidermal Growth Factor Receptor Degradation by Regulating Endocytic Trafficking from the Late Endosome. Journal of Biological Chemistry *281*, 1099-1106.

Chagpar, R.B., Links, P.H., Pastor, M.C., Furber, L.A., Hawrysh, A.D., Chamberlain, M.D., and Anderson, D.H. (2010). Direct positive regulation of PTEN by the p85 subunit of

phosphatidylinositol 3-kinase. Proc Natl Acad Sci U S A *107*, 5471-5476.

Chamberlain, M.D., Berry, T.R., Pastor, M.C., and Anderson, D.H. (2004). The p85alpha subunit of phosphatidylinositol 3'-kinase binds to and stimulates the GTPase activity of Rab proteins. J Biol Chem *279*, 48607-48614.

Chamberlain, M.D., Chan, T., Oberg, J.C., Hawrysh, A.D., James, K.M., Saxena, A., Xiang, J., and Anderson, D.H. (2008). Disrupted RabGAP function of the p85 subunit of phosphatidylinositol 3-kinase results in cell transformation. J Biol Chem *283*, 15861-15868.

Chamberlain, M.D., Oberg, J.C., Furber, L.A., Poland, S.F., Hawrysh, A.D., Knafelc, S.M., McBride, H.M., and Anderson, D.H. (2010). Deregulation of Rab5 and Rab4 proteins in p85R274A-expressing cells alters PDGFR trafficking. Cell Signal *22*, 1562-1575.

Chappie, J.S., Acharya, S., Liu, Y.W., Leonard, M., Pucadyil, T.J., and Schmid, S.L. (2009). An intramolecular signaling element that modulates dynamin function in vitro and in vivo. Molecular Biology of the Cell *20*, 3561-3571.

Chen, C.L., Hou, W.H., Liu, I.H., Hsiao, G., Huang, S.S., and Huang, J.S. (2009). Inhibitors of clathrin-dependent endocytosis enhance TGFbeta signaling and responses. Journal of Cell Science *122*, 1863-1871.

Chompret, A., Kannengiesser, C., Barrois, M., Terrier, P., Dahan, P., Tursz, T., Lenoir, G.M., and Bressac-De Paillerets, B. (2004). PDGFRA germline mutation in a family with multiple cases of gastrointestinal stromal tumor. Gastroenterology *126*, 318-321.

Citri, A., Alroy, I., Lavi, S., Rubin, C., Xu, W., Grammatikakis, N., Patterson, C., Neckers, L., Fry, D.W., and Yarden, Y. (2002). Drug-induced ubiquitylation and degradation of ErbB receptor tyrosine kinases: implications for cancer therapy. EMBO Journal *21*, 2407-2417.

Clark, R.A., Folkvord, J.M., Hart, C.E., Murray, M.J., and McPherson, J.M. (1989). Platelet

isoforms of platelet-derived growth factor stimulate fibroblasts to contract collagen matrices. Journal of Clinical Investigation *84*, 1036-1040.

Clarke, I.D., and Dirks, P.B. (2003). A human brain tumor-derived PDGFR-alpha deletion mutant is transforming. Oncogene *22*, 722-733.

Clarke, K., Smith, K., Gullick, W.J., and Harris, A.L. (2001). Mutant epidermal growth factor receptor enhances induction of vascular endothelial growth factor by hypoxia and insulin-like growth factor-1 via a PI3 kinase dependent pathway. Br J Cancer *84*, 1322-1329.

Coligan, Dunn, Speicher, and Wingfield., a. (2007). Current Protocols in Protein Science (Somerset, Wiley).

Coussens, L., Van Beveren, C., Smith, D., Chen, E., Mitchell, R.L., Isacke, C.M., Verma, I.M., and Ullrich, A. (1986). Structural alteration of viral homologue of receptor proto-oncogene fms at carboxyl terminus. Nature *320*, 277-280.

Coux, O., Tanaka, K., and Goldberg, A.L. (1996). Structure and functions of the 20S and 26S proteasomes. Annual Review of Biochemistry *65*, 801-847.

Daumke, O., Roux, A., and Haucke, V. (2014). BAR Domain Scaffolds in Dynamin-Mediated Membrane Fission. Cell *156*, 882-892.

De Donatis, A., Comito, G., Buricchi, F., Vinci, M.C., Parenti, A., Caselli, A., Camici, G., Manao, G., Ramponi, G., and Cirri, P. (2008). Proliferation versus migration in platelet-derived growth factor signaling: the key role of endocytosis. Journal of Biological Chemistry *283*, 19948-19956.

Di Guglielmo, G.M., Le Roy, C., Goodfellow, A.F., and Wrana, J.L. (2003). Distinct endocytic pathways regulate TGF-beta receptor signalling and turnover.[Erratum appears in Nat Cell Biol. 2003 Jul;5(7):680]. Nature Cell Biology *5*, 410-421.

Dikic, I., Wakatsuki, S., and Walters, K.J. (2009). Ubiquitin-binding domains - from structures to functions. Nature Reviews Molecular Cell Biology *10*, 659-671.

Doherty, G.J., and McMahon, H.T. (2009a). Mechanisms of endocytosis. Annu Rev Biochem *78*, 857-902.

Doherty, G.J., and McMahon, H.T. (2009b). Mechanisms of endocytosis. Annual Review of Biochemistry *78*, 857-902.

Dolloff, N.G., Shulby, S.S., Nelson, A.V., Stearns, M.E., Johannes, G.J., Thomas, J.D., Meucci, O., and Fatatis, A. (2005). Bone-metastatic potential of human prostate cancer cells correlates with Akt/PKB activation by alpha platelet-derived growth factor receptor. Oncogene *24*, 6848-6854.

Dong, J., Grunstein, J., Tejada, M., Peale, F., Frantz, G., Liang, W.C., Bai, W., Yu, L., Kowalski, J., Liang, X.*, et al.* (2004). VEGF-null cells require PDGFR alpha signaling-mediated stromal fibroblast recruitment for tumorigenesis. EMBO Journal *23*, 2800-2810.

Doolittle, R.F., Hunkapiller, M.W., Hood, L.E., Devare, S.G., Robbins, K.C., Aaronson, S.A., and Antoniades, H.N. (1983). Simian sarcoma virus onc gene, v-sis, is derived from the gene (or genes) encoding a platelet-derived growth factor. Science *221*, 275-277.

Dutta, D., Williamson, C.D., Cole, N.B., and Donaldson, J.G. (2012). Pitstop 2 is a potent inhibitor of clathrin-independent endocytosis. PLoS ONE [Electronic Resource] *7*, e45799.

Eskelinen, E.L., Tanaka, Y., and Saftig, P. (2003). At the acidic edge: emerging functions for lysosomal membrane proteins. Trends in Cell Biology *13*, 137-145.

Ettenberg, S.A., Magnifico, A., Cuello, M., Nau, M.M., Rubinstein, Y.R., Yarden, Y., Weissman, A.M., and Lipkowitz, S. (2001). Cbl-b-dependent coordinated degradation of the epidermal growth factor receptor signaling complex. Journal of Biological Chemistry *276*, 27677-27684.

Falcon, B.L., Pietras, K., Chou, J., Chen, D., Sennino, B., Hanahan, D., and McDonald, D.M. (2011). Increased vascular delivery and efficacy of chemotherapy after inhibition of platelet-derived growth factor-B. American Journal of Pathology *178*, 2920-2930.

Farsad, K., and De Camilli, P. (2003). Mechanisms of membrane deformation. Current Opinion in Cell Biology *15*, 372-381.

Fleming, T.P., Saxena, A., Clark, W.C., Robertson, J.T., Oldfield, E.H., Aaronson, S.A., and Ali, I.U. (1992). Amplification and/or overexpression of platelet-derived growth factor receptors and epidermal growth factor receptor in human glial tumors. Cancer Research *52*, 4550-4553.

Ford, M.G., Pearse, B.M., Higgins, M.K., Vallis, Y., Owen, D.J., Gibson, A., Hopkins, C.R., Evans, P.R., and McMahon, H.T. (2001). Simultaneous binding of PtdIns(4,5)P2 and clathrin by AP180 in the nucleation of clathrin lattices on membranes. Science *291*, 1051-1055.

Fujiwara, K., Tenno, T., Sugasawa, K., Jee, J.G., Ohki, I., Kojima, C., Tochio, H., Hiroaki, H., Hanaoka, F., and Shirakawa, M. (2004). Structure of the ubiquitin-interacting motif of S5a bound to the ubiquitin-like domain of HR23B. J Biol Chem *279*, 4760-4767.

Gallagher, P.G. (2005). Hematologically important mutations: ankyrin variants in hereditary spherocytosis. Blood Cells Mol Dis *35*, 345-347.

Gao, Y., Dickerson, J.B., Guo, F., Zheng, J., and Zheng, Y. (2004). Rational design and characterization of a Rac GTPase-specific small molecule inhibitor. Proceedings of the National Academy of Sciences of the United States of America *101*, 7618-7623.

Gerhardt, H., and Semb, H. (2008). Pericytes: gatekeepers in tumour cell metastasis? J Mol Med *86*, 135-144.

Glinsky, G.V., Berezovska, O., and Glinskii, A.B. (2005). Microarray analysis identifies a death-from-cancer signature predicting therapy failure in patients with multiple types of cancer. J Clin

Invest *115*, 1503-1521.

Gold, S., Monaghan, P., Mertens, P., and Jackson, T. (2010). A Clathrin Independent Macropinocytosis-Like Entry Mechanism Used by Bluetongue Virus-1 during Infection of BHK Cells. PLoS ONE *5*, e11360.

Goldberg, A.L. (2012). Development of proteasome inhibitors as research tools and cancer drugs. Journal of Cell Biology *199*, 583-588.

Gotzmann, J., Fischer, A.N., Zojer, M., Mikula, M., Proell, V., Huber, H., Jechlinger, M., Waerner, T., Weith, A., Beug, H.*, et al.* (2006). A crucial function of PDGF in TGF-beta-mediated cancer progression of hepatocytes. Oncogene *25*, 3170-3185.

Grimmer, S., van Deurs, B., and Sandvig, K. (2002). Membrane ruffling and macropinocytosis in A431 cells require cholesterol. Journal of Cell Science *115*, 2953-2962.

Gullberg, D., Tingstrom, A., Thuresson, A.C., Olsson, L., Terracio, L., Borg, T.K., and Rubin, K. (1990). Beta 1 integrin-mediated collagen gel contraction is stimulated by PDGF. Experimental Cell Research *186*, 264-272.

Hamasaki, M., Araki, N., and Hatae, T. (2004). Association of early endosomal autoantigen 1 with macropinocytosis in EGF-stimulated A431 cells. Anat Rec A Discov Mol Cell Evol Biol *277*, 298-306.

Hanson, P.I., Shim, S., and Merrill, S.A. (2009). Cell biology of the ESCRT machinery. Curr Opin Cell Biol *21*, 568-574.

Heinrich, M.C., Corless, C.L., Duensing, A., McGreevey, L., Chen, C.J., Joseph, N., Singer, S., Griffith, D.J., Haley, A., Town, A.*, et al.* (2003). PDGFRA activating mutations in gastrointestinal stromal tumors. Science *299*, 708-710.

Heldin, C.-H., and Lennartsson, J. (2013). Structural and Functional Properties of Platelet-Derived Growth Factor and Stem Cell Factor Receptors. Cold Spring Harbor Perspectives in Biology *5*.

Heldin, C.-H., and Westermark, B. (1999). Mechanism of Action and In Vivo Role of Platelet-Derived Growth Factor. Physiological Reviews *79*, 1283-1316.

Heldin, C.H. (2004). Development and possible clinical use of antagonists for PDGF and TGF-beta. Ups J Med Sci *109*, 165-178.

Heldin, C.H., Rubin, K., Pietras, K., and Ostman, A. (2004). High interstitial fluid pressure - an obstacle in cancer therapy. Nature Reviews. Cancer *4*, 806-813.

Heldin, C.H., Wasteson, A., and Westermark, B. (1982). Interaction of platelet-derived growth factor with its fibroblast receptor. Demonstration of ligand degradation and receptor modulation. J Biol Chem *257*, 4216-4221.

Henley, J.R., Krueger, E.W., Oswald, B.J., and McNiven, M.A. (1998). Dynamin-mediated internalization of caveolae. Journal of Cell Biology *141*, 85-99.

Hermanson, M., Funa, K., Koopmann, J., Maintz, D., Waha, A., Westermark, B., Heldin, C.H., Wiestler, O.D., Louis, D.N., von Deimling, A.*, et al.* (1996). Association of loss of heterozygosity on chromosome 17p with high platelet-derived growth factor alpha receptor expression in human malignant gliomas. Cancer Research *56*, 164-171.

Hicke, L. (2001). Protein regulation by monoubiquitin. Nat Rev Mol Cell Biol *2*, 195-201.

Hinrichsen, L., Harborth, J., Andrees, L., Weber, K., and Ungewickell, E.J. (2003). Effect of clathrin heavy chain- and alpha-adaptin-specific small inhibitory RNAs on endocytic accessory proteins and receptor trafficking in HeLa cells. Journal of Biological Chemistry *278*, 45160-45170.

Hommelgaard, A.M., Roepstorff, K., Vilhardt, F., Torgersen, M.L., Sandvig, K., and van Deurs, B. (2005). Caveolae: stable membrane domains with a potential for internalization. Traffic *6*, 720-724.

Hoock, T.C., Peters, L.L., and Lux, S.E. (1997). Isoforms of ankyrin-3 that lack the NH2-terminal repeats associate with mouse macrophage lysosomes. J Cell Biol *136*, 1059-1070.

Huang, F., Goh, L.K., and Sorkin, A. (2007). EGF receptor ubiquitination is not necessary for its internalization. Proc Natl Acad Sci U S A *104*, 16904-16909.

Huang, F., Kirkpatrick, D., Jiang, X., Gygi, S., and Sorkin, A. (2006). Differential regulation of EGF receptor internalization and degradation by multiubiquitination within the kinase domain. Mol Cell *21*, 737-748.

Ignatiuk, A., Quickfall, J.P., Hawrysh, A.D., Chamberlain, M.D., and Anderson, D.H. (2006). The Smaller Isoforms of Ankyrin 3 Bind to the p85 Subunit of Phosphatidylinositol 3'-Kinase and Enhance Platelet-derived Growth Factor Receptor Down-regulation. J Biol Chem *281*, 5956-5964.

Ippoliti, R., Ginobbi, P., Lendaro, E., D'Agostino, I., Ombres, D., Benedetti, P.A., Brunori, M., and Citro, G. (1998). The effect of monensin and chloroquine on the endocytosis and toxicity of chimeric toxins. Cellular & Molecular Life Sciences *54*, 866-875.

Jechlinger, M., Grunert, S., Tamir, I.H., Janda, E., Ludemann, S., Waerner, T., Seither, P., Weith, A., Beug, H., and Kraut, N. (2003). Expression profiling of epithelial plasticity in tumor progression. Oncogene *22*, 7155-7169.

Jechlinger, M., Sommer, A., Moriggl, R., Seither, P., Kraut, N., Capodiecci, P., Donovan, M., Cordon-Cardo, C., Beug, H., and Grunert, S. (2006). Autocrine PDGFR signaling promotes mammary cancer metastasis. Journal of Clinical Investigation *116*, 1561-1570.

Jenkins, S.M., and Bennett, V. (2001). Ankyrin-G coordinates assembly of the spectrin-based membrane skeleton, voltage-gated sodium channels, and L1 CAMs at Purkinje neuron initial segments. J Cell Biol *155*, 739-746.

Johnsson, A., Betsholtz, C., Heldin, C.H., and Westermark, B. (1985). Antibodies against platelet-derived growth factor inhibit acute transformation by simian sarcoma virus. Nature *317*, 438-440.

Jones, A.T. (2007). Macropinocytosis: searching for an endocytic identity and role in the uptake of cell penetrating peptides. J Cell Mol Med *11*, 670-684.

Jones, A.V., and Cross, N.C. (2004). Oncogenic derivatives of platelet-derived growth factor receptors. Cell Mol Life Sci *61*, 2912-2923.

Jousset, C., Carron, C., Boureux, A., Quang, C.T., Oury, C., Dusanter-Fourt, I., Charon, M., Levin, J., Bernard, O., and Ghysdael, J. (1997). A domain of TEL conserved in a subset of ETS proteins defines a specific oligomerization interface essential to the mitogenic properties of the TEL-PDGFR beta oncoprotein. EMBO Journal *16*, 69-82.

Kaplan, D.R., Chao, F.C., Stiles, C.D., Antoniades, H.N., and Scher, C.D. (1979). Platelet alpha granules contain a growth factor for fibroblasts. Blood *53*, 1043-1052.

Karch, C.M., Jeng, A.T., and Goate, A.M. (2012). Extracellular Tau Levels Are Influenced by Variability in Tau That Is Associated with Tauopathies. Journal of Biological Chemistry *287*, 42751-42762.

Katz, M., Shtiegman, K., Tal-Or, P., Yakir, L., Mosesson, Y., Harari, D., Machluf, Y., Asao, H., Jovin, T., Sugamura, K.*, et al.* (2002). Ligand-independent degradation of epidermal growth factor receptor involves receptor ubiquitylation and Hgs, an adaptor whose ubiquitin-interacting motif targets ubiquitylation by Nedd4. Traffic *3*, 740-751.

Kazazic, M., Roepstorff, K., Johannessen, L.E., Pedersen, N.M., van Deurs, B., Stang, E., and Madshus, I.H. (2006). EGF-induced activation of the EGF receptor does not trigger mobilization of caveolae. Traffic *7*, 1518-1527.

Kerr, M.C., Lindsay, M.R., Luetterforst, R., Hamilton, N., Simpson, F., Parton, R.G., Gleeson, P.A., and Teasdale, R.D. (2006). Visualisation of macropinosome maturation by the recruitment of sorting nexins. Journal of Cell Science *119*, 3967-3980.

Kerr, M.C., and Teasdale, R.D. (2009). Defining macropinocytosis. Traffic *10*, 364-371.

Kesarwala, A.H., Samrakandi, M.M., and Piwnica-Worms, D. (2009). Proteasome inhibition blocks ligand-induced dynamic processing and internalization of epidermal growth factor receptor via altered receptor ubiquitination and phosphorylation. Cancer Research *69*, 976-983.

King, T.R., Fang, Y., Mahon, E.S., and Anderson, D.H. (2000). Using a Phage Display Library to Identify Basic Residues in A-Raf Required to Mediate Binding to the Src Homology 2 Domains of the p85 Subunit of Phosphatidylinositol 3'-Kinase. J Biol Chem *275*, 36450-36456.

Kirchhausen, T. (2000). Clathrin. Annual Review of Biochemistry *69*, 699-727.

Kiuru-Kuhlefelt, S., El-Rifai, W., Fanburg-Smith, J., Kere, J., Miettinen, M., and Knuutila, S. (2001). Concomitant DNA copy number amplification at 17q and 22q in dermatofibrosarcoma protuberans. Cytogenet Cell Genet *92*, 192-195.

Kizhatil, K., Baker, S.A., Arshavsky, V.Y., and Bennett, V. (2009). Ankyrin-G promotes cyclic nucleotide-gated channel transport to rod photoreceptor sensory cilia. Science *323*, 1614-1617.

Kizhatil, K., Davis, J.Q., Davis, L., Hoffman, J., Hogan, B.L., and Bennett, V. (2007a). Ankyrin-G is a molecular partner of E-cadherin in epithelial cells and early embryos. J Biol Chem *282*, 26552-26561.

Kizhatil, K., Yoon, W., Mohler, P.J., Davis, L.H., Hoffman, J.A., and Bennett, V. (2007b). Ankyrin-G and beta2-spectrin collaborate in biogenesis of lateral membrane of human bronchial epithelial cells. J Biol Chem *282*, 2029-2037.

Kjeken, R., Mousavi, S.A., Brech, A., Griffiths, G., and Berg, T. (2001). Wortmannin-sensitive trafficking steps in the endocytic pathway in rat liver endothelial cells. Biochem J *357*, 497-503.

Krendel, M., Osterweil, E.K., and Mooseker, M.S. (2007). Myosin 1E interacts with synaptojanin-1 and dynamin and is involved in endocytosis. FEBS Letters *581*, 644-650.

Krucker, T., Siggins, G.R., and Halpain, S. (2000). Dynamic actin filaments are required for stable long-term potentiation (LTP) in area CA1 of the hippocampus. Proceedings of the National Academy of Sciences of the United States of America *97*, 6856-6861.

Kumabe, T., Sohma, Y., Kayama, T., Yoshimoto, T., and Yamamoto, T. (1992). Amplification of alpha-platelet-derived growth factor receptor gene lacking an exon coding for a portion of the extracellular region in a primary brain tumor of glial origin. Oncogene *7*, 627-633.

Labrecque, L., Royal, I., Surprenant, D.S., Patterson, C., Gingras, D., and Beliveau, R. (2003). Regulation of vascular endothelial growth factor receptor-2 activity by caveolin-1 and plasma membrane cholesterol. Molecular Biology of the Cell *14*, 334-347.

LaRochelle, W.J., Jeffers, M., McDonald, W.F., Chillakuru, R.A., Giese, N.A., Lokker, N.A., Sullivan, C., Boldog, F.L., Yang, M., Vernet, C.*, et al.* (2001). PDGF-D, a new protease-activated growth factor. Nature Cell Biology *3*, 517-521.

Lassila, M., Allen, T.J., Cao, Z., Thallas, V., Jandeleit-Dahm, K.A., Candido, R., and Cooper, M.E. (2004). Imatinib attenuates diabetes-associated atherosclerosis. Arteriosclerosis, Thrombosis & Vascular Biology *24*, 935-942.

Le Clainche, C., Pauly, B.S., Zhang, C.X., Engqvist-Goldstein, A.E., Cunningham, K., and

Drubin, D.G. (2007). A Hip1R-cortactin complex negatively regulates actin assembly associated with endocytosis. EMBO Journal *26*, 1199-1210.

Le Roy, C., and Wrana, J.L. (2005). Clathrin- and non-clathrin-mediated endocytic regulation of cell signalling. Nature Reviews Molecular Cell Biology *6*, 112-126.

Less, J.R., Posner, M.C., Boucher, Y., Borochovitz, D., Wolmark, N., and Jain, R.K. (1992). Interstitial hypertension in human breast and colorectal tumors. Cancer Research *52*, 6371-6374.

Leveen, P., Pekny, M., Gebre-Medhin, S., Swolin, B., Larsson, E., and Betsholtz, C. (1994). Mice deficient for PDGF B show renal, cardiovascular, and hematological abnormalities. Genes & Development *8*, 1875-1887.

Levkowitz, G., Waterman, H., Ettenberg, S.A., Katz, M., Tsygankov, A.Y., Alroy, I., Lavi, S., Iwai, K., Reiss, Y., Ciechanover, A.*, et al.* (1999). Ubiquitin ligase activity and tyrosine phosphorylation underlie suppression of growth factor signaling by c-Cbl/Sli-1. Molecular Cell *4*, 1029-1040.

Levkowitz, G., Waterman, H., Zamir, E., Kam, Z., Oved, S., Langdon, W.Y., Beguinot, L., Geiger, B., and Yarden, Y. (1998). c-Cbl/Sli-1 regulates endocytic sorting and ubiquitination of the epidermal growth factor receptor. Genes & Development *12*, 3663-3674.

Li, X., Ponten, A., Aase, K., Karlsson, L., Abramsson, A., Uutela, M., Backstrom, G., Hellstrom, M., Bostrom, H., Li, H.*, et al.* (2000). PDGF-C is a new protease-activated ligand for the PDGF alpha-receptor. Nature Cell Biology *2*, 302-309.

Lim, J.P., and Gleeson, P.A. (2011). Macropinocytosis: an endocytic pathway for internalising large gulps. Immunol Cell Biol *89*, 836-843.

Lindahl, P., and Betsholtz, C. (1998). Not all myofibroblasts are alike: revisiting the role of PDGF-A and PDGF-B using PDGF-targeted mice. Curr Opin Nephrol Hypertens *7*, 21-26.

Lindahl, P., Hellstrom, M., Kalen, M., Karlsson, L., Pekny, M., Pekna, M., Soriano, P., and Betsholtz, C. (1998). Paracrine PDGF-B/PDGF-Rbeta signaling controls mesangial cell development in kidney glomeruli. Development *125*, 3313-3322.

Lindahl, P., Johansson, B.R., Leveen, P., and Betsholtz, C. (1997a). Pericyte loss and microaneurysm formation in PDGF-B-deficient mice. Science *277*, 242-245.

Lindahl, P., Karlsson, L., Hellstrom, M., Gebre-Medhin, S., Willetts, K., Heath, J.K., and Betsholtz, C. (1997b). Alveogenesis failure in PDGF-A-deficient mice is coupled to lack of distal spreading of alveolar smooth muscle cell progenitors during lung development. Development *124*, 3943-3953.

Linding, R., Russell, R.B., Neduva, V., and Gibson, T.J. (2003). GlobPlot: exploring protein sequences for globularity and disorder. Nucleic Acids Research *31*, 3701-3708.

Lipkowitz, S. (2003). The role of the ubiquitination-proteasome pathway in breast cancer: ubiquitin mediated degradation of growth factor receptors in the pathogenesis and treatment of cancer. Breast Cancer Res *5*, 8-15.

Longva, K.E., Blystad, F.D., Stang, E., Larsen, A.M., Johannessen, L.E., and Madshus, I.H. (2002). Ubiquitination and proteasomal activity is required for transport of the EGF receptor to inner membranes of multivesicular bodies. Journal of Cell Biology *156*, 843-854.

Lu, Z., and Hunter, T. (2009). Degradation of activated protein kinases by ubiquitination. Annual Review of Biochemistry *78*, 435-475.

Luzio, J.P., Pryor, P.R., and Bright, N.A. (2007). Lysosomes: fusion and function. Nature Reviews Molecular Cell Biology *8*, 622-632.

Macia, E., Ehrlich, M., Massol, R., Boucrot, E., Brunner, C., and Kirchhausen, T. (2006a). Dynasore, a cell-permeable inhibitor of dynamin. Developmental Cell *10*, 839-850.

Macia, E., Ehrlich, M., Massol, R., Boucrot, E., Brunner, C., and Kirchhausen, T. (2006b). Dynasore, a cell-permeable inhibitor of dynamin. Dev Cell *10*, 839-850.

Magnusson, M.K., Meade, K.E., Brown, K.E., Arthur, D.C., Krueger, L.A., Barrett, A.J., and Dunbar, C.E. (2001). Rabaptin-5 is a novel fusion partner to platelet-derived growth factor beta receptor in chronic myelomonocytic leukemia. Blood *98*, 2518-2525.

Magnusson, M.K., Meade, K.E., Nakamura, R., Barrett, J., and Dunbar, C.E. (2002). Activity of STI571 in chronic myelomonocytic leukemia with a platelet-derived growth factor beta receptor fusion oncogene. Blood *100*, 1088-1091.

Manes, S., Ana Lacalle, R., Gomez-Mouton, C., and Martinez, A.C. (2003). From rafts to crafts: membrane asymmetry in moving cells. Trends in Immunology *24*, 320-326.

Marina-Garcia, N., Franchi, L., Kim, Y.G., Hu, Y., Smith, D.E., Boons, G.J., and Nunez, G. (2009). Clathrin- and dynamin-dependent endocytic pathway regulates muramyl dipeptide internalization and NOD2 activation. Journal of Immunology *182*, 4321-4327.

Marmor, M.D., and Yarden, Y. (2004). Role of protein ubiquitylation in regulating endocytosis of receptor tyrosine kinases. Oncogene *23*, 2057-2070.

Martin-Granados, C., Prescott, A.R., Van Dessel, N., Van Eynde, A., Arocena, M., Klaska, I.P., Görnemann, J., Beullens, M., Bollen, M., Forrester, J.V.*, et al.* (2012). A Role for PP1/NIPP1 in Steering Migration of Human Cancer Cells. PLoS ONE *7*, e40769.

Matsui, T., Itoh, T., and Fukuda, M. (2011). Small GTPase Rab12 regulates constitutive degradation of transferrin receptor. Traffic *12*, 1432-1443.

Mayor, S., and Pagano, R.E. (2007). Pathways of clathrin-independent endocytosis. Nat Rev Mol Cell Biol *8*, 603-612.

McArthur, G.A., Demetri, G.D., van Oosterom, A., Heinrich, M.C., Debiec-Rychter, M., Corless, C.L., Nikolova, Z., Dimitrijevic, S., and Fletcher, J.A. (2005). Molecular and clinical analysis of locally advanced dermatofibrosarcoma protuberans treated with imatinib: Imatinib Target Exploration Consortium Study B2225. Journal of Clinical Oncology *23*, 866-873.

Meier, O., Boucke, K., Hammer, S.V., Keller, S., Stidwill, R.P., Hemmi, S., and Greber, U.F. (2002). Adenovirus triggers macropinocytosis and endosomal leakage together with its clathrin-mediated uptake. The Journal of Cell Biology *158*, 1119-1131.

Melikova, M.S., Kondratov, K.A., and Kornilova, E.S. (2006). Two different stages of epidermal growth factor (EGF) receptor endocytosis are sensitive to free ubiquitin depletion produced by proteasome inhibitor MG132. Cell Biology International *30*, 31-43.

Mellor, P., Furber, L.A., Nyarko, J.N., and Anderson, D.H. (2012). Multiple roles for the p85alpha isoform in the regulation and function of PI3K signalling and receptor trafficking. Biochem J *441*, 23-37.

Miled, N., Yan, Y., Hon, W.C., Perisic, O., Zvelebil, M., Inbar, Y., Schneidman-Duhovny, D., Wolfson, H.J., Backer, J.M., and Williams, R.L. (2007). Mechanism of two classes of cancer mutations in the phosphoinositide 3-kinase catalytic subunit. Science *317*, 239-242.

Mimnaugh, E.G., Chavany, C., and Neckers, L. (1996). Polyubiquitination and proteasomal degradation of the p185c-erbB-2 receptor protein-tyrosine kinase induced by geldanamycin. Journal of Biological Chemistry *271*, 22796-22801.

Mitchell, H., Choudhury, A., Pagano, R.E., and Leof, E.B. (2004). Ligand-dependent and -independent Transforming Growth Factor-β Receptor Recycling Regulated by CME and Rab11. Molecular Biology of the Cell *15*, 4166-4178.

Mohler, P.J., and Bennett, V. (2005). Ankyrin-based cardiac arrhythmias: a new class of channelopathies due to loss of cellular targeting. Curr Opin Cardiol *20*, 189-193.

Mohler, P.J., Healy, J.A., Xue, H., Puca, A.A., Kline, C.F., Allingham, R.R., Kranias, E.G., Rockman, H.A., and Bennett, V. (2007). Ankyrin-B syndrome: enhanced cardiac function balanced by risk of cardiac death and premature senescence. PLoS One *2*, e1051.

Mohler, P.J., Hoffman, J.A., Davis, J.Q., Abdi, K.M., Kim, C.R., Jones, S.K., Davis, L.H., Roberts, K.F., and Bennett, V. (2004a). Isoform specificity among ankyrins. An amphipathic alpha-helix in the divergent regulatory domain of ankyrin-b interacts with the molecular co-chaperone Hdj1/Hsp40. J Biol Chem *279*, 25798-25804.

Mohler, P.J., Schott, J.J., Gramolini, A.O., Dilly, K.W., Guatimosim, S., duBell, W.H., Song, L.S., Haurogne, K., Kyndt, F., Ali, M.E*., et al.* (2003). Ankyrin-B mutation causes type 4 long-QT cardiac arrhythmia and sudden cardiac death. Nature *421*, 634-639.

Mohler, P.J., Yoon, W., and Bennett, V. (2004b). Ankyrin-B targets beta2-spectrin to an intracellular compartment in neonatal cardiomyocytes. Journal of Biological Chemistry *279*, 40185-40193.

Monier, S., Dietzen, D.J., Hastings, W.R., Lublin, D.M., and Kurzchalia, T.V. (1996). Oligomerization of VIP21-caveolin in vitro is stabilized by long chain fatty acylation or cholesterol. FEBS Letters *388*, 143-149.

Mooren, O.L., Galletta, B.J., and Cooper, J.A. (2012). Roles for Actin Assembly in Endocytosis. Annual Review of Biochemistry *81*, 661-686.

Mori, S., Claesson-Welsh, L., and Heldin, C.H. (1991). Identification of a hydrophobic region in the carboxyl terminus of the platelet-derived growth factor beta-receptor which is important for ligand-mediated endocytosis. J Biol Chem *266*, 21158-21164.

Mori, S., Claesson-Welsh, L., Okuyama, Y., and Saito, Y. (1995a). Ligand-induced polyubiquitination of receptor tyrosine kinases. Biochemical & Biophysical Research

Communications *213*, 32-39.

Mori, S., Heldin, C.H., and Claesson-Welsh, L. (1992). Ligand-induced polyubiquitination of the platelet-derived growth factor beta-receptor. Journal of Biological Chemistry *267*, 6429-6434.

Mori, S., Heldin, C.H., and Claesson-Welsh, L. (1993). Ligand-induced ubiquitination of the platelet-derived growth factor beta-receptor plays a negative regulatory role in its mitogenic signaling. Journal of Biological Chemistry *268*, 577-583.

Mori, S., Kanaki, H., Tanaka, K., Morisaki, N., and Saito, Y. (1995b). Ligand-activated platelet-derived growth factor beta-receptor is degraded through proteasome-dependent proteolytic pathway. Biochemical & Biophysical Research Communications *217*, 224-229.

Mori, S., Tanaka, K., Omura, S., and Saito, Y. (1995c). Degradation process of ligand-stimulated platelet-derived growth factor beta-receptor involves ubiquitin-proteasome proteolytic pathway. Journal of Biological Chemistry *270*, 29447-29452.

Mosesson, Y., Shtiegman, K., Katz, M., Zwang, Y., Vereb, G., Szollosi, J., and Yarden, Y. (2003). Endocytosis of receptor tyrosine kinases is driven by monoubiquitylation, not polyubiquitylation. Journal of Biological Chemistry *278*, 21323-21326.

Motley, A., Bright, N.A., Seaman, M.N., and Robinson, M.S. (2003). CME in AP-2-depleted cells. Journal of Cell Biology *162*, 909-918.

Mukherjee, S., Tessema, M., and Wandinger-Ness, A. (2006). Vesicular trafficking of tyrosine kinase receptors and associated proteins in the regulation of signaling and vascular function. Circ Res *98*, 743-756.

Mullock, B.M., Bright, N.A., Fearon, C.W., Gray, S.R., and Luzio, J.P. (1998). Fusion of lysosomes with late endosomes produces a hybrid organelle of intermediate density and is NSF dependent. Journal of Cell Biology *140*, 591-601.

Nankoe, S.R., and Sever, S. (2006). Dynasore puts a new spin on dynamin: a surprising dual role during vesicle formation. Trends in Cell Biology *16*, 607-609.

Navarro, A., Anand-Apte, B., and Parat, M.O. (2004). A role for caveolae in cell migration. FASEB Journal *18*, 1801-1811.

Neckers, L. (2002). Hsp90 inhibitors as novel cancer chemotherapeutic agents. Trends in Molecular Medicine *8*, S55-61.

Nobes, C., and Marsh, M. (2000). Dendritic cells: new roles for Cdc42 and Rac in antigen uptake? Current Biology *10*, R739-741.

Nossal, R. (2001). Energetics of clathrin basket assembly. Traffic *2*, 138-147.

Oh, P., McIntosh, D.P., and Schnitzer, J.E. (1998). Dynamin at the neck of caveolae mediates their budding to form transport vesicles by GTP-driven fission from the plasma membrane of endothelium. Journal of Cell Biology *141*, 101-114.

Olson, L.E., and Soriano, P. (2009). Increased PDGFRalpha activation disrupts connective tissue development and drives systemic fibrosis. Developmental Cell *16*, 303-313.

Ortiz-Lazareno, P.C., Hernandez-Flores, G., Dominguez-Rodriguez, J.R., Lerma-Diaz, J.M., Jave-Suarez, L.F., Aguilar-Lemarroy, A., Gomez-Contreras, P.C., Scott-Algara, D., and Bravo-Cuellar, A. (2008). MG132 proteasome inhibitor modulates proinflammatory cytokines production and expression of their receptors in U937 cells: involvement of nuclear factor-kappaB and activator protein-1. Immunology *124*, 534-541.

Ostman, A. (2004). PDGF receptors-mediators of autocrine tumor growth and regulators of tumor vasculature and stroma. Cytokine Growth Factor Rev *15*, 275-286.

Ostman, A., and Heldin, C.H. (2001). Involvement of platelet-derived growth factor in disease:

development of specific antagonists. Adv Cancer Res *80*, 1-38.

Parton, R.G., Hanzal-Bayer, M., and Hancock, J.F. (2006). Biogenesis of caveolae: a structural model for caveolin-induced domain formation. Journal of Cell Science *119*, 787-796.

Peters, L.L., John, K.M., Lu, F.M., Eicher, E.M., Higgins, A., Yialamas, M., Turtzo, L.C., Otsuka, A.J., and Lux, S.E. (1995). Ank3 (epithelial ankyrin), a widely distributed new member of the ankyrin gene family and the major ankyrin in kidney, is expressed in alternatively spliced forms, including forms that lack the repeat domain. J Cell Biol *130*, 313-330.

Peters, P.J., Mironov, A., Jr., Peretz, D., van Donselaar, E., Leclerc, E., Erpel, S., DeArmond, S.J., Burton, D.R., Williamson, R.A., Vey, M.*, et al.* (2003). Trafficking of prion proteins through a caveolae-mediated endosomal pathway. Journal of Cell Biology *162*, 703-717.

Pietras, K., Ostman, A., Sjoquist, M., Buchdunger, E., Reed, R.K., Heldin, C.H., and Rubin, K. (2001). Inhibition of platelet-derived growth factor receptors reduces interstitial hypertension and increases transcapillary transport in tumors. Cancer Research *61*, 2929-2934.

Pietras, K., Pahler, J., Bergers, G., and Hanahan, D. (2008). Functions of paracrine PDGF signaling in the proangiogenic tumor stroma revealed by pharmacological targeting. PLoS Medicine / Public Library of Science *5*, e19.

Pietras, K., Rubin, K., Sjoblom, T., Buchdunger, E., Sjoquist, M., Heldin, C.H., and Ostman, A. (2002). Inhibition of PDGF receptor signaling in tumor stroma enhances antitumor effect of chemotherapy. Cancer Research *62*, 5476-5484.

Piper, R.C., and Luzio, J.P. (2007). Ubiquitin-dependent sorting of integral membrane proteins for degradation in lysosomes. Current Opinion in Cell Biology *19*, 459-465.

Praetorius, J., Andreasen, D., Jensen, B.L., Ainsworth, M.A., Friis, U.G., and Johansen, T. (2000). NHE1, NHE2, and NHE3 contribute to regulation of intracellular pH in murine duodenal

epithelial cells. American Journal of Physiology - Gastrointestinal and Liver Physiology *278*, G197-G206.

Pryor, P.R., Mullock, B.M., Bright, N.A., Gray, S.R., and Luzio, J.P. (2000). The role of intraorganellar Ca(2+) in late endosome-lysosome heterotypic fusion and in the reformation of lysosomes from hybrid organelles. Journal of Cell Biology *149*, 1053-1062.

Pucadyil, T.J., and Schmid, S.L. (2009). Conserved functions of membrane active GTPases in coated vesicle formation. Science *325*, 1217-1220.

Pyorala, K., Laakso, M., and Uusitupa, M. (1987). Diabetes and atherosclerosis: an epidemiologic view. Diabetes Metab Rev *3*, 463-524.

Qian, Y., Corum, L., Meng, Q., Blenis, J., Zheng, J.Z., Shi, X., Flynn, D.C., and Jiang, B.-H. (2003). PI3K induced actin filament remodeling through Akt and p70S6K1: implication of essential role in cell migration. American Journal of Physiology - Cell Physiology *286*, C153-C163.

Racoosin, E.L., and Swanson, J.A. (1993). Macropinosome maturation and fusion with tubular lysosomes in macrophages. Journal of Cell Biology *121*, 1011-1020.

Raiborg, C., and Stenmark, H. (2009). The ESCRT machinery in endosomal sorting of ubiquitylated membrane proteins. Nature *458*, 445-452.

Ramachandran, R., and Schmid, S.L. (2008). Real-time detection reveals that effectors couple dynamin's GTP-dependent conformational changes to the membrane. EMBO Journal *27*, 27-37.

Ravid, T., and Hochstrasser, M. (2008). Diversity of degradation signals in the ubiquitin-proteasome system. Nature Reviews Molecular Cell Biology *9*, 679-690.

Roberts, W.M., Look, A.T., Roussel, M.F., and Sherr, C.J. (1988). Tandem linkage of human

CSF-1 receptor (c-fms) and PDGF receptor genes. Cell *55*, 655-661.

Rodal, S.K., Skretting, G., Garred, Ø., Vilhardt, F., van Deurs, B., and Sandvig, K. (1999). Extraction of Cholesterol with Methyl-β-Cyclodextrin Perturbs Formation of Clathrin-coated Endocytic Vesicles. Molecular Biology of the Cell *10*, 961-974.

Rosnet, O., Marchetto, S., deLapeyriere, O., and Birnbaum, D. (1991). Murine Flt3, a gene encoding a novel tyrosine kinase receptor of the PDGFR/CSF1R family. Oncogene *6*, 1641-1650.

Ross, R. (1993). The pathogenesis of atherosclerosis: a perspective for the 1990s. Nature *362*, 801-809.

Rothberg, K.G., Heuser, J.E., Donzell, W.C., Ying, Y.S., Glenney, J.R., and Anderson, R.G. (1992). Caveolin, a protein component of caveolae membrane coats. Cell *68*, 673-682.

Rubin, K., Sjoquist, M., Gustafsson, A.M., Isaksson, B., Salvessen, G., and Reed, R.K. (2000). Lowering of tumoral interstitial fluid pressure by prostaglandin E(1) is paralleled by an increased uptake of (51)Cr-EDTA. International Journal of Cancer *86*, 636-643.

Russell, M.R., Jamieson, W.L., Dolloff, N.G., and Fatatis, A. (2009). The alpha-receptor for platelet-derived growth factor as a target for antibody-mediated inhibition of skeletal metastases from prostate cancer cells. Oncogene *28*, 412-421.

Rutherford, C., Martin, W., Carrier, M., Anggard, E.E., and Ferns, G.A. (1997). Endogenously elicited antibodies to platelet derived growth factor-BB and platelet cytosolic protein inhibit aortic lesion development in the cholesterol-fed rabbit. Int J Exp Pathol *78*, 21-32.

Sak, M.M., Breen, K., Ronning, S.B., Pedersen, N.M., Bertelsen, V., Stang, E., and Madshus, I.H. (2012). The oncoprotein ErbB3 is endocytosed in the absence of added ligand in a clathrin-dependent manner. Carcinogenesis *33*, 1031-1039.

Saksena, S., Sun, J., Chu, T., and Emr, S.D. (2007). ESCRTing proteins in the endocytic pathway. Trends Biochem Sci *32*, 561-573.

Saksena, S., Wahlman, J., Teis, D., Johnson, A.E., and Emr, S.D. (2009). Functional reconstitution of ESCRT-III assembly and disassembly. Cell *136*, 97-109.

Sargiacomo, M., Scherer, P.E., Tang, Z., Kubler, E., Song, K.S., Sanders, M.C., and Lisanti, M.P. (1995). Oligomeric structure of caveolin: implications for caveolae membrane organization. Proceedings of the National Academy of Sciences of the United States of America *92*, 9407-9411.

Schafer, D.A., D'Souza-Schorey, C., and Cooper, J.A. (2000). Actin assembly at membranes controlled by ARF6. Traffic *1*, 892-903.

Schmees, C., Villasenor, R., Zheng, W., Ma, H., Zerial, M., Heldin, C.H., and Hellberg, C. (2012). Macropinocytosis of the PDGF -receptor promotes fibroblast transformation by H-RasG12V. Molecular Biology of the Cell *23*, 2571-2582.

Schmid, E.M., Ford, M.G., Burtey, A., Praefcke, G.J., Peak-Chew, S.Y., Mills, I.G., Benmerah, A., and McMahon, H.T. (2006). Role of the AP2 beta-appendage hub in recruiting partners for clathrin-coated vesicle assembly. Plos Biology *4*, e262.

Sepp-Lorenzino, L., Ma, Z., Lebwohl, D.E., Vinitsky, A., and Rosen, N. (1995). Herbimycin A induces the 20 S proteasome- and ubiquitin-dependent degradation of receptor tyrosine kinases. Journal of Biological Chemistry *270*, 16580-16587.

Sever, S., Muhlberg, A.B., and Schmid, S.L. (1999). Impairment of dynamin's GAP domain stimulates receptor-mediated endocytosis. Nature *398*, 481-486.

Shim, A.H., Liu, H., Focia, P.J., Chen, X., Lin, P.C., and He, X. (2010). Structures of a platelet-derived growth factor/propeptide complex and a platelet-derived growth factor/receptor complex.

Proceedings of the National Academy of Sciences of the United States of America *107*, 11307-11312.

Shimizu, A., O'Brien, K.P., Sjoblom, T., Pietras, K., Buchdunger, E., Collins, V.P., Heldin, C.H., Dumanski, J.P., and Ostman, A. (1999). The dermatofibrosarcoma protuberans-associated collagen type Ialpha1/platelet-derived growth factor (PDGF) B-chain fusion gene generates a transforming protein that is processed to functional PDGF-BB. Cancer Research *59*, 3719-3723.

Shpetner, H.S., Herskovits, J.S., and Vallee, R.B. (1996). A binding site for SH3 domains targets dynamin to coated pits. Journal of Biological Chemistry *271*, 13-16.

Sigismund, S., Woelk, T., Puri, C., Maspero, E., Tacchetti, C., Transidico, P., Di Fiore, P.P., and Polo, S. (2005). Clathrin-independent endocytosis of ubiquitinated cargos. Proceedings of the National Academy of Sciences of the United States of America *102*, 2760-2765.

Singh, R.D., Liu, Y., Wheatley, C.L., Holicky, E.L., Makino, A., Marks, D.L., Kobayashi, T., Subramaniam, G., Bittman, R., and Pagano, R.E. (2006). Caveolar Endocytosis and Microdomain Association of a Glycosphingolipid Analog Is Dependent on Its Sphingosine Stereochemistry. Journal of Biological Chemistry *281*, 30660-30668.

Smits, A., Funa, K., Vassbotn, F.S., Beausang-Linder, M., af Ekenstam, F., Heldin, C.H., Westermark, B., and Nister, M. (1992). Expression of platelet-derived growth factor and its receptors in proliferative disorders of fibroblastic origin. American Journal of Pathology *140*, 639-648.

Soriano, P. (1994). Abnormal kidney development and hematological disorders in PDGF beta-receptor mutant mice. Genes & Development *8*, 1888-1896.

Soriano, P. (1997). The PDGF alpha receptor is required for neural crest cell development and for normal patterning of the somites. Development *124*, 2691-2700.

Sorkina, T., Huang, F., Beguinot, L., and Sorkin, A. (2002). Effect of Tyrosine Kinase Inhibitors on Clathrin-coated Pit Recruitment and Internalization of Epidermal Growth Factor Receptor. Journal of Biological Chemistry *277*, 27433-27441.

Sorokin, A.V., Kim, E.R., and Ovchinnikov, L.P. (2009). Proteasome system of protein degradation and processing. Biochemistry (Mosc) *74*, 1411-1442.

Spritz, R.A., Strunk, K.M., Lee, S.T., Lu-Kuo, J.M., Ward, D.C., Le Paslier, D., Altherr, M.R., Dorman, T.E., and Moir, D.T. (1994). A YAC contig spanning a cluster of human type III receptor protein tyrosine kinase genes (PDGFRA-KIT-KDR) in chromosome segment 4q12. Genomics *22*, 431-436.

Spudich, G., Chibalina, M.V., Au, J.S., Arden, S.D., Buss, F., and Kendrick-Jones, J. (2007). Myosin VI targeting to clathrin-coated structures and dimerization is mediated by binding to Disabled-2 and PtdIns(4,5)P2. Nature Cell Biology *9*, 176-183.

Stahlhut, M., and van Deurs, B. (2000). Identification of filamin as a novel ligand for caveolin-1: evidence for the organization of caveolin-1-associated membrane domains by the actin cytoskeleton. Molecular Biology of the Cell *11*, 325-337.

Stenmark, H. (2009). Rab GTPases as coordinators of vesicle traffic. Nat Rev Mol Cell Biol *10*, 513-525.

Strous, G.J., van Kerkhof, P., Govers, R., Ciechanover, A., and Schwartz, A.L. (1996). The ubiquitin conjugation system is required for ligand-induced endocytosis and degradation of the growth hormone receptor. EMBO Journal *15*, 3806-3812.

Stuffers, S., Sem Wegner, C., Stenmark, H., and Brech, A. (2009). Multivesicular endosome biogenesis in the absence of ESCRTs. Traffic *10*, 925-937.

Surviladze Z, W.A., Strouse JJ, et al (2010). A Potent and Selective Inhibitor of Cdc42 GTPase.

In In: Probe Reports from the NIH Molecular Libraries Program [Internet]. Bethesda (MD): National Center for Biotechnology Information (US); .

Swaminathan, S., Amerik, A.Y., and Hochstrasser, M. (1999). The Doa4 deubiquitinating enzyme is required for ubiquitin homeostasis in yeast. Molecular Biology of the Cell *10*, 2583-2594.

Swanson, J.A. (2008). Shaping cups into phagosomes and macropinosomes. Nature Reviews Molecular Cell Biology *9*, 639-649.

Tallquist, M., and Kazlauskas, A. (2004). PDGF signaling in cells and mice. Cytokine Growth Factor Rev *15*, 205-213.

Tang, Y., Katuri, V., Dillner, A., Mishra, B., Deng, C.-X., and Mishra, L. (2003). Disruption of Transforming Growth Factor-β Signaling in ELF β-Spectrin-Deficient Mice. Science *299*, 574-577.

Tanno, H., and Komada, M. (2013). The ubiquitin code and its decoding machinery in the endocytic pathway. Journal of Biochemistry *153*, 497-504.

Tejada, M.L., Yu, L., Dong, J., Jung, K., Meng, G., Peale, F.V., Frantz, G.D., Hall, L., Liang, X., Gerber, H.P.*, et al.* (2006). Tumor-driven paracrine platelet-derived growth factor receptor alpha signaling is a key determinant of stromal cell recruitment in a model of human lung carcinoma. Clinical Cancer Research *12*, 2676-2688.

Thiery, J.P., Acloque, H., Huang, R.Y., and Nieto, M.A. (2009). Epithelial-mesenchymal transitions in development and disease. Cell *139*, 871-890.

Thomsen, P., Roepstorff, K., Stahlhut, M., and van Deurs, B. (2002). Caveolae are highly immobile plasma membrane microdomains, which are not involved in constitutive endocytic trafficking. Molecular Biology of the Cell *13*, 238-250.

Tikhomirov, O., and Carpenter, G. (2000). Geldanamycin induces ErbB-2 degradation by proteolytic fragmentation. Journal of Biological Chemistry *275*, 26625-26631.

Tomasson, M.H., Sternberg, D.W., Williams, I.R., Carroll, M., Cain, D., Aster, J.C., Ilaria, R.L., Jr., Van Etten, R.A., and Gilliland, D.G. (2000). Fatal myeloproliferation, induced in mice by TEL/PDGFbetaR expression, depends on PDGFbetaR tyrosines 579/581. Journal of Clinical Investigation *105*, 423-432.

Uhrbom, L., Hesselager, G., Nister, M., and Westermark, B. (1998). Induction of brain tumors in mice using a recombinant platelet-derived growth factor B-chain retrovirus. Cancer Research *58*, 5275-5279.

Ullrich, O., Reinsch, S., Urbe, S., Zerial, M., and Parton, R.G. (1996). Rab11 regulates recycling through the pericentriolar recycling endosome. J Cell Biol *135*, 913-924.

Ungewickell, E.J., and Hinrichsen, L. (2007). Endocytosis: clathrin-mediated membrane budding. Current Opinion in Cell Biology *19*, 417-425.

Uusitupa, M.I., Niskanen, L.K., Siitonen, O., Voutilainen, E., and Pyorala, K. (1990). 5-year incidence of atherosclerotic vascular disease in relation to general risk factors, insulin level, and abnormalities in lipoprotein composition in non-insulin-dependent diabetic and nondiabetic subjects. Circulation *82*, 27-36.

van Kerkhof, P., Govers, R., Alves dos Santos, C.M., and Strous, G.J. (2000). Endocytosis and degradation of the growth hormone receptor are proteasome-dependent. Journal of Biological Chemistry *275*, 1575-1580.

Verschooten, L., Barrette, K., Van Kelst, S., Rubio Romero, N., Proby, C., De Vos, R., Agostinis, P., and Garmyn, M. (2012). Autophagy Inhibitor Chloroquine Enhanced the Cell Death Inducing Effect of the Flavonoid Luteolin in Metastatic Squamous Cell Carcinoma Cells. PLoS ONE *7*, e48264.

von Kleist, L., and Haucke, V. (2012). At the Crossroads of Chemistry and Cell Biology: Inhibiting Membrane Traffic by Small Molecules. Traffic *13*, 495-504.

von Kleist, L., Stahlschmidt, W., Bulut, H., Gromova, K., Puchkov, D., Robertson, M.J., MacGregor, K.A., Tomilin, N., Pechstein, A., Chau, N.*, et al.* (2011). Role of the clathrin terminal domain in regulating coated pit dynamics revealed by small molecule inhibition.[Erratum appears in Cell. 2011 Sep 2;146(5):841 Note: Tomlin, Nikolay [corrected to Tomilin, Nikolay]]. Cell *146*, 471-484.

von Tell, D., Armulik, A., and Betsholtz, C. (2006). Pericytes and vascular stability. Experimental Cell Research *312*, 623-629.

von Zastrow, M., and Sorkin, A. (2007). Signaling on the endocytic pathway. Curr Opin Cell Biol *19*, 436-445.

Wang, F., Herzmark, P., Weiner, O.D., Srinivasan, S., Servant, G., and Bourne, H.R. (2002). Lipid products of PI(3)Ks maintain persistent cell polarity and directed motility in neutrophils. Nat Cell Biol *4*, 513-518.

Wang, J., Coltrera, M.D., and Gown, A.M. (1994). Cell proliferation in human soft tissue tumors correlates with platelet-derived growth factor B chain expression: an immunohistochemical and in situ hybridization study. Cancer Research *54*, 560-564.

West, M.A., Bretscher, M.S., and Watts, C. (1989). Distinct endocytotic pathways in epidermal growth factor-stimulated human carcinoma A431 cells.[Erratum appears in J Cell Biol 1990 Mar;110(3):859]. Journal of Cell Biology *109*, 2731-2739.

West, M.A., Prescott, A.R., Eskelinen, E.L., Ridley, A.J., and Watts, C. (2000). Rac is required for constitutive macropinocytosis by dendritic cells but does not control its downregulation. Current Biology *10*, 839-848.

Wilson, G.D. (2007). Hypoxia and prognosis: the oxygen tension mounts. Frontiers in Bioscience *12*, 3502-3518.

Xian, X., Hakansson, J., Stahlberg, A., Lindblom, P., Betsholtz, C., Gerhardt, H., and Semb, H. (2006). Pericytes limit tumor cell metastasis. Journal of Clinical Investigation *116*, 642-651.

Xu, W., Mimnaugh, E., Rosser, M.F., Nicchitta, C., Marcu, M., Yarden, Y., and Neckers, L. (2001). Sensitivity of mature Erbb2 to geldanamycin is conferred by its kinase domain and is mediated by the chaperone protein Hsp90. Journal of Biological Chemistry *276*, 3702-3708.

Yang, J., Liu, X., Nyland, S.B., Zhang, R., Ryland, L.K., Broeg, K., Baab, K.T., Jarbadan, N.R., Irby, R., and Loughran, T.P., Jr. (2010). Platelet-derived growth factor mediates survival of leukemic large granular lymphocytes via an autocrine regulatory pathway. Blood *115*, 51-60.

Yang, L., Lin, C., and Liu, Z.R. (2006). P68 RNA helicase mediates PDGF-induced epithelial mesenchymal transition by displacing Axin from beta-catenin. Cell *127*, 139-155.

Yang, Y., Yuzawa, S., and Schlessinger, J. (2008). Contacts between membrane proximal regions of the PDGF receptor ectodomain are required for receptor activation but not for receptor dimerization. Proceedings of the National Academy of Sciences of the United States of America *105*, 7681-7686.

Yarar, D., Waterman-Storer, C.M., and Schmid, S.L. (2005). A dynamic actin cytoskeleton functions at multiple stages of CME. Molecular Biology of the Cell *16*, 964-975.

Yarden, Y., Escobedo, J.A., Kuang, W.J., Yang-Feng, T.L., Daniel, T.O., Tremble, P.M., Chen, E.Y., Ando, M.E., Harkins, R.N., Francke, U.*, et al.* (1986). Structure of the receptor for platelet-derived growth factor helps define a family of closely related growth factor receptors. Nature *323*, 226-232.

Yarden, Y., Kuang, W.J., Yang-Feng, T., Coussens, L., Munemitsu, S., Dull, T.J., Chen, E.,

Schlessinger, J., Francke, U., and Ullrich, A. (1987). Human proto-oncogene c-kit: a new cell surface receptor tyrosine kinase for an unidentified ligand. EMBO Journal *6*, 3341-3351.

Yu, J., Zhang, Y., McIlroy, J., Rordorf-Nikolic, T., Orr, G.A., and Backer, J.M. (1998). Regulation of the p85/p110 phosphatidylinositol 3'-kinase: stabilization and inhibition of the p110alpha catalytic subunit by the p85 regulatory subunit. Mol Cell Biol *18*, 1379-1387.

Zerial, M., and McBride, H. (2001). Rab proteins as membrane organizers. Nat Rev Mol Cell Biol *2*, 107-117.

Zheng, X., Baker, H., Hancock, W.S., Fawaz, F., McCaman, M., and Pungor, E. (2006). Proteomic Analysis for the Assessment of Different Lots of Fetal Bovine Serum as a Raw Material for Cell Culture. Part IV. Application of Proteomics to the Manufacture of Biological Drugs. Biotechnology Progress *22*, 1294-1300.

Zigrino, P., Loffek, S., and Mauch, C. (2005). Tumor-stroma interactions: their role in the control of tumor cell invasion. Biochimie *87*, 321-328.